Isolation and Characterization of Anti-Inflammatory and Immunomodulatory Compounds from Higher Plants

Inauguraldissertation

zur
Erlangung der Würde eines Doktors der Philosophie
vorgelegt der
Philosophisch-Naturwissenschaftlichen Fakultät
der Universität Basel

von

Morris Keller

2023

Genehmigt von der Philosophisch-Naturwissenschaftlichen Fakultät

auf Antrag von

Erstbetreuer:	Prof. Dr. Olivier Potterat
Zweitbetreuer:	Prof. Dr. Alex Odermatt
Externer Experte:	Prof. Dr. Pierre Champy

Basel, den 20.06.2023

Prof. Dr. Marcel Mayor

Dekan

"We choose to go to the Moon in this decade and do the other things, not because they are easy, but because they are hard; because that goal will serve to organize and measure the best of our energies and skills, because that challenge is one that we are willing to accept, one we are unwilling to postpone, and one we intend to win, and the others, too."

From "*We choose to go to the Moon*", John F. Kennedy, September 12, 1962

Acknowledgments

First and foremost, I would like to express my deepest gratitude to Prof. Dr. Olivier Potterat, as well as to Prof. Dr. Matthias Hamburger, and Prof. Dr. Robin Teufel, for providing me the opportunity to pursue my doctoral degree in the Pharmaceutical Biology research group at the Pharmacenter in Basel. In particular, I am extremely grateful to Prof. Dr. Olivier Potterat for his invaluable guidance, expertise, and support over the past five years, which have been instrumental in both my scientific and personal growth. I am truly appreciative of the time you spent sharing your knowledge and insights with me, as well as for your patience, encouragement, and feedback, which have helped me to overcome many challenges throughout the project. Thank you for being a remarkable mentor!

Next, I am deeply thankful to Prof. Dr. Alex Odermatt, my second supervisor, for his valuable inputs during our annual meetings. I also want to express my appreciation to Prof. Dr. Pierre Champy for serving as the external examiner and reviewing my doctoral thesis.

Furthermore, I want to convey my heartfelt thanks to several collaborators, including Prof. Dr. Carsten Gründemann and Dr. Moritz Winker from the Translational Complementary Medicine research group in Basel, Prof. Dr. Amel Boudjelal and Dr. Sarra Chabane from the Mohamed Boudiaf University in M'Sila Algeria, and Prof. Dr. Veronika Butterweck from the Max Zeller Söhne AG in Romanshorn. I highly valued the opportunity to work alongside such distinguished experts in their field of research. Our fruitful collaborations led to the successful publication of wonderful research findings, and I am truly grateful for their expertise and insights.

I would like to extend special thanks to Dr. Ombeline Danton for her instrumental role in teaching me the techniques of NMR spectroscopy and imparting the proper skills for solving chemical structures. Furthermore, I am also grateful to Dr. Jakob Reinhardt for his excellent teaching and invaluable assistance in the lab, particularly in the field of circular dichroism.

Next, I woud like to acknowledge Dr. Alessandro Prescimone and Dr. Roman Jakob for introducing me to the field of single X-ray crystallography and providing guidance and support throughout my work in this area.

In addition, I am appreciative for the assistance offered by Franziska Keresztes and Nino Sperisen during their Master projects in isolating substances.

Then, I would like to thank Orlando Fertig for his invaluable support as a colleague and friend. His technical expertise and advices were instrumental in the success of this project, and his insights and guidance on personal matters were greatly appreciated. Additionally, I would like to extend my appreciation to Manuela Rogalski for her invaluable support with administrative tasks.

I extend my heartfelt gratitude to my colleagues Tanja, Lara, Vanessa, Antoine, Theresa, Teresa, Ming, Nova, Justine, Pascaline, Halim, Mouhssin, Eliane, Andrea, Ahmed, Valeria, Ruzhe, Tamara, Lars, Maria, Lei, Sven, Malik, Heiner, Andreas, and Xinja. I want to express my appreciation to all of you for creating such a wonderful atmosphere and for imparting so much knowledge to me throughout these five years. Our time together has led to some special friendships that I cherish.

Many thanks go to my best friends "The Coons" for always being at my side and for all the great memories we share.

I am extremely thankful to my family, particularly my parents, for their unwavering support and guidance throughout my life. They taught me the essential skills and values needed to navigate life's challenges and have set a great example of the rewards of hard work. Thank you, mom and dad, for everything!

Basel *Morris Keller*

Summer 2023

Table of Contents

Abbreviations

8-MOP	8-methoxypsoralen
ALG	Anti-lymphoglobulin
AP-1	Activator protein 1
APC	Antigen-presenting cell
ATG	Anti-thymoglobulin
Ca^{2+}	Calcium ion
CAR	Chimeric antigen receptor
CB2R	Cannabinoid-2 receptor
CBD	Cannabidiol
CBM	Cutaneous biodistribution method
CCL	CC-chemokine ligand
CD	Cluster of differentiation
CDK	Cyclin-dependent kinase
CFSE	Carboxyfluorescein diacetate succinimidyl ester
CSF	Colony-stimulating factor
CTLA4	Cytotoxic T-lymphocyte-associated protein 4
CXCL	CXC-motif chemokine ligand
CYP3A4	Cytochrome P450 3A4
DAG	Diacylglycerol
DC	Dendritic cell
ECD	Electronic circular dichroism
EGF	Epidermal growth factor
ELISA	Enzyme-linked immunosorbent assay
ESI	Electrospray ionization
EtOH	Ethanol
FACS	Fluorescence-activated cell sorting
Fc region	Fragment crystallizable region
FGF	Fibroblast growth factor
FKBP12	FK506-binding protein 12
FRB	FKBP12-rapamycin-binding
G1 phase	Gap phase 1

G2 phase	Gap phase 2
G-CSF	Granulocyte-colony stimulating factor
GAPDH	Glyceraldehyde 3-phosphate dehydrogenase
GM-CSF	Granulocyte-macrophage colony-stimulating factor
HO-1	Heme oxygenase 1
HGF	Hepatocyte growth factor
HILIC	Hydrophilic interaction liquid chromatography
HIV	Human immunodeficiency virus
HLA	Human leukocyte antigen
HPLC	High-performance liquid chromatography
HR	High resolution
IFN	Interferon
IgE	Immunoglobulin E
IgG	Immunoglobulin G
IκBα	Nuclear factor of kappa light polypeptide gene enhancer in B cells inhibitor alpha
IL	Interleukin
ILCs	Innate lymphoid cells
IP_3	Inositol trisphosphate
JAK	Janus kinase
LAT	Linker for activation of T cells
Lck	Lymphocyte-specific protein tyrosine kinase
MAPK	Mitogen-activated protein kinase.
MCP-1	Monocyte chemotactic protein 1
MeOH	Methanol
MHC	Major histocompatibility complex
MLR	Mixed lymphocyte reaction
M phase	Mitosis phase
MS	Mass spectrometry
MSI	Mass spectrometry imaging
mTOR	Mammalian target for rapamycin
NFAT	Nuclear factor of activated T cells
NFκB	Nuclear factor kappa-light-chain-enhancer of activated B cells

NK cell	Natural killer cell
NMR	Nuclear magnetic resonance
NOD-like receptor	Nucleotide-binding oligomerization domain-like receptor
OKT3	Ortho Kung T3
PBMCs	Peripheral blood mononuclear cells
PDA	Photodiode array
PDGF	Platelet-derived growth factor
PGE1	prostaglandin E1
PGE2	Prostagalndin E2
PI3K	Phosphoinositide 3-kinase
PIP_2	Phosphatidylinositol 4,5-bisphosphate
PKC-θ	Protein kinase C theta
PLC-γ	Phospholipase C gamma
PRRs	Pattern recognition receptors
PUVA	Psoralen plus UV-A
RANTES	Regulated upon activation normal T cell expressed and secreted
RasGRP1	Ras guanyl-releasing protein 1
ROS	Reactive oxygen species
S1P	Sphingosine-1-phosphate
Siglecs	Sialic acid-binding immunoglobulin-type lectins
S phase	Synthesis phase
TCR	T cell receptor
TFH cell	T follicular helper cell
TGF	Transforming growth factor
THC	Tetrahydrocannabinol
TH cell	T helper cell
TNF-α	Tumor necrosis factor, alpha
Treg	Regulatory T cell
UV	Ultraviolet
VAC	Vacuum-assisted closure therapy
VCAM-1	Vascular cell adhesion molecule-1
VEGF	Vascular endothelial growth factor
Zap-70	Zeta-chain-associated protein kinase 70

Summary

Autoimmunity is a pathological chronic inflammatory state that arises when the immune system mistakenly targets healthy cells and tissues in the human body. Clinically, there are more than 80 types of autoimmune diseases described, including well-known conditions like psoriasis, rheumatoid arthritis, type I diabetes, multiple sclerosis, and Crohn's disease. The incidence of autoimmune diseases in the human population is around 5−10% and continues to rise. Although current treatment options with immunosuppressant drugs like cyclosporine or biologic agents have shown excellent efficacy, they are often associated with unwanted side effects such as increased susceptibility to infections and malignancies, drug-drug interactions, cytokine release syndrome, hypersensitivity reactions, or anti-drug antibodies. Additionally, current drugs often lose efficacy over time, which leads to non-responsiveness, or to a lack of long-lasting relief of symptoms. Finally, the treatment of autoimmune diseases is very expensive and generates high treatment costs. Thus, there is a need for continued research into new therapies.

In the pathogenesis of chronic inflammation and autoimmune diseases enhanced activation and proliferation of T cells plays a crucial role. To address this issue, targeted therapies that specifically enhance inhibitory pathways in T cells are an attractive approach to treat human autoimmune diseases. Thus, the first aim of this study was to discover novel immune-modulating substances from plant extracts that specifically inhibit human T cell activation and proliferation. To achieve this goal, an in-house library of 600 extracts from plants endemic to Panama was screened for potential T cell inhibition. As one of the hits, an ethyl acetate extract from the aerial parts of *Hyptis brachiata* Briq. (Lamiaceae) was found to have strong inhibitory effects on T cell activation and proliferation. Seven aryltetralin lignans, five arylnaphthalene lignans, two flavonoids, three triterpenes, and cinnamyl cinnamate were isolated using an HPLC-based activity profiling approach. The aryltetralin lignans inhibited T cell proliferation in a concentration-dependent manner without inducing apoptosis. Additionally, the ethyl acetate extract and isolated triterpenes weakly lowered the secretion of inflammatory cytokines like IL-2 and TNF-α by activated T cells. The suppressive effects on activated T cells could be attributed to a synergistic interplay between the aryltetralin lignans and triterpenes. These findings suggest that the

extract from *Hyptis brachiata* could be further investigated as a potential treatment for T cell-mediated inflammatory and autoimmune diseases. The findings of this study have been published in *Biomedicine & Pharmacotherapy*, 160 in 2023.

Another aspect of this work aimed to explore the potential use of saffron corms (*Crocus sativus* L., Iridaceae) that arise as a waste product from saffron cultivation. A 70% ethanol extract of the corms and a sugar-depleted methanol fraction of the extract have been found to inhibit the TNF-α/IFN-γ-induced gene expression and secretion of the chemokines IL-8, MCP-1, and RANTES in human HaCaT keratinocytes. The effects were in part stronger than those of the positive control hydrocortisone. These chemokines are responsible for monocyte and T cell attraction, as well as for keratinocyte proliferation, making them critical in wound healing and in the development of inflammatory skin diseases like psoriasis and atopic dermatitis. A series of unusual bidesmosidic glycosides of echinocystic acid, which bear a 3,16-dihydroxy-10-oxo-hexadecanoic acid residue attached to the glycosidic moiety at C-28, were isolated using centrifugal partition chromatography and different C18 and HILIC HPLC stationary phases. Two previously reported compounds, azafrines 1 and 2, and eight new congeners named as azafrines 3−10 were identified. Saffron saponins significantly inhibited TNF-α/IFN-γ-induced secretion of RANTES in human HaCaT cells at 1 μM ($p < 0.001$). *In vitro* data suggest that saffron saponins possess anti-inflammatory properties by affecting the expression and secretion of chemotactic cytokines, and could therefore potentially be used as topical agents for treating inflammatory skin diseases. These results have been published in the *Journal of Natural Products*, 84, 2021.

The treatment of wounds is an increasingly important challenge, particularly in the case of chronic wounds associated with complex pathophysiology that may arise from autoimmune diseases such as psoriasis or type I diabetes. These wounds reduce the quality of life of many patients and current wound healing therapies are only partially effective. The lack of effective treatments for non-healing chronic wounds has become a growing clinical concern, and ongoing research is focused on obtaining more effective options to reduce treatment costs, provide long-term relief, and facilitate effective scar healing.

Historically, medicinal plants have been successfully used in wound treatment, and today they remain widely applied. Plant-based products have gained increasing interest as cost-efficient treatment options for wounds, as they represent mixtures of various phytochemicals that could act beneficially in a synergistic manner during the complex wound healing process. In this context, the last project described in this work investigated the wound healing properties of *Teucrium polium* subsp. *capitatum* (L.) Arcang (syn. *Teucrium capitatum* L.; Lamiaceae), a plant traditionally used in Algeria as a decoction or ointment to treat hypertension, diabetes, and wounds. Initially, a wound excision model in rabbits confirmed beneficial wound healing effects of a methanol extract from the aerial parts of *T. polium*. An ointment prepared from the *T. polium* extract demonstrated significant wound healing properties, superior to those of the reference drug Cicatryl-Bio containing allantoin as the active ingredient. A comprehensive analysis by HPLC-PDA-ESIMS led to the isolation and identification of 12 flavonoids and two phenylethanoid glycosides as the main constituents of the extract. Further investigation led to the isolation of six acetoxylated neo-clerodane diterpenes, including 20-acetylauropolin and 6-acetylteucjaponin A, along with four previously undescribed congeners. Some of the isolated diterpenes possess unusual structural features in the class of neo-clerodane diterpenes, such as a rare C-20 acetal function that forms an oxepane ring to C-7 of the *trans*-decalin core structure. The beneficial wound healing effect of *T. polium* is thought to be due to the combined effects of its polyphenolic constituents. Overall, the data support the use of *T. polium* as a wound healing agent in Algerian traditional medicine. The results have been published in the *South African Journal of Botany*, 137, 2021, and the *Journal of Molecular Structure*, 1284, 2023.

In conclusion, various approaches have been employed to investigate plant extracts and their secondary metabolites in the context of T cell-mediated autoimmunity, inflammatory skin diseases, such as psoriasis and atopic dermatitis, and wound healing. These diseases are challenging to treat due to their complex pathophysiology, involving numerous mechanisms and targets. However, plants, with their complex mixtures of phytochemical substances, can exert their effects on various targets, offering a potential advantage in treating multifactorial diseases. Complementary modes of action from structurally diverse

substance classes may act synergistically on different target cell types or proteins, contributing to improved clinical outcomes. Therefore, preparations containing various phytochemical substances from plant extracts may have the potential as alternative treatment options for these complex disorders. This work provides insights into how extracts and pure substances from *H. brachiata*, *C. sativus*, and *T. polium* may exert beneficial effects in the treatment of multifactorial conditions such as T cell-mediated autoimmunity, inflammatory skin diseases, and wound healing.

Zusammenfassung

Autoimmunität ist ein pathologisch chronischer Entzündungszustand, der entsteht, wenn das Immunsystem fälschlicherweise gesunde Zellen und Gewebe im menschlichen Körper angreift. Klinisch gesehen gibt es über 80 Arten von Autoimmunerkrankungen, darunter bekannte Erkrankungen wie Psoriasis, rheumatoider Arthritis, Typ I Diabetes, Multiple Sklerose und Morbus Crohn. Die Inzidenz von Autoimmunerkrankungen in der Bevölkerung beträgt etwa 5−10% und steigt weiter an. Obwohl aktuelle Behandlungsmöglichkeiten mit Immunsuppressiva wie Cyclosporin oder Biopharmazeutika eine hervorragende klinische Wirksamkeit zeigen, sind sie oft mit unerwünschten Nebenwirkungen wie z. B. erhöhte Anfälligkeit für Infektionen und Malignitäten, Arzneimittelwechselwirkungen, Zytokin-Freisetzungssyndrom, Überempflindlichkeitsreaktionen oder der Bildung von Antikörpern gegen verabreichte Medikamente verbunden. Darüber hinaus verlieren aktuelle Medikamente oft im Laufe der Zeit ihre Wirksamkeit, was zu Nichtansprechen oder zu einem Verlust an langanhaltender Symptomlinderung führt. Ausserdem ist die Behandlung von Autoimmunerkrankungen sehr kostspielig und generiert hohe Behandlungskosten. Daher besteht ein Bedarf an weiterführender Erforschung neuer Therapien.

In der Pathogenese von chronischen Entzündungen und Autoimmunerkrankungen spielt eine verstärkte Aktivierung und Proliferation von T-Zellen eine entscheidende Rolle. Um dieses Problem anzugehen, sind gezielte Therapien, die spezifisch hemmende Signalwege in T-Zellen verstärken, ein attraktiver Ansatz zur Behandlung menschlicher Autoimmunerkrankungen. Das erste Ziel dieser Arbeit war es, neuartige immunmodulatorische Substanzen aus Pflanzenextrakten zu finden, die spezifisch die Aktivierung und Proliferation von humanen T-Zellen hemmen. Um dieses Ziel zu erreichen, wurde eine interne Bibliothek bestehend aus 600 Extrakten von in Panama endemischen Pflanzen auf potenzielle T-Zell-Hemmung untersucht. Als einer der Treffer wurde ein Ethylacetat-Extrakt aus den oberirdischen Teilen von *Hyptis brachiata* Briq. (Lamiaceae) gefunden, der eine stark hemmende Wirkung auf die T-Zell Aktivierung und Proliferation aufwies. Durch einen HPLC-basierten Aktivitätsprofiling-Ansatz wurden sieben Aryltetralin-Lignane, fünf Arylnaphthalin-Lignane, zwei Flavonoide, drei

Triterpene und Cinnamyl-Cinnamat isoliert. Die Aryltetralin-Lignane hemmten die T-Zell Proliferation konzentrationsabhängig, ohne Apoptose auszulösen. Darüber hinaus senkten der Ethylacetat-Extrakt und isolierte Triterpene schwach die Sekretion von entzündlichen Zytokinen wie IL-2 und TNF-α durch aktivierte T-Zellen. Die hemmenden Effekte auf aktivierten T-Zellen konnten auf ein synergistisches Zusammenspiel zwischen den Aryltetralin-Lignanen und Triterpenen zugeschrieben werden. Diese Ergebnisse legen nahe, dass der Extrakt aus *Hyptis brachiata* als potenzielle Behandlungsmöglichkeit für T-Zell-vermittelte entzündliche Autoimmunerkrankungen weiter untersucht werden könnte. Die Ergebnisse dieser Studie wurden 2023 in *Biomedicine & Pharmacotherapy*, 160 veröffentlicht.

Ein weiterer Aspekt dieser Arbeit hatte zum Ziel, das Potenzial der Safranknollen (*Crocus sativus* L., Iridaceae) zu untersuchen, die als Abfallprodukt aus dem Safrananbau entstehen. Es wurde festgestellt, dass ein 70%-iger Ethanolextrakt der Knollen und eine zuckerfreie Methanolfraktion dieses Extraktes die TNF-α/IFN-γ-induzierte Genexpression und Sekretion der Chemokine IL-8, MCP-1 und RANTES in menschlichen HaCaT-Keratinozyten hemmten. Die Wirkungen waren teilweise stärker als die der Positivkontrolle Hydrocortison. Diese Chemokine sind für die Anlockung von Monozyten und T-Zellen, sowie für die Proliferation von Keratinozyten verantwortlich und spielen daher bei der Wundheilung, als auch bei der Entstehung entzündlicher Hauterkrankungen wie Psoriasis und Atopischer Dermatitis eine entscheidende Rolle. Mithilfe der Zentrifugalpartitions-Chromatographie und verschiedener stationären C18- und HILIC-HPLC-Phasen wurden eine Reihe ungewöhnlicher bidesmosidischer Glykoside der Echinocystinsäure isoliert, die an der glykosidischen Einheit an C-28 einen 3,16-Dihydroxy-10-oxo-Hexadecansäurerest tragen. Es wurden zwei bereits bekannte Verbindungen namens Azafrin 1 und 2, sowie acht neue Verbindungen, die als Azafrin 3−10 bezeichnet wurden, identifiziert. Safran Saponine hemmten die TNF-α/IFN-γ-induzierte Sekretion von RANTES in menschlichen HaCaT-Zellen signifikant bei 1 μM ($p < 0.001$). Die *in vitro* Daten deuten darauf hin, dass Safran Saponine entzündungshemmende Eigenschaften besitzen, indem sie die Expression und Sekretion chemotaktischer Zytokine beeinflussen. Daher könnten sie möglicherweise als topische

Behandlung für entzündliche Hauterkrankungen verwendet werden. Diese Ergebnisse wurden im *Journal of Natural Products*, 84, 2021 publiziert.

Die Behandlung von Wunden stellt eine zunehmend wichtige Herausforderung dar, insbesondere im Falle von chronischen Wunden, die mit komplexer Pathophysiologie assoziiert sind und durch Autoimmunerkrankungen wie Psoriasis oder Typ I Diabetes verursacht werden können. Diese Wunden beeinträchtigen die Lebensqualität vieler Patienten und die derzeitigen Therapien zur Wundheilung sind nur teilweise wirksam. Der Mangel an effektiven Behandlungen für nicht-heilende chronische Wunden ist zu einem wachsenden Anliegen in der Klinik geworden und laufende Forschungen zielen darauf ab, effektivere Behandlungsmöglichkeiten zu finden, um Behandlungskosten zu reduzieren, langfristige Linderung zu bieten und eine effektive Narbenheilung zu erleichtern.

Historisch betrachtet wurden viele Heilpflanzen erfolgreich zur Wundbehandlung eingesetzt und auch heute finden sie dafür noch breite Anwendung. Pflanzenbasierte Produkte haben zunehmendes Interesse als kosteneffiziente Alternative zur Wundbehandlung gewonnen, da sie Mischungen verschiedener Phytochemikalien darstellen, die während des komplexen Wundheilungsprozesses auf synergistische Weise vorteilhaft wirken können. In diesem Zusammenhang untersuchte das letzte Projekt, das in dieser Arbeit beschrieben wird, die Wundheilungseigenschaften von *Teucrium polium* subsp. *capitatum* (L.) Arcang (syn. *Teucrium capitatum* L.; Lamiaceae), einer Pflanze, die in Algerien traditionell als Aufguss oder Salbe zur Behandlung von Bluthochdruck, Diabetes und Wunden verwendet wird. Zunächst wurde ein Wundexzisionsmodell an Kaninchen durchgeführt, das vorteilhafte Wundheilungseffekte eines Methanolextraktes bestätigte, welches aus den oberirdischen Pflanzenteilen von *T. polium* hergestellt wurde. Eine aus dem *T. polium* Extrakt hergestellte Salbe zeigte Wundheilungseigenschaften, die denen des Referenzmedikaments Cicatryl-Bio, das Allantoin als Wirkstoff enthält, überlegen waren. Eine umfassende Analyse durch HPLC-PDA-ESIMS führte zur Isolierung und Identifizierung von 12 Flavonoiden und zwei Phenylethanoidglykosiden als Hauptbestandteile des Extrakts. Weitere Untersuchungen führten zur Isolierung von sechs acetoxylierten Neo-Clerodan Diterpenen, einschliesslich 20-Acetylauropolin und 6-

Acetylteucjaponin A, sowie vier zuvor unbeschriebenen Kongenern. Einige der isolierten Diterpene weisen ungewöhnliche strukturelle Merkmale in der Klasse der Neo-Clerodan Diterpene auf, wie beispielsweise eine seltene C-20 Acetal-Funktion, die einen Oxepan-Ring zum C-7 des *trans*-Decalin Grundgerüstes bildet. Die vorteilhafte Wundheilungswirkung von *T. polium* wird vermutlich auf die synergistischen Effekte seiner polyphenolischen Bestandteile zurückzuführen sein. Insgesamt unterstützen die Daten die Verwendung von *T. polium* als Wundheilmittel in der algerischen traditionellen Medizin. Die Ergebnisse wurden im *South African Journal of Botany*, 137, 2021, und im *Journal of Molecular Structure*, 1284, 2023, veröffentlicht.

Zusammenfassend wurden verschiedene Ansätze angewandt, um Pflanzenextrakte und ihre Sekundärenmetabolite im Kontext T-Zell-vermittelter Autoimmunität, in entzündlichen Hauterkrankungen wie Psoriasis und Atopischer Dermatitis, sowie der Wundheilung zu untersuchen. Diese Erkrankungen sind aufgrund ihrer komplexen Pathophysiologie, die zahlreiche Mechanismen und Zielstrukturen umfasst, schwierig zu behandeln. Pflanzen können jedoch aufgrund ihrer komplexen phytochemischen Zusammensetzung auf verschiedene Zielstrukturen einwirken und somit einen möglichen Vorteil bei der Behandlung multifaktorieller Erkrankungen bieten. Ergänzende Wirkeffekte durch strukturell unterschiedliche Substanzklassen können synergistisch auf verschiedene Zielzellen oder Proteine wirken, und so zu einer verbesserten klinischen Wirksamkeit beitragen. Daher könnten pflanzliche Zubereitungen, die aus verschiedenen Phytochemikalien bestehen, als alternative Behandlungsmethode für solch komplexe Erkrankungen in Frage kommen. Diese Arbeit gibt Einblicke darüber, wie Extrakte und isolierte Reinsubstanzen von *H. brachiata*, *C. sativus* und *T. polium* in der Behandlung multifaktorieller Erkrankungen wie T-Zell-vermittelter Autoimmunität, entzündlichen Hauterkrankungen und Wundheilung vorteilhafte Wirkungen entfalten können.

1. Introduction[1]

[1] Chapters 1.1−1.4 have been written based on following literature, which is not further cited in detail in the text:

- [1] Parham, P. *The Immune System.* (W.W. Norton & Company, New York, 2021).
- [2] V Kumar, V., Abbas, A. K. & Aster, J. C. *Robbins & Cotran Pathologic Basis of Disease.* (Elsevier, Philadelphia, 2020).
- [3] Murphy, K. & Weaver, C. *Janeway's Immunobiology.* (Garland Science, New York, 2016).
- [4] Abbas, A., Lichtmann, A. H. & Pillai, S. *Cellular and Molecular Immunology.* (Elsevier Saunders, Philadelphia, 2014).

1.1 The Immune System

Immunology is the study of the physiological mechanisms that mammals use to defend their bodies from invasion by other organisms. In response to an infection, the human body develops and produces tissues, cells, and molecules, which form together the immune system that serves as a defense against infectious agents. Thus, the immune system is crucial to protect the human body from invading pathogens and ensures human survival. In the absence of a working immune system, as it is the case in immune deficiencies, even minor infections take hold and can be fatal. The effective protection of the human body against invading microorganisms relies on the intricate and coordinated interaction among cells and tissues of the immune system.

On the other hand, the immune system can also contribute to tissue damage and the development of diseases. This can occur in conditions where immune responses inadvertently target harmless environmental substances, like in allergies, or when the immune system mistakenly attacks the body's own tissues and cells, as seen in autoimmune disorders. The classical definition of immunity is therefore protection against infectious pathogens, but in a broader sense it includes also host reactions against cancers (tumor immunity), tissue transplants (transplant rejection), and self-antigens (autoimmunity).

The mechanisms of immunity are broadly distinguished by innate immunity and adaptive immunity. Innate immunity, alternatively referred to as native immunity, is characterized by immediate immune responses triggered by an infection, serving as the body's initial defense mechanism. It involves the activation of cells and molecules that recognize pathogens and dead cells, leading to a rapid and protective response by the host. Adaptive immunity, also known as acquired immunity, includes mechanisms stimulated by invading microbes that are more slowly compared to those of innate immunity, but are more powerful in combating infections.

1.2 The Normal Immune Response

1.2.1 Innate Immunity and Inflammation

In confronting the microbial universe, the human body has developed several types of defense mechanisms to fight against pathogens. The first line of defense is mediated by innate immunity, which is always ready to provide immediate defense against microbes and to eliminate damaged cells within a few days. Innate immunity mainly comprises epithelial barriers that block the entry of microbes, a variety of plasma proteins, and different phagocytic and granulating cells.

The overall effect of innate immunity is to induce a state of inflammation in the infected tissue. Inflammation is a response of vascularized tissues that delivers circulating leukocytes and molecules of host defense from the circulation to the sites of infection and cell damage aiming to eliminate the offending agents. Thus, inflammation is a crucial response that plays a vital role in ensuring human survival. Without inflammation, infections would not be effectively controlled, wounds would fail to heal, and damaged tissues could persist as chronic and unhealed sores. An ancient concept of inflammation is *calor*, *rubor*, *tumor*, *dolor*, and *functio laesa*: The Latin words for heat, redness (erythema), swelling (edema), pain, and disturbed function. Protective inflammatory reactions to infections during innate immunity are accompanied by vascular dilation of nearby blood capillaries, which results in higher blood volumes with slowly moving red blood cells that cause the inflamed tissue to warm and redden. Vasodilation increases the permeability of endothelium which causes the leakage of blood plasma resulting in the accumulation of fluid in the tissue. This exudation process causes swelling of the tissue, resulting in edema, which increases the pressure on tissue and nerves that finally generates pain. Furthermore, when tissue is injured, leukocytes leave the bloodstream and migrate to the affected site, where they eliminate the harmful pathogen and release molecules such as cytokines and proteases that can induce inflammation and tissue damage. As a consequence, this process often leads to local pain and potential impairment of the normal tissue function. Normally, these harmful effects remain

localized and resolve within a few days as the inflammation diminishes, causing little or no lasting damage.

Nevertheless, there are numerous diseases in which the inflammatory response becomes misdirected, such as targeting the body's own tissues in autoimmune diseases, or inappropriately reacting to typically harmless environmental substances in allergies. In these cases, the typically beneficial inflammatory response becomes the primary contributor to the disease, and the resulting damage develops disease specific characteristic. Inflammatory reactions play a fundamental role in various chronic conditions like rheumatoid arthritis, psoriasis, and lung fibrosis, as well as in severe hypersensitivity reactions triggered by insect bites, foods, drugs, and toxins, which can pose life-threatening risks.

1.2.2 Mechanisms of Innate Immunity

The first type of protection of the innate immunity is the so-called immediate defense, which comprises physical and chemical barriers like the skin and mucosal epithelia with their commensal microorganisms. These barriers prevent most pathogens from gaining access to the cells and tissues and directly face them with soluble antimicrobial peptides, called defensins, that effectively destroy pathogens. On the other hand, actions such as touching, rubbing, and scratching the eyes, nose, and mouth can facilitate the entry of pathogens through mucosal surfaces. Similarly, inhaling polluted air, consuming contaminated food, and being in close proximity to infected individuals can also serve as pathways for pathogens to enter the body. Additionally, wounds create direct openings in the skin that can allow pathogens to penetrate.

If pathogens can invade the soft tissues further defense mechanisms of the innate immunity get activated that are summarized as the induced innate immune response. Induced innate immune response comprises a series of sequential steps to develop a state inflammation that is needed to get rid of the pathogen. These steps include pathogen recognition, recruitment of effector immune cells, destruction of the pathogen, and finally repair of damaged tissues to restore normal

tissue function. All these processes are regulated by a variety of soluble plasma proteins and different immune cells.

The initial step of the induced innate immune response is recognition, during which plasma proteins such as mannose-binding lectin, C-reactive protein, and the various proteins of the complement system function as opsonins. These opsonins attach to the surface structures of pathogens to aid in their identification. Opsonization marks invaders for effector immune cells as agents to kill and attracts further effector cells into the invaded tissue. The effector cells of the immune system are the white blood cells, called leukocytes. Beside plasma proteins also leukocytes of the innate immunity are involved in pathogen recognition. These cells include mainly tissue-resident sentinel cells like macrophages that are equipped with receptors that recognize microbial products and substances released from damaged cells. After sensing foreign substances, they produce and emit mediators of inflammation, which then trigger subsequent steps of innate immunity and inflammation.

Macrophages are long-lived leukocytes that are resident in every tissue and are among the first cells that respond to any pathogen that invades the human body. Tissue-resident macrophages include the Langerhans cells in the skin, the Kupffer cells in the liver, the microglia in the brain, the histiocytes in spleen and lymph nodes, or the alveolar macrophages in the lungs. In infected tissues the resident macrophages orchestrate the induced innate immune response to infection by directly killing pathogens by phagocytosis and by recruiting other immune cells through secretion of inflammatory cytokines. Macrophages and other leukocytes of the innate immune system possess a wide range of cell surface, endosomal, and cytoplasmic receptors. These receptors recognize specific chemical characteristics found in macromolecules such as carbohydrates, lipids, peptides, proteins, and nucleic acids derived from pathogens, as well as from damaged or deceased human cells. Since these receptors recognize structural features that are common to many different types of pathogens, they are called pattern recognition receptors (PRRs) including Toll-like, NOD-like, or mannose receptors.

Once a pathogenic agent has been captured by such surface receptors of a resident macrophage, the next step of the induced innate immunity is initiated, namely the step of pathogen removal. The captured pathogen is internalized and killed by an acidic environment and enzymatic degradation, a process called phagocytosis. Phagocytosis by tissue-resident macrophages stops most incursions at an early stage before the aspiring pathogen can proliferate and disrupt tissue. If the tissue-resident macrophages fail to eliminate the invading microorganism, recruitment steps are initiated by emission of alarm signals that attract other effector cells of the immune system to the infected tissue helping to eliminate the pathogen. These alarm signals are messenger proteins called cytokines. In this case, the cytokines are called inflammatory or pro-inflammatory cytokines, because they will induce a state of inflammation throughout the infected tissue.

Binding of pathogens by PRRs stimulates resident macrophages to synthesize and secrete inflammatory cytokines that alter the permeability of local blood vessels and actively recruit other leukocytes of innate immunity from the blood circulation to the infected tissue including neutrophils, monocytes, and natural killer (NK) cells. One of these cytokines is interleukin-1β (IL-1β), known as the master mediator of inflammation, since it activates different cells throughout the infected tissue, attracts leukocytes from blood circulation, and induces fever. The immediate effect of IL-1β is to activate further tissue-resident macrophages, which improves the speed and efficiency of phagocytosis, and hence the elimination of the pathogen. The second effect is triggering macrophages to secrete additional inflammatory cytokines including CC-chemokine ligand 2 (CCL2), CXC-motif chemokine ligand 8 (CXCL8), tumor necrosis factor-alpha (TNF-α), IL-6, and IL-12 that recruit further effector leukocytes and plasma proteins to the infected tissue, where they work together to create a state of inflammation at the site of infection (Fig. 1).

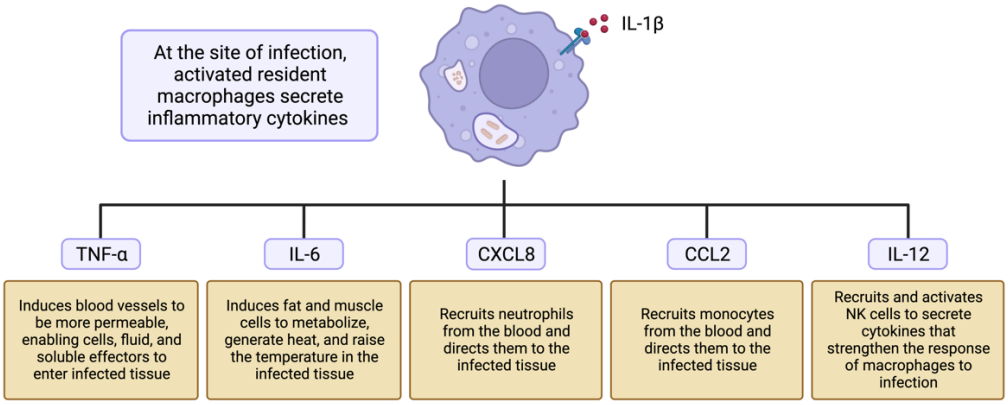

Fig. 1. Tissue resident macrophages respond to the presence of infection and IL-1β by generating and releasing inflammatory cytokines. Among these cytokines, TNF-α, IL-6, CXCL8, CCL2, and IL-12 play essential roles and are produced by macrophages following the release of IL-1β. The cytokines recruit effector cells and plasma proteins to the infected tissue, where they contribute to the development of a state of inflammation. Adapted from[1]; Created with BioRender.com.

Under healthy conditions, leukocytes normally cannot leave the blood circulation and enter the tissue. However, the presence of IL-1β, followed by TNF-α, induces local blood vessel to dilate and become more permeable which decreases the blood flow, allowing fluid and cells to leave the blood and enter the tissue. Furthermore, TNF-α induces endothelial cells to express surface adhesion molecules, that support leukocytes to cross the endothelium to reach the infected tissue. CCL2 and CXCL8 (also known as IL-8) are chemoattractant cytokines, called chemokines, which attract effector cells by chemotaxis from the blood circulation into the infected tissue. Guided by the chemokine CXCL8 neutrophils get recruited from the blood to sites of infection.

Neutrophils are the first population of effector cells recruited to an infected tissue (during the first 6 to 24 hours) where they become the dominant leukocyte. The arrival of neutrophils is the start of the inflammatory response. Similar to tissue-resident macrophages, neutrophils possess various PRRs which detect extracellular microbial components. Upon binding to these components, the neutrophils proceed to phagocytose and destroy the microorganisms. Neutrophils are short-lived leukocytes and die directly after phagocytosing microorganisms by apoptosis,

thereby forming the creamy pus at infected wounds and other sites of infection. The remains of dead neutrophils are removed by phagocytosis through macrophages.

After 24 to 48 hours neutrophils are replaced by monocytes. The chemokine CCL2, also known as monocyte chemotactic protein 1 (MCP-1), recruits monocytes from the blood to the site of infection. Upon entering the inflamed tissue, monocytes promptly undergo proliferation to increase their population and differentiate into macrophages. These newly formed macrophages exhibit functions and phenotype that are nearly identical to those of tissue-resident macrophages, thereby providing additional support in the phagocytosis of pathogens. Beside the neutrophils, the macrophages are the dominant cells in the development of inflammation. Phagocytic cells that engulf and kill microorganisms are the principal means by which the immune system destroys invading pathogens.

Further effector cells of the innate immune system are granulocytes like eosinophils, basophils, and mast cells. Granulocytes contain cytoplasmic granules filled with reactive biochemical molecules that kill microorganisms and enhance inflammation. They play a significant role in allergic reactions and in protecting the body against parasites like helminth worms. To accomplish this, they release granules that contain various chemical mediators capable to induce inflammation and spasms of smooth muscles, which can effectively expel parasites from the respiratory and gastrointestinal tract. Degranulation of granulocytes releases histamine, prostaglandins, and other vasoactive substances that cause dilation of blood vessels, and increase vascular permeability, which facilitates the exit of plasma proteins and immune cells from the blood and their passage to sites of infection in the tissues.

During the induced innate immune response, beside leukocytes also lymphocytes are involved, so-called innate lymphoid cells (ILCs). One type of ILCs are the helper innate lymphoid cells which are tissue-resident lymphocytes. They can be activated directly by a pathogen or by cytokines. Upon activation, they release additional inflammatory cytokines, which aid in the activation of other innate immune cells,

like macrophages and granulocytes, during the initial phases of an innate immune response. The other type of an ILC is the cytotoxic NK cell. Naïve NK cells circulate in the blood and are recruited by the inflammatory cytokines CXCL8 and IL-12 secreted by tissue-resident macrophages. Tissue cells that are infected with intracellular pathogens, such as viruses, bacteria, or protozoan parasites, start expressing and secreting the type I interferons, interferon alpha (IFN-α) and IFN-β. These cytokines induce naïve NK cells to differentiate and proliferate into cytotoxic effector NK cells that kill infected cells aiming to prevent the spread of the infection. The main weapons of NK cells are cytoplasmic granules, which are loaded with toxins and degradative enzymes. NK cells deliver the lethal contents of its granules directly into the cytoplasm of infected target cells, which induces their apoptosis. Finally, macrophages dispose what remains of the killed cells. If naïve NK cells get activated by IL-2, IL-12, and especially by IL-15 secreted by macrophages, in the concomitant absence of the type I interferons, they proliferate and differentiate into cytokine-producing effector NK cells that are not cytotoxic, and secrete the type II interferon IFN-γ instead. IFN-γ is a potent inflammatory cytokine and the principal cytokine produced by NK cells. The increasing presence of the cytokines IL-15 and IFN-γ produces a heightened state of inflammation. Especially, IFN-γ activates further macrophages to secrete more cytokines and improves the efficiency of phagocytosis, aimed at increased elimination of extracellular virus particles and virus-infected cells that have been killed by NK cells. In this way, NK cells provide defense against intracellular and extracellular pathogens.

Dendritic cells (DCs) are specialized tissue-resident leukocytes that just sample the environment for infectious particles and form together with the tissue-resident macrophages the first line of induced innate immunity. Unlike macrophages, DCs are not key participants in the phagocytic destruction of microbes and in the creation of inflammation. Instead their critical function is to capture particles of pathogens, degrade and process them intracellularly, and take them to lymphoid tissues. There, DCs finally display processed pathogen-derived protein fragments

as antigens for recognition by T cells to initiate an adaptive immune response (see chapter 1.2.4). If the DC becomes infected by intracellular pathogens, it changes its protein expression and starts secreting IL-15, which is monitored by naïve NK cells. This results in activation of naïve NK cells resulting in increased proliferation and differentiation into cytotoxic effector NK cells that will kill pathogen-infected cells, including the DCs that successfully induced NK cell differentiation. But if the NK cell response is inadequate and fails to contain the infection, the NK cells secrete cytokines that induce the DCs to differentiate into a motile form that leaves the infected tissue and travels in the draining lymph to a secondary lymphoid tissue where they present the pathogen's antigen to the cells of the adaptive immune system. This event marks the failure of the innate immune response to clear the infection and the initiation of the adaptive immune response. Within the infected tissue, interactions between NK cells and DCs determine whether the innate immune response is sufficient to clear the infection or if an adaptive immune response should be made. Therefore, DCs are the component of the immune system that connects the innate immune response with the adaptive immunity.

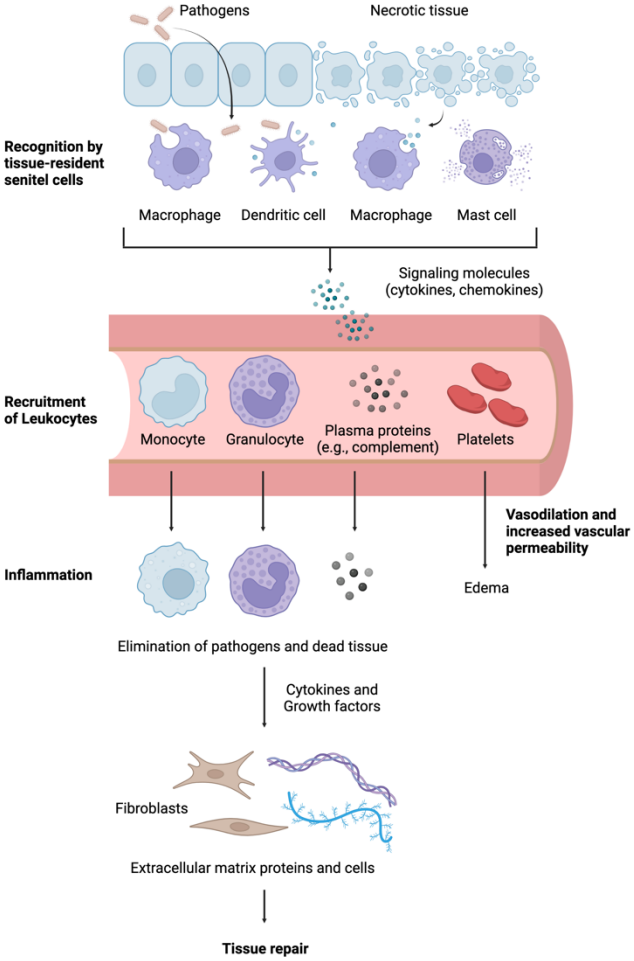

Fig. 2. This illustration summarizes the sequences of the inflammatory reaction during the innate immune response. Sentinel cells such as macrophages and dendritic cells recognize pathogens and damaged cells, and secrete inflammatory cytokines that trigger the vascular and cellular processes of inflammation. Adapted from[2]; Created with BioRender.com.

1.2.3 Adaptive Immunity

Innate immunity usually terminates most infections within 4 days and keeps most humans healthy. However, some infections can evade the mechanisms of innate immunity. If the innate immune response is unable to effectively eliminate the infection, it aims to limit the spread of the infection and recruits assistance from lymphocytes, the white blood cells belonging to the adaptive immune system. The involvement of lymphocytes helps to enhance the potency and specificity of the immune response. This powerful contribution of lymphocytes is called the adaptive immune response, which is specific to the disease-causing pathogen, long-lasting, and complements the mechanisms of innate immunity. Adaptive immune responses progress through distinct stages, beginning with the recognition of antigens. This is followed by the activation of antigem-specific lymphocytes, which undergo proliferation and differentiation into effector and memory cells. These effector cells work together to eliminate the specific antigen, which finally leads to a gradual decline of the immune response. Memory cells remain as long-lived cells and provide immune protection for the future.

The innate immunity uses the PRR cell surface receptors that are structurally of many different types, which recognize similar features shared by different groups of pathogens, but none of them is specific for a particular pathogen. In contrast, the lymphocytes of the adaptive immunity recognize pathogens specifically using only one type of cell surface receptor, but this one is made in billions of different versions. Billions of different receptor variants enable the immune system to recognize and eliminate all possible types of pathogens, and the high receptor specificity for a particular pathogen makes sure that only this specific pathogen will be killed, and that no immunity is provided against an unrelated pathogen. During an adaptive immune response only lymphocytes bearing receptors that recognize the specific pathogen are recruited to the site of infection. They then proliferate and differentiate to form an army of pathogen specific effector cells. Lymphocytes recognizing the same specific antigen are referred to as clones. This means that all the members of a single clone express identical surface receptors, which differ from

the receptors of other clone populations. The selective activation of a specific clone, and its subsequent proliferation are known as clonal selection and expansion, respectively. Consequently, each clone of a lymphocyte expresses a unique form of antigen receptor, but the clones themselves exhibit distinct specificities for antigens.

To expand a few selected pathogen-specific lymphocytes into an army of effector cells takes time, and therefore the benefit of the adaptive immune response is noticed only 7–10 days after the onset of infection, while the innate immune response starts immediately within hours. Although slower, the adaptive immune response terminates almost all infections that outrun innate immunity. After successful elimination of a pathogen by the adaptive immune response, some of the contributing lymphocytes persist in the body and are selected to provide long-term immunological memory of the pathogen. These so-called memory cells enable rapid recognition of the same pathogen in a following infection and elicit an adaptive immune response, known as the secondary immune response, directly from the very beginning of the infection. Therefore, this secondary immune response is faster, stronger, and more effective than the primary response. Throughout the secondary response, innate immunity works in partnership with the adaptive immunity, which decreases both the time taken to clear the infection and the collateral damage to tissues caused by inflammation. Due to the high effectivity of the secondary immune response, the disease caused by a second infection is shorter and less severe than that arising from the first, and is often terminated before any significant symptoms of disease may occur. However, in some cases, the adaptive immunity fails to suppress the pathogen and the infected individual either dies of the acute infection (as it may occur for many infections with Ebola virus) or develops a chronic infection leading to premature death (as it was the case for the human immunodeficiency virus (HIV) in the era before effective drug therapy was available).

Lymphocytes are distinguished by their cell surface receptors into B lymphocytes and T lymphocytes, commonly referred to as B cells and T cells. These two cell types are responsible for two types of adaptive immunity, humoral and cell-

mediated adaptive immunity. The humoral adaptive immunity protects against extracellular pathogens and is mediated by B cells expressing a pathogen specific B cell receptor. Activated B cells, called plasma cells, secrete a soluble form of the B cell receptor which is called antibody or immunoglobulin (Ig). Secreted antibodies neutralize extracellular microbes and mark them for destruction by phagocytic cells, or activate the complement system to initiate the innate immune response and provoke inflammation.

The cell-mediated or cellular adaptive immunity is responsible for defense against intracellular pathogens and is mediated by T cells. T cells have many functions ranging from activation of macrophages and supporting inflammation to directly killing of infected cells, and suppression or termination of the immune response. T cells are characterized by expressing the so-called T cell receptor (TCR), which differs from the B cell receptor, since TCRs are only expressed as cell surface receptors and not as soluble effector molecules. During adaptive immunity B and T cell receptors recognize and bind macromolecules, virus particles, or cell-surface components, which are referred to as their antigens. Therefore, B and T cell receptors are also called antigen receptors.

1.2.4 Mechanisms of Cell-mediated Adaptive Immunity

As many cells of the immune system also lymphocytes are not fixed to certain tissues, instead they constantly circulate among lymphoid and other tissues via the blood and the lymphatic system. This promotes immune surveillance throughout the human body and allows lymphocytes to home to any site of infection. Only a small fraction of lymphocytes is in the peripheral blood circulation. The great majority is present in specialized lymphoid tissues. Primary lymphoid tissues are the bone marrow and the thymus, and are the locations where lymphocytes develop and mature to the stage at which they become competent to recognize and respond to pathogens. After small lymphocytes have developed in primary lymphoid tissues, they enter the bloodstream as naïve lymphocytes, which describes lymphocytes that have not yet encountered their specific antigens, and therefore are inactive

(immunologically inexperienced). If they reach the blood capillaries in secondary lymphoid tissue like lymph nodes or spleen, they can leave the blood and enter these tissues. After a while they leave the secondary lymphoid tissues again and move back to the blood circulation. This movement between blood and lymphoid tissues is called lymphocyte recirculation. Secondary lymphoid tissues are the sites where naïve lymphocytes encounter pathogen-derived antigens and are activated to become effector cells that attack and eliminate the microbial invader. Thus, secondary lymphoid organs are the places where antigens are concentrated and brought together with B and T cells to initiate adaptive immune responses.

T cells recognize and bind antigens through the highly variable and antigen-specific TCR. The TCR is a membrane-bound glycoprotein that consists of two polypeptide chains, the α and the β chain. The αβ TCR recognizes only small pathogen-derived peptide antigens that are bound to a glycoprotein, called major histocompatibility complex (MHC) molecule, presented on the cell surfaces of antigen-presenting cells (APCs). Therefore, the ligand for a TCR is not simply a peptide-antigen, it is the combination of a peptide and an MHC molecule, which is called the peptide-MHC complex. Thus, the function of MHC molecules is to display peptide fragments of protein antigens for recognition by antigen specific T cells (Fig. 3).

At the site of infection, resident DCs capture pathogens and their protein antigens, and bring them via the lymph to secondary lymphoid tissues. During this transport the DCs mature, process the carried antigens, and display them in the secondary lymphoid tissues as antigenic peptide-MHC complexes to naïve T cells. Presented antigens are short peptide fragments, typically consisting of 8 to 25 amino acids, that are generated through a process called antigen-processing. During antigen processing, phagocytosed pathogen-derived proteins are degraded into small antigenic peptides, which are intracellularly loaded onto MHC glycoproteins to form the peptide-MHC complex. The antigenic peptide-MHC complexes are transported to the cell surface where they are presented to TCRs of circulating naïve T cells, which is referred to as antigen-presentation (Fig. 3, Fig. 6).

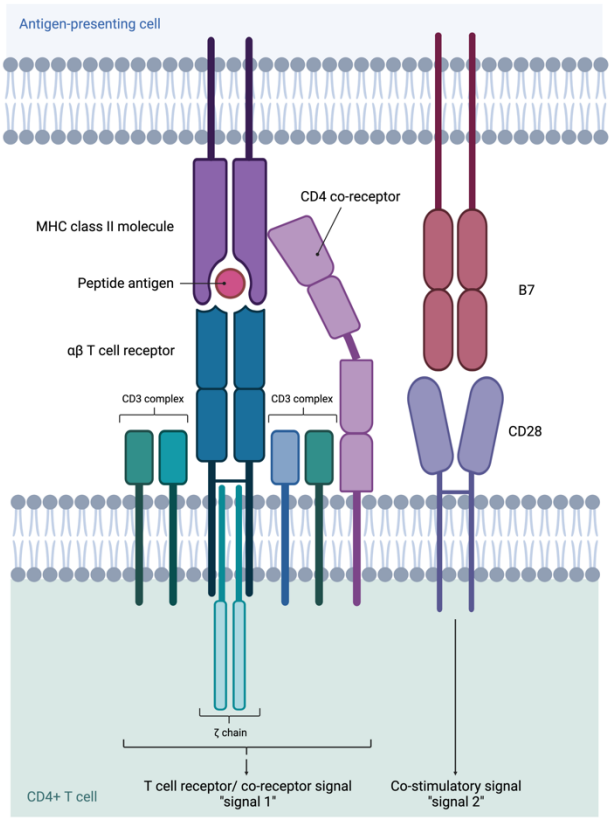

Fig. 3. Illustration of the TCR complex and the CD28-B7 co-stimulatory signal complex. The TCR heterodimer, consisting of an α and β chain, recognizes the antigen, which is bound as a peptide-MHC complex expressed on an antigen-presenting cell. The TCR is linked to the CD3 complex and the ζ chains, which together form the TCR complex. Both the TCR complex and the CD4 co-receptor are needed to elicit the antigen specific signal ("signal 1") for T cell activation. The co-stimulatory signal ("signal 2") is delivered when the CD28 co-stimulatory receptor of the T cell binds to the B7 co-stimulator on the antigen-presenting cell. Activation and clonal expansion of the antigen-specific naïve T cell occurs only if the antigen-specific and the co-stimulatory signals are delivered together. This applies for both naïve CD4+ and naïve CD8+ T cells. Adapted from[1,2]; Created with BioRender.com.

Naïve T cells continuously enter the lymphoid tissues through circulation where they undergo screening by antigen-presenting DCs. This screening process persists until the pathogen-specific naïve T cell is identified and binds to the peptide-MHC complex. Each naïve T cell that conjugates with a DC stays in the lymphoid tissue where it gets activated to proliferate and differentiate to form a clone of several hundreds of effector and memory T cells that will be recruited for the adaptive immune response against the invading pathogen. This process of T cell activation is the first stage of the primary adaptive immune response and takes around one week. This accounts for the delay between the onset of infection and the appearance of a primary adaptive immune response. Effector T cells are diverse in function and phenotype. Some effector T cells leave the secondary lymphoid tissues and migrate to sites of infection where they work together with the cells of innate immunity to terminate local infections. Other effector T cells remain in the secondary lymphoid tissues where they help antigen-activated B cells to become antibody-producing plasma cells (Fig. 6).

During an adaptive immune response, antigen-activated T cells demonstrate diverse functions that are determined by several factors. These factors include the surface co-receptor glycoproteins known as cluster of differentiation (CD) ligands, the cytokines to which they respond, the cytokines they release, and the specific type of target cell with which they interact. The main subdivision of effector T cells is defined by the cell-surface expression of either CD4 or CD8, which are described as T cell co-receptors. Co-receptors cooperate with TCRs in the recognition of peptide-MHC complexes and are necessary to initiate signals needed for T cell activation (Fig. 3). Naïve T cells expressing CD8 recognize peptides that are presented as so-called peptide-MHC class I complexes. After binding to peptide-MHC class I complexes they get activated to become cytotoxic CD8+ effector T cells. MHC class I molecules are expressed on all nucleated cells and display peptides that are derived from cytoplasmic proteins of intracellular pathogens. Thus, cytotoxic CD8+ T cells counter intracellular infections by killing the infected cells through induction of apoptosis. Naïve T cells expressing CD4 bind to peptides

displayed as peptide-MHC class II complexes and become activated to differentiate into helper CD4+ effector T cells. MHC class II molecules present the antigens of extracellular pathogens like bacteria, and their expression is restricted to professional APCs like macrophages, DCs, and B cells. The main function of helper CD4+ T cells is to secrete cytokines that enable other cell types, such as B cells and phagocytes, to become fully activated effector cells that respond to infection. CD4+ T cells stimulate B cells to differentiate into plasma cells and to produce pathogen-specific antibodies. In addition, they stimulate macrophages to secrete cytokines that enhance the ability of other innate immune cells to phagocytose extracellular pathogens. Furthermore, CD4+ T cells support macrophages to secrete inflammatory cytokines and chemokines that facilitate and maintain the adaptive immune response. Finally, they also trigger mechanisms of tissue repair.

To initiate the activation of naïve T cells, both the binding of the αβ TCR to the peptide-MHC complex and the interaction between the co-receptors CD4 or CD8, are necessary to generate an intracellular signaling cascade. The binding of the αβ TCR and the co-recpeptors to the peptide-MHC complex delivers a signal to the CD3 complex, which is a polypeptidic protein complex directly linked to the αβ TCR. The CD3 complex transmits this signal and initiates an intracellular signaling cascade that leads to the activation of the naïve T cell ("signal 1"). An additional signal needed for T cell activation is the co-stimulatory signal delivered by the engagement of the co-stimulatory receptor CD28 on the T cell surface and the co-stimulator B7 (also known as CD80 or CD86), a membrane protein expressed on activated antigen-presenting DCs ("signal 2"). Proliferation and differentiation of the antigen-specific naïve T cell occurs only if the intracellular signals of the αβ TCR, co-receptor, and co-stimulatory receptor are generated simultaneously (Fig. 3).

Interactions of the MHC ligand with the αβ TCR and the co-receptor, as well as of the co-stimulatory receptor with the co-stimulator, activate within the naïve T cell an intracellular cascade of different cytoplasmic protein kinases, which finally triggers three different signaling pathways that drive T cell proliferation and

differentiation into the different effector T cells. One pathway leads to the activation of nuclear factor of activated T cells (NFAT) and involves inositol trisphosphate (IP_3) as second messenger. The second pathway leads to the activation of protein kinase C theta (PKC-θ), which induces the transcription of transcription factor nuclear factor kappa-light-chain-enhancer of activated B cells (NFκB). The third pathway initiated leads to the activation of transcription factor activator protein 1 (AP-1). The combined effect of NFAT, NFκB, and AP-1 is to initiate the transcription of genes that direct T cell proliferation and differentiation, as well as the acquisition of effector functions like the expression and secretion of IL-2, and the expression of the high affinity IL-2 receptor. The pro-inflammatory cytokine IL-2 plays a crucial role in promoting the proliferation of activated naïve T cells in an autocrine manner ("signal 3"). It also facilitates the differentiation of these cells into effector T cells, resulting in an expansion of antigen-specific effector T cell populations. Intracellular signaling pathways are summarized in Fig. 4.

How proliferating T cells differentiate into the different subsets of effector T cells is influenced by the nature of the pathogen, the anatomical site of infection, and the type of innate immune response stimulated by the pathogen. These factors influence the cytokine environment within the secondary lymphoid tissue and drive the production of effector T cells that are best suited for controlling the infection and eliminating the pathogen. The six types of effector T cells are the cytotoxic CD8+ T cells, and the helper CD4+ T cell subsets including the T helper cell 1 (TH1), TH2, TH17, T follicular helper cell (TFH), and the regulatory T cell (Treg), which all have complementary roles during the immune response (Fig. 5). To get activated by APCs in infected tissues, fully differentiated effector T cells only need the engagement of the αβ TCR with the peptide-MHC complex, and the interaction with the co-receptor. Compared to the activation of naïve T cells in the secondary lymphoid tissues, the co-stimulatory signal of CD28 and B7 is not required anymore for the activation of T cell effector functions in the infected tissues.

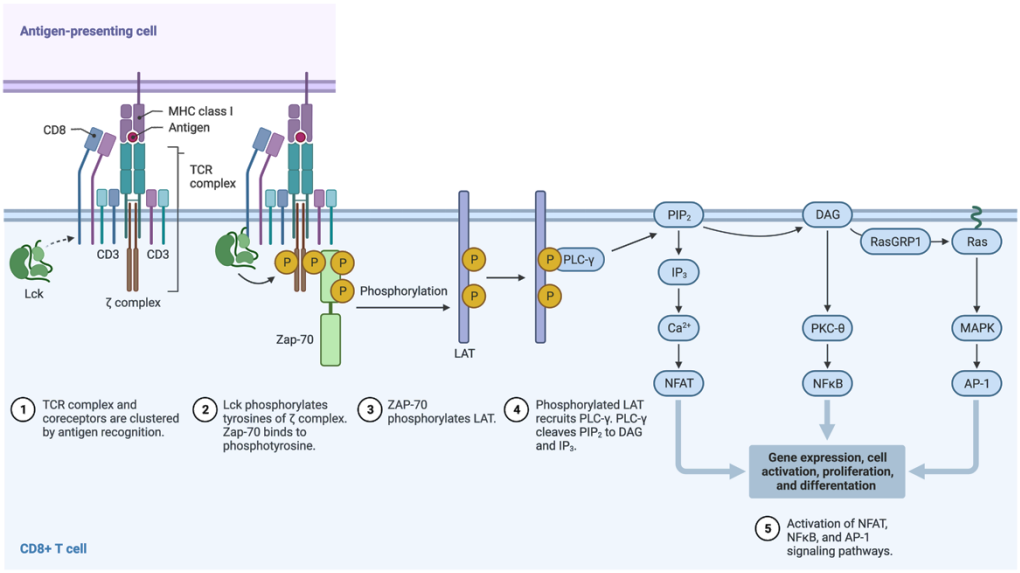

Fig. 4. Summary of the intracellular signaling pathways initiated by the interaction of the αβ TCR complex and the CD8+ co-receptor with the APC (interaction with the CD28 co-stimulatory receptor is not shown). Similar pathways operate in CD4+ T cells, because CD4, like CD8, interacts with Lck. Interaction of the naïve T cell with the specific antigen, presented by an APC, sets different pathways of signal transduction in motion that lead to its clonal expansion and differentiation. First, Lck gets activated, which phosphorylates the ζ chains and the kinase Zap-70. Activated Zap-70 initiates a series of phosphorylations that finally lead to the activation of PLC-γ. PLC-γ cleaves PIP_2 into DAG and IP_3. DAG initiates two pathways: On one hand, DAG activates PKC-θ, which itself activates NFκB. On the other hand DAG activates RasGRP1, which in turn initiates a Ras-induced MAPK cascade leading to the activation of AP-1. IP_3 increases the intracellular Ca^{2+} concentration, which finally activates calcineurin phosphatase. Calcineurin activates NFAT. NFAT, NFκB, and AP-1 change the pattern of gene expression, resulting in T cell activation, proliferation, and differentiation into effector T cells. LcK, Lymphocyte-specific protein tyrosine kinase; Zap-70, Zeta-chain-associated protein kinase 70; LAT, Linker for activation of T cells; PLC-γ, Phospholipase C-gamma; PIP_2, Phosphatidylinositol 4,5-bisphosphate; DAG, Diacylglycerol; IP_3, Inositol trisphosphate; RasGRP1, Ras guanyl-releasing protein 1; MAPK, Mitogen-activated protein kinase. Adapted from[1,3] and from "TCR Signaling Network" & "TCR Downstream Signaling" by BioRender.com (2023). Retrieved from https://app.biorender.com/biorender-templates.

After binding, the effector T cell delivers effector molecules that induce changes in the target cell. Cytotoxins delivered by cytotoxic CD8+ T cells kill the target cell directly by inducing its apoptosis, whereas helper CD4+ T cells deliver cytokines that help the target cell to either increase or decrease its immune response against the pathogen. The differentiation of activated naïve CD4+ T cells into various subsets of CD4+ T cells is influenced by the cytokine environment. These subsets are characterized by their unique surface receptors and the specific cytokines they produce, enabling them to carry out diverse immune effector functions. Compared to cytotoxic CD8+ T cells, helper CD4+ T cells only interact with other immune cells to support them fulfilling their specific effector functions aiming to eliminate the pathogen. After differentiation cytotoxic CD8+ T cells and helper CD4+ TH1, TH2, and TH17 cells leave the secondary lymphoid tissues, and travel to the infected tissue where they start to interact with the target cells. Some activated T cells remain in the lymphoid organs and either help B cells to produce antibodies or differentiate into long-lived memory T cells (Fig. 5, Fig. 6).

During the innate immune response, DCs and macrophages secrete IL-12, and NK cells secrete IFN-γ, two cytokines that stimulate the differentiation of naïve CD4+ T cells towards TH1 cells. TH1 cells are producers of cytokines IFN-γ and IL-2, which increase in secondary lymphoid tissue the production of further TH1 cells in an autocrine manner. Both, IFN-γ and IL-2 are pro-inflammatory cytokines, that are involved in the activation of macrophages to make them more proficient in the uptake and killing of pathogens.

Basophils, eosinophils, and mast cells secrete IL-4 during the innate immune defense against helminthic parasites, which induces naïve helper CD4+ T cells to differentiate into TH2 cells. Upon activation by IL-4, TH2 cells subsequently produce further IL-4 in an autocrine manner. Once TH2 cells start to secrete IL-4, IL-5, and transforming growth factor beta (TGF-β), the local environment becomes one that promotes anti-inflammatory mechanisms which decreases the production of TH1 cells, and therefore reduces their pro-inflammatory effects. Toxic microbicidal substances produced by TH1-activated macrophages can harm human

cells and tissues, which inevitably suffer collateral damage from the macrophage response to the pathogen. Regulatory mechanisms that suppress macrophage activation reduce this damage. These mechanisms are mainly regulated by IL-4 that promotes repair and recovery of damaged tissues by inducing the alternative pathway of macrophage activation, which causes macrophages to differentiate into so-called M2 macrophages (see chapter 1.3). Furthermore, IL-4, stimulates B cells to differentiate into IgE-secreting plasma cells, while IL-5 stimulates the production and activation of eosinophils. Eosinophils and mast cells bind to IgE-coated microbes such as helminthic parasites, and function together to eliminate them.

The cytokines IL1-β, TGF-β, IL-6, IL-21, and IL-23, secreted by macrophages and DCs, lead to the development and proliferation of naïve CD4+ T cells into TH17 cells, which are characterized by the secretion of IL-17 and IL-22. IL-17 activates fibroblasts, epithelial cells, and endothelial cells to secrete cytokines that recruit neutrophils to infected tissues, aiming to control fungal and extracellular bacterial infections. Additionally, IL-17 induces the secretion of colony-stimulating factors (CSFs), such as granulocyte-macrophage colony-stimulating factor (GM-CSF) or granulocyte-colony stimulating factor (G-CSF), which stimulate the growth, production, and recruitment of granulocytes, macrophages, and neutrophils. The CSFs stimulate leukocyte recruitment during immune and inflammatory responses to increase the amount of leukocytes, and to replace leukocytes that die during such responses at the site of infection. All these processes lead to inflammatory effects in infected tissues. Therefore, TH17 cells are the most inflammatory type of T helper cells, and are involved in the manifestation of many inflammatory autoimmune diseases.

Under the influence of IL-6 and IL-21 naïve CD4+ T cells develop into TFH cells. In contrast to other effector T cell types, TFH cells are the only effector CD4+ T cell subtype that resides in secondary lymphoid tissues where they activate naïve pathogen-specific B cells to become antibody-producing plasma cells. After binding to naïve B cells, the TFH cell gets activated to secrete IL-4, IL-5, and IL-21, which support naïve B cells to proliferate, differentiate, and mature into plasma cells.

Therefore, TFH cells are responsible for initiating the antibody response against any infecting pathogen.

In the presence of TGF-β and in the absence of inflammatory cytokines, such as IL-6, naïve CD4+ T cells differentiate into Treg cells. If IL-6 or IL-21 is present, naïve T cells develop into TH17 cells. Treg cells are not directly involved in the primary immune response against infections, but they help to control the response and regulate it down once the pathogen is defeated. They facilitate repair mechanisms in tissues that have been damaged by the immune response, and interact with other effector T cells with the aim to decrease pro-inflammatory effects. Treg cells produce immunosuppressive and anti-inflammatory cytokines like TGF-β and IL-10, which downregulate the immune response. In the absence of Treg cells immune responses targeting self-antigens can occur, which potentially result in attacks against various healthy tissues within the body, such as the gut, skin, and endocrine glands. Therefore, a reduced activity of Treg cells is assumed to be involved in the development autoimmune diseases. Fig. 5 summarizes effector T cell cytokines and their effector functions, and Fig. 6 gives an overview about the single steps of cell-mediated adaptive immunity.

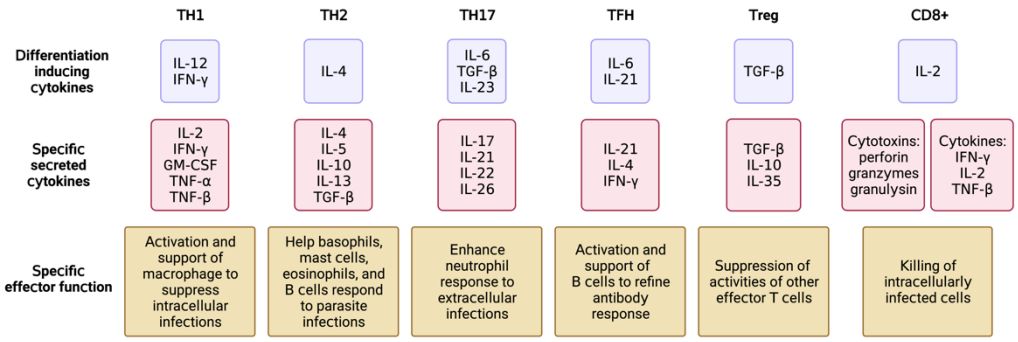

Fig. 5. Overview of the different effector T cell subtypes. Summarized are the cytokines that induce the differentiation into the specific T cell subtypes, the cytokines made by each effector T cell subtype, and the effector function of these subtypes during cell-mediated adaptive immune responses. The differentiation of CD4+ and CD8+ T cells is based on their co-receptor. Adapted from[1]; Created with BioRender.com.

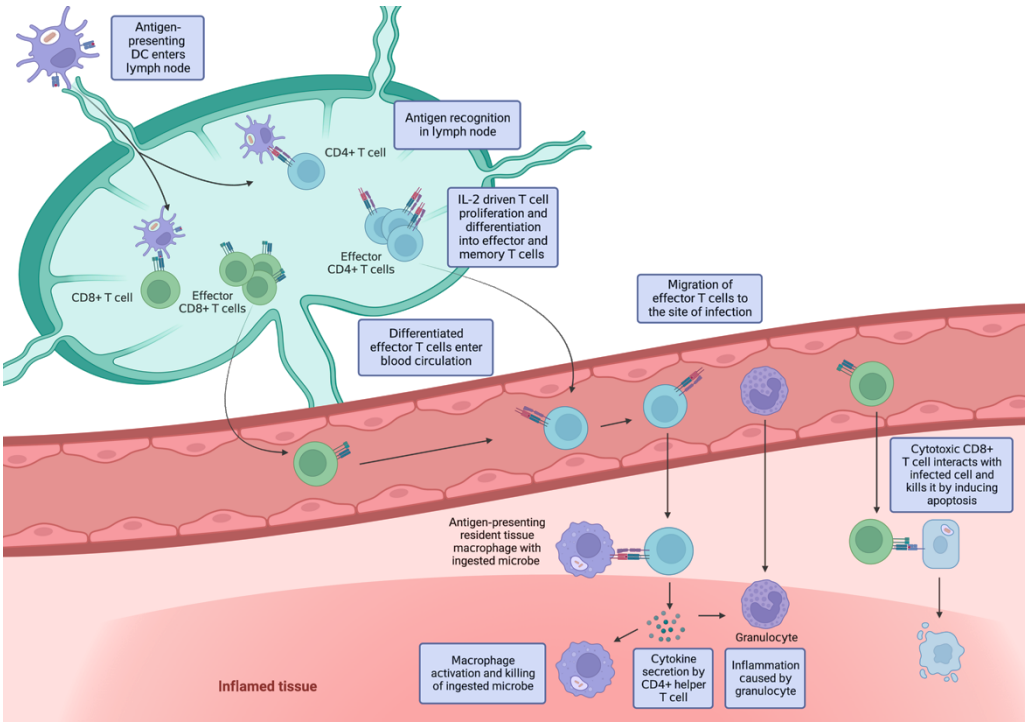

Fig. 6. This illustration provides an overview of the single events involved in the cell-mediated adaptive immune response. Firstly, DCs capture and transport pathogenic antigens from the tissues to the lymph nodes. Naïve T cells recognize these antigens, which are displayed as peptide-MHC complexes by DCs. Upon binding, the naïve T cell is activated to proliferate and differentiate into effector and memory T cells. Effector T cells migrate to the site of infection and perform various functions in cell-mediated adaptive immunity. Helper CD4+ T cells recognize pathogen antigens displayed on phagocytes (e.g., macrophages) and secrete various cytokines to mediate different effector functions. Cytotoxic CD8+ T cells eliminate cells infected with intracellular pathogens. Some effector CD4+ T cells remain in the lymph node and support B cells to produce antibodies. Furthermore, some T cells differentiate into long-lived memory T cells (not shown). Adapted from[2] and from "Stimulated T Cells Migrate Out of Lymph Nodes and Enter Inflamed Tissue" by BioRender.com (2023). Retrieved from https://app.biorender.com/biorender-templates.

1.3 Mechanisms in Wound Healing

Critical to the survival of a human is the ability to repair tissue damage caused by pathogenic insults and inflammation. The inflammatory response to microbes and injured tissues not only serves to eliminate these dangers, but also sets into motion the process of repair. Thus, the last step of immune reactions includes mechanisms that consist of a series of events causing repair of damaged tissue. Repair of tissue damage, also called healing or wound healing, is a process that restores tissue architecture and its physiological function after an injury. During this process the injured tissue is restored by regeneration of surviving cells and by filling residual defects with connective tissue, a process called scarring.

Inflammatory reactions typically have one of three outcomes, namely resolution, healing by fibrosis, or chronic inflammation. Healing by resolution refers to the restoration of normal physiological function at the site of inflammation after inflammatory mechanisms have successfully eliminated the offending agents. This is the usual outcome when the injury is limited, short-lived, or when only little tissue destruction has been caused. Resolution involves removal of cellular debris and microbes by macrophages, and resorption of edema fluid by lymphatics, followed by regeneration of the damaged tissue. The second possibility is healing by connective tissue replacement, also called scarring or fibrosis. This occurs after substantial tissue destruction and if the inflamed tissue is incapable of regeneration. In this situation, connective tissue grows into the area of damage, converting it into a mass of fibrous tissue, a process also called organization. The last case in wound healing is the progression from acute inflammation to chronic inflammation. Acute to chronic transition occurs when the acute inflammatory response cannot be resolved, because of either the persistence of the injurious agent or some interference with the normal healing process.

The first step of tissue repair is regeneration, a process that replaces damaged tissue by healthy cells to restore normal physiological function. This involves cell proliferation and differentiation of tissue-resident stem cells, and tissue cells that

have survived the injury. However, humans possess a restricted ability to regenerate most of their damaged tissues and organs, and only certain parts of these tissues are capable of complete restoration. Therefore, very often scar formation is involved, which basically "patches" the tissue. Various cell types participate in tissue repair like remaining epithelial cells that strive to restore the normal tissue structure. Furthermore, vascular endothelial cells play a significant role in generating new blood vessels to supply nutrients that are essential for the repair process. Additionally, fibroblasts contribute to tissue repair by producing fibrous tissue, which fills up defects that cannot be repaired through regeneration, and which eventually forms a scar. Cell survival, growth, and proliferation during tissue repair is driven by various cytokines and growth factors. Growth factors like epidermal growth factor (EGF) and TGF-α, produced by macrophages and epithelial cells (e.g., keratinocytes), act on activated parenchymal cells and fibroblasts to stimulate cell proliferation and migration. Hepatocyte growth factor (HGF), produced by fibroblasts and endothelial cells, enhances proliferation and cell migration of other epithelial cells during wound healing in the skin. Fibroblast growth factors (FGFs) are mainly produced by macrophages at sites of injury, which promote proliferation and migration of fibroblasts that are involved in the synthesis of extracellular matrix proteins. Furthermore, FGFs stimulate angiogenesis. Thus, these growth factors play a crucial role in the formation of granulation tissue during the wound healing process. If repair of a tissue cannot be accomplished by the increased proliferation and differentiation of parenchymal cells alone, injured cells need to be replaced by connective tissue, leading to the formation of a scar. In general, the term scar describes the replacement of parenchymal cells in any tissue by collagen.

In the case of a skin wound, the process of tissue repair starts within a few minutes after an injury with hemostasis, a process consisting of vasoconstriction and the formation of a hemostatic clot composed of platelets and polymerized fibrin, which stops bleeding. During clot formation the platelets granulate and release pro-inflammatory molecules like prostaglandins and growth factors that contribute to the recruitment of innate immune cells, antimicrobial defense, and tissue repair.

Additionally, at the site of injury the mechanisms of the innate immune system start to develop a state of inflammation.

The coagulation process is followed by a state of inflammation that endures around one week. Within the initial 6-48 hours, cytokines secreted by tissue-resident macrophages attract neutrophils and monocytes, which then work together to remove any harmful agents, including microbes that might have entered the wound. Tissue repair is primarily facilitated by macrophages, which perform multiple functions including the removal of offending agents and dead tissue, providing growth factors that promote proliferation of various cells, and secret cytokines, such as IL-1, that stimulate fibroblast proliferation and deposition of connective tissue. In the beginning, macrophages are mainly involved in developing and sustaining a state of inflammation. During the inflammatory phase, macrophages and neutrophils can cause so-called leukocyte-mediated tissue injury. This describes the damage of healthy tissue by mechanisms that are usually used to eliminate microbes and dead cells during innate immunity. Under normal circumstances, leukocytes produce lysosomal granules filled with reactive oxygen species (ROS) and various proteases that kill pathogens and remove cell debris. If phagocytes encounter particles that cannot be easily ingested these harmful substances may be released during phagocytosis into the extracellular space, a process called frustrated phagocytosis or respiratory burst. Released ROS and proteases potentiate further inflammatory processes that result in tissue damage. Plasma, tissue fluids, and host cells contain a system of anti-proteases that control harmful proteases, and possess antioxidant mechanisms including enzymes like superoxide dismutase, catalase, and glutathione peroxidase that protect healthy cells from destructive effects caused by ROS. If not adequately controlled, leukocyte-dependent tissue injury can lead to acute and chronic inflammatory diseases in humans.

Because of the inherent capacity to cause tissue injury, it is essential to terminate acute inflammatory processes during wound healing. Inflammation declines after the offending agents are removed, because the mediators of inflammation like cytokines are produced for only as long as the stimulus persists. Furthermore,

neutrophils have short half-lives in tissues and die by apoptosis within several hours. In addition, as inflammation develops, the process itself triggers a variety of stop signals that actively terminate inflammatory reactions. These active termination mechanisms include an increase in anti-inflammatory cytokines like TGF-β, IL-4, IL-13, and IL-10 produced by TH2 and Treg cells. Especially, macrophages become influenced by IL-4 and IL-13, which gradually induce macrophages to differentiate into so-called M2 macrophages. These M2 macrophages lose their pro-inflammatory activity, and instead start producing growth factors that serve important roles in the repair of injured tissues by supporting scar formation and fibrosis.

Following intense inflammation, a process of increased cell proliferation and tissue growth starts. During the following 10−20 days damaged tissue is replaced by connective tissue which is accomplished by angiogenesis and fibrosis, two essential processes in wound healing and repair. In these processes several cell types, including endothelial cells, epithelial cells, and fibroblasts proliferate and migrate to close the wound. Locally produced growth factors stimulate epithelial cells, for example keratinocytes in the skin, to migrate and proliferate to cover the wound. Endothelial cells start to grow and proliferate to form new blood vessels, a process known as angiogenesis. Angiogenesis plays a crucial role in facilitating adequate blood supply to the healing tissue. This process is regulated by various growth factors, including vascular endothelial growth factors (VEGFs). VEGFs promote vasodilation, increase vascular permeability, and stimulate the migration and proliferation of endothelial cells, a process called capillary sprouting. The formation of connective tissue is mainly driven by migration and proliferation of fibroblasts at the site of injury, followed by production and deposition of extracellular tissue proteins. All these processes are orchestrated by locally produced cytokines and growth factors like platelet-derived growth factor (PDGF), FGF-2, and TGF-β, produced by various cells at the site of injury including macrophages, platelets, endothelial cells, mast cells, keratinocytes, and lymphocytes. Migration and proliferation of fibroblasts, along with the deposition of loose connective tissue, as

well as the formation of new and delicate blood capillaries, contribute to the formation of granulation tissue. Additionally, leukocytes that remain from the precedent inflammation process are still present within the granulation tissue.

As the wound healing process progresses, fibroblasts increase their collagen production which re-builds the extracellular matrix, and the high vascularization within the granulation tissue regresses. These processes finally transform the highly vascularized granulation tissue into a pale, largely avascular scar. Some of the fibroblasts also acquire features of smooth muscle cells, and are called myofibroblasts, which contribute to the contraction of the scar over time. By the end of the first month, the scar comprises a cellular connective tissue largely devoid of inflammatory cells. The tensile strength of myofibroblasts in the wound increases with time, which helps to contract the wound.

After intense cell proliferation, angiogenesis, deposition of collagen, and scar formation, a phase of scar remodeling takes place, also known as maturation phase. This process can take several weeks or even years and is characterized by modification and reorganization of collagen. A summary of the wound healing process is given in Fig. 7.

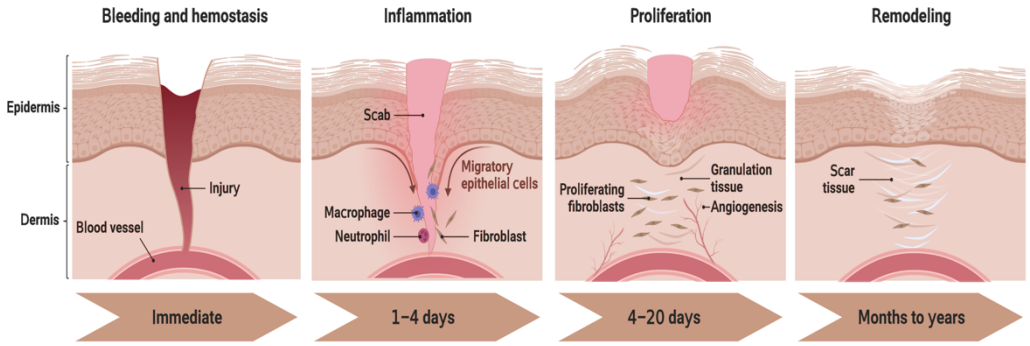

Fig. 7. Overview of the single steps during tissue repair in the skin. Adapted from[2,5] and from "Wound Healing" by BioRender.com (2023). Retrieved from https://app.biorender.com/biorender-templates.

1.4 Autoimmunity

When the adaptive immune system is misdirected to healthy cells and tissues, a pathologic chronic inflammatory state, known as autoimmunity, may develop. The cause of autoimmune diseases is the failure of mechanisms that regulate self-tolerance, which allows to develop responses of the adaptive immune system against normal components of the healthy human body, called self-antigens. Thus, the autoimmune response tries to eliminate all self-antigens (also known as auto-antigens) from the body which generates a chronic state of inflammation, leading to comprised tissue functions. This results in the development of chronic diseases, in which the immune response remains in its destructive phase and never reaches the point at which inflammation is overcome by tissue repair and reconstruction. Although much is known of the molecular and cellular effects of autoimmune diseases, little is known of the events that break self-tolerance and initiate an autoimmune response. However, it is assumed that autoimmunity may arise from a combination of genetic predispositions (mainly human leukocyte antigens (HLA) gene polymorphisms), which may contribute to the breakdown of self-tolerance, and from environmental triggers, such as infections, tissue damage, and inflammation, that promote the activation of self-reactive lymphocytes. Once an autoimmune response is initiated, it usually continues throughout a person's life and increases its severity. With cell death and tissue disruption physiological functions become compromised, and for some conditions this is the direct cause of death.

There are clinically more than 80 different autoimmune diseases described, from which the most famous are psoriasis, rheumatoid arthritis, type I diabetes, multiple sclerosis, and Crohn's disease. Autoimmune dysfunctions affect around 5–10% of the human population, with increasing incidence. For most autoimmune diseases the incidence differs between females and males, with females being more frequently affected. The clinical manifestation of autoimmune disorders varies widely in the tissues they affect and the symptoms they cause. Some are organ-specific, and others act systemically on widespread antigens in the human body.

Examples for organ-specific autoimmune diseases are type I diabetes in which the autoreactive T cells and antibodies are specific for β-cells of the pancreatic islets, or multiple sclerosis, where autoreactive T cells react against myelin in the central nervous system. An example of a systemic autoimmune disease is systemic lupus erythematosus, in which auto-antibodies are made against different components of the cell nucleus (so-called anti-nuclear antibodies), including DNA, RNA, and nucleoproteins, resulting in the formation antigen-antibody complexes, also called as immune complexes. Such immune complexes get deposited in various tissues like blood vessels and kidney where they activate inflammatory reactions causing widespread lesions throughout the body.

Autoimmune diseases can be classified as type II, III, and IV corresponding to the mechanisms of the damaging effects of hypersensitivity reactions type II, III, and IV, respectively. Since no autoimmune disease is mediated by IgE antibodies, type I does not exist for autoimmunity. The autoimmune diseases that correspond to type II hypersensitivities are caused by IgG antibodies that bind to antigens on cell surfaces or the extracellular matrix as in diseases like Pemphigus vulgaris, Graves' disease, or myasthenia gravis. Autoimmune diseases corresponding to type III hypersensitivities are caused by the deposition of soluble antigen-antibody complexes in the walls of blood vessels like in systemic lupus erythematosus. Corresponding to type IV hypersensitivities are autoimmune reactions caused by effector T cells like type I diabetes, rheumatoid arthritis, or multiple sclerosis. The majority of chronic inflammatory autoimmune diseases are caused by effector T cells that lost tolerance against self-antigens. Especially excessive responses of CD4+ effector T cells like TH1 and TH17 are known to play crucial roles in the pathogenesis of type IV autoimmune diseases.

1.5 Treatment of T cell-mediated Autoimmune Diseases

Many autoimmune diseases correspond to type IV, and thus increased activation, proliferation, and migration of T cells play an essential role in the pathogenesis of chronic inflammation and autoimmune diseases. Targeted therapies that specifically inhibit activating pathways in T cells are an attractive approach to improve disease resolution in human autoimmune diseases. For this purpose, various immunosuppressive drugs are clinically available that specifically interfere with T cell activity[1].

1.5.1 Glucocorticoids

Autoimmune disorders are often treated with glucocorticoids like betamethasone, dexamethasone, or prednisone. Although glucocorticoids have wide-ranging physiological effects on different organs, they are mainly used for their anti-inflammatory and immunosuppressive properties. The effect of glucocorticoids is based on inhibiting the expression of pro-inflammatory genes, whereas the expression of anti-inflammatory and immunosuppressive genes is increased. Glucocorticoids diffuse across the plasma membrane and bind to the specific cytosolic glucocorticoid receptor to form a glucocorticoid-receptor complex. The glucocorticoid-receptor complex binds to NFκB which reduces the expression of inflammatory mediators, including prostaglandins, nitric oxide, and some cytokines like IL-1β, IL-2, IL-6, and TNF-α. Furthermore, the glucocorticoid-receptor complex dimerizes, enters the nucleus, and binds specific DNA sequences in the promoter regions of glucocorticoid-responsive genes to activate the transcription of a wide variety of anti-inflammatory genes. For instance, they increase the expression of nuclear factor of kappa light polypeptide gene enhancer in B cells inhibitor alpha (IκBα), which is an inhibitory regulator that prevents the transcription factor NFκB from gaining access to the nucleus and initiating expression of genes that cause inflammation. Additionally, glucocorticoids prevent immune cell migration to sites of inflammation by inhibiting the expression of

adhesion molecules, and promote apoptotic death of leukocytes and lymphocytes. Because of their multifarious effects on gene expression and cellular metabolism, corticosteroids have many adverse side effects. Among them are fluid retention, weight gain, diabetes, loss of bone mineral, and thinning of the skin[1,6].

1.5.2 Inhibitors of T cell Receptor Signaling During T cell Activation

Among the first immunosuppressive drugs found to selectively inhibit T cell activation were cyclosporine and tacrolimus. Cyclosporine, also known as cyclosporine A, is a cyclic peptide consisting of eleven amino acids derived from the soil fungus *Tolypocladium inflatum*. Tacrolimus, also called FK506, is a macrolide lactone isolated from the soil actinomycete *Streptomyces tsukubaensis*[7].

The binding of the TCR to its antigen induces the T cell to release calcium ions (Ca^{2+}) from intracellular stores and promotes intracellular signaling leading to the activation of the transcription factor AP-1. Elevated cytosolic Ca^{2+} directly binds and activates calmodulin. Then, activated calmodulin induces the serine/threonine phosphatase calcineurin to dephosphorylate the transcription factor NFAT. Once dephosphorylated, the active NFAT migrates to the nucleus to form a complex with AP-1. The AP-1-NFAT complex initiates the transcription of genes required for T cell activation, including the genes encoding for IL-2 and TNF-α.

Both, cyclosporine and tacrolimus suppress T cell activation by similar mechanisms of calcineurin inhibition, which interferes with AP-1 activation. In the cytosol, they bind peptidyl-prolyl isomerase enzymes called immunophillins. Cyclosporine forms a complex with the immunophillin called cyclophilin, and tacrolimus a complex with the immunophillin FK506-binding protein 12 (FKBP12). Both complexes bind to calcineurin, thereby blocking its phosphatase activity and preventing it from activating NFAT. Therefore, in the presence of cyclosporine or tacrolimus, IL-2 and other T cell activating cytokines are not made, aborting T cell activation at an early stage. However, both drugs are associated with various side effects including nephro- and hepatotoxicity, and drug sensitization. Additionally, there are many

possibilities for drug-drug interactions with drugs that interfere with cytochrome P450 3A4 (CYP3A4). Therefore, therapies with these drugs are only made in experienced institutions[1].

Pimecrolimus is a semisynthetic derivative of ascomycin, which has been isolated from *Streptomyces hygroscopicus* var. *ascomyceticus*. Since pimecrolimus is structurally closely related to tacrolimus it shares the same mode of action by binding FKBP12 and inhibiting calcineurin activity[8,9].

Rapamycin (syn. sirolimus) is an immunosuppressive macrolide produced by several actinomycetes, but was initially isolated from *Streptomyces rapamycinicus* (formerly, *Streptomyces hygroscopicus* ATCC 29253)[7]. As tracolimus and pimecrolimus, also rapamycin associates with FKBP12, but the FKBP12-rapamycin complex does not bind to calcineurin. Instead it interferes with T cell activation by directly binding to the FKBP12-rapamycin-binding (FRB) domain of the protein kinase mammalian target for rapamycin (mTOR). The resulting FKBP12-rapamycin-mTOR complex interferes with signals coming from the IL-2 surface receptor and causes a decrease in cyclin expression. As a result, the mTOR complex inhibits cell cycle progression from G1 to S, thereby suppressing T cell proliferation[10]. Currently, rapamycin is approved for clinical use of solid organ transplants. But due to its anti-proliferative effects, rapamycin and semi-synthetic analogs thereof become increasingly investigated in the treatment of various cancers and in autoimmune diseases like rheumatoid arthritis, systemic lupus erythematosus, or multiple sclerosis[10–12]. For example, its semi-synthetic derivative everolimus is approved for the prevention of organ rejection and for the treatment of different types of tumors. Furthermore, it is currently under investigation for use in rheumatoid arthritis[12–14].

Antibodies that bind to the TCR complex have the potential to inhibit the signaling that directly arises from antigen recognition. Most of these antibodies are initially discovered and used for inhibiting organ rejection, but become more frequently used in autoimmune dysfunctions. CD3-specific monoclonal antibody Ortho Kung T3 (OKT3), marketed under the name muromonab, binds the CD3 complex of the

TCR and induces T cell apoptosis, or causes internalization of the TCR, resulting in the effect that the T cell loses the abiliy to recognize its antigen, a process called antigenic modulation. Due to numerous severe side effects and its immunogenicity in humans OKT3 was withdrawn from the market in 2008. However, a new generation of anti-CD3 monoclonal antibodies is currently in clinical development showing reduced side effects that are particularly intended for the use in autoimmune diseases. For example, otelixizumab and teplizumab are investigated for the use in type I diabetes, and foralumab for the treatment of inflammatory bowel disease[15,16].

Beside the signal from the TCR complex, T cell activation also needs the signal coming from the CD28 co-stimulatory receptor ("signal 2"). The latter signal is generated when CD28 interacts with a B7 co-stimulator expressed on APCs. Cytotoxic T-lymphocyte-associated protein 4 (CTLA4) is an additional surface receptor on T cells that binds to B7, resulting in inhibition of T cell activation. Therefore, CTLA4 is described as the negative regulator of T cell activation. Abatacept and belatacept are two fusion proteins that combine the extracellular B7-binding domains of CTLA4 with the Fc fragment of the immunoglobulin IgG1. These fusion proteins use their CTLA4 component to bind to the B7, which prevents the CD28 receptors of naïve T cells from binding and thereby inhibit T cell activation. Abatacept is used in the treatment of autoimmune diseases and belatacept for graft rejection[17,18].

1.5.3 Blocking Cytokine Signaling Prevents Activation of T cells

Once a naïve T cell has received activating signals from the TCR and the co-stimulatory receptor, further signals from the IL-2 receptor are needed for activation ("signal 3"). High-affinity IL-2 receptors consist of three different proteins called α, β, and γ chain. Anti-CD25 antibodies like basiliximab bind specifically to the α chain (also called CD25) of the high-affinity IL-2 receptor, preventing IL-2 from interacting with the IL-2 receptor. This blocks intracellular signals necessary for stimulating the proliferation and differentiation of antigen-

activated T cells. Basiliximab was primary developed for the treatment of organ rejection, but showed also beneficial effects in the treatment of immune-mediated bowel disease and lichen planus[19–21].

Tocilizumab is a monoclonal antibody that acts as an IL-6 receptor antagonist, and is used in the treatment of rheumatoid arthritis and Crohn's disease. By binding to the IL-6 receptor, tocilizumab blocks the diverse effects of pro-inflammatory IL-6 during innate immunity, such as induction of acute-phase response and fever, as well as the activation and differentiation of macrophages, B cells, and T cells during adaptive immunity[22,23].

1.5.4 Inhibitors of DNA Synthesis

DNA synthesis inhibitors are cytostatic drugs that suppress T cell proliferation by interfering with different processes involved in DNA synthesis. These drugs are used as immunosuppressants in transplantation and autoimmunity, but also in the treatment of cancer.

Azathioprine is a widely used purine analog in the treatment of rheumatoid arthritis, inflammatory bowel disease, multiple sclerosis, and in the prevention of transplant rejection[24]. Azathioprine is the pro-drug of 6-thioinosinic acid, which itself gets enzymatically further metabolized to afford the active metabolites 6-methyl thioinosine 5-phosphate and 6-thioguanosine. These metabolites interfere with different enzymes involved in purine and nucleic acid synthesis, and damage the newly synthesized DNA through the incorporation of thiopurine analogues. This inhibits DNA replication leading to reduced clonal expansion of B and T cells[25].

Methotrexate is widely used in cancer chemotherapy and as an immunosuppressant in the treatment of psoriasis, rheumatoid arthritis, and Crohn's disease. Structurally, methotrexate is an analog of folate (vitamin B9) and acts as a folate antagonist by inhibiting dihydrofolate reductase, an enzyme essential for thymidine biosynthesis, and thereby it inhibits DNA replication. Recent investigations revealed that methotrexate further inhibits NFκB activity and reduces the production of pro-inflammatory cytokines like IL-2[26].

Mycophenolate mofetil is a pro-drug that is metabolized to mycophenolic acid, a compound that has previously been isolated from different *Penicillium* sp. like *Penicillium stoloniferum* or *Penicillium brevicompactum*. Mycophenolic acid inhibits inosine monophosphate dehydrogenase, an enzyme necessary for guanine synthesis. This decreases the synthesis of guanine nucleotides, hinders DNA synthesis, and consequently reduces lymphocyte proliferation. Mycophenolate mofetil is used in organ transplantation and in autoimmune diseases like rheumatoid arthritis, systemic lupus erythematosus, or psoriasis[27].

Leflunomide is used in the treatment of rheumatoid arthritis. Its active metabolite teriflunomide is an inhibitor of dihydroorotate dehydrogenase a key enzyme involved in the biosynthesis of uridine and cytidine, which causes a decrease in T cell proliferation[28].

Cyclophosphamide is a pro-drug that is metabolized to phosphoramide mustard, which alkylates and cross-links DNA. Such disruption renders cells incapable of DNA replication and transcription, that finally leads to apoptosis. Cyclophosphamide has clinically been used in treatment of various cancers, and as an immunosuppressive agent in the treatment of transplant rejection and different autoimmune diseases like multiple sclerosis[29].

1.5.5 Direct Blocking of Cytokines

In the treatment of autoimmune diseases, monoclonal antibodies that directly target and inhibit inflammatory cytokines can be used. For example, in the treatment of rheumatoid arthritis, Morbus Crohn, or psoriasis infusion with monoclonal antibodies specific for TNF-α are rather successful in alleviating symptoms by eliminating TNF-α. Widely used anti-TNF-α antibodies are infliximab and adalimumab[30,31]. Etanercept is a fusion protein consisting of a recombinant human TNF receptor that is bound to the Fc portion of an immunoglobulin, which binds strongly to soluble TNF-α[32].

1.5.6 Complement-induced Depletion of T cells

To achieve immune suppression antibodies can be given that broadly and unspecifically react with leukocytes, which causes leukocyte depletion resulting in a weakened immune system. The antibody preparations anti-thymoglobulin (ATG) and anti-lymphoglobulin (ALG) are obtained from purified serum of rabbits and horses that have been previously immunized with human thymocytes and lymphocytes, respectively[33,34]. Both ATG and ALG are polyclonal mixtures of high-affinity IgG antibodies that specifically bind different antigens expressed on lymphocytes, which marks them for complement proteins for destruction. ATG and ALG are mainly used in preventing graft rejection, but have also successfully been studied in different autoimmune diseases like aplastic anemia, type I diabetes, or multiple sclerosis[1,35–37].

Alemtuzumab is an anti-CD52 antibody used to treat multiple sclerosis, which binds to CD52 expressed on the cell surface of lymphocytes. The physiological function of CD52 is unknown, but the cell-surface complex of CD52 and anti-CD52 binds covalently to Cb3, and activates the complement system to induce phagocytosis of lymphocytes by the cells of innate immunity[1,38].

1.5.7 Inhibitors of Lymphocyte Migration

After activation and differentiation in secondary lymphoid tissues effector T cells need to migrate to the infected tissue. For this purpose, they first must leave the lymphoid tissues in the efferent lymph. This departure is controlled by the sphingosine-1-phosphate receptor expressed on the surface of activated T cells that recognizes sphingosine-1-phosphate (S1P), a lipid made in all cells, which has chemotactic activity. Under the influence of an S1P gradient, T cells expressing an S1P receptor are directed to move out of the lymph node into the efferent lymph to join the blood circulation. If this signal is blocked, activated effector T cells do not enter the blood and remain in the lymph node, which prevents effector T cells to fulfill their actions during adaptive immunity. This principle is used in the treatment of multiple sclerosis with fingolimod. Fingolimod was synthesized by

chemical modification of myriocin, an immunosuppressive substance isolated from the entomopathogenic fungus *Isaria sinclairii*. As a pro-drug fingolimod gets phosphorylated by sphingosine kinase 2 to become fingolimod-phosphate, which is a high affinity agonist for the S1P receptor. Binding of fingolimod-phosphate to the S1P receptor causes internalization of the S1P receptor, which inhibits the S1P-dependent egress of lymphocytes from lymphoid tissues. Consequently, this effect decreases the concentration of lymphocytes in the peripheral blood circulation and reduces infiltration of effector T cells into inflammatory sites of autoimmune diseases, which causes the immunosuppressive activity[1,39].

Another way to prevent infiltration of effector T cells into inflamed tissue is achieved by integrin inhibitors. The transition of T cells from the blood into the inflamed tissue is supported by adhesion molecules on T cell surfaces, called integrins, which bind to adhesion molecules on endothelial cells. At inflammatory sites endothelial cells are activated to express numerous cell adhesion molecules, such as vascular cell adhesion molecule-1 (VCAM-1), that allow T cells entering the tissue. Inhibition of this transition has been shown to be beneficial in the treatment of multiple sclerosis and Crohn's disease. Natalizumab and vedolizumab are monoclonal antibodies that binds to the α4 subunit of integrins expressed on T cells. This prevents T cells from binding to adhesion molecules expressed on epithelial cells, and to leave the blood circulation to enter the tissues[40,41].

1.5.8 Immunosuppressive Agents with Different or Unclear Modes of Action

Chloroquine and hydroxychloroquine, initially used as antimalarial drugs, are currently also used in the treatment of autoimmune diseases, primarily in rheumatoid arthritis and systemic lupus erythematosus. Despite the widespread use in clinics, the mode of action is still not completely understood. However, chloroquine and hydroxychloroquine have been shown to interfere with different processes during the immune response. They inhibit the process of antigen processing and subsequent presentation as MHC class II complexes in APCs. Through inhibition of Toll-like receptors both substances decrease the production

of pro-inflammatory cytokines including IFN-γ, TNF-α, IL-1, IL-2, and IL-6. Additionally, these drugs also interfere with Ca^{2+} signaling in T cells, which consequently inhibits T cell activation. The combination of these effects result in a reduced T cell response, which consequently decreases the aberrant adaptive immune response in autoimmune diseases[42].

Sulfasalazine is a widely used drug in the treatment of autoimmune diseases like rheumatoid arthritis and ulcerative colitis. Its mode of action is not fully understood, and is believed to be mediated by several immunomodulatory and anti-inflammatory effects. Among these effects sulfasalazine has been shown to inhibit the release of pro-inflammatory cytokines produced by various cell types, including IL-2 by T cells, which showed to reduce T cell activation and proliferation[43,44].

Therapy with IFN-β is commonly used in the treatment of multiple sclerosis since it reduces the relapse rates and slows the progression of the disease. The primary physiological effect of IFN-β lies in its antiviral activity by supporting NK cells to destroy virus infected cells. However, IFN-β also revealed immunosuppressive and anti-inflammatory effects whose mode of action is still not fully understood. The beneficial effect is explained by different mechanisms, such as the downregulation of MHC class II complexes in APCs, which diminishes T cell activation, the induction of IL-10 production by T cells, which shifts the balance towards anti-inflammatory TH2 cells, and the inhibition of T cell migration based on decreased expression of adhesion molecules, which prevents T cells to leave the blood stream[45].

An additional treatment option applied in multiple sclerosis is the heterogeneous mixture of large synthetic polypeptides randomly composed of L-alanine, L-lysine, L-glutamic acid, and L-tyrosine, called glatiramer acetate. The mode of action is not fully understood, but multiple ways of action are discussed for its therapeutic activity, which are mainly explained by its effect on autoreactive T cells. It has been shown that glatiramer acetate binds directly to MHC class II molecules expressed by APCs, or displaces other peptides from the MHC binding groove. This prevents

the presentation of antigens and hinders T cell activation. Furthermore, glatiramer acetate binds as an antagonist directly to the TCR which inhibits T cell activation. Like the IFN-β, glatiramer acetate treatment promotes the differentiation of naïve T cells towards TH2 and Treg cells, which secrete anti-inflammatory cytokines and showed to reduce the number of pro-inflammatory TH1 and TH17 cells. Currently, glatiramer acetate is also investigated in transplant rejection and inflammatory bowel disease[46].

Dimethyl fumarate is a fumaric acid ester used in the treatment of multiple sclerosis and psoriasis. Initially, dimethyl fumarate has been synthesized from fumaric acid obtained from *Fumaria officinalis* (Papaveraceae), a plant that has traditionally been used for ailments of the skin such as chronic eczema and cutaneous eruptions. The mechanisms behind the immunosuppressive effect of dimethyl fumarate are multifactorial and are still being unraveled. In general, dimethyl fumarate has been shown to inhibit T cell activation and proliferation, and even induced T cell apoptosis, resulting in reduced number of lymphocytes in blood circulation. This could be explained by inhibition of the NFκB pathway in activated T cells through blocking PKC-θ, which leads to inhibition of IL-2 secretion. Furthermore, dimethyl fumarate can deplete circulating glutathione levels and subsequently induces heme oxygenase 1 (HO-1), which reduces pro-inflammatory cytokine secretion in activated T cells. Dimethyl fumarate also interferes with glycolysis of T cells by inhibiting glyceraldehyde 3-phosphate dehydrogenase (GAPDH), which reduces the capacity of T cells to proliferate, to survive, and to produce cytokines[47–49].

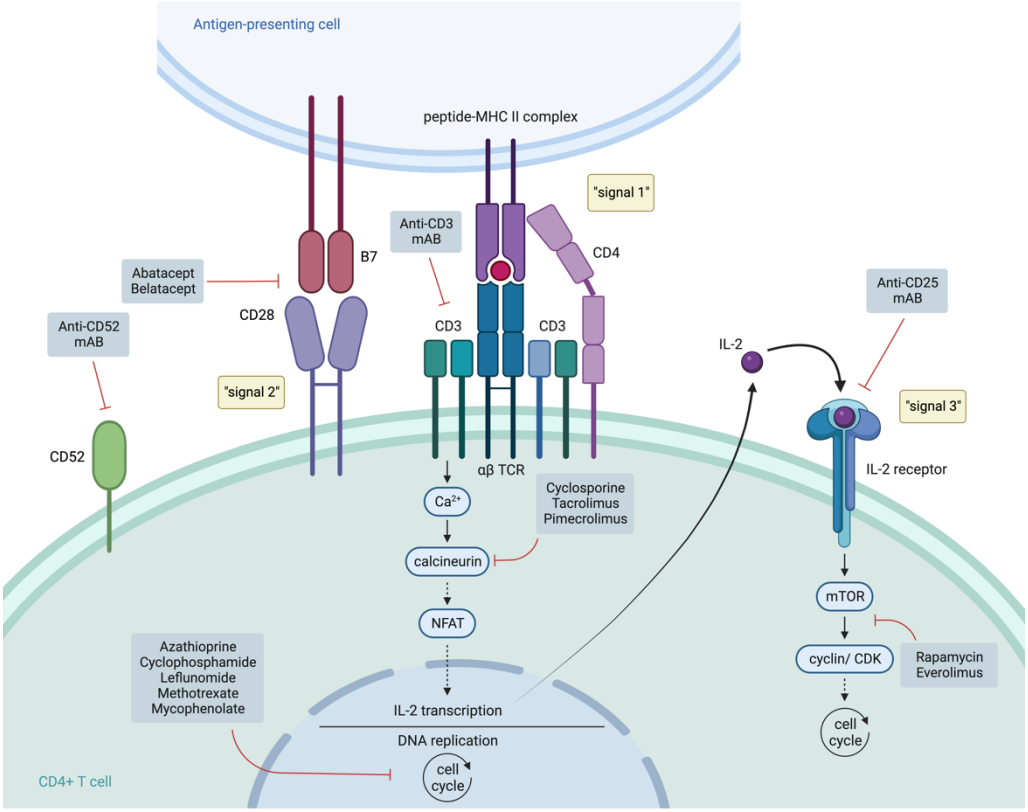

Fig. 8. Overview of immunosuppressive drugs and their target structures in T cells. CDK, Cyclin-dependent kinase. Adapted from[1]; Created with BioRender.com.

1.6 Treatment of Wounds

The treatment of wounds depends on the wound type (abrasion, cut, burning, bruise), the degree of infection, and the state of health of the patient (e.g., diabetes, edema). However, wound treatment usually follows the TIME principle. "T" for tissue means wound cleaning and debridement, "I" stands for infection/ inflammation and means the treatment of the infected wound with topical antiseptics or oral antibiotics, "M" stands for moisture and includes measures to manage wound exudate and wound moistening, and "E" means edge, which describes the assessment of wound edges and the surrounding skin[50,51].

Wound cleaning describes the procedure of removing microbes, foreign bodies, and necrotic tissue (called debridement) from the wound using isotonic saline or antimicrobial wound irrigation solutions (autolytic debridement), or in more severe cases surgical measures. Antiseptic wound irrigation solutions contain antimicrobials such as polihexanide, octenidine dihydrochloride, or hypochlorous acid[52]. In chronic non-healing wounds with necrotic tissue like in diabetic foot ulcer, autolytic or surgical debridement methods sometimes fail. In such cases bio-surgery can be used, also known as maggot debridement therapy. Medical grade live larvae of the common green bottle fly *Lucilia sericata* are given onto the wound where they remove the sloughy, necrotic tissue. They secrete proteolytic enzymes that extracorporeal digest and remove infected and dead tissue of the wound. Concomitantly, this proteolysis promotes tissue repair and reconstruction by inducing collagen degradation, keratinocyte migration, and activation of endothelial cells and fibroblasts. Furthermore, maggots exhibit antimicrobial activity by directly ingesting bacteria and secreting antimicrobial substances like defensins[53].

During the disinfection phase different antiseptics are directly applied onto the wound for approximately 2−6 days. The different substances used as antiseptics are polihexanide, octenidine dihydrochloride, alcohols (e.g., ethanol, *iso*-propanol, phenoxyethanol), quaternary ammonia compounds (e.g., benzoxonium chloride), iodine (e.g., povidone-iodine) and chlorine containing compounds (e.g., triclosan,

chlorhexidine), as well as silver containing substances (e.g., elemental silver, silver chloride, silver sulfate, silver sulfadiazine)[52,54].

To support fast regeneration of the injured tissue it is important to keep the wound moistened. The goal is to balance the moistening of the wound and skin by retaining the right amount of moisture to support epithelization, cell migration, and neo-angiogenesis, and by removing excessive exudate that could lead to wound maceration or biofilm formation[51]. To regulate the moistening in the skin, various wound dressings have been developed. To prevent drying of the wound, hydrogel dressings containing antiseptics can be used. If the wound is wet and bleeding, hydroactive dressings like sodium carboxymethyl cellulose, polyvinyl alcohol, or calcium alginate dressings, containing alginic acid obtained from brown algae, can be applied, which are able to soak a lot of wound exudate and stop bleeding to prevent wound maceration[51,55]. If the wound is wet and wound maceration has been developed, wound healing is impaired and delayed. In this case, the wound must be treated dry with a dry dressing. This can be supported with zinc oxide containing ointments or medicinal honey (e.g., Manuka honey from New Zealand obtained from *Leptospermum scoparium* nectar), which have skin drying, antiseptic, and wound healing promoting properties[56,57]. To re-moisten the wound afterwards, often therapeutic moisturizers like petrolatum or siloxane-based ointments, which contain dimethicone and related siloxane polymers (also called silicone oils) are used to build-up a firm film that regulates skin hydration and supports re-epithelization[58,59]. A more recent therapeutic moisturizer is a spray containing red oil from *Hypericum perforatum* (oleum hyperici) and neem oil from the seeds of *Azadirachta indica* (oleum azadirachtae). It is believed that the oil constituents work synergistically to aid the wound healing process. They exhibit antimicrobial properties and create a moist wound environment that facilitates cell proliferation while preventing wound maceration[60–62].

Further possibilities to treat non-healing wounds include skin replacement therapies with biosynthetic and tissue-engineered living skin transplants. For example, Apligraf® is a tissue-engineered human skin product which consists of an

epidermal layer of living human keratinocytes and of a dermal layer made out of bovine collagen containing human fibroblasts. Once transplanted, tissue-engineered human skin adapts to the physiological and structural environment at the site of the wound and supports tissue repair by secreting growth factors[63]. Improved wound healing is also achieved with acellular fish skin transplantation, which enhances wound healing by promoting angiogenesis and collagen deposition based on different growth factors, and reduces the state of inflammation due to the high content of omega-3 fatty acids[5,64]. A further type of therapy in the treatment of non-healing wounds is the vacuum-assisted closure therapy (VAC). The wound is airtight sealed and is connected to a vacuum pump which aspirates continuously wound exudate. The applied vacuum stabilizes the wound environment, reduces wound edema and bacterial load, improves tissue perfusion, and stimulates granulation tissue and angiogenesis. All this improves wound closure and reduces the need of plastic surgeries[65].

To support wound healing of smaller wounds and scars often special ointments, gels, creams, or adhesive silicone bandages are locally applied. The goal of such topical dosage forms is to regularly disinfect the wound and support its re-epithelization while avoiding hypertrophic scarring and hyperkeratosis. Usual active ingredients include heparin sodium, allantoin, dexpanthenol, zinc oxide, vitamins, antiseptics, hyaluronic acid, collagen, siloxane polymers, and herbal remedies[66,67].

Heparin is a natural occurring glycosaminoglycan mostly obtained from porcine intestine mucosa and is used as an anticoagulant that binds antithrombin III. In wound healing it is used for its antithrombotic, anti-inflammatory, analgesic, and collagen remodeling properties[68]. Often, heparin sodium-containing topical dosage forms are combined with substances that support re-epithelization like dexpanthenol (pantothenic acid) and allantoin.

Dexpanthenol is a skin moisturizer and prevents skin irritation, stimulates skin regeneration, and promotes wound healing. When applied topically, dexpanthenol as a prodrug gets enzymatically transformed to pantothenic acid (vitamin B5), a

constituent of coenzyme A. Coenzyme A is involved in many metabolic processes including fatty acid and sphingosine synthesis, which promotes epidermal regeneration. Furthermore, pantothenic acid increases fibroblast proliferation, collagen synthesis, accelerated epithelialization, and induces fibroblasts to produce cytokines involved in wound healing mechanisms[69].

Allantoin is a natural occurring degradation product of nucleic acids and from purine metabolism in various organisms, but can be found in higher concentrations in certain plants, especially from the genus *Symphytum*, such as *Symphytum officinale*[70,71]. Furthermore, it is also produced during maggot debridement by the larvae of *Lucilia sericata*[53]. Allantoin exhibits wound regeneration promoting effects by its slightly keratolytic and skin hydrating properties. Additionally, allantoin supports granulation tissue formation by stimulating fibroblast proliferation and collagen synthesis[71,72].

Beside heparin, dexpanthenol, and allantoin, it is quite common that wound healing ointments contain onion extract (Allii cepae extractum) or the oil of *Hyoscyamus niger* (Hyoscyami maceratum oleosum, Grünöl in German). *Allium cepa* extract shows anti-inflammatory effects, and reduces proliferation and collagen synthesis by fibroblasts, which prevents hypertrophic scarring during wound healing. The effects of *Allium cepa* are believed due to its increased flavonoid content, mainly due to quercetin[73,74]. Topical formulations containing oil of *Hyoscyamus niger* in the treatment of wounds and scars are commonly used in Austria and Switzerland[75]. Even though, no scientific data is available about its wound healing effects, it seems to be rather effective against hypertrophic scar formation. Active constituents are believed to be the parasympathic-blocking tropane alkaloids atropine, scopolamine, and hyoscyamine[76].

Adhesive silicone bandages and siloxane polymer-containing ointments can be used with or without other active ingredients to reduce pain and itching of wounds. Silicone based wound treatment supports re-epithelization by keeping the wound

occluded, hydrated, and smooth, and additionally silicone reduces fibroblast proliferation preventing hypertrophic scar formation[77].

Hyaluronic acid is a human glycosaminoglycan that is used in tissue regeneration alone or in combination with other drugs due to its wound healing promoting effects. By its hydrating effect, it supports wound moistening, which promotes re-epithelization, neo-angiogenesis, and granulation tissue formation. As an essential component of the extracellular matrix hyaluronic acid supports cell differentiation, proliferation, adhesion, and migration of keratinocytes, fibroblasts and immune cells during tissue regeneration. Additionally, hyaluronic acid binds to hyaluronic acid receptors on skin and immune cells, which supports the production of cytokines, chemokines, and growth factors that regulate the wound healing process[78].

Collagens are the most abundant structural proteins in the extracellular matrix found throughout connective tissues in mammals and contribute to hydration, mechanical strength, and elasticity of the skin. In their native and fibrillar conformation, or as soluble components in the wound milieu, they are important in the regulation of the different wound healing phases. In the healing wound, collagens are synthesized by fibroblasts and are involved in immune cell activation. Collagens stimulate immune cells to secrete cytokines, which influence the migration of fibroblasts, endothelial cells, and epithelial cells within the wound. Simultaneously, collagen degradation releases fragments that promote fibroblast to proliferate and to synthesize growth factors that support angiogenesis and re-epithelialization. One driving factor in the development of chronic wounds is persistent and increased destruction of extracellular matrix by elevated levels of matrix metalloproteinases. Beside the ability to support the recruitment of immune cells, fibroblasts, and keratinocytes to sites of healing wounds, collagens applied on wounds have been shown to bind matrix metalloproteinases which reduces destructive and inflammatory processes. Furthermore, collagens promote neo-angiogenesis in granulation tissue, and support wound healing by their moisturizing properties[79].

Beside dexpanthenol or rather pantothenic acid, different other vitamins are applied topically to support wound healing. Vitamin A (retinol) is used in the treatment of skin diseases like acne and psoriasis where it supports the healing of skin lesions. The beneficial effects during wound healing are explained by promoting keratinocyte migration, collagen synthesis by fibroblasts, and by inhibiting matrix metalloproteinases, which supports re-epithelization. Vitamin C (ascorbic acid) supports wound healing by promoting collagen synthesis, modulating immune cell functions, and by its antioxidative effects. Vitamin E (tocopherols) is believed to act similarly as vitamin C as an antioxidant, which counteracts the elevated level of tissue damaging ROS in inflamed wounds caused by neutrophils during the processes of innate immunity. Vitamin D3 is known to accelerate wound closure by promoting re-epithelization through increasing proliferation and differentiation of keratinocytes and fibroblasts[80,81].

1.7 Traditional Natural Products in Autoimmune Diseases and Wound Healing

Many of the immunosuppressive drugs currently used in clinics are natural products like cyclosporine, tacrolimus, or rapamycin, or are natural product-derived semi-synthetic derivatives like mycophenolate mofetil, pimecrolimus, everolimus, fingolimod, and dimethyl fumarate. The modern idea of the immune system, its components, and how they interact do defeat pathogens started to develop in the middle of the 19th century. However, the understanding on how immune reactions develop, what type of cells are involved, and how they interact, especially also the idea of autoimmune diseases in which immune cells attack own body structures only emerged in the middle of the 20th century. Therefore, to have traditional natural remedies with the intention to treat autoimmune diseases specifically does basically not exist. However, the clinical manifestation of autoimmune diseases like psoriasis or rheumatoid arthritis was already known many hundred years before the cellular and molecular understanding of these diseases developed. Hence, such clinical pictures have commonly been treated symptomatically with traditional medicinal products, mainly with traditional medicinal plants.

Rheumatic disorders comprise diseases causing chronic pain in the joints and connective tissues, which can develop a chronic joint inflammation, as it is the case in rheumatoid arthritis. Therefore, inflammatory rheumatic disorders affecting the joints have mainly been treated traditionally with herbal preparations having analgesic properties. Typical oral applications include devil's claw root of *Harpagophytum procumbens* (Harpagophyti radix), willow bark (Salicis cortex) from different *Salix* sp. (e.g., *Salix alba*, *Salix purpurea*), preparations made out of *Populus tremula*, *Solidago virgaurea*, and *Fraxinus excelsior* (Phytodolor®), or green-lipped mussel (*Perna canaliculus*). As topical treatment options *Capsicum* fruit (*Capsicum annuum*, *Capsicum frutescens*) or *Arnica montana* (Arnicae flos) containing ointments are applied. More recently, olibanum (*Boswellia carteri*, *Boswellia serrata*) or rose hip fruits (*Rosa canina*, Cynosbati fructus) as oral preparations gained more interests in the usage for rheumatic disorders[82–84].

The effects of *H. procumbens*, *Salix* sp., and Phytodolor® are mainly described as anti-inflammatory and analgesic by influencing the expression of different pro-inflammatory cytokines and the inhibition of cyclooxygenases[82–84].

The capsaicinoids of *Capsicum*-containing drugs interfere directly with nerves resulting in the analgesic effect. The beneficial effects *A. montana* in rheumatoid arthritis are explained due to the sesquiterpene lactones helenalin and its derivatives that directly inhibit the activation of transcription factors NFκB and NFAT, which reduces the activation of T cells and the secretion of pro-inflammatory cytokines like TNF-α and IL-2[82–84].

Green-lipped mussel preparations are used for their analgesic, anti-inflammatory, and joint protective properties. The effects are explained by omega-3 fatty acids interfering with cyclooxygenases, as well as by glucosamine and chondroitin which promote chondrocyte proliferation and collagen production counteracting cartilage degradation[85].

Olibanum is used in traditional ayurvedic medicine to treat rheumatic diseases. Boswellic acids were identified as active ingredient showing anti-inflammatory, anti-proliferative, and immunosuppressive properties, and demonstrated *in vivo* promising effects in the treatment of autoimmune diseases, such as rheumatoid arthritis, inflammatory bowel disease, and psoriasis. The beneficial effects of boswellic acids are mostly explained by the inhibition of cathepsin G and microsomal prostaglandin-E-synthase 1[83,84,86,87]. Cathepsin G is a serine protease mainly produced by neutrophils and stored in their granula. During the normal innate immune response, it is involved in the intra- and extracellular destruction of pathogens. As a component of the neutrophil proteolytic machinery, cathepsin G regulates inflammatory responses by stimulating the production of cytokines and chemokines, which are responsible for the activation and mobilization of immune cells to the site of infection. Furthermore, during inflammation, cathepsin G plays an important role in the degradation of extracellular matrix in the tissues, and is crucial for the formation of neutrophil extracellular traps[88]. Through inhibition of

microsomal prostaglandin-E-synthase 1, boswellic acids reduced the synthesis of prostaglandin E2 (PGE2), resulting in reduced inflammation[86]. Furthermore, similarly to the sesquiterpene lactones of *A. montana*, boswellic acids can inhibit NFκB and NFAT pathways, and thereby inhibiting T cell activation and proliferation[84,89].

Food supplements containing rose hip fruits to treat rheumatic disorders are gaining interests in Switzerland. Despite promising clinical outcomes, including decreased joint damage and pain with concomitant improved joint mobility, the active constituents of rose hip preparations and their mode of action remain unclear. In various *in vitro* studies, extracts have shown to possess anti-inflammatory properties, which are mainly explained by the reduced expression of pro-inflammatory cytokines and chemokines, the inhibition of NFκB signaling, and the suppression of cyclooxygenases and pro-inflammatory metalloproteases[90].

For the treatment of inflammatory skin diseases like psoriasis, as well as for wound treatment, a wide range of different traditional medicinal products have been effectively used in clinics[91–93]. Skin diseases and wounds are mostly topically treated with ointments, creams, or gels, and the base for such dosage forms often contains excipients coming from natural products. Often these base substances are not only intended to be inert excipients, they also have supporting effects like moistening or greasing of the skin, which may be beneficial in certain circumstances, or they have antioxidant and anti-inflammatory properties that support health promoting effects.

For dry and scaly skin, as it may be the case in diseases like psoriasis or atopic dermatitis, often oily base excipients are used, such as olive oil (*Olea europaea*) peanut oil (*Arachis hypogaea*), avocado oil (*Persea americana*), almond oil (*Prunus dulcis* var. *dulcis*), sesame oil (*Sesamum indicum*), soy oil (*Glycine max*), linseed oil (*Linum usitatissimum*), coconut oil (*Cocos nucifera*), palm oil (*Elaeis guineensis*), castor oil (*Ricinus communis*), and wheat germ oil (*Triticum aestivum*). Beside the plant oils also plant fats like cacao butter (*Theobroma cacao*) and shea butter (*Vitellaria paradoxa*), or waxes, such as jojoba wax (*Simmondsia chinensis*), carnauba wax (*Copernicia prunifera*), beeswax

(Cera flava, Cera alba; *Apis mellifera*), or sheep wool wax (lanolin, Adeps lanae; *Ovis aries*) are applied onto dry skin. To keep the skin moistened, especially in the treatment of wounds and burns, gels containing *Aloe vera* (syn. *Aloe barbadensis*) are used. Compared to the fatty base excipients, *Aloe vera* is often also used as the active ingredient, because beside its skin hydrating properties, polysaccharides such as acemannan showed to have anti-inflammatory and wound healing promoting effects by stimulating collagen synthesis and neo-angiogenesis[83,84,94].

Smaller wounds and slight inflammation on the skin are traditionally treated with herbal-based ointments containing marigold (Calendulae flos, *Calendula officinalis*), witch-hazels (Hamamelidis folium, *Hamamelis virginiana*), chamomile (Matricariae flos, *Matricaria chamomilla*, syn. *Matricaria recutita*), oak bark (Quercus cortex, *Quercus robur*, *Quercus petraea*, *Quercus pubescens*), *Arnica montana* (Arnicae flos), comfrey roots (Symphyti radix, *Symphytum officinale*), yarrow (Millefolii herba, *Achillea millefolium*), and red oil from *Hypericum perforatum* (oleum hyperici)[82–84].

For chronic skin inflammation, like in the various types of dermatitis, oral herbal preparations containing bittersweet stems (Dulcamarae stipites, *Solanum dulcamara*) or evening prime rose seed oil (Oenotherae seminis oleum, *Oenothera biennis*) are commonly used. For the topical treatment of dermatitis and psoriasis, traditionally used medicinal products contain chrysarobin (*Andira araroba*; syn. *Vataireopsis araroba*), wild pansy (Violae tricoloris herba, *Viola tricolor*), lesser balloon vine (*Cardiospermum halicacabum*), *Mahonia aquifolium* bark, birch bark (*Betula pendula*, *Betula pubescens*), olibanum (*Boswellia carteri*, *Boswellia serrata*), or Indian pennywort (*Centella asiatica*). In the psoralen plus UV-A (PUVA) photo chemotherapy of psoriasis, furanocoumarins obtained from plants like *Psoralea corylifolia* (syn. *Cullen corylifolium*) or *Ammi majus* have traditionally been used[82–84,91].

The beneficial effects on skin inflammation and wound healing of marigold are explained by antibacterial, anti-inflammatory, and granulation tissue promoting effects caused by triterpene alcohols like faradiol and their fatty acid 3-monoester derivatives of lauric, myristitic, and palmitic acid, as well as by flavonoids and

triterpene saponins. The antibacterial, anti-inflammatory, and wound healing properties of chamomile are mainly due to inhibitory effects on lipoxygenases and cyclooxygenases by flavonoids, sesquiterpenoids, the sesquiterpene lactone matricin, chamazulene, and chamazulene carboxylic acid. The use of yarrow in skin lesions is also mainly explained by its content of sesquiterpene lactones. The advantageous effects of witch-hazels and oak bark are caused by the astringent and anti-inflammatory effects of the tanning agents[82–84].

Evening primrose seed oil contains a high amount of γ-linolenic acid and is mainly used as an oral treatment for atopic dermatitis. The pathophysiology of atopic dermatitis is still not understood and it is thought to be multifactorial. One of the discussed pathological pathways is a decreased activity of δ-6-desaturase, an enzyme that converts linoleic acid, which is taken up by diet, into γ-linolenic acid. A decrease in γ-linolenic acid results in a decrease of prostaglandin E1 (PGE1). PGE1 exhibits anti-inflammatory properties by promoting the differentiation of Treg cells, leading to decreased activity of effector B cells and reduced production of IgE. An increased level of IgE is a typical indicator of atopic dermatitis. Hence, the supplementation of γ-linolenic acid through evening primrose seed oil is thought to enhance the levels of PGE1. This, in turn, is believed to amplify Treg cell activity, leading to a reduction in inflammatory processes caused by effector B cells producing IgE. Finally, this improvement in PGE1 levels and the resulting Treg cell activity helps to ameliorate the clinical symptoms of atopic dermatitis. However, different clinical studies provide conflicting results about the effectivity of evening primrose seed oil[82–84].

Extracts of the stems of *Solanum dulcamara* are used for the oral treatment of inflammatory skin diseases. The effect is explained by anti-inflammatory effects caused by steroid alkaloids and steroid saponins. However, literature about bittersweet stems is scarce[82–84].

One of the oldest traditional treatments specifically indicated for psoriasis was the topical application of Goa-powder obtained from the medullary rays of the

heartwood of *Andira araroba*. Extraction of the Goa-powder with benzene afforded so-called crude chrysarobin, a crystalline powder consisting of several anthrone derivatives, which substituted the Goa-powder in the treatment of psoriatic skin. Crude chrysarobin contains mainly pure chrysarobin (syn. chrysaphanol anthrone, 3-methyl-1,8-dihydroxyanthrone), as well as its enol form chrysaphanol anthranol, and physcion anthrone with its enol form physcion anthronol. In a smaller amount the oxidation product of chrysarobin the chrysophanic acid (syn. chrysophanol, 1,8-dihydroxy-3-methylanthraquinone) is found. Chrysarobin and chrysophanic acid are considered as the active constituents of the Goa-powder. Due to side effects and limited availability in the early 20th century, chrysarobin was replaced by the synthetic analog dithranol (syn. anthralin, cignolin). Since 2022, dithranol has been withdrawn from the market for the treatment of psoriasis due to the availability of more effective and less toxic alternatives[95,96]. The mode of action of anthrone derivatives is described by their low stability and their ability for fast oxidation to form danthrone derivatives. The oxidation process releases ROS and anthrone radicals that interfere with the respiration process in mitochondria and with DNA replication, resulting in anti-proliferative and anti-inflammatory effects in psoriatic skin[83,84,97]. Recently, there has been growing interest in the use of chrysophanic acid derived from *Rumex crispus* or *Rheum palmatum* for treating atopic dermatitis and inflammatory bowel disease. Chrysophanic acid demonstrated anti-inflammatory effects by reducing keratinocyte and T cell activation and proliferation. These effects are based on directly inhibiting NFκB signaling, which leads to a decrease in the secretion of pro-inflammatory cytokines[98–101].

A further treatment option used in psoriasis is the PUVA photo chemotherapy. PUVA is a therapy which applies UV-A light (380−315 nm) in combination with the previously administered psoralen derivative methoxsalen (8-methoxypsoralen, 8-MOP, xanthotoxin) to destroy psoriatic plaques. The cytotoxic and anti-proliferative effect of linear furanocoumarins of the psoralen type is based on their ability to interact directly with the DNA double strand. Firstly, furanocoumarins intercalate with pyrimidine bases. After applying UV-A light thymidine bases get

activated to bind covalently to intercalated furanocoumarins, which finally results in cross-linking of the single DNA strands. This prevents DNA replication and transcription, and leads finally to the apoptosis of affected cells. Furanocoumarins were usually obtained from *Psoralea corylifolia* or from the fruits of *Ammi majus*. However, furanocoumarins can also be obtained from other plants, such as *Heracleum mantegazzianum*, *Heracleum sphondylium*, *Angelica archangelica*, *Ficus carica*, or from several *Citrus*-species (e.g., pericarp or essential oils of bergamot orange *Citrus bergamia*)[83,84].

The beneficial anti-inflammatory, anti-proliferative, and keratolytic effects in the topical treatment of psoriasis with *Mahonia aquifolium* bark is explained by its content of bisbenzylisoquinoline, protoberberine (e.g., berberine), and aporphine alkaloids. It is assumed that the alkaloids may inhibit keratinocyte proliferation by reversible intercalation with DNA. Additionally, the whole extract reduced the activity of cyclooxygenases and lipoxygenases, *in vitro*. However, data about the effects of *Mahonia* bark is scarce[91,102].

Wild pansy contains flavonoids, salicylic acid ester derivatives, cyclotides, and mucilage. Its traditional use in inflammatory skin diseases may be explained by anti-inflammatory and keratolytic effects caused by salicylic acid ester derivatives. However, recent research demonstrated that *Viola* extracts reduce neutrophil infiltration into the skin, and that isolated cyclotides inhibit T cell activation and proliferation[91,103,104]. Willow bark has traditionally been used as anti-inflammatory, analgesic, and keratolytic treatment option for psoriasis. These beneficial effects are explained by the content of salicyl alcohol derivatives. Still to date, salicylic acid is routinely used as active ingredient in ointments for its keratolytic effects to treat psoriasis. Salicylic acid is often combined with urea, which is also frequently applied for its good keratolytic properties[105,106].

Cardiospermum halicacabum is traditionally applied topically for treating inflammatory skin diseases due to its anti-inflammatory and antipruritic effects. Beneficial properties are explained by its content of flavonoids and triterpene saponins[107]. The

ethanolic extract showed *in vitro* an inhibition of NFκB signaling, and reduced the expression of cyclooxygenases in macrophages and T cells. However, so far, no secondary metabolites have been identified that could be involved in these effects[108]. In small clinical studies beneficial effects could be shown, but more investigation is needed to assess the effectivity of lesser balloon vine preparations[107,109].

In the last few years two further plants gained interest in the treatment of dermatological issues, namely Indian pennywort (*Centella asiatica*) and *Betula pendula*. Indian pennywort showed *in vitro* and *in vivo* improvements in wound healing, scar treatment, and in psoriatic skin. As active constituents the triterpenes asiaticoside, madecassoside, asiatic acid, and madecassic acid have been identified. In wound healing *C. asiatica* extracts and isolated triterpenes promoted neo-angiogenensis, and induced fibroblast activation and proliferation, which resulted in increased collagen synthesis. Additionally, inhibitory effects on keratinocyte proliferation was shown. Asiatic acid and madecassic acid demonstrated anti-inflammatory potential by reducing the secretion of pro-inflammatory cytokines in macrophages[110,111]. Furthermore, asiatic acid and madecassoside improved psoriatic skin lesions by reducing the activity of TH17 cells, *in vivo*[112,113].

In 2016 the ointment Episalvan®, which contains a triterpene-enriched extract obtained from birch bark got approval for the treatment of wounds, and is also off-label used in psoriasis. The effects are not fully understood, but are explained by a high concentration of betulin. The betulin-containing ointment improved wound closure and re-epithelization in clinical studies. The dry triterpene-enriched extract demonstrated anti-inflammatory and keratinocyte migration promoting properties[114].

In the treatment of skin disorders, especially of wounds, resins and balsams are commonly used. Resins are brittle solids or highly viscous lipophilic exudates with yellow, brown, or red colors from plants with low essential oil content. If resins contain a high content of essential oil, the resin becomes more ductile and less

viscous, and is then called balsam. Emulsions of resins with mucilage are called gum resins. Resins and balsams contain mainly resin acids, which include carboxylic acids of terpenes (especially diterpene and triterpene acids), resin alcohols (lignans or benzyl alcohols), resin esters (esters of resin acids), benzoic and cinnamic acid derivatives, and essential oils. In history resins and balsams such as olibanum, myrrh (the gum resin from different *Commiphora* sp., mainly of *Commiphora myrrha*), turpentine and rosin (the resin of different conifers, especially of *Pinus* and *Larix* sp.), styrax benzoin (siam-benzoin from *Styrax tonkinensis*, sumatra-benzoin from *Styrax benzoin*), mastic (*Pistacia lentiscus*), and the *Myroxylon* balsams Peru balsam (*Myroxylon balsamum* var. *pereirae*) and tolu balsam (*Myroxylon balsamum* var. *balsamum*) are used for various ailments including skin irritations and wounds[83,84,115–117]. The beneficial effects for skin disorders and wounds are mainly explained by their greasing, anti-bacterial, anti-inflammatory, and granulation-tissue promoting properties, and their ability to support wound closure[118]. Recent research in this field demonstrated that lignans and diterpene resin acids, as main constituents of different conifer balsams, are able to support re-epithelization by increased migration and proliferation of keratinocytes *in vitro*[119,120]. Additionally, clinical trials revealed beneficial outcomes if wounds are treated with coniferous resins[118,121,122].

Propolis, or bee glue, is a natural resinous substance made by honey bees (*Apies mellifera*) that has traditionally been used to treat inflammatory skin diseases and wounds. The composition highly varies and comprises balsams, waxes, essential oil, and pollen components. Propolis is rich in flavonoids, phenylpropanoids, terpenoids, and lignans. The beneficial effects for the treatment of skin disorders and wounds are mainly explained by its anti-bacterial, anti-inflammatory, and wound healing promoting properties. Recent research, supported its traditional use in wound healing, since propolis has shown to accelerate tissue repair by stimulating hyaluronic acid synthesis, which is necessary for granulation tissue formation and wound closure[123,124].

In the last few years, in the field of traditional medicinal natural products a lot of herbal preparations have been investigated for possible immunosuppressive effects.

Some of the investigated plant species gained quite some interests for further investigation and development in the field of autoimmunity[7,125–129].

Curcuma longa extracts and its active ingredient curcumin has been shown to reduce T cell activation and proliferation in the mixed lymphocyte reaction. Curcumin exhibits anti-inflammatory effects by interfering with cyclooxygenases and NFκB signaling, and showed to interfere with the differentiation of effector T cells towards inflammatory TH1 and TH17 cells. In *in vivo* studies and small randomized controlled clinical studies, both *C. longa* extracts and curcumin showed beneficial effects in autoimmune diseases like psoriasis, inflammatory bowel disease, and multiple sclerosis. The mode of action is not fully understood and believed to be multifactorial by influencing different molecular targets. However, more clinical data is needed to confirm its effectivity in autoimmune diseases[127,128,130–133].

Triperygium wilfordii, a plant widely used in traditional Chinese medicine to treat rheumatoid arthritis, is currently undergoing intensive research to explore its potential in treating autoimmune diseases. The investigation comprises different extracts of the plant, as well as its major constituent triptolide and derivatives thereof, along with the triterpene celastrol. Extracts and triptolide effectively reduced activation and proliferation of T cells by inhibition of IL-2-mediated signal transduction. Additionally, inhibition of expression and secretion of various pro-inflammatory cytokines by T cells could be demonstrated. Furthermore, effectivity in rheumatoid arthritis could be established in *in vivo* and clinical studies. However, during clinical studies some toxic side effects have been identified[7,127,134–138].

A few years ago the traditional Chinese medicinal plant *Dichroa febrifuga* gained some attention in the media for the treatment of autoimmune diseases. The semi-synthetic drug halofuginone, synthesized from quinazoline alkaloid febrifugine, which has been isolated from the hydrangea roots, was found to exhibit strong inhibitory effects on the development of TH17 effector T cells without affecting other types of T cells. Therefore, halofuginone is considered as a new treatment

option for diverse autoimmune diseases and has been studied in animal models for rheumatoid arthritis and multiple sclerosis[139–142].

Due to high media influences in the last few years also cannabis (*Cannabis sativa*) and cannabinoids gained interest in autoimmunity research. Cannabis and its active ingredients demonstrated immune modulating effects by reducing the expression and secretion of pro-inflammatory cytokines through interaction with the cannabinoid-2 receptor (CB2R), which is mainly expressed on immune cells. The binding to cannabinoid receptors has been shown to reduce immune system activation and the migration of immune cells. Furthermore, the binding to cannabinoid receptors in immune cells induces apoptosis, suppresses transcription factors, and inhibits the release of cytokines. Tetrahydrocannabinol (THC) and cannabidiol (CBD) decreased *in vitro* the activation of TH17 cells resulting in a reduced secretion of pro-inflammatory IL-17. In murine models cannabinoids reduced T cell activation, proliferation, and the secretion of pro-inflammatory cytokines like IL-2. Even though, *in vitro* data and animal studies indicated beneficial effects in terms of autoimmunity, the mode of action is not fully understood and clinical studies for multiple sclerosis, rheumatoid arthritis, and inflammatory bowel disease are still lacking of clinical evidence[143,144].

More rather recent efforts in natural product research for autoimmune diseases are nicely summarized in the publications of Asadi-Samani *et al.* and Saurin *et al.*[127,128].

1.8 Current Research on Natural Products in Autoimmunity and Wound Healing

Currently, research in finding new therapeutics in the treatment of autoimmunity is mainly driven by the developments of novel biologics, such as monoclonal antibodies and fusion proteins, that are specific for certain targets. Due to this target specificity, it is assumed that such therapeutic interventions cause less side effects through hitting off-targets. Despite great specificity and effectivity, biologics have been shown to cause a variety of adverse side effects, such as cytokine release syndrome, hypersensitivity reactions, anti-drug antibodies, or loss of efficacy over time[145–149]. Therefore, huge efforts are undertaken to develop novel biologics that are less immunogenic, and more specific for certain targets. In this regard, a lot of research is done to unravel the modes of action involved in the pathogenesis of autoimmune diseases, aiming to find new target structures that can be tackled with novel therapeutics[145,147,150,151]. This, for example, led to the development of novel molecules interfering with Janus kinases (JAK) and phosphoinositide 3-kinases (PI3K), or to investigations how targeting sialic acid-binding immunoglobulin-type lectins (Siglecs) could impact the progress of autoimmune diseases[152–154]. Another recent approach comprises the usage of cellular therapies in which Treg cells or chimeric antigen receptor (CAR) Treg cells are investigated as potential novel therapeutics in the treatment of autoimmunity[155].

In the field of wound healing research a similar trend is observed, which is based on exploring in more detail the physiological interplay between immune cells, extracellular matrix, and epidermal cells, aiming to unravel novel molecular pathways or targets that are involved in the wound healing process[156–159]. When it comes to wound treatment, the emphasis is less on discovering new drugs and more on developing innovative formulations to enhance drug accessibility to the skin. This involves for example the improvement of wound dressings that incorporate components of the extracellular matrix, such as hyaluronic acid and collagen, along with growth factors. Additionally, the use of stem cells is explored as they have the potential to stimulate neo-angiogenesis, keratinocyte proliferation, and fibroblast

activity. Further approaches are aimed to develop new skin transplants, or to improve physical interventions like cryotherapy, pressure therapy, or laser therapy[78,79,158,160–163].

In order to address complex multifactorial diseases, such as autoimmunity and wound healing, researchers are exploring additional approaches that focus on identifying novel multi-target therapeutics. Such therapeutics have the potential to simultaneously hit multiple targets involved in disease pathogenesis, which may offer a more comprehensive approach to treat this group of diseases. The goal is either to develop one molecule that interferes on multiple molecular targets, or to use a therapeutic interventions that are composed of several substances, which may act synergistically on the same or on different targets[151,164–166].

One approach that goes into the direction of multi-component treatments includes the investigation of natural products and extracts coming from herbals, fungi, bacteria, or animals[92,94,167–170]. Natural products and their diverse chemical scaffolds remain a crucial and valuable source for the discovery of novel chemical entities in the field of drug development. Therefore, such approaches have the potential to uncover novel chemical structures from nature that could be used as single drug treatments or serve as lead structures for subsequent improvements by medicinal chemistry, leading to the development of new semi-synthetic derivatives[39,171,172]. This natural product based approach led to the discovery of some of the most famous and most frequently used drugs in the treatment of autoimmune diseases like cyclosporine, tacrolimus, rapamycin, fingolimod, or mycophenolate mofetil[173].

The search of novel potential immunosuppressive natural products often starts with an *in vitro* lymphocyte proliferation assay. In such assays human peripheral blood mononuclear cells (PBMCs) or the mixed lymphocyte reaction (MLR) is used. These assays can be combined by evaluating the expression and secretion of various cytokines with fluorescence-activated cell sorting (FACS) or enzyme-linked immunosorbent assay (ELISA) based approaches[1]. Natural extracts that are able to reduce the activation and proliferation of T cells can be further investigated in

additional *in vitro*, *ex vivo*, or *in vivo* test systems that are specific for certain autoimmune diseases[174–178]. Follow-up steps often include the chemical characterization of active extracts using chromatographic and spectroscopic methods, which can be combined with dereplication strategies, such as advanced MS/MS-based annotation, to identify and annotate the compounds present in the extract[179–186]. Chemical components of the extract can be isolated by an activity-guided approach with the goal to identify the specific compounds responsible for the observed effects of the extract[89,187–194]. A recent successful case by applying this approach is the identification of novel immunosuppressive cyclotides derived from *Oldenlandia affininis* and *Viola tricolor*, that are now entering early stage clinical trials for the treatment of multiple sclerosis and ulcerative colitis, respectively[103,195,196].

A wide range of *in vitro*, *ex vivo*, and *in vivo* test systems specific to autoimmune diseases are available, offering diverse experimental endpoints. For example, extracts that may have an impact on psoriasis can be explored *in vitro* on HaCaT keratinocytes, in different *ex vivo* test systems, and in animal models with experimental endpoints ranging from keratinocyte migration and proliferation, expression and secretion of inflammatory cytokines, up to *in vivo* plaque formation[197–201]. Similar approaches are followed for different autoimmune diseases, such as multiple sclerosis, rheumatoid arthritis, and type I diabetes[202–205].

The study of natural products in the field of wound healing is basically similar to that described for autoimmune diseases. However, the goal is not focused on finding new and extraordinary drugs as it might be the case for autoimmunity. The primary objective is to explore natural preparations that have a well-established traditional usage in promoting wound healing, since these preparations are sought as cost-effective and affordable alternatives for wound treatment[94,206]. Due to the well-established foundational knowledge gained from traditional use, research on herbal preparations for wound healing predominantly focuses on *in vitro* or *ex vivo* studies, which is in contrast to the research in the field of autoimmunity that often places greater emphasis on *in vivo* studies[206]. The most routinely used *in vitro* assays are scratch and proliferation assays using different types of cells, such as

keratinocytes, fibroblasts, endothelial cells, and immune cells, to examine cell migration and proliferation. Scratch assays are often combined with ELISAs to study expression and secretion of various cytokines that are involved in the wound healing process[199,206–213]. Frequently, fibroblasts are investigated in 3D *in vitro* models to study their migration, as well as their influence on the production of collagen and other components of the extracellular matrix[206,212,213]. Although *in vitro* and *ex vivo* models offer valuable insights into the potential mechanisms of action in wound healing, it is recommended to further investigate herbal preparations in *in vivo* and clinical studies. Such attempts are crucial to assess the influence of herbal preparations on all phases of the wound healing process, and to confirm their traditional usage. Unfortunately, despite promising effects in *in vitro* and *ex vivo* studies, many herbal preparations remain largely unexplored in the pre-clinical stage without further investigation[206]. Therefore, the next phase includes *in vivo* studies using animal models, such as wound incision, excision, or burn models. These models are employed to examine tissue repair, assess the time-dependent reduction of wound size, and evaluate histological changes. Furthermore, *in vivo* models are used to study granulation tissue formation, neo-vascularization, extracellular matrix remodeling, wound contraction, and scar formation[206,213,214].

2. Aim of the Work

Autoimmune dysfunction affects around 5–10% of the human population, with increasing incidence. Increased activation and proliferation of T cells plays an essential role in the development of chronic inflammation and autoimmune diseases. Currently used immunosuppressive drugs often do not provide long-lasting relief of symptoms and show a gradual loss of efficacy over time. Moreover, they are frequently associated with various side effects. Certain autoimmune diseases, such as psoriasis or type I diabetes, are commonly accompanied by the formation of chronic and non-healing inflammatory wounds. Worldwide, millions of people suffer from difficult-to-treat wounds, and currently available treatment options provide only partial effectiveness. The treatment of non-healing wounds often needs hospitalization and generates steadily increasing healthcare costs. Therefore, for both, autoimmunity and wound healing novel therapies are needed.

The first goal of this work is to discover novel immunosuppressive lead substances. For this purpose, an in-house library consisting of 600 extracts of plants from Panama should be screened for inhibition of human T cell proliferation. Given that plant extracts are complex mixtures of chemical substances, HPLC-based activity profiling will be performed, aiming to identify substances that are considered to be responsible for effects, observed with the whole extracts. After bioactivity-guided and scaled-up isolation procedures through a combination of various chromatographic techniques, obtained compounds will be characterized by high-resolution mass spectrometry (HRMS) and spectroscopic methods, such as UV spectroscopy, nuclear magnetic resonance (NMR), electronic circular dichroism (ECD), optical rotation, and single X-ray crystallography. As autoimmune diseases are influenced by different inflammatory cytokines, next steps include to explore the impact of plant extracts and isolated secondary metabolites on the expression and secretion of cytokines by activated T cells.

The second project aims at the valorization of saffron corms, that currently arise in significant amounts during saffron spice production as a biowaste product without any use. Extracts and isolated substances from corms will be tested in HaCaT keratinocytes for possible effects on the expression and secretion of pro-

inflammatory cytokines. Potential active substances will be further characterized with the goal to find compounds that may exert beneficial effects in the treatment of inflammatory skin diseases, such as psoriasis or atopic dermatitis.

For the last project, an ethnopharmacological approach is followed to search plant extracts that might be useful alternatives in the treatment of wounds. In this regard, the wound healing activity of a plant used in Algerian traditional medicine should be confirmed in a rabbit excision model. The active extract should then be phytochemically characterized to identify compounds, which might be involved in the observed beneficial wound healing effects.

Thus, the primary objective of this work is to identify and isolate secondary metabolites from plant extracts that possess wound healing and immunomodulatory properties. Both, *in vitro* and *in vivo* approaches will be applied to discover and identify plant-based preparations and novel molecules that might have the potential to be further developed for the treatment of inflammatory conditions, such as autoimmunity or non-healing wounds.

3. Results

The chapters "*Results*" and "*Discussion, Conclusion, and Outlook*" is based on following peer-reviewed publications:

Publication 1

Aryltetralin lignans from *Hyptis brachiata* inhibiting T lymphocyte proliferation

Keller M., Winker M., Zimmermann-Klemd A. M., Sperisen N., Gupta M. P., Solis P. N., Hamburger M., Potterat O., Gründemann C.

Publication 2

Saponins from saffron corms inhibit the gene expression and secretion of pro-inflammatory cytokines

Keller M., Fankhauser S., Giezendanner N., König M., Keresztes F., Danton O., Fertig O., Marcourt L., Hamburger M., Butterweck V., and Potterat O.

Publication 3

Teucrium polium – wound healing potential, toxicity and polyphenolic profile

Chabane S., Boudjelal A., Keller M., Doubakh S., Potterat O.

Publication 4

New neo-clerodane diterpenes from *Teucrium polium* subsp. *capitatum*

Keller M., Chabane S., Boudjelal A., Danton O., Prescimone A., Hamburger M., Potterat O.

3.1 Publication 1

Aryltetralin lignans from *Hyptis brachiata* inhibiting T lymphocyte proliferation

Morris Keller‡, Moritz Winker‡, Amy Marisa Zimmermann-Klemd, Nino Sperisen, Mahabir P. Gupta, Pablo N. Solis, Matthias Hamburger, Olivier Potterat, Carsten Gründemann

Biomedicine & Pharmacotherapy **160**, 114328 (2023)
doi: 10.1016/j.biopha.2023.114328

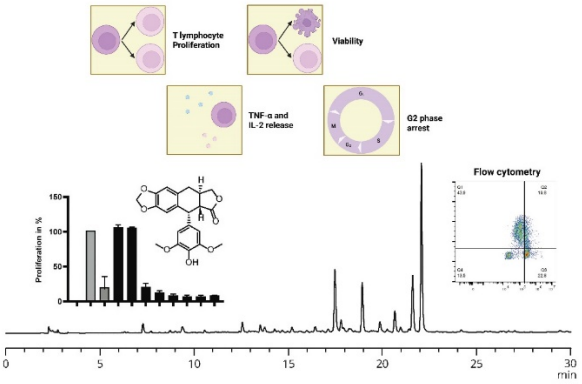

An in-house library of 600 plant extracts from plants endemic in Panama was screened to find extracts that inhibit T lymphocyte proliferation, with the aim of discovering potential leads for autoimmune disease treatment. As one of the hits, an ethyl acetate extract of *Hyptis brachiata* exhibited strong inhibitory effects and was further investigated. Seven aryltetralin lignans, five arylnaphthalene lignans, two flavonoids, three triterpenes, and cinnamyl cinnamate were isolated and tested for their inhibitory effects on T lymphocyte proliferation. The aryltetralin lignans were particularly effective, inhibiting T lymphocyte proliferation without inducing apoptosis and causing cell cycle arrest in G2/M phase. The extract and isolated triterpenes showed weak suppression of IL-2 and TNF-α production. *H. brachiata* could be further studied as an herbal alternative for treating T lymphocyte-mediated autoimmune diseases.

‡ These authors contributed equally

The supporting information is available in the appendix

Contribution to this publication:
Extraction, isolation, and structure elucidation of the compounds from *H. brachiata*

Biomedicine & Pharmacotherapy 160 (2023) 114328

Contents lists available at ScienceDirect

Biomedicine & Pharmacotherapy

journal homepage: www.elsevier.com/locate/biopha

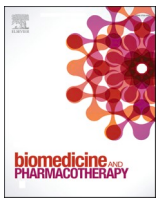

Aryltetralin lignans from *Hyptis brachiata* inhibiting T lymphocyte proliferation

Morris Keller [a,1], Moritz Winker [b,1], Amy Marisa Zimmermann-Klemd [b], Nino Sperisen [a], Mahabir P. Gupta [c], Pablo N. Solis [c], Matthias Hamburger [a], Olivier Potterat [a,*,2], Carsten Gründemann [b,*,3]

[a] Division of Pharmaceutical Biology, University of Basel, Klingelbergstrasse 50, CH-4056 Basel, Switzerland
[b] Translational Complementary Medicine, Department of Pharmaceutical Sciences, University of Basel, Campus Rosental – Mattenstrasse 22, CH-4058 Basel, Switzerland
[c] Centro de Investigaciones Farmacognosticas de la Flora Panamena (CIFLORPAN), Facultad de Farmacia, Universidad de Panama, Panama City, Republic of Panama

ARTICLE INFO

Keywords:
T lymphocyte proliferation
Autoimmune diseases
Flow cytometry
Hyptis brachiata
Aryltetralin lignans

ABSTRACT

Increased activation and proliferation of T lymphocytes plays an essential role in the development of chronic inflammation and autoimmune diseases. Currently used immunosuppressive drugs often do not provide long-lasting relief of symptoms and show a gradual loss of efficacy over time, and are accompanied by various side effects. Therefore, novel immunosuppressive lead substances are needed. For this purpose, an in-house library consisting of 600 extracts of plants from Panama was screened for inhibition of human T lymphocyte proliferation. As one of the hits, an ethyl acetate extract from the aerial parts of *Hyptis brachiata* (Lamiaceae) exhibited strong inhibitory effects. Subsequent investigation resulted in the isolation of seven aryltetralin lignans, five arylnaphthalene lignans, two flavonoids, three triterpenes, and cinnamyl cinnamate. Aryltetralin lignans inhibited T lymphocyte proliferation in a concentration-dependent manner without induction of apoptosis. No relevant inhibition was observed for the arylnaphthalene lignans, flavonoids, and triterpenes. Additional cell cycle arrest investigations revealed that isolated aryltetralin lignans potently inhibited cell division in G2/M phase similarly to podophyllotoxin. Multifluorescence panel analyses of the extract also showed weak suppressive effects on the production of IL-2 and TNF-α. Therefore, preparations made out of *H. brachiata* could be further explored as an interesting herbal alternative in the treatment of autoimmune diseases.

1. Introduction

Autoimmune dysfunction affects 5% of the population and refers to a disorder in which the body's immune tolerance is impaired, resulting in a reaction to the body's own cells and tissues [1]. Autoimmune diseases are treated symptomatically, as no causal therapy is currently available [2]. Moreover, therapy with current drugs suffers from several limitations, such as various side effects, nonresponding, increased susceptibility to infections, and high treatment costs [3–6]. Therefore, continued research into new therapies is mandatory.

Enhanced activation and proliferation of T lymphocytes is known to play a crucial role in the pathogenesis of autoimmune diseases and chronic inflammation, such as type I diabetes, rheumatoid arthritis, psoriasis, or multiple sclerosis [7]. Therefore, targeted therapies that specifically enhance inhibitory pathways in lymphocytes are an attractive approach to augment disease resolution in an attempt to effectively treat human autoimmune diseases [8]. In this context, we started a project aimed at the discovery of new plant-derived immune-modulating substances which specifically inhibit the activation and proliferation of human T lymphocytes. For this purpose, an in-house library consisting of 600 extracts of plants from Panama was screened for potential T lymphocyte inhibition. As one of the hits, an ethyl acetate extract from the aerial parts of *Hyptis brachiata* Briq. (Lamiaceae) exhibited strong inhibitory effects.

H. brachiata is native to Central America. In Venezuela the infusion of the whole plant is traditionally used as an antiseptic, a wound-healing

* Corresponding authors.
E-mail addresses: olivier.potterat@unibas.ch (O. Potterat), carsten.gruendemann@unibas.ch (C. Gründemann).
[1] These authors contributed equally to the work.
[2] Orcid.org/0000–0001-5962–6516
[3] Orcid.org/ 0000–0003-0240–0342

https://doi.org/10.1016/j.biopha.2023.114328
Received 18 November 2022; Received in revised form 23 January 2023; Accepted 27 January 2023
Available online 3 February 2023

agent, and as a treatment of ulcers and cancers [9]. Pharmacological data on *H. brachiata* are scarce. Recently, an ethyl acetate extract of the aerial parts showed moderate inhibition of aberrant AKT signaling in MM121224 human melanoma cells, and the methoxylated flavonoid sideritoflavone was identified as active compound [10]. Apart from that very little is known about chemical constituents from *H. brachiata*. In a study on the essential oil obtained from the leaves of *H. brachiata,* various compounds such as α-humulene, germacrene A, germacrene D, *E*-caryophyllene, and γ-cadinene were identified [11].

We report here on a comprehensive phytochemical profiling of *H. brachiata*, and on the identification of the constituents inhibiting T lymphocyte proliferation. The active aryltetralin lignans were further investigated in a cell cycle arrest assay. In addition, the impact of the extract and isolated substances on functional T lymphocyte suppression was explored.

2. Material and methods

2.1. General chromatographic procedures

Flash chromatography was carried out on a PuriFlash® 4100 system equipped with an UV detector and fraction collector (Interchim, Montluçon, France).

Preparative HPLC was done on a Preparative LC/MSD System (Agilent Technologies, Santa Clara, CA, USA) consisting of a binary pump (1260 Prep Bin Pump), a quaternary pump (Infinity II 1290), a PDA detector (1100 Series), and a 6120 single quadrupole MS detector. A SunFire Prep C18 OBD column (5 μm, 150 × 30 mm i.d., Waters, Milford, MA, USA), equipped with a C18 Prep Guard Cartridge (10 × 30 mm i.d.) was used. MeCN and water, both containing 0.1% formic acid (FA), was used as mobile phase for all preparative separations. A flow rate of 20 mL/min was applied. A 1290 Infinity II Valve Drive manual injection system (Agilent Technologies) was used for injection. Data acquisition and processing was done by ChemStation software (Agilent Technologies).

For semi-preparative separations an Agilent HP1100 Series HPLC instrument (Agilent Technologies, Santa Clara, CA, USA) equipped with a binary pump (G1312A bin pump), auto sampler (G1357A WPALS), column oven (G1316A COLCOM), and a diode array detector (G1315A DAD), or an Alliance 2690 HPLC system equipped with a DAD 996 detector (Waters, Milford, MA, USA) were used. Chromatography was performed either on a SunFire C18 column (5 μm, 150 × 10 mm i.d., Waters) or on a ReproSIL-Pur 120 C18-AQ column (3 μm, 150 ×10 mm i.d., Dr. Maisch GmbH, Ammerbuch-Entringen, Germany), both equipped with a guard column (10 × 10 mm i.d.). The mobile phases used consisted of MeCN or MeOH and water, all containing 0.1% FA. The flow rate was 4 mL/min. Data acquisition and processing was performed using ChemStation (Agilent Technologies, Santa Clara, CA, USA) or Empower software (Waters, Milford, MA, USA).

Microfractionation and HPLC-PDA-ELSD-ESIMS analyses were performed on a LC-MS 8030 system (Shimadzu, Kyoto, Japan) consisting of a degasser, auto-sampler, quaternary pump (LC-20 CE), a column oven (CTO-20AC), a PDA detector (SPD-M20A) connected via a T-split to a triple quadrupole MS and an ELSD 3300 detector (Alltech, Deerfield, IL, USA). Separations were either carried out on a SunFire C18 column (3.5 μm, 150 × 3 mm i.d., Waters, Milford, MA, USA), or on a ReproSIL-Pur 120 C18-AQ column (3 μm, 150 × 3 mm i.d., Dr. Maisch GmbH, Ammerbuch-Entringen, Germany), both equipped with a guard column (10 × 3 mm i.d.). The mobile phases consisted of MeCN or MeOH and water, all containing 0.1% FA. The flow rate was 0.4 mL/min. The LabSolutions software (Shimadzu) was used for data acquisition and processing.

TLC was performed on silica gel 60 F254-coated aluminum plates (ALUGRAM Xtra Nano-SIL G, Macherey-Nagel, Düren, Germany). Detection was with UV 254 nm, UV 366 nm, and after spraying with 1% ethanolic vanillin and 10% sulfuric acid in EtOH followed by heating at 110 °C.

Silica gel 60 (0.040–0.063 mm) used for flash chromatography was obtained from Merck (Darmstadt, Germany). HPLC-grade solvents MeCN, MeOH (Avantor, Radnor, PA, USA), and water from a Milli-Q water purification system (Merck Millipore, Billerica, USA) were used for HPLC separations. HPLC-grade formic acid (FA) and DMSO were obtained from Scharlau (Scharlab S.L., Spain). Technical grade EtOAc, MeOH, and *n*-hexane (Rheuss Chemie, Tägerig, Switzerland) were redistilled before use for extraction and MPLC. Rosmarinic acid was purchased from Sigma (Darmstadt, Germany).

2.2. General procedures for physicochemical characterization

NMR spectra were recorded on a Bruker Avance III NMR spectrometer operating at 500.13 MHz for ^{1}H and 125.77 MHz for ^{13}C at 23 °C, or on a Bruker Avance NEO NMR spectrometer operating at 600.15 MHz for ^{1}H at 25 °C (both Bruker BioSpin, Rheinstetten, Germany). ^{1}H NMR, COSY, HSQC, HMBC, NOESY, and ROESY spectra were measured in a 1 mm TXI, a 5 mm BBO, or a 3 mm TCI cryoprobe. Spectra were recorded in $CDCl_3$ (Sigma-Aldrich, St. Louis, MO, USA) or DMSO-d_6 (ARMAR Chemicals, Döttingen, Switzerland). Data were analyzed using Bruker Topspin 3.5 and ACD/Labs NMR Workbook suites software. Chemical shifts are reported as δ values (ppm) using the solvent signal (δ_H 2.50; δ_C 39.51 for DMSO-d_6 or δ_H 7.27; δ_C 77.00 for $CDCl_3$) as internal reference; coupling constants (J) are given in Hz.

Optical rotations were measured in $CHCl_3$ or MeOH (1 mg/mL) on a JASCO P-2000 polarimeter (Brechbühler AG, Schlieren, Switzerland) equipped with a 10 cm temperature-controlled microcell and a sodium light source (589 nm).

2.3. Plant material

Aerial parts of *Hyptis brachiata* Briq. were collected in August 1990 in El Valle de Antón, El Pinar, Coclé Province (Panama) by CIFLORPAN. The taxonomic identity was confirmed by Carmen Galdames, botanist at CIFLORPAN, and a voucher specimen (no. 89710) deposited at the herbarium of the University of Panama. A voucher specimen is also available at the Division of Pharmaceutical Biology, Department of Pharmaceutical Sciences, University of Basel (no. 1181).

2.4. HPLC-based activity profiling

The EtOAc extract of *H. brachiata* aerial parts stored in our in-house library was used for HPLC-based activity profiling. Microfractionation was carried out by analytical RP-HPLC on an LC-MS 8030 system (Shimadzu, Kyoto, Japan) connected to an FC 204 fraction collector (Gilson, Mettmenstetten, Switzerland) adapted for 96-deep-well plates. Three injections of the extract (10 mg/mL in DMSO) were performed: 2 × 30 μL (corresponding to 600 μg of extract) using only a PDA detector for collection of microfractions, and 1 × 10 μL with PDA-ELSD-ESIMS detection without collection. As mobile phase MeCN and water was used, both containing 0.1% FA. The gradient was 5–100% MeCN in 30 min, followed by a final hold for 5 min at 100% MeCN. Fractions of 1 min each were collected from 0 to 35 min. Microfractions of two successive injections were collected into the same wells of a 96-deep-well plate. The plate was dried in a Genevac EZ-2 evaporator (Genevac, Ipswich, England).

The dried microfractions were re-suspended in 25 μL of DMSO for use in the proliferation assays. 1 μL of this dilution was used in 100 μL of cell suspension (2 * 10^6 cells/mL) as maximal concentration, and 1:3 titrations were performed for a total of six concentrations. With this approach the relative activity of the fractions was assessed in a concentration-dependent manner. The HPLC-PDA-ELSD-ESIMS chromatograms were correlated with the activity of the fractions to generate the activity profile.

2.5. Large scale extraction and isolation

The ground plant material (712 g) was percolated with EtOAc (9 L), followed by MeOH (17 L) as previously reported [10]. Evaporation under reduced pressure yielded 9.4 g of EtOAc (1.3%) and 27.4 g of MeOH extract (3.8%).

The EtOAc extract (9.3 g) was separated by flash chromatography. The sample was dissolved, mixed with 35 g of silica gel 60 (0.040–0.063 mm) and dried, prior to loading onto a self-packed silica 60 glass column (0.040–0.063 mm, column size: 46 × 7 cm, i.d.). A gradient of EtOAc in *n*-hexane [2% (0–10 min), 2–70% (10–450 min), 70–100% (450–570 min), 100% (570–615 min)], followed by MeOH in EtOAc [0–50% (615–735 min), 50–100% (735–750 min), 100% (750–810 min)] was applied at a flow rate of 20 mL/min. A total of 808 fractions were collected and combined into 28 fractions (F1–F28) based on TLC analysis.

Further separation of F19 (206 mg) by preparative HPLC with a gradient of 30–100% MeCN in water in 30 min afforded 8 fractions (F19.1–F19.8). Follow-up purification of F19.1 (4.2 mg) by semi-preparative HPLC on a ReproSil-Pur 120 C18-AQ column eluted with a gradient of 30–60% MeCN in water in 30 min yielded compound **2** (1.9 mg, t_R 14.7 min). Compound **1** (25.2 mg, t_R 13.3 min) was isolated by semi-preparative HPLC from F19.2 (37.2 mg) on a ReproSil-Pur 120 C18-AQ column eluted with 38% MeCN in water. Further separation of F19.4 (12 mg) using a combination of semi-preparative HPLC with a SunFire C18 column with 37% MeCN in water, followed by semi-preparative HPLC using a ReproSil-Pur 120 C18-AQ column with 48% MeCN in water afforded a crude lignan mixture F19.4.3.1 (10.6 mg) and **17** (1.3 mg, t_R 10.2 min). F19.4.3.1 was further purified using semi-preparative HPLC on a SunFire C18 column with a gradient of 45–70% MeOH in water in 30 min, yielding **3** (8.7 mg, t_R 17.4 min) and **4** (2.4 mg, t_R 18.6 min). Separation of F19.7 (11.8 mg) by semi-preparative HPLC on a ReproSil-Pur 120 C18-AQ column with a gradient of 47–62% MeCN in water in 30 min gave **15** (5.5 mg, t_R 14.9 min) and **10** (6.3 mg, t_R 15.8 min). F19.8 (10.3 mg) was further purified over a semi-preparative SunFire C18 HPLC column with 45% MeCN in water resulting in **9** (5.7 mg, t_R 19.1 min). F20 (707 mg) was further fractionated by preparative HPLC applying a gradient of 30–100 MeCN in water in 30 min to yield fractions F20.1–F20.4. Fraction F20.3 (35.0 mg) was purified by semi-preparative HPLC on a ReproSil-Pur 120 C18-AQ column using a gradient of 35–75% MeCN in water in 30 min yielding fraction F20.3.4 (22.4 mg). Further purification of F20.3.4 by semi-preparative HPLC on a ReproSil-Pur 120 C18-AQ column using a gradient of 55–75% MeOH in water in 30 min gave **7** (5.2 mg, t_R 11.8 min) and **8** (16.3 mg, t_R 18.6 min). Fractionation of F21 (249 mg) by preparative HPLC with a gradient of 5–100% MeCN in water in 30 min gave 21 fractions F21.1–F21.21. F21.21 was identified as **13** (18.6 mg, t_R 29.6 min). Further separation of F21.11 (6.4 mg) by semi-preparative HPLC with a SunFire C18 column and a MeCN gradient in water of 30–85% in 30 min afforded **12** (1.7 mg, t_R 9.7 min), **11** (0.5 mg, t_R 16.8 min), and **18** (0.6 mg, t_R 30.0 min). Further separation of F21.12 (7.1 mg) using semi-preparative HPLC with a SunFire C18 column with 36% MeCN in water afforded **5** (3.3 mg, t_R 11.1 min). Fraction F21.13 (17.9 mg) was further purified using semi-preparative HPLC with a gradient of 30–60% MeCN in water in 30 min on a ReproSil-Pur 120 C18-AQ column to yield **6** (2.5 mg, t_R 15.2 min) and **16** (8.9 mg, t_R 15.9 min). Purification of F21.16 (21.5 mg) by semi-preparative HPLC on a SunFire C18 column with a gradient of 42–62% MeCN in water in 30 min yielded **14** (4.7 mg, t_R 15.5 min). NMR and HPLC purity of the compounds was > 90% except for **11** and **14** (both approximately 85%), for **13** (approximately 80%), and for **15** (approximately 75%). The impurity in compounds **11**, **13**, and **15** was an unidentified triterpene.

In addition, a minor peak at t_R 12.2 min in the HPLC chromatographic trace of the EtOAc extract was identified as rosmarinic acid (**19**) based on UV and MS data and chromatographic comparison with a commercial reference. Rosmarinic acid was a major peak in the UV 254 nm trace of the MeOH extract (Data not shown).

2.6. Ethics approval statement

All adult, healthy blood donors gave written informed consent for blood collection. The blood samples were obtained in an anonymized and coded form, without any visible ID number, from the central blood donation of the University Hospital in Basel. The work therefore does not fall within the scope of the Swiss Human Research Act. Thus, no ethics vote by the Ethics Committee Central and Northwestern Switzerland is required for the methods used to work with the blood samples.

2.7. Preparation and cultivation of human peripheral lymphocytes

Isolation of PBMCs was performed by centrifugation over a LymphoPrep™ gradient (1.077 g/cm^3, 20 min, 500 g, 20 °C; Progen). White blood cells were isolated and washed twice with phosphate-buffered saline (PBS, GE Healthcare). Cultivation was performed in an incubator at 37 °C, 5% CO_2, and 95% air atmosphere using RPMI 1640 medium supplemented with 10% fetal calf serum (FCS, GE Healthcare Life Sciences), 2 mM L-glutamine, 100 U/mL penicillin, and 100 U/mL streptomycin (all from Sigma-Aldrich).

2.8. Treatment with extracts and compounds

Isolated cells were treated with extracts (0.3–100 μg/mL) and compounds (0.01–100 μM). Cyclosporine (5 μg/mL; Sandimmun®), staurosporine (0.3 μM; Tocris), and vinblastine (0.03 μM; Tocris) were used as controls. Commercial podophyllotoxin (Sigma-Aldrich) was also included as a reference substance and was named **5** in the manuscript. All cells were stimulated with soluble CD3 and CD28 monoclonal antibodies (mAbs) (eBioscience) at 100 ng/mL, except the unstimulated controls. Experiments were repeated at least three times.

2.9. T lymphocyte proliferation assay

Isolated PBMCs (5 *10^6 cells/mL) were stained with carboxyfluorescein diacetate succinimidyl ester (CFSE; 5 μM: Sigma-Aldrich) for 10 min at 37 °C with carboxyfluorescein diacetate succinimidyl ester (CFSE; 5 μM: Sigma-Aldrich). The staining was stopped by addition of RPMI complete medium. Excess of CFSE was removed by washing. Cells (2 * 10^6 cells/mL) were treated for 72 h and cell proliferation was analyzed by CytoflexS (Beckman Coulter) and FlowJo software (BD Biosciences).

2.10. Cell death assay

Isolated PBMCs (2 * 10^6 cells/mL) were treated for 72 h and then stained with Annexin V-FITC (eBioscience) as recommended by the manufacturer's instructions. The percentage of apoptotic cells was determined using CytoflexS (Beckman Coulter) and FlowJo software (BD Biosciences).

2.11. Cell cycle assay

Isolated PBMCs (2 * 106 cells/mL) were treated for 72 h and subsequently washed with 4 °C cold PBS. Cells were re-suspended in 3 mL ice cold 70% ethanol and fixed overnight at −20 °C. After fixation, cells were washed and stained in 200 μL staining solution (1 μL propidium iodide (1 mg/mL; Sigma-Aldrich) in 199 μL PBS) for 30 min at room temperature in the dark. The measurement was performed with a CytoflexS (Beckman Coulter).

2.11.1. Analysis of the activation status and cytokine production of human T lymphocytes

Isolated PBMCs were treated with anti-CD3 and anti-CD28 mAbs for 40 h before restimulation and afterwards re-stimulated with phorbol-12-myristate-13-acetate (PMA, 50 ng/mL; Sigma-Aldrich) and ionomycin (1 μg/mL; Sigma-Aldrich) (except the unstimulated control) for further 4 h. To block the Golgi apparatus, cells were treated with GolgiPlugTM (1 μL/mL; BD Biosciences) and GolgiStopTM (0.65 μL/mL; BD Biosciences) and incubated simultaneously due to the restimulation process. The cell surface was stained with two separate panels (panel 1: CD3-APC AlexaFluor750, CD4-AlexaFluor700, CD69-PC7; panel 2: CD3-APC Alexa Fluor750, CD8-AlexaFluor700, CD69-PC7 (all Abs from Beckman-Coulter)) for 30 min at room temperature in the dark. Cells were re-suspended in 100 μL Cytofix/Cytoperm solution for 15 min at 4 °C. Cells were intracellularly stained with two different panels (panel 1: IFN-γ FITC (Beckman-Coulter), IL-2 APC (BD), TNF-α PE (Beckman-Coulter), IL-21 BV421 (BD); panel 2: IFN-γ FITC, TNF-α PE, MIP1-β BV421 (all Abs from Beckman-Coulter)) for 30 min at 4 °C. Afterwards, the cells were fixed with 2% paraformaldehyde (PFA; Electron Microscopy Sciences) for 10 min at 4 °C. Analysis was performed using a CytoflexS flow cytometer (Beckman Coulter) and FlowJo software (BD Biosciences).

2.12. Data analysis

For statistical analysis, data were processed with PRISM software (version 9.3.1 for PC, GraphPad Software). The Shapiro-Wilk test was used to test for a normal distribution. A multiple group comparison was performed with the Brown-Forsythe and Welch ANOVA, followed by Dunnetś T3 post-hoc test. Values are presented as mean ± standard deviation differences from controls (*$p < 0.05$, **$p < 0.01$, ***$p < 0.001$, ****$p < 0.0001$.).

3. Results

3.1. Effect of H. brachiata EtOAc extract on proliferation and apoptosis of human T lymphocytes

An in-house library consisting of 600 extracts of plants collected in Panama was screened at a single concentration of 20 μg/mL for inhibition of human T lymphocyte proliferation using carboxyfluorescein succinimidyl ester (CFSE) staining and flow cytometric analysis. The active extracts were subsequently tested for suppression of T lymphocyte division at six concentrations ranging from 0.3 to 100 μg/mL. Among the hits, an ethyl acetate extract obtained from the aerial parts of *H. brachiata* significantly inhibited the proliferation of human T lymphocytes in a concentration range from 1 to 100 μg/mL (Fig. 1). Apoptosis induction in the concentration range was excluded by annexin V-FITC staining (Fig. 1). Cytotoxicity of the vehicle (DMSO) was also tested. The data showed that the overall inhibitory effects of only the highest tested concentrations (100 μg/mL for extract and 30 μM for single substances) were mediated by the cytotoxicity of the DMSO solvent. The data are provided as supplementary information (Fig. S1). To identify the active constituents, the EtOAc extract was submitted to HPLC-based activity profiling, a procedure which combines analytical HPLC separation with on-line recorded spectroscopic data and with biological information obtained in parallel from microfractions collected from the column effluent. Separation of the extract into 35 one-minute microfractions and subsequent testing of the fractions on T lymphocytes proliferation revealed a main active time window between 16 and 22 min (Fig. 2). Several peaks were detected which could be tentatively assigned to lignans, flavonoids, and triterpenes based on their UV and MS spectra, and with the aid of chemotaxonomic data.

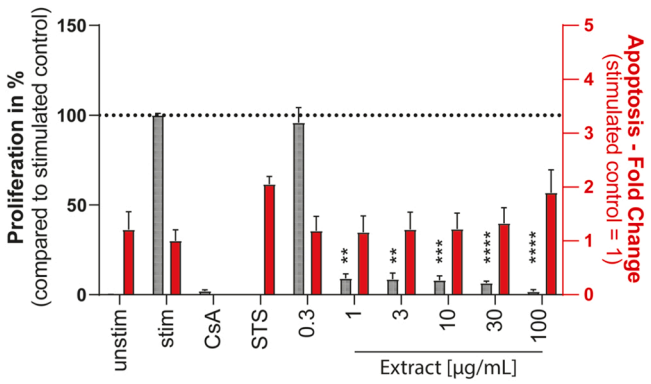

Fig. 1. Effect of the *H. brachiata* EtOAc extract on T lymphocyte proliferation and apoptosis. T lymphocyte proliferation is shown in gray (left y-axis) and apoptosis induction in red (right y-axis). Primary human lymphocytes were stained either with CFSE or Annexin V-FITC stainings in proliferation or apoptosis experiments, respectively. Lymphocytes were stimulated with anti-CD3 and anti-CD28 mAbs (except the unstimulated control) and incubated for 72 h in the presence of medium (unstimulated (unstim), stimulated (stim)), cyclosporine A (CsA; 4.16 μM), staurosporine (STS, 0.3 μM), or *H. brachiata* EtOAc extract (μg/mL). Both, proliferation and apoptosis induction were analyzed by flow cytometry. Only the proliferation results were normalized to stimulated control. Results are depicted as mean ± standard deviation. n = 3; *$p < 0.05$; **$p < 0.01$; ***$p < 0.005$; ****$p < 0.001$. The Shapiro-Wilk test was used to test for a normal distribution. A multiple group comparison was performed with the Brown-Forsythe and Welch ANOVA, followed by Dunnetś T3 post-hoc test.

3.2. Isolation of compounds, and effect on proliferation and apoptosis induction of human T lymphocytes

For preparative isolation, a larger amount of aerial parts was extracted with EtOAc. Targeted fractionation of the extract by a combination of chromatographic methods resulted in the isolation of 18 compounds, including seven aryltetralin lignans (**1**–**7**), five arylnaphthalene lignans (**8**–**12**), three triterpenes (**13**–**15**), two flavonoids (**16**–**17**), and cinnamyl cinnamate (**18**). Compounds were identified with the aid of ESI-MS and NMR analysis. The absolute configuration was established by comparison of optical rotation data with literature values. In addition, rosmarinic acid (**19**) was identified in the extract from its UV and MS data, and by chromatographic comparison with a commercial reference sample (Figs. 2 and 3). Physicochemical and spectroscopic data of compounds **1**-**18** are provided as Supplementary Information (Tables S1-S18).

The aryltetralin lignans **1**–**4** and **7**, arylnaphthalene lignans **8**–**10**, triterpenes **14** and **15**, and flavonoids **16** and **17** were obtained in sufficient amounts and purity to be tested for T lymphocyte proliferation inhibition and apoptosis induction. The lignan **5** identified as podophyllotoxin was isolated as a minor substance of insufficient purity. Therefore, a commercially available reference of **5** was used for all bioassays. Except for **4**, all aryltetralin lignans significantly inhibited proliferation in a concentration-dependent manner at concentrations of 0.1 μM for **1** and **2**, 0.3 μM for podophyllotoxin (**5**) and **7**, and 3 μM for **3** (Fig. 4A). Apoptosis correlated with proliferation inhibition, but these effects were weak and not significant. (Fig. 4 A). No effects on T lymphocyte proliferation were observed for arylnaphthalene lignans, triterpenes, and flavonoids (Fig. 4B).

3.3. Effect of H. brachiata EtOAc extract and aryltetralin lignans on the cell cycle of human T lymphocytes

To characterize the proliferation inhibition by the extract and the aryltetralin lignans in more detail, cell cycle arrest analyses were performed. The distribution of stimulated T lymphocytes in different cell

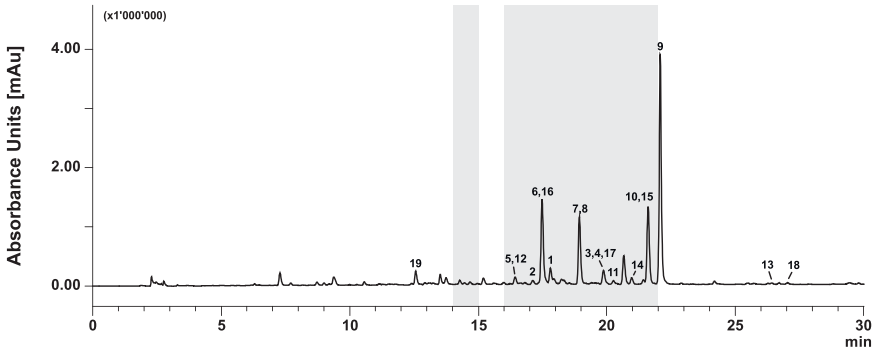

Fig. 2. HPLC-based activity profile of the *H. brachiata* EtOAc extract. HPLC-PDA chromatographic trace at 254 nm (SunFire C18, 3.5 µM. 3.0 × 150 mm i.d.). 5–100% MeCN (0.1% FA) in 30 min. The active one-minute microfractions are highlighted in grey. Numbers refer to the identified compounds.

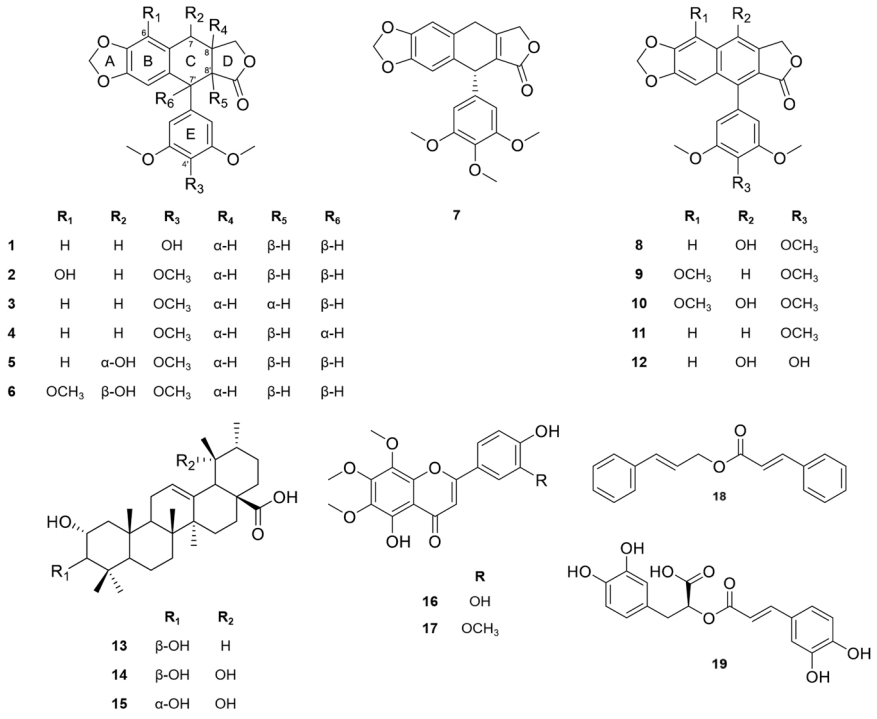

	R_1	R_2	R_3	R_4	R_5	R_6
1	H	H	OH	α-H	β-H	β-H
2	OH	H	OCH_3	α-H	β-H	β-H
3	H	H	OCH_3	α-H	α-H	β-H
4	H	H	OCH_3	α-H	β-H	α-H
5	H	α-OH	OCH_3	α-H	β-H	β-H
6	OCH_3	β-OH	OCH_3	α-H	β-H	β-H

	R_1	R_2	R_3
8	H	OH	OCH_3
9	OCH_3	H	OCH_3
10	OCH_3	OH	OCH_3
11	H	H	OCH_3
12	H	OH	OH

	R_1	R_2
13	β-OH	H
14	β-OH	OH
15	α-OH	OH

	R
16	OH
17	OCH_3

Fig. 3. Chemical structures of identified compounds.

cycle phases was observed by flow cytometric sorting analysis. Cyclosporine A and vinblastine were used as references that inhibit T lymphocyte proliferation via two different pathways to characterize the effects of our tested substances. As can be seen in Fig. 5, unstimulated cells remained mainly in G1 phase. Compared to unstimulated cells, stimulated cells showed an increased number in S and G2. The calcineurin inhibitor cyclosporine A inhibited cell division immediately after T lymphocyte activation, leading to an accumulation of cells in G1. The microtubule inhibitor vinblastine blocked cell division during mitosis and led to a higher accumulation of dividing T lymphocytes in S and G2 compared to stimulated cells (Fig. 5). At concentrations between 0.003 and 0.3 µg/mL the *Hyptis* extract showed a concentration-dependent increase of of T lymphocytes with a G2 phase arrest. However, this trend decreased again at higher concentrations (3–30 µg/mL). The same was observed for the pure compounds, since **1**, **2**, **5** and **7** showed as well an increased G2 arrest at concentrations between 0.01 and 1 µM for **1**, and between 0.01 and 0.1 µM for **2**, **5**, and **7**. At higher concentrations the number of cells in the G2 phase decreased similarly as seen for the extract. Only **3** showed a continuous dose-dependent G2 phase arrest over the whole tested concentration range between 0.01 and 10 µM (Fig. 5).

3.4. *Effect of H. brachiata EtOAc extract and isolated substances on the activation state and cytokine production of human T lymphocytes*

During an immune response, T helper cells ($CD4^+$) and cytotoxic T cells ($CD8^+$) secrete various cytokines that promote the immune response. In addition, the activation marker CD69 is expressed on the cell surface of both cell types [12]. To evaluate a functional T lymphocyte suppression by the *H. brachiata* EtOAc extract and the pure compounds, the production of different cytokines and the expression of surface markers was investigated. A multifluorescence panel was used to examine the production of CD69, IFN-γ, IL-2, TNF-α, and IL-21 of $CD4^+$ lymphocytes, and CD69, IL-2, TNF-α, and MIP1-β of $CD8^+$ lymphocytes.

The extract decreased the secretion of IL-2 (Fig. 6A) and IL-21 (Fig. 6B) of $CD4^+$ lymphocytes, and of IL-2 (Fig. 6C), TNF-α (Fig. 6D), and MIP1-β (Fig. 6E) of $CD8^+$ lymphocytes in a concentration-dependent manner. The inhibition of IL-2 secretion of $CD4^+$ lymphocytes by the extract was significant between concentrations of 30 and 100 µg/mL (Fig. 6A). The remaining effects are merely trends, without statistical

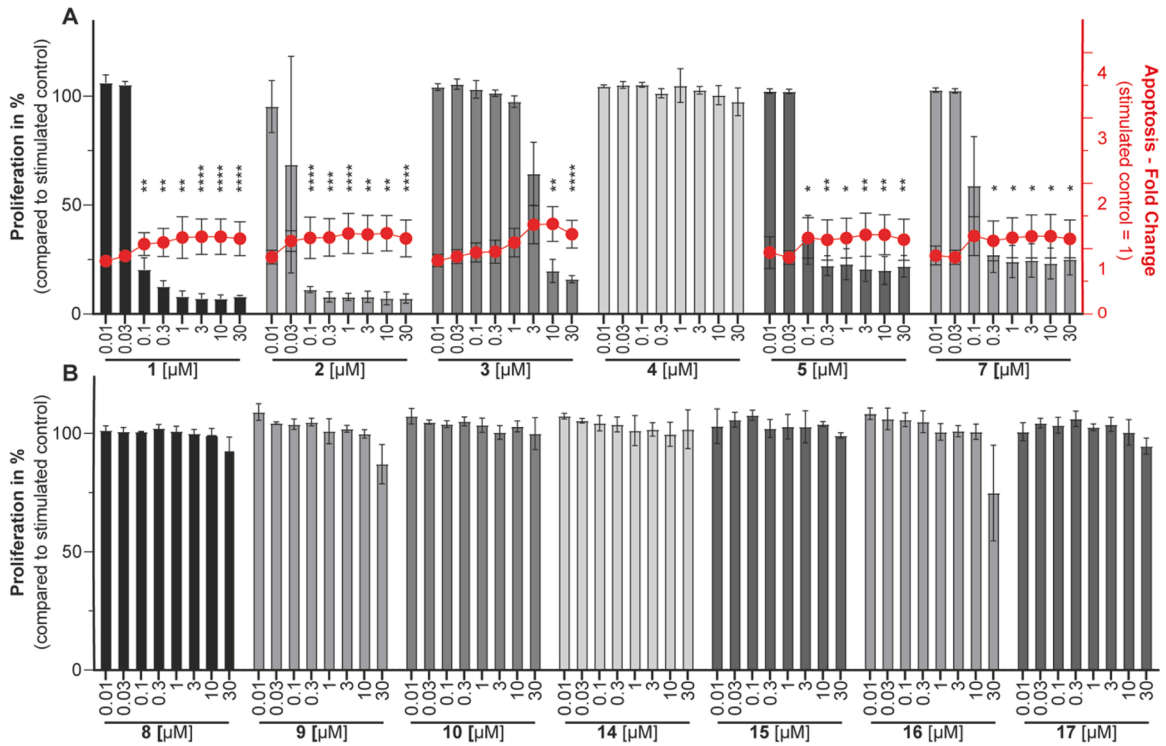

Fig. 4. Effects of compounds on T lymphocyte proliferation and apoptosis. Effects on proliferation is shown as black and gray bars (left y-axis), and apoptosis induction as red dots (right y-axis). Primary human lymphocytes were stained either with CFSE or Annexin V-FITC stainings in proliferation or apoptosis experiments, respectively. Lymphocytes were stimulated with anti-CD3 and anti-CD28 mAbs and incubated for 72 h in the presence of isolated compounds or commercial podophyllotoxin. Concentrations tested in µM. Both, proliferation and apoptosis induction were analyzed by flow cytometry. Only the proliferation results were normalized to stimulated control. Results are depicted as mean ± standard deviation. The controls are shown in Fig. 1. n = 3; *p < 0.05; **p < 0.01; ***p < 0.005; * ** *p < 0.001. The Shapiro-Wilk test was used to test for a normal distribution. A multiple group comparison was performed with the Brown-Forsythe and Welch ANOVA, followed by Dunnetś T3 post-hoc test.

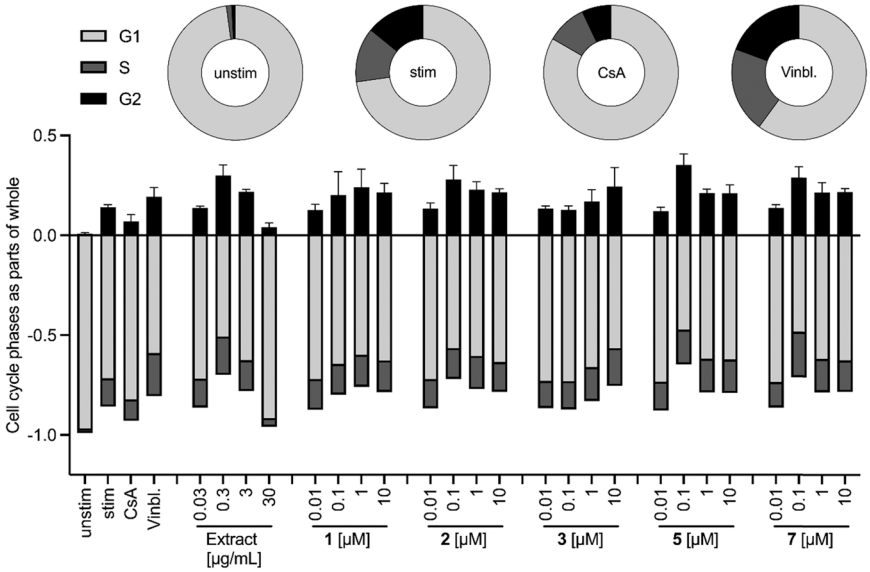

Fig. 5. Effects of *H. brachiata* EtOAc extract and aryltetralin lignans on the cell cycle of human T lymphocytes. Primary human lymphocytes were stimulated with anti-CD3 and anti-CD28 mAbs. Stimulated cells were incubated for 72 h in the presence of H. brachiata EtOAc extract, or isolated aryltetralin lignans. PI staining of the DNA was performed. The mean number of lymphocytes in G2 phase ± standard deviation is shown above the x-axis. The proportions of lymphocytes in G1 and S phase are depicted below the x-axis. Concentrations tested for the extract in µg/mL and for substances in µM. Controls (unstim, stim, cyclosporine (CsA; 4.16 µM), vinblastine (Vinbl.; 0.03 µM)) are shown as pie charts and indicate the proportions of lymphocytes in each phase. n = 3. The Shapiro-Wilk test was used to test for a normal distribution. A multiple group comparison was performed with the Brown-Forsythe and Welch ANOVA, followed by Dunnetś T3 post-hoc test.

significance.

Of the isolated substances only the triterpenes **14** and **15** weakly inhibited the secretion of IL-2 (Fig. 6A) and IL-21 (Fig. 6B) by $CD4^+$ lymphocytes, and of IL-2 (Fig. 6C), TNF-α (Fig. 6D), and MIP1-β (Fig. 6E) by $CD8^+$ lymphocytes in a concentration range between 0.3 and 30 µM. Expression of IL-21 by $CD4^+$ lymphocytes, and of TNF-α and MIP1-β by $CD8^+$ lymphocytes was concentration-dependent, but not significant. The effects on IL-2 secretion of $CD4^+$ and $CD8^+$ T lymphocytes were not concentration-dependent. The other activation markers and cytokines were neither affected by the extract nor by the triterpenes (data not shown). No significant effects on the secretion of cytokines were observed for aryltetralin and arylnaphthalene lignans, as well as for flavonoids (data not shown).

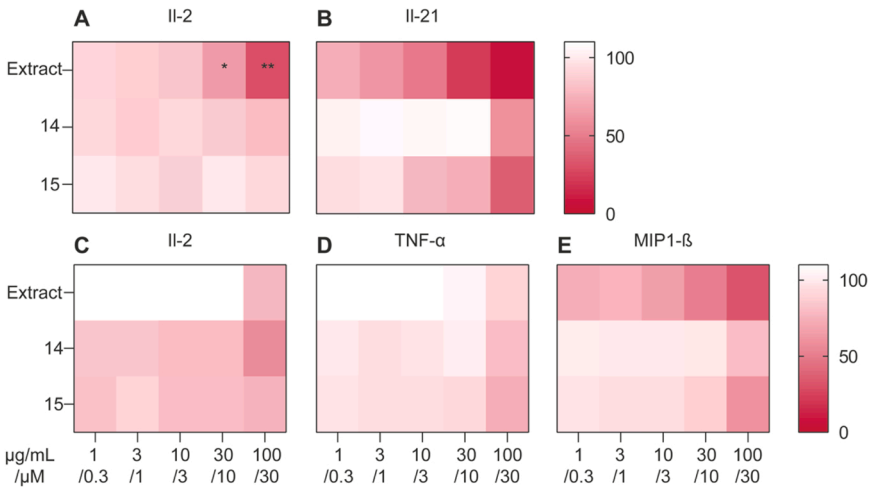

Fig. 6. Effects of *H. brachiata* EtOAc extract and triterpenes **14** and **15** on the activation state and cytokine production of primary human lymphocytes. After treatment with extract and triterpenes for 44 h $CD4^+$ lymphocytes and $CD8^+$ lymphocytes were separately analyzed by their functional status using two flow cytometric staining panels. The effects of the extract and triterpenes **14** and **15** on the secretion of IL-2 (A) and IL-21 (B) by $CD4^+$ lymphocytes and of IL2 (C), TNF-α (D), and MIP1-β (E) by $CD8^+$ lymphocytes are shown as heat maps. $n = 3$; *$p < 0.05$; * *$p < 0.01$. The Shapiro-Wilk test was used to test for a normal distribution. A multiple group comparison was performed with the Brown-Forsythe and Welch ANOVA, followed by Dunnetś T3 post-hoc test.

4. Discussion

Continued research into new therapies for the treatment of autoimmune diseases is of great importance to overcome current therapeutic limitations. Plants are a promising source for the discovery of novel immunosuppressive substances given the high structural diversity of their secondary metabolites. In the screening of a library of 600 plant extracts for T lymphocyte proliferation inhibition an EtOAc extract from the aerial parts of *H. brachiata* showed strong inhibitory effects (Fig. 1). Subsequent investigation resulted in the isolation of seven aryltetralin lignans, five arylnaphthalene lignans, three triterpenes, two flavonoids, and cinnamyl cinnamate (Figs. 2 and 3; Tables S1-S18). This study represents the first detailed report on the phytochemical composition of *H. brachiata*. However, most of the isolated lignans have already been identified in other species of the Hyptidinae subtribe, such as *Condea verticillata* (syn. *Hyptis verticillata*), *Mesosphaerum suaveolens* (syn. *Hyptis suaveolens*), or *Eriope latifolia* (syn. *Hyptis latifolia*) [13]. Lignans **6** and **12** are described for the first time in a species of the Hyptidinae subtribe, but were previously isolated from *Libocedrus chevalieri* (Cupressaceae) [14], *Dysosma versipellis* (Berberidaceae) [15], and *Sinopodophyllum hexandrum* (Berberidaceae) [16,17]. Most of the triterpenes, flavonoids, and cinnamic acid derivatives have also been previously reported in other Hyptidinae species [13], except the flavonoid **17**, which has been identified in various other Lamiaceae species [18,19] and the cinnamic acid derivative **18,** a metabolite known for example from *Cinnamomum cassia* (Lauraceae) [20].

Of the isolated substances only the aryltetralin lignans strongly suppressed T lymphocyte proliferation, whereas the other compounds were inactive. Both the EtOAc extract and the aryltetralin lignans slightly increased the induction of apoptosis (Figs. 1 and 4). However, compared to unstimulated T lymphocytes the effect on apoptosis induction was weak, and apoptosis as such could, therefore, not explain the observed proliferation inhibition.

Podophyllotoxin is a widely investigated substance that mainly gained attention because of its antimitotic effects, and therefore for its anti-tumor properties [21]. Even though podophyllotoxin and its analogues proved to be highly effective as antitumor agents they failed in clinical investigations mainly due to severe gastrointestinal side effects [22].

Aryltetralin lignans have also gained interest as immunosuppressive agents [23–25]. Proresid®, podophyllotoxin, and Reumacon® even reached the stage of clinical studies in the treatment of rheumatoid arthritis because they clearly improved the clinical manifestation of the disease by significant reduction of inflammatory activity through inhibitory effects on lymphocyte proliferation [23,26–36]. Additionally, podophyllotoxin was investigated in clinical studies for the treatment of psoriasis because it effectively reduced IL-1 and TNF-α serum levels, as well as lymphocyte activity [37]. All observed effects could be explained by aryltetralin lignans that bind to tubulin and inhibit microtubule formation [25,38,39].

From these findings we can conclude that the aryltetralin lignans from *H. brachiata* also inhibit T lymphocyte proliferation by binding to tubulin monomers and therefore inhibit the formation of the mitotic spindle. The most active lignans were **1** and **2**, followed by **5**, **7**, and **3**, while lignan **4** did not show any effect (Fig. 4A). The differences observed between the aryltetralin lignans on antimitotic activity can be explained in the light of reported structure-activity relationships. For tubulin polymerization inhibition, the almost co-planar orientation of a 7′-(*R*), 8′-(*R*), and 8-(*R*) configuration at the C-ring and the *trans*-fused γ-lactone D-ring is important (Fig. 3) [40,41]. The most active aryltetralin lignans **1**, **2**, and **5** show the 7′-(*R*), 8′-(*R*), and 8-(*R*) configuration. Compound **3** shows a 7′-(*R*), 8′-(*S*), and 8-(*R*) configuration, resulting in a *cis*-fused γ-lactone D-ring. This changes the quasi-axial orientation of the E-ring in trans-fused ring systems to a quasi-equatorial orientation of the E-ring, which in turn results in a decreased activity (Fig. 4) [22,40,42]. The 7′-(*S*), 8′-(*R*), 8-(*S*) configuration of lignan **4** leads to an inversed spatial orientation of the E-ring that prevents binding to the colchicine binding site (Fig. 4) [22,43,44]. Although lignan **7** possesses a double bond between C-8 and C-8′ the almost co-planar disposition remains, and the E-ring keeps a quasi-axial orientation. Therefore, it shows a comparable potency as the *trans*-lactone **5** (Fig. 4) [45]. Removal of the 4′-O-methyl group of the E-ring and of the 7-hydroxy group at the C-ring, as well as an additional 6-hydroxy group at the B-ring is known to increase potency [40,46]. Accordingly, the 4′-O-demethyl lignan **1** and the 6-hydroxy lignan **2** were the most active substances from *H. brachiata* (Fig. 4). Arylnaphthalene lignans show a rigid flat aromatic core structure resulting in a loss of activity [42,43], as seen with arylnaphthalenes **8**–**10** (Fig. 4).

Since podophyllotoxin (**5**) and similar aryltetralin lignans are known to cause G2/M arrest in dividing cells [22,23,32,39,47,48], the isolated lignans were tested in a cell cycle arrest assay to get insight in their mode of action (Fig. 5). The distribution of cells in each cell cycle phase was determined using a flow cytometric analysis. Vinblastine was used as positive control, and cyclosporine A was included to compare different mode of actions. As expected, the EtOAc extract as well as the aryltetralin lignans **1**, **2**, **3**, **7**, and podophyllotoxin (**5**) showed a dose dependent accumulation of cells in G2 phase. The same was observed for vinblastine, thereby suggesting an interaction with microtubule assembly in early stage of mitosis. For the extract as well as for **1**, **2**, **7**, and podophyllotoxin (**5**) this G2 arrest was observed at only lower test concentrations. At higher concentrations the G2 phase arrest declined again, presumably due to cytotoxicity, because dead cells cannot be

measured as G2 cells. Even though aryltetralin lignans increase dose-dependently apoptosis rate, apoptosis data of this study could not explain this decrease in G2 cells at higher test concentrations, because the change in apoptosis was not significantly different from that of unstimulated or stimulated cells (Figs. 1 and 4). Only lignan **3** showed a dose dependent increased G2 phase arrest without any decline over the investigated concentration range. Furthermore, the slight induction of apoptosis observed for **3** occurred only at higher concentrations compared to the other lignans. As expected, unstimulated, stimulated, and cells treated with cyclosporin A are accumulated mainly in G1 phase.

Beside antimitotic effects, the production and secretion of cytokines and the expression of surface activation markers of activated $CD4^+$ lymphocytes, like CD69, IFN-γ, IL-2, TNF-α, and IL-21, and of activated $CD8^+$ lymphocytes, like CD69, IL-2, TNF-α, and MIP1-β, was investigated. Podophyllotoxin and other aryltetralin lignans have been shown to influence the expression and secretion of different cytokines [29,37,49,50]. The EtOAc extract showed a weak concentration-dependent decrease in the secretion of IL-2 and IL-21 by $CD4^+$ lymphocytes, and a weak concentration-dependent decrease in the secretion of IL-2, TNF-α, and MIP1-β by $CD8^+$ lymphocytes. To trace back the observed effects to single substances, we tested all isolated compounds. Even though effects of aryltetralin lignans on cytokines have been reported in literature, we did not observe any effects on expression of activation markers and on cytokine release for both aryltetralin and arylnaphthalene lignans. No effects were also found for flavonoids. Although they did not show any effects on proliferation and apoptosis, the triterpenes **14** and **15** showed weak inhibitory effects on the secretion of IL-2 and IL21 in $CD4^+$ lymphocytes, and of IL-2, TNF-α, and MIP1-β in $CD8^+$ lymphocytes. From that we assume that the suppressive effects on T lymphocytes by the EtOAc extract from *H. brachiata* may be explained by synergistic effects between structurally different substance classes, the aryltetralin lignans inhibiting cell division and triterpenes reducing the secretion inflammatory cytokines. This is an interesting aspect since little is known about super additive and synergistic properties of different substance classes in this area. The groups of Onlamoon [51] and Gertsch [52] demonstrated that the flavonoids hispidulin and neptin as well as N-alkylamide combinations from different plants modulate immune cellular function of human peripheral lymphocytes in a synergistic and superadditive manner, respectively.

5. Conclusion

In conclusion, the EtOAc extract of *H. brachiata* exhibited strong inhibitory effects on T lymphocyte proliferation. The observed effect could be traced back to a synergistic interplay between different aryltetralin lignans and triterpenes. The aryltetralin lignans showed an antimitotic effect, while the triterpenes weakly lowered the production of inflammatory cytokines such as IL-2 and TNF-α by activated T lymphocytes. This makes the extract worthy of further investigation in the treatment of inflammatory and autoimmune diseases. Especially the aryltetralin lignans, which have already been investigated as antimitotic substances and as T lymphocyte proliferation inhibitors seem to be interesting candidates for further development in the field of T lymphocyte driven autoimmune diseases. In this context, research is ongoing on the development of new aryltetralin-like lignans, which combine the strong antimitotic effects with a decreased development of drug resistance and lower toxicity [53]. Beside single compounds, extracts of *H. brachiata* which contain both lignans and triterpenes with complementary modes of actions may also have a potential for future developments.

Funding

CG and AZK are supported by PRIAM-BS (Verein Stiftungsprofessur für Integrative und Anthroposophische Medizin an der Universität Basel).

CRediT authorship contribution statement

Matthias Hamburger, Olivier Potterat, Carsten Gründemann: Conceptualization, Validation. **Morris Keller, Moritz Winker**: Data curation. **Morris Keller, Moritz Winker, Nino Sperisen**: Formal analysis, Investigation. **Morris Keller, Moritz Winker, Mahabir P. Gupta, Matthias Hamburger, Olivier Potterat, Carsten Gründemann**: Methodology. **Amy Marisa Zimmermann-Klemd, Olivier Potterat, Carsten Gründemann**: Project administration. **Mahabir P. Gupta, Matthias Hamburger, Olivier Potterat, Carsten Gründemann**: Resources. **Morris Keller, Moritz Winker, Amy Marisa Zimmermann-Klemd, Nino Sperisen, Mahabir P. Gupta, Pablo N. Solis, Matthias Hamburger, Olivier Potterat, Carsten Gründemann**: Software. **Amy Marisa Zimmermann-Klemd, Matthias Hamburger, Olivier Potterat, Carsten Gründemann**: Supervision. **Morris Keller, Moritz Winker, Amy Marisa Zimmermann-Klemd, Olivier Potterat, Carsten Gründemann**: Visualization. **Morris Keller, Moritz Winker, Amy Marisa Zimmermann-Klemd**: Writing – original draft. **Morris Keller, Moritz Winker, Amy Marisa Zimmermann-Klemd, Olivier Potterat, Carsten Gründemann**: Writing – review & editing.

Conflict of interest statement

The authors declare no competing interests.

Data availability

The datasets generated for this study are available on request to the corresponding author.

Acknowledgement

Thanks are due to Carmen Galdames (botanist at CIFLORPAN) for the botanical identification of the plant material. Parts of this work was presented at the Annual Fall Meeting of the Swiss Chemical Society, Zürich, Switzerland, September 8, 2022, as a poster contribution.

Appendix A. Supporting information

Supplementary data associated with this article can be found in the online version at doi:10.1016/j.biopha.2023.114328.

References

[1] U. Khan, H. Ghazanfar, T Lymphocytes and autoimmunity, Int. Rev. Cell Mol. Biol. 341 (2018) 125–168, https://doi.org/10.1016/bs.ircmb.2018.05.008.
[2] M. Her, A. Kavanaugh, Alterations in immune function with biologic therapies for autoimmune disease, J. Allergy Clin. Immunol. 137 (2016) 19–27, https://doi.org/10.1016/j.jaci.2015.10.023.
[3] A.C. Allison, Immunosuppressive drugs: the first 50 years and a glance forward, Immunopharmacology 47 (2000) 63–83, https://doi.org/10.1016/S0162-3109(00)00186-7.
[4] S. Mathur, C. Hoskins, Drug development: lessons from nature (review), Biomed. Rep. 6 (2017) 612–614, https://doi.org/10.3892/br.2017.909.
[5] J. Río, M. Comabella, X. Montalban, Predicting responders to therapies for multiple sclerosis, Nat. Rev. Neurol. 5 (2009) 553–560, https://doi.org/10.1038/nrneurol.2009.139.
[6] C. Daubert, N. Behar, R.P. Martins, P. Mabo, C. Leclercq, Avoiding non-responders to cardiac resynchronization therapy: a practical guide, Eur. Heart J. 38 (2017) 1463–1472, https://doi.org/10.1093/eurheartj/ehw270.
[7] D.D. Chaplin, Overview of the immune response, J. Allergy Clin. Immunol. 125 (2010) S3–S23, https://doi.org/10.1016/j.jaci.2009.12.980.
[8] M.D. Rosenblum, K.A. Remedios, A.K. Abbas, Mechanisms of human autoimmunity, J. Clin. Invest. 125 (2015) 2228–2233, https://doi.org/10.1172/JCI78088.
[9] D. Velázquez, E. de Arrioja, S. Tillett, Usos populares de Lamiaceae en Venezuela, Acta Botánica Venezuélica 18 (1995) 5–20.
[10] T. Hell, A. Rutz, L. Dürr, M. Dobrzyński, J.K. Reinhardt, T. Lehner, M. Keller, A. John, M. Gupta, O. Pertz, M. Hamburger, J.L. Wolfender, E. Garo, Combining activity profiling with advanced annotation to accelerate the discovery of natural

products targeting oncogenic signaling in melanoma, J. Nat. Prod. 2022 (2022) 1540–1554, https://doi.org/10.1021/acs.jnatprod.2c00146.
[11] G. Tafurt-Garcia, A. Munoz-Acevedo, A.M. Calvo, L.F. Jimenez, W.A. Delgado, Volatile compounds of analysis of *Eriope crassipes*, *Hyptis conferta*, *H. dilatata*, *H. brachiata*, *H. suaveolens* and *H. mutabilis* (Lamiaceae), Bol. Latinoam. Y. Del. Caribe Plantas Med. Y. Aromát 13 (2014) 254–269.
[12] S.F. Ziegler, F. Ramsdell, M.R. Alderson, The activation antigen CD69, Stem Cells 12 (1994) 456–465, https://doi.org/10.1002/stem.5530120502.
[13] H. Bridi, G. de Carvalho Meirelles, G. Lino von Poser, Subtribe Hyptidinae (Lamiaceae): a promising source of bioactive metabolites, J. Ethnopharmacol. 264 (2021), 113225, https://doi.org/10.1016/j.jep.2020.113225.
[14] Y.J. Zhang, M. Litaudon, H. Bousseroue, M.T. Martin, O. Thoison, S. Léonce, V. Dumontet, T. Sévenet, F. Guéritte, Sesquiterpenoids and cytotoxic lignans from the bark of *Libocedrus chevalieri*, J. Nat. Prod. 70 (2007) 1368–1370, https://doi.org/10.1021/np070124q.
[15] Z. Yang, P. Guo, R. Han, J.M. Gao, Preparative separation of flavone dimers from *Dysosma versipellis* by counter-current chromatography: trifluoroacetic acid as a solvent system modifier, J. Sep. Sci. 41 (2018) 3631–3643, https://doi.org/10.1002/jssc.201800530.
[16] M. Atta-ur-Rahman, M.Iqbal Ashraf, Choudhary, M.H. Habib-ur-Rehman, Kazmi, Antifungal aryltetralin lignans from leaves of *Podophyllum hexandrum*, Phytochemistry 40 (1995) 427–431, https://doi.org/10.1016/0031-9422(95)00195-D.
[17] Y.J. Sun, Z.L. Li, H. Chen, X.Q. Liu, W. Zhou, H.M. Hua, Three new cytotoxic aryltetralin lignans from *Sinopodophyllum emodi*, Bioorg. Med. Chem. Lett. 21 (2011) 3794–3797, https://doi.org/10.1016/j.bmcl.2011.04.036.
[18] C.O. Van Den Broucke, R.A. Dommisse, E.L. Esmans, J.A. Lemli, Three methylated flavones from *Thymus vulgaris*, Phytochemistry 21 (1982) 2581–2583, https://doi.org/10.1016/0031-9422(82)85261-8.
[19] M.A. El-Ansari, D. Barron, M.F. Abdalla, N.A.M. Saleh, J.L.Le Quéré, Flavonoid constituents of *Stachys aegyptiaca*, Phytochemistry 30 (1991) 1169–1173, https://doi.org/10.1016/S0031-9422(00)95197-5.
[20] X. Liu, J. Fu, X.J. Yao, J. Yang, L. Liu, T.G. Xie, P.C. Jiang, Z.H. Jiang, G.Y. Zhu, Phenolic constituents isolated from the twigs of *Cinnamomum cassia* and their potential neuroprotective effects, J. Nat. Prod. 81 (2018) 1333–1342, https://doi.org/10.1021/acs.jnatprod.7b00924.
[21] H.N. Brandão, H.H.S. Medrado, J.P. David, J.M. David, J.F.B. Pastore, M. Meira, Determination of podophyllotoxin and related aryltetralin lignans by HPLC/DAD/MS from Lamiaceae species, Microchem. J. 130 (2017) 179–184, https://doi.org/10.1016/j.microc.2016.09.002.
[22] M. Antúnez-Mojica, J. Rodríguez-Salarichs, M. Redondo-Horcajo, A. León, I. Barasoain, Á. Canales, F.J. Cañada, J. Jiménez-Barbero, L. Alvarez, J.F. Díaz, Structural and biochemical characterization of the interaction of tubulin with potent natural analogues of podophyllotoxin, J. Nat. Prod. 79 (2016) 2113–2121, https://doi.org/10.1021/acs.jnatprod.6b00428.
[23] S.R. Dahlqvist, B. Norberg, K. Sondell, I. Nordenson, G. Holmgren, The effect of CPH 82 on the growth of human lymphocytes in vitro. Definition of cytobiological action, Rheumatology 28 (1989) 418–421, https://doi.org/10.1093/rheumatology/28.5.418.
[24] T. Hirano, A. Wakasugi, M. Oohara, K. Oka, Y. Sashida, Suppression of mitogen-induced proliferation of human peripheral blood lymphocytes by plant lignans, Planta Med 57 (1991) 331–334, https://doi.org/10.1055/s-2006-960110.
[25] C. Brigati, B. Sander, CPH-86, a highly purified podophyllotoxin, efficiently suppresses in vivo and in vitro immune responses, Immunopharmacol. Immunotoxicol. 7 (1985) 285–302, https://doi.org/10.3109/08923978509026477.
[26] J. Lysholm, T. Weitoft, Proresid in the long-term treatment of rheumatoid arthritis, Scand. J. Rheumatol. 17 (1988) 465–468, https://doi.org/10.3109/03009748809098808.
[27] L. Truedsson, P. Geborek, G. Sturfelt, Antiproliferative effects on human peripheral blood mononuclear cells and inhibition of in vitro immunoglobulin synthesis by podophyllotoxin (CPH86) and by semisynthetic lignan glycosides (CPH82), Clin. Exp. Rheumatol. 11 (1993) 179–182.
[28] S. Rantapää-Dahlqvist, E. Löfvenbert, B. Norberg, Effect of CPH82 in rheumatoid arthritis. Accumulation of bone marrow cells in mitosis and clinical response, Clin. Rheumatol. 12 (1993) 541–542, https://doi.org/10.1007/BF02231790.
[29] K. Carlström, P.J. Hedin, L. Jönsson, T. Lerndal, J. Lien, T. Weitoft, M. Axelson, Endocrine effects of the podophyllotoxine derivative drug CPH 82 (Reumacon®) in patients with rheumatoid arthritis, Scand. J. Rheumatol. 29 (2000) 89–94, https://doi.org/10.1080/030097400750001888.
[30] E.S. Gudmundsdóttir, H. Jónsson, CPH 82 (Reumacon®) in refractory inflammatory arthritis, Scand. J. Rheumatol. 29 (2000) 323–325, https://doi.org/10.1080/030097400447723.
[31] T. Lerndal, B. Svensson, A clinical study of CPH 82 vs methotrexate in early rheumatoid arthritis, Rheumatology 39 (2000) 316–320, https://doi.org/10.1093/rheumatology/39.3.316.
[32] S.R. Dahlqvist, G. Landberg, G. Roos, B. Norberg, Cell cycle effects of the anti-rheumatic agent CPH82, Rheumatology 33 (1994) 327–331, https://doi.org/10.1093/rheumatology/33.4.327.
[33] A. Larsen, I. Petersson, B. Svensson, Podophyllum derivatives (CPH 82) compared with placebo in the treatment of rheumatoid arthritis, Rheumatology 28 (1989) 124–127, https://doi.org/10.1093/rheumatology/28.2.124.
[34] B. Svensson, K. Herlyn, B. Rosén, CPH 82 (Reumacon®): A new and promising basic therapy in rheumatoid arthritis, Aktuelle Rheumatol. 24 (1999) 58–61, https://doi.org/10.1055/s-2008-1043548.
[35] B. Mansson, P. Geborek, T. Hallberg, G. Sturfelt, Inhibition of ConA-induced proliferate response in human lymphocytes by podophyllotoxin and a detergent, Tween80, Clin. Exp. Rheumatol. 6 (1988) 405–407.
[36] S. Meske, H.H. Peter, Podophyllotoxin therapy in rheumatoid arthritis: a clinical open dose-response study, Aktuelle Rheumatol. 15 (1990) 154–155, https://doi.org/10.1055/s-2008-1047442.
[37] L. Bohlin, B. Rosén, Podophyllotoxin derivatives: drug discovery and development, Drug Discov. Today 1 (1996) 343–351, https://doi.org/10.1016/1359-6446(96)10028-3.
[38] M. Antúnez-Mojica, A. León, A.M. Rojas-Sepúlveda, S. Marquina, M.A. Mendieta-Serrano, E. Salas-Vidal, M.L. Villarreal, L. Alvarez, Aryldihydronaphthalene-type lignans from *Bursera fagaroides* var. *fagaroides* and their antimitotic mechanism of action, RSC Adv. 6 (2016) 4950–4959, https://doi.org/10.1039/c5ra23516b.
[39] M. Antúnez-Mojica, A.M. Rojas-Sepúlveda, M.A. Mendieta-Serrano, L. Gonzalez-Maya, S. Marquina, E. Salas-Vidal, L. Alvarez, Lignans from *Bursera fagaroides* affect in vivo cell behavior by disturbing the tubulin cytoskeleton in zebrafish embryos, Molecules 24 (2019) 8, https://doi.org/10.3390/molecules24010008.
[40] M. Gordaliza, M.A. Castro, M.D. García-Grávalos, P. Ruiz, J.M.M. Del Corral, A.S. Feliciano, Antineoplastic and antiviral activities of podophyllotoxin related lignans, Arch. Pharm. (Weinh.). 327 (1994) 175–179, https://doi.org/10.1002/ardp.19943270309.
[41] B. Botta, G. Monache, D. Misiti, A. Vitali, G. Zappia, Aryltetralin lignans: chemistry, pharmacology and biotransformations, Curr. Med. Chem. 8 (2001) 1363–1381, https://doi.org/10.2174/0929867013372292.
[42] A. San Feliciano, M. Gordaliza, J.M. Miguel Del Corral, M.A. Castro, M.D. Garcia-Gravalos, P. Ruiz-Lazaro, Antineoplastic and antiviral activities of some cyclolignans, Planta Med 59 (1993) 246–249, https://doi.org/10.1055/s-2006-959660.
[43] M. Novelo, J.G. Cruz, L. Hernández, R. Pereda-Miranda, H. Chai, W. Mar, J. M. Pezzuto, Cytotoxic constituents from *Hyptis verticillata*, J. Nat. Prod. 56 (1993) 1728–1736, https://doi.org/10.1021/np50100a011.
[44] F. Zavala, D. Guenard, J.P. Robin, E. Brown, Structure-antitubulin activity relationships in steganacin congeners and analogs. Inhibition of tubulin polymerization in vitro by (±)-isodeoxypodophyllotoxin, J. Med. Chem. 23 (1980) 546–549, https://doi.org/10.1021/jm00179a014.
[45] M. Gordaliza, G.T. Faircloth, M.A. Castro, J.M. Miguel Del Corral, M.L. López-Vázquez, A. San Feliciano, Immunosuppressive cyclolignans, J. Med. Chem. 39 (1996) 2865–2868, https://doi.org/10.1021/jm960023h.
[46] E. Ter Haar, H.S. Rosenkranz, E. Hamel, B.W. Day, Computational and molecular modeling evaluation of the structural basis for tubulin polymerization inhibition by colchicine site agents, Bioorg. Med. Chem. 4 (1996) 1659–1671, https://doi.org/10.1016/0968-0896(96)00158-7.
[47] M. Ángeles Castro, J.M. Miguel Del Corral, P.A. García, M. Victoria Rojo, A. C. Bento, F. Mollinedo, A.M. Francesch, A. San Feliciano, Lignopurines: a new family of hybrids between cyclolignans and purines. Synthesis and biological evaluation, Eur. J. Med. Chem. 58 (2012) 377–389, https://doi.org/10.1016/j.ejmech.2012.10.026.
[48] Y. Yong, S.Y. Shin, Y.H. Lee, Y. Lim, Antitumor activity of deoxypodophyllotoxin isolated from *Anthriscus sylvestris*: induction of G2/M cell cycle arrest and caspase-dependent apoptosis, Bioorg. Med. Chem. Lett. 19 (2009) 4367–4371, https://doi.org/10.1016/j.bmcl.2009.05.093.
[49] N. Pugh, I.A. Khan, R.M. Moraes, D.S. Pasco, Podophyllotoxin lignans enhance IL-1β but suppress TNF-α mRNA expression in LPS-treated monocytes, Immunopharmacol. Immunotoxicol. 23 (2001) 83–95, https://doi.org/10.1081/IPH-100102570.
[50] X.-H. Gan, J.P. Robin, J.M.M. Huerta, P. Braquet, B. Bonavida, Inhibition of tumor necrosis factor-alpha (TNF-α) and interleukin-1 beta (IL-1β) secretion but not IL-6 from activated human peripheral blood monocytes by a new synthetic demethylpodophyllotoxin derivative, J. Clin. Immunol. 14 (1994) 280–288, https://doi.org/10.1007/BF01540981.
[51] P. Thitilertdecha, V. Tantithavorn, P. Poungpairoj, N. Onlamoon, Synergistic immunosuppressive effect of hispidulin and nepetin mixtures on human T lymphocytes, Immunopharmacol. Immunotoxicol. 44 (2022) 693–703, https://doi.org/10.1080/08923973.2022.2077216.
[52] A. Chicca, S. Raduner, F. Pellati, T. Strompen, K.H. Altmann, R. Schoop, J. Gertsch, Synergistic immunomopharmacological effects of N-alkylamides in *Echinacea purpurea* herbal extracts, Int. Immunopharmacol. 9 (2009) 850–858, https://doi.org/10.1016/j.intimp.2009.03.006.
[53] S. Shen, Y. Tong, Y. Luo, L. Huang, W. Gao, Biosynthesis, total synthesis, and pharmacological activities of aryltetralin-type lignan podophyllotoxin and its derivatives, Nat. Prod. Rep. 39 (2022) 1856–1875, https://doi.org/10.1039/d2np00028h.

3.2 Publication 2

Saponins from saffron corms inhibit the gene expression and secretion of pro-Inflammatory cytokines

Morris Keller, Sarah Fankhauser, Noreen Giezendanner, Michelle König, Franziska Keresztes, Ombeline Danton, Orlando Fertig, Laurence Marcourt, Matthias Hamburger, Veronika Butterweck, and Olivier Potterat

Journal of Natural Products **84**, 630−645 (2021)
doi: 10.1021/acs.jnatprod.0c01220

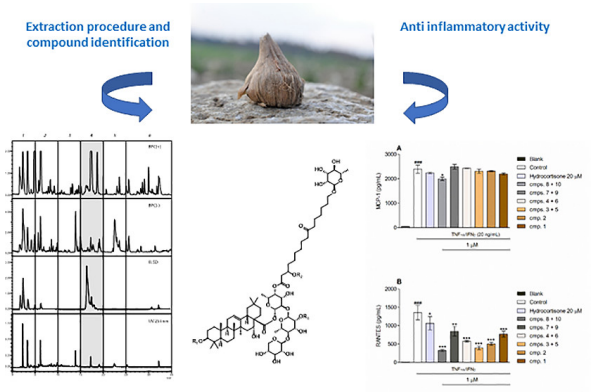

During the cultivation of saffron (*Crocus sativus* L.), corms are obtained as a byproduct. In an effort to valorize this waste product, a 70% EtOH extract of the corms and a sugar-depleted MeOH fraction of this extract was found to inhibit the TNF-α/IFN-γ-induced gene expression and secretion of the chemokines IL-8, MCP-1, and RANTES in human HaCaT cells. The effects were in part stronger than those of the positive control hydrocortisone. The 70% EtOH extract was further studied, and a series of bidesmosidic glycosides of echinocystic acid with a 3,16-dihydroxy-10-oxo-hexadecanoic acid residue were isolated. These saponins, including azafrines 1 and 2, and eight new congeners named as azafrines 3−10, significantly inhibited the TNF-α/IFN-γ-induced gene expression and secretion of RANTES in human HaCaT cells. These findings suggest that saffron corms could be further explored as a potential source for the development of topical agents for the treatment of inflammatory skin diseases, such as psoriasis or atopic dermatitis.

The supporting information is available in the appendix

Contribution to this publication: Extraction, isolation, and structure elucidation of the compounds from *C. sativus*

JOURNAL OF NATURAL PRODUCTS

pubs.acs.org/jnp

Article

Saponins from Saffron Corms Inhibit the Gene Expression and Secretion of Pro-Inflammatory Cytokines

Morris Keller, Sarah Fankhauser, Noreen Giezendanner, Michelle König, Franziska Keresztes, Ombeline Danton, Orlando Fertig, Laurence Marcourt, Matthias Hamburger,* Veronika Butterweck,* and Olivier Potterat

Cite This: *J. Nat. Prod.* 2021, 84, 630−645

Read Online

ACCESS | Metrics & More | Article Recommendations | Supporting Information

ABSTRACT: Corms are obtained as a byproduct during the cultivation of saffron (*Crocus sativus*). In a project aimed at the valorization of this waste product, we observed that a 70% EtOH extract of the corms and a sugar-depleted MeOH fraction of the extract inhibited the TNF-α/IFN-γ-induced secretion and gene expression of the chemokines IL-8, MCP-1, and RANTES in human HaCaT cells. The effects were in part stronger than those of the positive control hydrocortisone. For preparative isolation, the 70% EtOH extract was partitioned between *n*-BuOH and water. Separation of the *n*-BuOH-soluble fraction by centrifugal partition chromatography, followed by preparative and semipreparative HPLC, afforded a series of bidesmosidic glycosides of echinocystic acid bearing a 3,16-dihydroxy-10-oxo-hexadecanoic acid residue attached to the glycosidic moiety at C-28. They include azafrines 1 and 2, previously reported in saffron, and eight new congeners named azafrines 3−10. Saffron saponins significantly inhibited TNF-α/IFN-γ-induced secretion of RANTES in human HaCaT cells at 1 μM ($p < 0.001$). Some of them further lowered TNF-α/IFN-γ-induced gene expression.

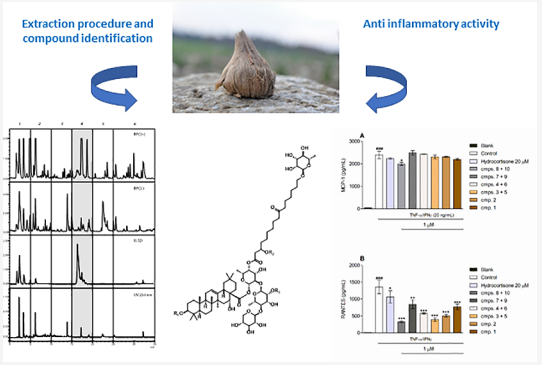

Saffron (*Crocus sativus* L., Iridaceae) is an autumn-flowering perennial geophyte forming underground corms.[1] As a triploid sterile plant, *C. sativus* only propagates by vegetative multiplication of the corms.[2] Saffron has been cultivated since antiquity for its characteristic and aromatic red stigmata, which are used as a precious spice, dye, herbal medicine, cosmetic ingredient, and odor-active substance in perfumes.[3] The earliest reports about saffron cultivation in eastern Mediterranean regions go back to 1700 to 1500 B.C.[4] Today, saffron is globally cultivated since it is one of the most expensive spices worldwide.[5] Top producers are Iran (90%), followed by Afghanistan, India, Greece, Morocco, Spain, Italy, and France.[6]

In traditional medicine, the stigmata, as well as extracts and tinctures, have been used to treat various health conditions such as insomnia, depression, pain, stomach ailments, tumors, asthma, sexual dysfunction, and kidney disorders. It has also been used as an emmenagogue and abortifacient agent.[7]

The phytochemistry and pharmacological properties of the stigmata have been extensively studied.[8,9] More than 160 volatile and nonvolatile constituents that contribute to the characteristic aroma and flavor of the spice have been identified.[10−13] The most characteristic secondary metabolites are carotenoids and apocarotenoids, which give the characteristic yellow to orange-red color, and monoterpenoid aldehydes such as picrocrocin and safranal, which are responsible for the bitter taste and the characteristic aroma, respectively.[10] In contrast, little is known about the phytochemicals of corms. They contain high amounts of sugars and amino and fatty acids.[14,15] A rhamnose-rich proteoglycan and several mannan-binding lectins were obtained from corm tissue,[16−18] and phytosterols, triterpenoid acids, and phenolic acids have been reported.[19] Crocetin and crocetin glycosides have been detected in developing corms.[20] The oil of corms contains large amounts of 2-furanone and long-chain fatty acids, along with smaller amounts of higher alkanes, volatile bisabolene-type sesquiterpenoids, and aldehydes such as safranal.[21,22] Finally, two oleanane-type triterpenoid saponins, azafrine 1 and azafrine 2, have been reported.[23]

Data on the pharmacological and biological properties of saffron corms are scarce. Proteins inducing or inhibiting platelet aggregation have been purified.[24,25] A proteoglycan was found to be cytotoxic against tumor cells in vitro[26] and to exhibit macrophage-activating effects at lower concentrations.[27] The triterpenoid saponins azafrines 1 and 2 showed cytotoxic activity

Special Issue: Special Issue in Honor of A. Douglas Kinghorn

Received: November 8, 2020
Published: February 18, 2021

https://dx.doi.org/10.1021/acs.jnatprod.0c01220
J. Nat. Prod. 2021, 84, 630−645

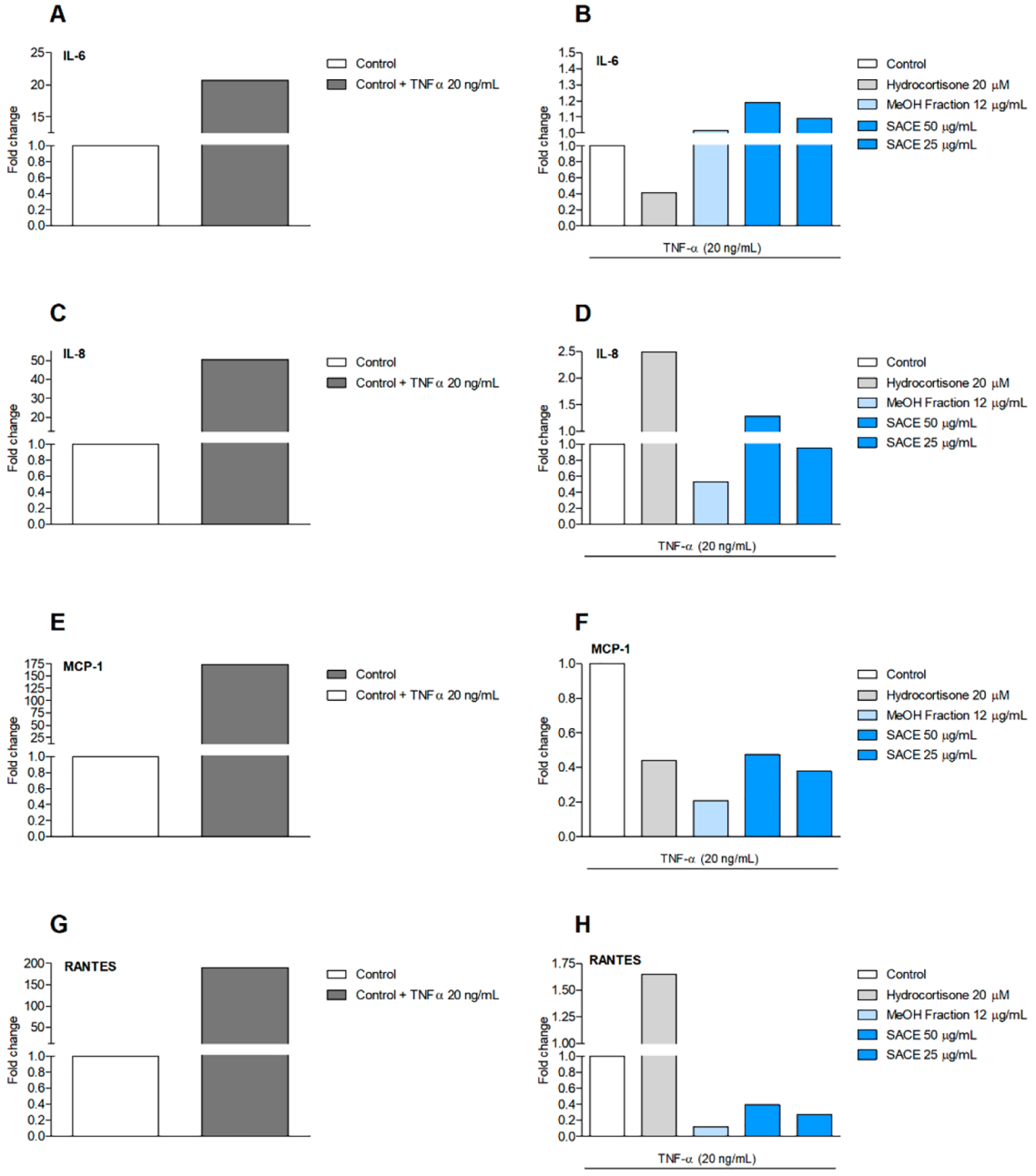

Figure 1. Effect of 70% EtOH saffron corm extract (SACE), sugar-depleted MeOH fraction, and hydrocortisone (20 μM) on TNF-α/IFN-γ-induced (20 ng/mL) gene expression of IL-6, IL-8, MCP-1, and RANTES in human HaCaT cells. Data represent changes in gene expression of the untreated control compared to TNF-α/IFN-γ (20 ng/mL) stimulation (A, C, E, G) and changes in gene expression of SACE and MeOH fraction after TNF-α/IFN-γ stimulation (B, D, F, H) compared to the TNF-α/IFN-γ (20 ng/mL)-stimulated control. The data represent the mean value of three independent experiments (n = 3).

in HeLa cells[23] and were patented as adjuvants for protein-based vaccines.[28] Lipophilic fractions of an EtOH corm extract showed antidepressant-like effects in animal behavioral models.[29]

For the production of saffron spice, significant amounts of corms are generated as a side product, and only a portion of them is replanted.[30,31] The other corms are either discarded or used as animal feed.[32] In a project aimed at the valorization of this biowaste product we observed that a 70% EtOH extract (SACE) of saffron corms inhibited tumor necrosis factor α (TNF-α)/interferon γ (IFN-γ)-induced gene expression of the chemokines monocyte chemotactic protein 1 (MCP-1) and regulated upon activation normal T-cell expressed and secreted (RANTES) and slightly increased the expression of interleukin 6 (IL-6) in human HaCaT keratinocytes (Figure 1). The secretion of IL-6 significantly increased in a concentration-dependent manner, while secretion of MCP-1 and RANTES decreased only at the highest concentration tested. IL-8 was not affected (Figure 2).

Keratinocytes produce a large number of pro- and anti-inflammatory cytokines upon stimulation by environmental triggers such as microorganisms, physical damage, or various cytokines. Under normal physiological conditions, levels of pro- and anti-inflammatory cytokines are balanced and highly regulated to control inflammatory processes, to initiate tissue repair, and to maintain cellular and intercellular homeostasis. A dysregulation of cytokines and an alteration of their receptors in

https://dx.doi.org/10.1021/acs.jnatprod.0c01220
J. Nat. Prod. 2021, 84, 630−645

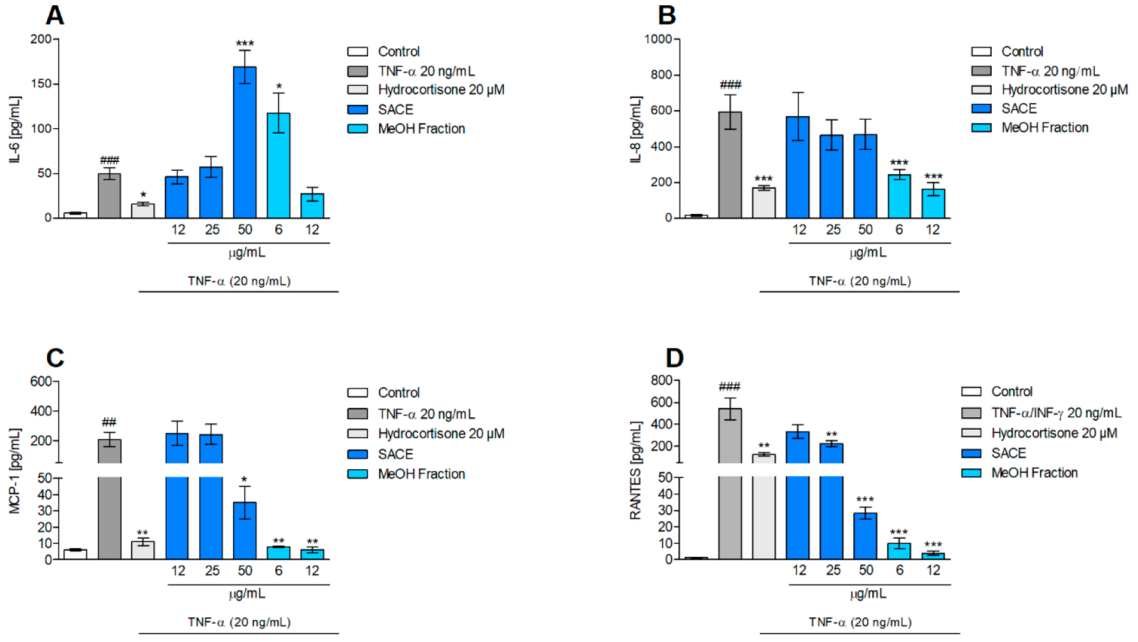

Figure 2. Effect of saffron corm extract (SACE), sugar-depleted MeOH fraction, and hydrocortisone (20 μM) on TNF-α/IFN-γ-induced (20 ng/mL) secretion of IL-6, IL-8, MCP-1, and RANTES in human HaCaT cells. Data represent the mean ± SEM of three independent experiments measured in duplicates (n = 3). $^{\#\#}p \leq 0.01$ vs control, $^{*}p \leq 0.05$ vs TNF-α, $^{**}p \leq 0.01$ vs TNF-α, $^{***}p \leq 0.001$ vs TNF-α.

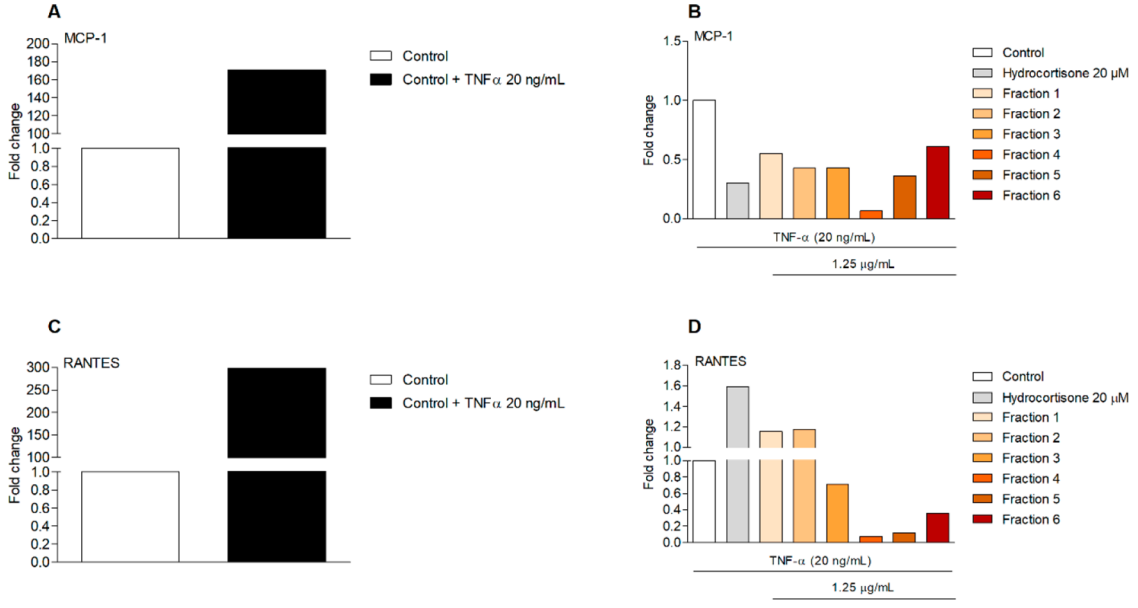

Figure 3. Effect of fractions 1−6 and hydrocortisone (20 μM) on TNF-α-induced (20 ng/mL) gene expression of MCP-1 and RANTES in human HaCaT cells. The data represent changes in gene expression of the untreated control compared to TNF-α (20 ng/mL) stimulation (A, C) and changes in gene expression of fractions 1−6 (1.25 μg/mL each) after TNF-α stimulation (B, D) compared to the TNF-α (20 ng/mL) stimulated control. The data represent the mean value of three independent experiments (n = 3).

inflammatory skin diseases lead to hyperproliferation of keratinocytes and infiltration of leukocytes, resulting in the clinical manifestation of skin diseases such as atopic dermatitis and psoriasis.[33,34] TNF-α and IFN-γ are primary inflammatory cytokines that activate the production of secondary inflammatory cytokines such as IL-6, IL-8, RANTES, and MCP-1.[35] Expression of IL-6 and IL-8 causes proliferation of keratinocytes and plays an important role in epidermal hyperplasia, psoriasis, and wound healing.[35−38] RANTES and MCP-1 are potent chemoattractants and activators for monocytes, granulocytes, and T-cells and are known to play a crucial role in atopic dermatitis, psoriasis, arthritis, and atherosclerosis.[34,35,39,40]

We here report on the activity-directed isolation and characterization of a series of unusual bidesmosidic triterpenoid saponins with a fatty acid residue attached to the pentasaccharide moiety at C-28 and on the testing of these saponins for inhibition of expression and release of proinflammatory cytokines.

https://dx.doi.org/10.1021/acs.jnatprod.0c01220
J. Nat. Prod. 2021, 84, 630−645

RESULTS AND DISCUSSION

Using a filtration of the 70% EtOH extract (SACE) over an HP-20 Diaion cartridge the sugars accounting for approximately 80% of the extract were removed by elution with water, and secondary metabolites were subsequently eluted with MeOH. The effects of the sugar-depleted MeOH fraction on the TNF-α/IFN-γ-induced gene expression and secretion of the chemokines IL-6, IL-8, MCP-1, and RANTES are shown in Figures 1 and 2, in comparison with SACE. Compared to the control, the expression of IL-6 was slightly increased, and it decreased for the other three chemokines. The secretion of IL-8, MCP-1, and RANTES was significantly decreased and comparable to or more pronounced than the effect of the positive control hydrocortisone. Given that the most prominent effects were seen on MCP-1 and RANTES, these two chemokines were subsequently used to track the active compounds in the MeOH fraction.

A portion of the sugar-depleted MeOH fraction was separated by semipreparative HPLC into six fractions, which were tested for their inhibitory activity on the TNF-α/IFN-γ-induced expression and secretion of RANTES and MCP-1 (Figures 3 and 4). An inhibition of expression of both chemokines was

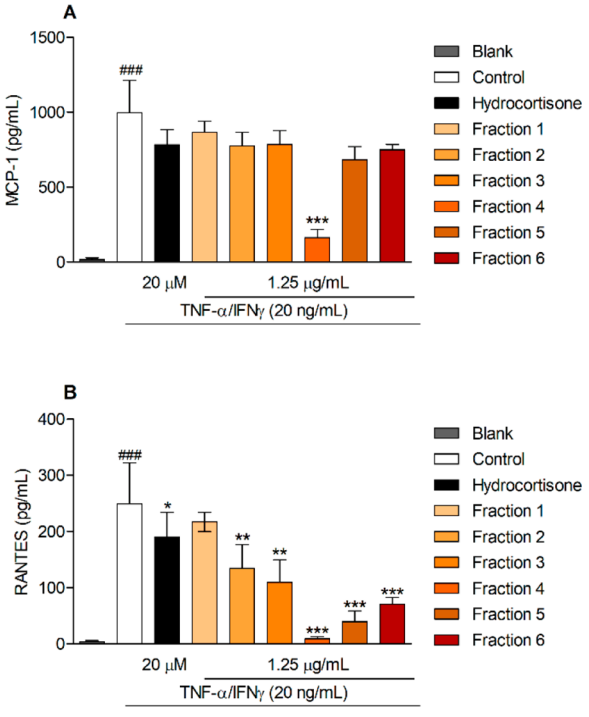

Figure 4. Effect of fractions 1−6 (1.25 μg/mL) and hydrocortisone (20 μM) on TNF-α/IFN-γ-induced (20 ng/mL) secretion of MCP-1 (A) and RANTES (B) in human HaCaT cells. The data represent the mean ± SEM of three independent experiments measured in triplicate (n = 3). $^{\#\#}p \leq 0.01$ vs control, $^{*}p \leq 0.05$ vs TNF-α, $^{**}p \leq 0.01$ vs TNF-α, $^{***}p \leq 0.001$ vs TNF-α.

mainly found in fraction 4 eluted between 15 and 20 min, and this was also in line with a potent inhibition of secretion (Figure 4). HPLC-UV-ELSD-MS analysis revealed the presence in the ELSD trace of a broad and non-UV-absorbing major peak (Figure 5) that eluted in the time window of the chromatogram corresponding to the active fraction.

For preparative isolation, a larger batch of corms was extracted with 70% EtOH. Removal of the sugar constituents was

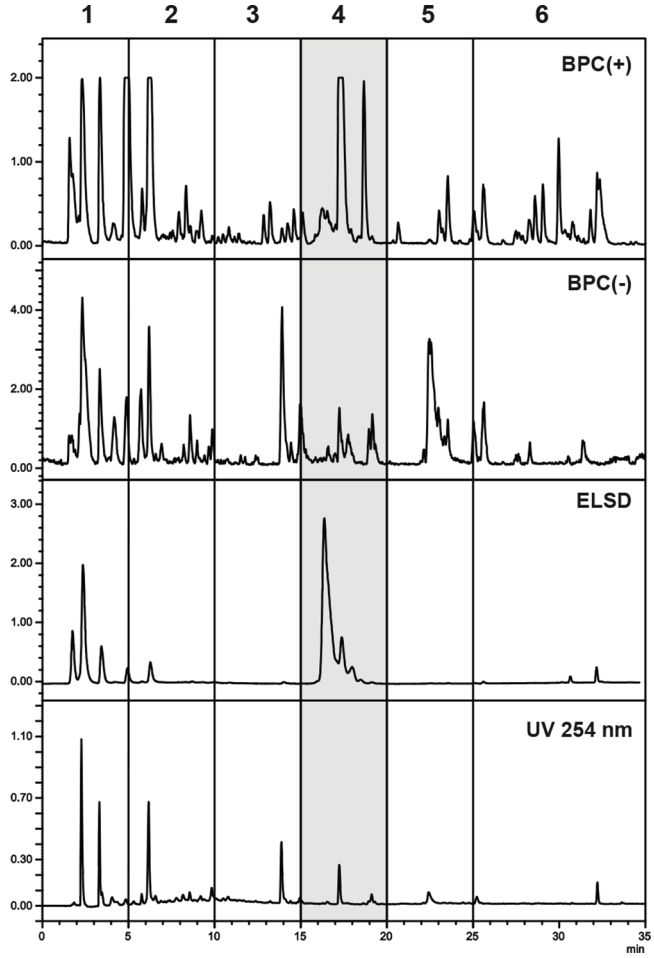

Figure 5. HPLC-PDA-ELSD-ESIMS analysis of the sugar-depleted MeOH fraction. Chromatographic conditions: SunFire C_{18}; 5−100% MeCN in water (both containing formic acid 0.1%) in 30 min; 0.4 mL/min; the region highlighted in gray corresponds to active fraction 4. BPC: base peak chromatograms in positive and negative modes.

performed by liquid/liquid partition between water and EtOAc, followed by water and n-BuOH. HPLC-UV-ELSD-MS analysis of the n-BuOH-soluble fraction confirmed the presence of the previously detected broad peak at t_R 15−20 min in the ELSD trace of the sugar-depleted MeOH fraction.

The n-BuOH-soluble fraction was separated by centrifugal partition chromatography (CPC). Further fractionation by flash chromatography on C_{18} and Diol cartridges, followed by semipreparative HPLC on a HILIC column, afforded six substances (I−VI) (Figure S2, Supporting Information). The substances that appeared chromatographically pure according to HPLC analysis on an RP-18 column were evaluated for their inhibitory effects on expression and secretion of MCP-1 and RANTES. Compared to the control, the substances increased expression of MCP-1 to varying degrees, while expression of RANTES was decreased (Figure 6). In contrast, no effect on MCP-1 secretion was observed, while all substances significantly decreased secretion of RANTES (Figure 7).

During structure elucidation, however, a close inspection of the NMR spectra revealed that four of these substances (I−IV) were in fact mixtures of two highly similar congeners, while substances V and VI were single compounds, which were subsequently identified as **1** and **2**. A total of 10 compounds were eventually obtained in pure form starting from a larger

https://dx.doi.org/10.1021/acs.jnatprod.0c01220
J. Nat. Prod. 2021, 84, 630−645

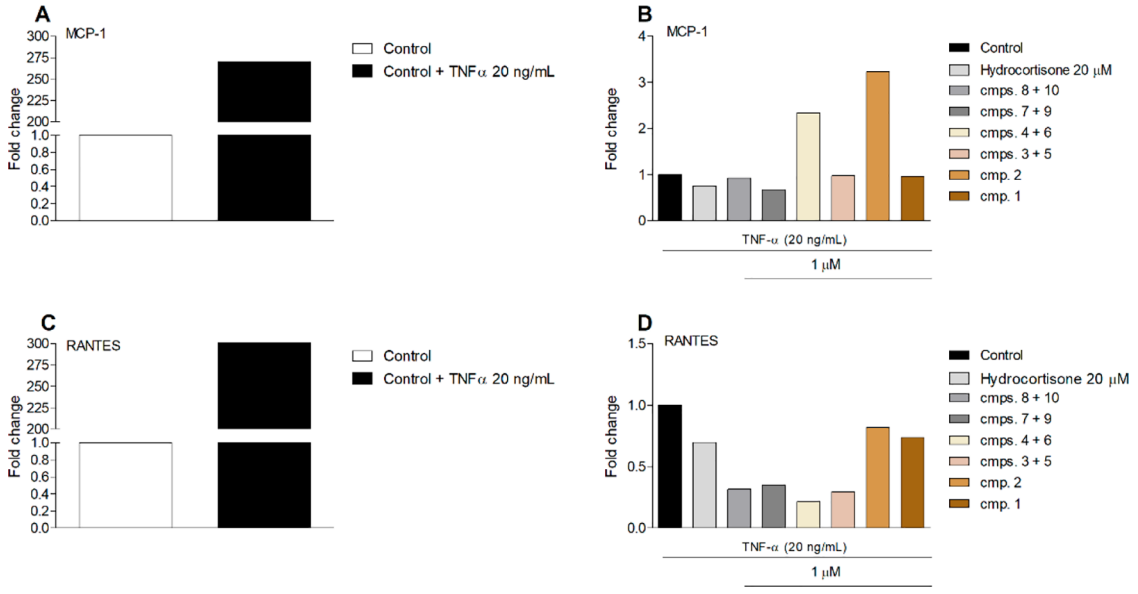

Figure 6. Effect of compounds **1**–**10** and hydrocortisone (20 μM) on TNF-α/IFN-γ-induced (20 ng/mL) gene expression of MCP-1 and RANTES in human HaCaT cells. Data represent changes in gene expression of the untreated control compared to TNF-α/IFN-γ (20 ng/mL) stimulation (A, C) and changes in gene expression of compounds **1**–**10** after TNF-α/IFN-γ stimulation (B, D) compared to TNF-α/IFN-γ (20 ng/mL)-stimulated control. The data represent the mean value of three independent experiments (n = 3).

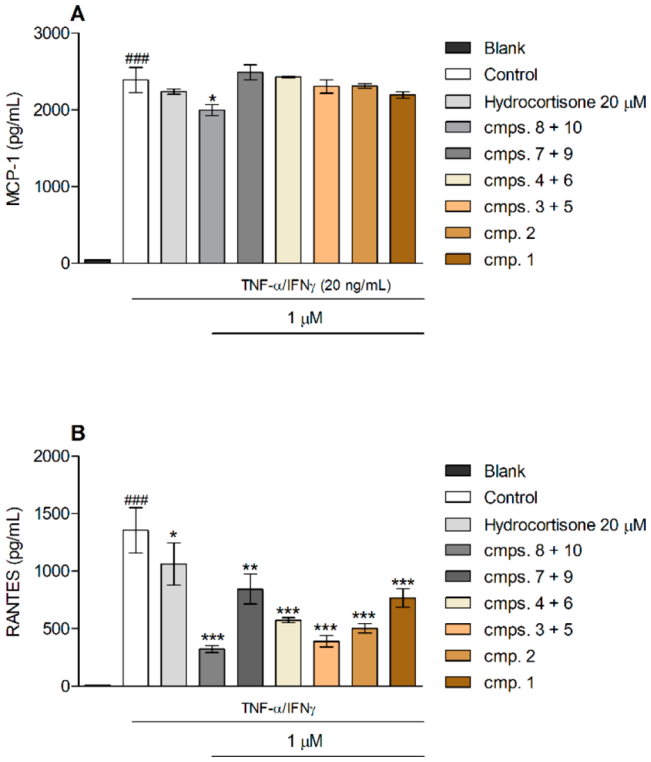

Figure 7. Effect of compounds **1**–**10** (1 μM) and hydrocortisone (20 μM) on TNF-α/IFN-γ-induced (20 ng/mL) secretion of MCP-1 (A) and RANTES (B) in human HaCaT cells. The data represent the mean ± SEM measured as triplicates (n = 3). $^{\#\#}p \leq 0.01$ vs control, $^{*}p \leq 0.05$ vs TNF-α, $^{**}p \leq 0.01$ vs TNF-α, $^{***}p \leq 0.001$ vs TNF-α.

portion of the n-BuOH-soluble fraction. CPC followed by preparative HPLC on an RP-18 column afforded a saponin fraction. This mixture was resolved into 10 saponins (**1**–**10**) by preparative HPLC on a HILIC column followed by semi-preparative HPLC on HILIC and C_{18}-AQ columns. Compounds **8** and **10** (and minor amounts of **7** and **9**), **7** and **9** (and minor amounts of **8** and **10**), **4** and **6** (and minor amounts of **3** and **5**), and **3** and **5** were contained in substances I–IV, respectively. The successful combination of RP-18, HILIC, and C_{18}-AQ columns for the separation of this complex mixture of structurally closely related saponins is shown in Figure 8 and in Figure S3 (Supporting Information).

Compounds **1** and **2** both had a molecular formula of $C_{92}H_{150}O_{43}$ (HRESIMS m/z 1965.9411 $[M + Na]^+$ and 1965.9493 $[M + Na]^+$; calcd for $C_{92}H_{150}NaO_{43}^+$, 1965.9443). 1D and 2D NMR spectra (Tables S1 and S2, Supporting Information) indicated that both compounds were bidesmosidic glycosides of echinocystic acid with a 3,16-dihydroxy-10-oxo-hexadecanoic acid residue attached to the pentasaccharide moiety at C-28. Acid hydrolysis followed by GC-MS analysis revealed the presence of L-rhamnose, D-fucose, D-xylose, L-arabinose, and D-galactose in both compounds. In addition, D-glucuronic acid was detected in the case of **1**, and D-galacturonic acid in that of **2**. The compounds were identified after extensive analysis of COSY, HSQC, HMBC, HSQC-TOCSY, and ROESY spectra (Tables S1 and S2, Figures S4–S15, Supporting Information) as azafrine 1 (**1**) and azafrine 2 (**2**), respectively. These two saponins have been previously reported in saffron corms.[23] They differ from each other only by the presence of a D-glucuronic acid or a D-galacturonic acid moiety at C-3. The key HMBC correlations confirming the connectivities between the aglycone, the sugar moieties, and the fatty acid residue in **1** are shown in Figure 9.

Compounds **3**–**10** had the same aglycone and fatty acid moieties as azafrines 1 (**1**) and 2 (**2**) but differed in their glycosylation pattern.

Saponins **3** and **4** had a molecular formula of $C_{86}H_{140}O_{38}$ (HRESIMS at m/z 1803.8844 $[M + Na]^+$ and 1803.8916 $[M + Na]^+$; calcd for $C_{86}H_{140}NaO_{38}^+$, 1803.8915), indicative of one hexosyl moiety less than in **1** and **2**. The 1D and 2D NMR data were very similar to those of **1** and **2** but lacked the signals of the galactosyl residue, which was obvious from the absence of the

https://dx.doi.org/10.1021/acs.jnatprod.0c01220
J. Nat. Prod. 2021, 84, 630–645

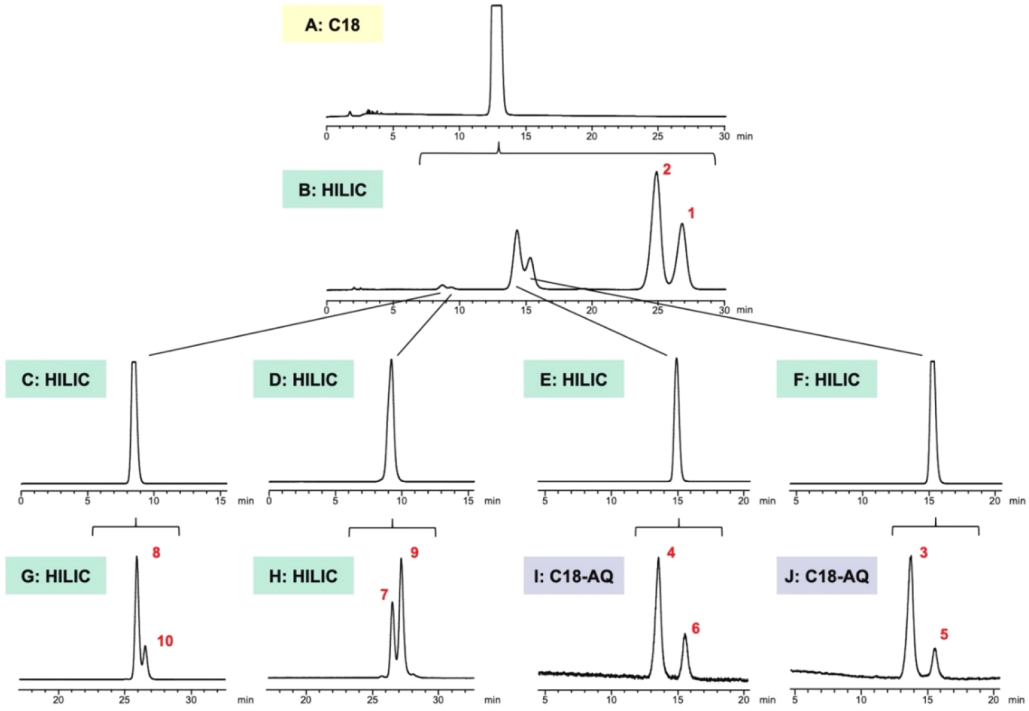

Figure 8. Combination of different HPLC column chemistries and mobile phases for the separation of compounds **1**−**10**. Evaporative light scattering detection (ELSD) chromatographic traces of analytical separations are shown. Chromatographic conditions: A: SunFire C_{18} (3.5 μm, 3 × 150 mm i.d.); 70−100% MeOH in water in 30 min; 0.4 mL/min; B: Nucleodur HILIC (5 μm, 3 × 150 mm i.d.); 83% MeCN in water; 0.4 mL/min; C−F: Nucleodur HILIC (5 μm, 3 × 150 mm i.d.); 83% MeCN in water; 0.4 mL/min; G, H: Nucleodur HILIC (5 μm, 3 × 150 mm i.d.); 90% MeCN in water; 0.4 mL/min; I, J: ReproSil-Pur 120 C_{18}-AQ (3 μm, 3 × 150 mm i.d.); 39% MeCN in water; 0.5 mL/min. All mobile phases contained 0.1% formic acid. Peak numbers **1**−**10** in red correspond to compound numbers **1**−**10**.

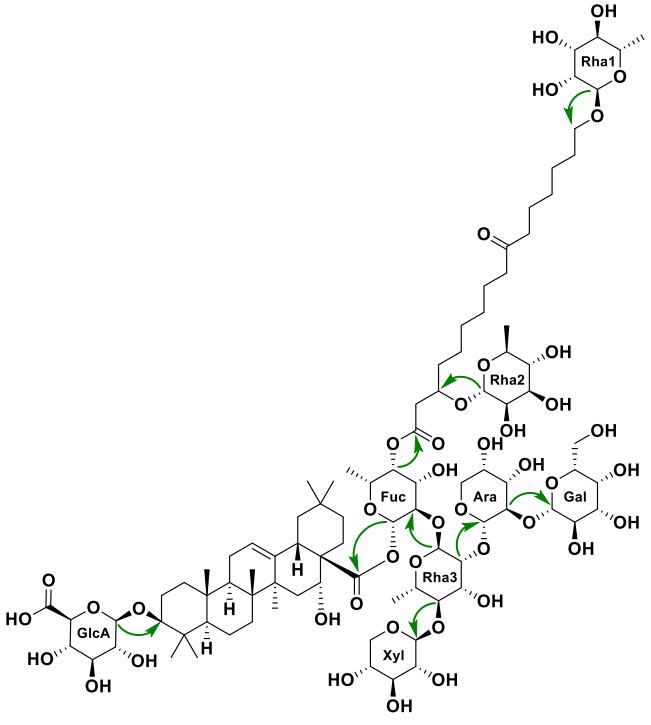

Figure 9. Key HMBC correlations (green arrows) for azafrine 1 (**1**).

anomeric signals observed in **1** (δ_H 4.33, δ_C 104.0) and **2** (δ_H 4.33, δ_C 104.0) for this sugar moiety (Tables 1 and 2). Compared to **1** and **2**, shielding of C-2_{Ara} and deshielding of C-1_{Ara} and C-3_{Ara} were seen. GC-MS analysis of sugars confirmed the absence of D-galactose and the presence of L-rhamnose, D-fucose, D-xylose, and L-arabinose. In addition, D-glucuronic acid was identified in the case of saponin **3**, and D-galacturonic acid in the case of **4**. Compounds **3** and **4** were new compounds and named azafrine 3 and azafrine 4, respectively.

A molecular formula of $C_{86}H_{140}O_{39}$ was assigned to compounds **5** and **6** (HRESIMS at m/z 1819.8827 $[M + Na]^+$ and 1819.8901 $[M + Na]^+$; calcd for $C_{86}H_{140}NaO_{39}^+$, 1819.8864). When compared to **1** and **2**, a difference of 146 amu suggested the lack of a deoxyhexosyl moiety. The 1D and 2D NMR data (Tables 1 and 2) were similar to those of **1** and **2** but without the signals of the rhamnosyl residue connected to the long-chain fatty acid moiety at C-3′. This was apparent from the absence of the anomeric signals for this sugar moiety observed in **1** (δ_H 4.70, δ_C 98.8) and **2** (δ_H 4.70, δ_C 98.8). Compared to **1** and **2**, shielding of C-3′ and deshielding of C-2′ and C-4′ of the 3,16-dihydroxy-10-oxo-hexadecanoic acid moiety were observed. The presence of L-rhamnose, D-fucose, D-xylose, and L-arabinose was confirmed by GC-MS analysis after acid hydrolysis. In addition, D-glucuronic acid was identified in the case of compound **5**, while D-galacturonic acid was obtained from **6**. Compounds **5** and **6** are new compounds and were named azafrines 5 and 6, respectively.

Compounds **7** and **8** had a molecular formula of $C_{80}H_{130}O_{34}$ (HRESIMS at m/z 1657.8340 $[M + Na]^+$ and 1657.8340 $[M + Na]^+$; calcd for $C_{80}H_{130}NaO_{34}^+$, 1657.8336), suggesting one hexosyl residue less than in **5** and **6**. The 1D and 2D NMR data (Tables 3 and 4) were very similar to those of **5** and **6** but lacked the signals of the galactosyl residue, and in particular the anomeric signals (**5**; δ_H 4.34, δ_C 103.9; **6**; δ_H 4.33, δ_C 103.9). Compared to **5** and **6**, shielding of C-2_{Ara} and deshielding of C-1_{Ara} and C-3_{Ara} were observed. Acid hydrolysis followed by GC-

https://dx.doi.org/10.1021/acs.jnatprod.0c01220
J. Nat. Prod. 2021, 84, 630−645

Chart 1

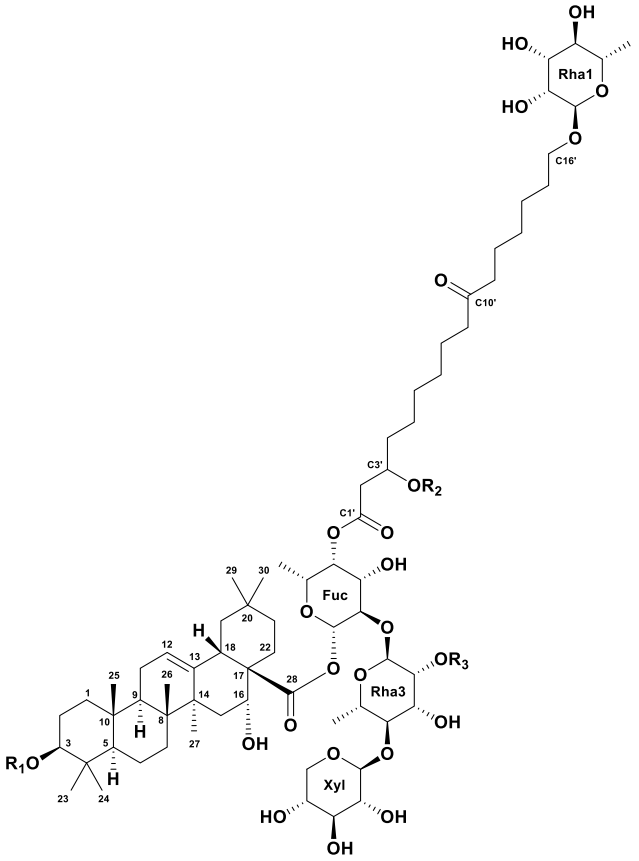

	R_1	R_2	R_3
1	D-GlcA	L-Rha	L-Ara-(2→1)-D-Gal
2	D-GalA	L-Rha	L-Ara-(2→1)-D-Gal
3	D-GlcA	L-Rha	L-Ara
4	D-GalA	L-Rha	L-Ara
5	D-GlcA	H	L-Ara-(2→1)-D-Gal
6	D-GalA	H	L-Ara-(2→1)-D-Gal
7	D-GlcA	H	L-Ara
8	D-GalA	H	L-Ara
9	D-GlcA	L-Rha	H
10	D-GalA	L-Rha	H

MS analysis confirmed the absence of D-galactose and the presence of L-rhamnose, D-fucose, D-xylose, and L-arabinose. In addition, D-glucuronic acid was identified in the case of saponin **7**, and D-galacturonic acid for **8**. Compounds **7** and **8** are new saponins and were named azafrine 7 and azafrine 8, respectively.

Compounds **9** and **10** both had a molecular formula of $C_{81}H_{132}O_{34}$(HRESIMS at m/z 1671.8415 $[M + Na]^+$ and 1671.8479 $[M + Na]^+$; calcd for $C_{81}H_{132}NaO_{34}^+$, 1671.8493). This suggested the lack of a pentosyl moiety compared to **3** and **4**. The 1D and 2D NMR data (Tables 3 and 4) indicated that both compounds differed from saponins **3** and **4** by the absence of the arabinosyl residue. Weak anomeric signals of an arabinosyl moiety (δ_H 4.23, δ_C 105.8) could be observed, which, given their low intensities, belonged to unidentified minor saponins bearing an arabinosyl moiety attached to the rhamnosyl residue as in **3** and **4**. The presence of L-rhamnose, D-fucose, and D-xylose was confirmed by GC-MS analysis, along with a minor amount of L-arabinose due to the presence of these unidentified minor saponins. In addition, D-glucuronic acid was identified for compound **9**, while D-galacturonic acid was found in the case of **10**. Compounds **9** and **10** are new saponins named azafrine 9 and azafrine 10, respectively. The configuration at C-3′ of the 3,16-dihydroxy-10-oxo-hexadecanoic acid residue in compounds **1**−**10** was not established.

From a chemotaxonomic perspective, the occurrence of triterpenoidal saponins in monocotyledonous plants is uncommon, as they usually produce steroidal saponins. Saponins bearing a long-chain fatty acid residue appear to be restricted to the family Iridaceae and have so far been found only in *C. sativus* and in the genus *Crocosmia*.[41]

The effects of the sugar-depleted MeOH fraction on the TNF-α/IFN-γ-induced gene expression and secretion of chemokines IL-6, IL-8, MCP-1, and RANTES in human HaCaT keratinocytes could be linked to a series of complex triterpenoidal saponins. Fractions and compounds overall inhibited expression and secretion of RANTES more potently than hydrocortisone. Expression but not secretion of MCP-1 was inhibited (Figures 6 and 7). Chemotactic cytokines RANTES and MCP-1 contribute to the recruitment of leukocytes to the skin and are involved in the pathogenesis of psoriasis and atopic dermatitis.[42−44] MCP-1 was shown to be induced by lipopolysaccharides (LPS), interleukins, and tumor necrosis factor (TNF-α). MCP-1 was observed in high concentrations in psoriasis patients, but also in other skin diseases. The expression of RANTES plays an active role in the inflammatory response and has been linked to various inflammatory diseases such as atopic dermatitis, psoriasis, arthritis, atherosclerosis, and others.[44]

Anti-inflammatory activities of oleanane-type saponins such as asiaticoside have been shown earlier. The compound was found to decrease the generation of antigen-induced tumor necrosis factor α, interleukin 4 (IL-4), IL-8, and IL-1β in RBL-2H3 cells sensitized by IgE.[45] Kimura et al. investigated the effects of asiaticoside in burn wound exudates and demonstrated that asiaticoside enhanced MCP-1 production in HaCaT cells, but had no direct effect on VEGF production.[46] The authors concluded that the enhancement of burn wound healing by asiaticoside was due to the stimulation of VEGF production caused by an increased expression of MCP-1 in keratinocytes. Cho et al. reported that Δ(11,13) oleanane-type triterpenoids from *Tetrapanax papyriferus* significantly reduced the LPS-

https://dx.doi.org/10.1021/acs.jnatprod.0c01220
J. Nat. Prod. 2021, 84, 630−645

Table 1. ^{1}H and ^{13}C NMR Spectroscopic Data of the Aglycone and Fatty Acid Residue in Compounds 3−6 (DMSO-d_6; 600 MHz for ^{1}H and 151 MHz for ^{13}C NMR; δ in ppm)

	3		4		5		6	
position	δ_C, type	δ_H (J in Hz)	δ_C, type	δ_H (J in Hz)	δ_C, type	δ_H (J in Hz)	δ_C, type	δ_H (J in Hz)
1	38.3, CH_2	0.90[a]	38.4, CH_2	0.87[a]	38.3, CH_2	0.89[a]	38.3, CH_2	0.89[a]
		1.53[a]		1.53[a]		1.52[a]		1.52[a]
2	25.4, CH_2	1.51[a]	25.5, CH_2	1.48[a]	25.5, CH_2	1.49[a]	25.5, CH_2	1.49[a]
		1.86[a]		1.85[a]		1.85[a]		1.83[a]
3	87.9, CH	3.05[a]	88.0, CH	3.01[a]	87.9, CH	3.03[a]	87.9, CH	3.01[a]
4	38.6, C		38.8, C		38.7, C		38.8, C	
5	55.1, CH	0.70[a]	55.2, CH	0.68[a]	55.1, CH	0.70[a]	55.2, CH	0.69[a]
6	17.8, CH_2	1.25[a]	17.9, CH_2	1.25[a]	17.9, CH_2	1.25[a]	18.0, CH_2	1.25[a]
		1.47[a]		1.45[a]		1.46[a]		1.46[a]
7	32.6, CH_2	1.29[a]	32.6, CH_2	1.32[a]	32.6, CH_2	1.32[a]	32.6, CH_2	1.31[a]
		1.39[a]		1.38[a]		1.39[a]		1.38[a]
8	39.2, C		39.1, C		39.1, C		39.1, C	
9	46.1, CH	1.52[a]	46.1, CH	1.51[a]	46.1, CH	1.52[a]	46.1, CH	1.51[a]
10	36.2, C		36.3, C		36.3, C		36.3, C	
11	23.0, CH_2	1.80[a]	23.0, CH_2	1.80[a]	22.9, CH_2	1.80[a]	22.9, CH_2	1.80[a]
12	121.3, CH	5.25[a]	121.4, CH	5.25, m	121.6, CH	5.23, m	121.6, CH	5.22[a]
13	143.2, C		143.3, C		143.1, C		143.0, C	
14	41.0, C		41.1, C		41.0, C		41.0, C	
15	34.6, CH_2	1.30[a]	34.7, CH_2	1.29[a]	34.7, CH_2	1.30[a]	34.7, CH_2	1.30[a]
		1.60[a]		1.56[a]		1.60[a]		1.62[a]
16	72.7, CH	4.32[a]	72.8, CH	4.30[a]	72.6, CH	4.33[a]	72.6, CH	4.31[a]
17	48.1, C		48.1, C		48.0, C		48.0, C	
18	40.4, CH	2.84[c]	40.4, CH	2.83, d (12.3)	40.4, CH	2.84, d (12.2)	40.4, CH	2.84, d (12.7)
19	46.5, CH_2	0.99[a]	46.6, CH_2	1.00[a]	46.5, CH_2	1.00[a]	46.5, CH_2	1.00[a]
		2.22[c]		2.21, dd (12.5, 12.5)		2.23, dd (12.5, 12.5)		2.24, dd (13.8, 13.8)
20	29.9, C		30.1, C		30.1, C		30.1, C	
21	35.0, CH_2	1.09[a]	35.1, CH_2	1.08[a]	35.0, CH_2	1.08[a]	35.0, CH_2	1.09[a]
		1.87[a]		1.88[a]		1.90[a]		1.89, m
22	30.4, CH_2	1.66[a]	30.6, CH_2	1.63[a]	30.6, CH_2	1.64[a]	30.6, CH_2	1.65[a]
		1.82[a]		1.81[a]		1.80[a]		1.79[a]
23	27.6, CH_3	0.98[c]	27.7, CH_3	0.98[a]	27.6, CH_3	0.98[a]	27.7, CH_3	0.98[a]
24	16.4, CH_3	0.76[c]	16.5, CH_3	0.76, s	16.5, CH_3	0.76, s	16.5, CH_3	0.75, s
25	15.3, CH_3	0.88[a]	15.5, CH_3	0.88[a]	15.4, CH_3	0.87[a]	15.4, CH_3	0.87[a]
26	16.8, CH_3	0.70[c]	16.9, CH_3	0.69[a]	16.8, CH_3	0.67[a]	16.8, CH_3	0.67[a]
27	26.1, CH_3	1.31[a]	26.2, CH_3	1.30[a]	26.2, CH_3	1.31[a]	26.2, CH_3	1.30[a]
28	175.0, C		175.1, C		175.0, C		175.1, C	
29	32.7, CH_3	0.83[c]	32.8, CH_3	0.82, s	32.8, CH_3	0.84, s	32.8, CH_3	0.83, s
30	24.2, CH_3	0.91[a]	24.2, CH_3	0.90[a]	24.2, CH_3	0.90[a]	24.2, CH_3	0.90[a]
C1′	170.5, C		170.7, C		171.1, C		171.1, C	
C2′	38.4, CH_2	2.48[a]	38.3, CH_2	2.47[a]	42.6, CH_2	2.46, m	42.6, CH_2	2.45[a]
		2.69[a]		2.71, dd (15.0, 4.1)				
C3′	72.5	3.92[c]	72.3, CH	3.91, tt (5.3, 5.3)	67.2, CH	3.83[a]	67.3, CH	3.82[a]
C4′	34.2	1.54[a]	34.3, CH_2	1.54[a]	36.7, CH_2	1.41[a]	36.7, CH_2	1.40[a]
C5′	24.4, CH_2	1.33[a]	24.5, CH_2	1.32[a]	24.9, CH_2	1.27[a]	24.9, CH_2	1.27[a]
						1.37[a]		1.37[a]
C6′	28.6, CH_2	1.23[a]	28.6, CH_2	1.21[a]	28.7, CH_2	1.21[a]	28.6, CH_2	1.26[a]
C7′	28.3, CH_2	1.26[a]	28.6, CH_2	1.25[a]	28.6, CH_2	1.23[a]	28.6, CH_2	1.23[a]
C8′	23.1, CH_2	1.44[a]	23.2, CH_2	1.43[a]	23.2, CH_2	1.44[a]	23.2, CH_2	1.44[a]
C9′	41.7, CH_2	2.37[c]	41.8, CH_2	2.37, t (6.7)	41.8, CH_2	2.38, t (7.1)	41.8, CH_2	2.37, t (7.1)
C10′	210.3, C		210.6, C		210.6, C		210.6, C	
C11′	41.7, CH_2	2.37[c]	41.8, CH_2	2.37, t (6.7)	41.8, CH_2	2.38, t (7.1)	41.8, CH_2	2.37, t (7.1)
C12′	23.1, CH_2	1.44[a]	23.2, CH_2	1.43[a]	23.3, CH_2	1.45[a]	23.3, CH_2	1.45[a]
C13′	28.8, CH_2	1.17[a]	28.7, CH_2	1.19[a]	28.7, CH_2	1.24[a]	28.6, CH_2	1.20[a]
C14′	25.5, CH_2	1.27[a]	25.6, CH_2	1.26[a]	25.6, CH_2	1.28[a]	25.6, CH_2	1.29[a]
C15′	29.0, CH_2	1.48[a]	29.0, CH_2	1.47[a]	29.0, CH_2	1.48[a]	29.0, CH_2	1.48[a]
C16′	66.4, CH_2	3.31[a]	66.4, CH_2	3.30[a]	66.3, CH_2	3.30[a]	66.3, CH_2	3.30[a]
		3.52[a]		3.51[a]		3.52[a]		3.52[a]

[a]Overlapping signals. [b]Signal not visible. [c]Signals are split, possibly due to the viscosity of the sample.

https://dx.doi.org/10.1021/acs.jnatprod.0c01220
J. Nat. Prod. 2021, 84, 630−645

Table 2. ^{1}H and ^{13}C NMR Spectroscopic Data of the Glycosidic Moiety in Compounds 3−6 (DMSO-d_6; 600 MHz for ^{1}H and 151 MHz for ^{13}C NMR; δ in ppm)

	3		4		5		6	
position	δ_C, type	δ_H (J in Hz)	δ_C, type	δ_H(J in Hz)	δ_C, type	δ_H (J in Hz)	δ_C, type	δ_H (J in Hz)
Sugar moiety at C-3								
GalA								
1			105.7, CH	4.11, br s			106.0, CH	4.07, br s
2			70.8, CH	3.30[a]			[b]	[b]
3			73.4, CH	3.24[a]			73.9, CH	3.17[a]
4			69.7, CH	3.86[a]			69.9, CH	3.87[a]
5			[b]	[b]			[b]	[b]
6			[b]				[b]	
GlcA								
1	105.2, CH	4.18[c]			105.3, CH	4.15, d (5.7)		
2	74.0, CH	2.99[a]			73.9, CH	2.96, m		
3	76.7, CH	3.10[a]			76.6, CH	3.13[a]		
4	[b]	[b]			[b]	[b]		
5	[b]	[b]			[b]	[b]		
6	[b]				[b]			
Sugar moiety at C-28								
Fuc								
1	93.0, CH	5.31[a]	93.0, CH	5.30, d (7.8)	92.8, CH	5.32[a]	92.8, CH	5.32[a]
2	74.6, CH	3.50[a]	74.4, CH	3.47[a]	74.8, CH	3.48[a]	74.7, CH	3.49[a]
3	71.5, CH	3.80[a]	71.5, CH	3.80[a]	71.7, CH	3.81[a]	71.7, CH	3.80[a]
4	73.5, CH	4.94, br s	73.4, CH	4.91, br s	73.2, CH	4.92, br s	73.2, CH	4.91, br s
5	68.8, CH	3.84[a]	68.8, CH	3.85[a]	68.9, CH	3.85[a]	68.9, CH	3.84[a]
6	15.8, CH_3	0.93[c]	16.0, CH_3	0.92, d (5.9)	16.0, CH_3	0.95, d (6.3)	15.9, CH_3	0.94, d (6.0)
Rha3								
1	98.7, CH	5.27[a]	98.7, CH	5.27, br s	98.6, CH	5.30[a]	98.5, CH	5.31[a]
2	79.0, CH	3.86[a]	79.3, CH	3.82[a]	78.1, CH	3.84[a]	78.2, CH	3.83[a]
3	70.4, CH	3.74[a]	70.5, CH	3.71[a]	70.3, CH	3.71[a]	70.2, CH	3.71[a]
4	81.9, CH	3.39[a]	81.7, CH	3.38[a]	82.1, CH	3.36[a]	82.0, CH	3.36[a]
5	67.1, CH	3.59[a]	67.0, CH	3.57[a]	67.0, CH	3.56[a]	66.9, CH	3.55[a]
6	17.8, CH_3	1.18[c]	17.9, CH_3	1.17, d (5.8)	18.0, CH_3	1.19, d (5.9)	18.0, CH_3	1.19, d (5.7)
Xyl								
1	105.1, CH	4.42[c]	105.1, CH	4.41, d (7.3)	104.7, CH	4.48, d (7.5)	104.7, CH	4.48, d (7.3)
2	74.4, CH	3.03[a]	74.4, CH	3.01[a]	74.6, CH	2.99[a]	74.6, CH	2.98[a]
3	76.5, CH	3.15[a]	76.6, CH	3.13[a]	76.3, CH	3.18[a]	76.3, CH	3.17[a]
4	69.6, CH	3.29[a]	69.5, CH	3.26[a]	69.6, CH	3.25[a]	69.6, CH	3.24[a]
5	65.8, CH_2	3.06[a]	65.9, CH_2	3.03[a]	65.7, CH_2	3.16[a]	65.7, CH_2	3.14[a]
		3.71[a]		3.70[a]		3.65[a]		3.65[a]
Ara								
1	105.1, CH	4.32[a]	105.3, CH	4.28[a]	102.0, CH	4.56, d (5.4)	102.0, CH	4.56, d (4.8)
2	70.9, CH	3.42[a]	70.7, CH	3.39[a]	78.1, CH	3.69[a]	78.1, CH	3.69[a]
3	72.4, CH	3.37[a]	72.4, CH	3.34[a]	71.1, CH	3.63[a]	71.1, CH	3.62[a]
4	67.4, CH	3.64[a]	67.6, CH	3.61[a]	66.2, CH	3.70[a]	66.2, CH	3.70[a]
5	65.2, CH_2	3.38[a]	65.5, CH_2	3.37[a]	63.7, CH_2	3.34[a]	63.7, CH_2	3.33[a]
		3.68[a]		3.66[a]		3.66[a]		3.66[a]
Gal								
1					103.9, CH	4.34[a]	103.9, CH	4.33[a]
2					71.0, CH	3.35[a]	71.1, CH	3.33[a]
3					73.3, CH	3.31[a]	73.3, CH	3.29[a]
4					67.7, CH	3.67[a]	67.7, CH	3.66[a]
5					75.4, CH	3.38[a]	75.4, CH	3.38[a]
6					60.0, CH_2	3.51[a]	59.9, CH_2	3.50[a]
						3.59[a]		3.58[a]
Sugar moiety at C-3′								
Rha2								
1	98.8, CH	4.72[c]	98.8, CH	4.70, br s				
2	70.8, CH	3.58[a]	70.8, CH	3.54[a]				
3	70.9, CH	3.42[a]	70.9, CH	3.39[a]				
4	72.0, CH	3.19[a]	71.9, CH	3.18[a]				

https://dx.doi.org/10.1021/acs.jnatprod.0c01220
J. Nat. Prod. 2021, 84, 630−645

Table 2. continued

	3		4		5		6	
position	δ_C, type	δ_H (J in Hz)	δ_C, type	δ_H(J in Hz)	δ_C, type	δ_H (J in Hz)	δ_C, type	δ_H (J in Hz)
5	68.9, CH	3.46[a]	69.0, CH	3.44[a]				
6	17.8, CH_3	1.13[a]	17.9, CH_3	1.12, d (6.0)				
Sugar moiety at C-16′								
Rha1								
1	99.9, CH	4.53[c]	100.0, CH	4.50, br s	99.9, CH	4.51, br s	100.0, CH	4.51, br s
2	70.6, CH	3.59[a]	70.6, CH	3.57[a]	70.6, CH	3.57[a]	70.6, CH	3.58[a]
3	70.9, CH	3.42[a]	71.1, CH	3.41[a]	70.8, CH	3.40[a]	70.8, CH	3.40[a]
4	72.0, CH	3.19[a]	72.0, CH	3.16[a]	72.0, CH	3.18[a]	72.0, CH	3.16[a]
5	68.2, CH	3.39[a]	68.4, CH	3.36[a]	68.4, CH	3.37[a]	68.4, CH	3.35[a]
6	17.8, CH_3	1.13[a]	17.8, CH_3	1.11, d (6.0)	17.9, CH_3	1.13, d (6.3)	17.9, CH_3	1.13, d (5.3)

[a]Overlapping signals. [b]Signal not visible. [c]Signals are split, possibly due to the viscosity of the sample.

induced expression of COX-2 and pro-inflammatory cytokines such as TNF-α and IL-6.[47]

In summary, our in vitro data suggest that saffron saponins possess anti-inflammatory properties by affecting expression and secretion of chemotactic cytokines and thus could be possibly used as topical agents against inflammatory skin diseases such as atopic dermatitis and psoriasis. This is in line with findings reported for other oleanane-type saponins such as asiaticoside. However, hitherto no clinical trial has been published using these triterpenoids in therapy.

EXPERIMENTAL SECTION

General Experimental Procedures. Centrifugal partition chromatography was performed on an ARMEN SPOT centrifugal partition chromatography instrument system (AlphaCrom, Switzerland) equipped with a ProStar 210 solvent delivery module pump, a ProStar 325 UV/vis detector, and a ProStar 704 fraction collector (all Varian Inc., USA).

Flash chromatography was carried out on a Sepacore flash chromatography system (Büchi, Switzerland) consisting of a C-660 fraction collector, a C-605 pump module, a C-640 UV photometer, and a C-620 control unit. Data acquisition and processing was carried out by SepacoreRecord software. C_{18} (80 g, 40−63 μm) and Diol (80 g, 40−63 μm) Sepacore flash cartridges were used.

HPLC-PDA-ELSD-ESIMS analysis was performed on a chromatographic system consisting of a degasser, quaternary pump (LC-20AD), a column oven (CTO-20AC), a PDA detector (SPD-M20A), a triple quadrupole mass spectrometer (LCMS-8030) (all Shimadzu, Kyoto, Japan), and an ELSD 3300 detector (Alltech). Separations were carried out on a SunFire C_{18} column (3.5 μm, 3 × 150 mm i.d., Waters) equipped with a guard column (3 × 10 mm i.d.), a Nucleodur HILIC column (5 μm, 3 × 150 mm i.d., Macherey-Nagel), or a ReproSil-Pur 120 C_{18}-AQ column (3 μm, 3 × 150 mm i.d., Dr. Maisch GmbH). The flow rate for analytical investigations was 0.4 or 0.5 mL/min. The LabSolutions software (Shimadzu) was used for data acquisition and processing.

Preparative HPLC was carried out on a Preparative LC/MSD system (Agilent Technologies, Santa Clara, CA, USA) consisting of a binary pump (1260 Prep bin pump, 1290 Infinity II), a quaternary pump (G1311A Quat pump, 1200 Series), a 1290 Infinity II valve drive manual injection system, a PDA detector (1100 Series), and a 6120 quadrupole LC/MS. A SunFire Prep C_{18} OBD column (5 μm, 30 × 150 mm i.d., Waters, Milford, MA, USA), equipped with a C_{18} Prep guard column (10 × 30 mm i.d.), or a Nucleodur HILIC column (5 μm, 32 × 150 mm i.d., Macherey-Nagel), equipped with a Nucleodur HILIC guard column (10 × 32 mm i.d.), was used. MeCN (or MeOH) and water, both containing 0.1% formic acid, were used as mobile phase. The flow rate was 20 mL/min. Data acquisition and processing was performed using ChemStation software (Agilent Technologies).

Semipreparative HPLC separations were performed on an HP 1100 Series system (Agilent Technologies, Santa Clara, CA, USA) consisting of a binary pump (G1312A bin pump), auto sampler (G1367A WPALS), column oven (G1316A COLCOM), and a diode array detector (G1315A DAD). Separations were carried out on a SunFire Prep C_{18} column (5 μm, 10 × 150 mm i.d., Waters) equipped with a guard column (10 × 10 mm i.d.), a Nucleodur HILIC column (5 μm, 10 × 150 mm i.d., Macherey-Nagel) equipped with a guard column (8 × 10 mm i.d.), or a ReproSil-Pur 120 C_{18}-AQ column (3 μm, 10 × 150 mm i.d., Dr. Maisch GmbH). MeCN and water, both containing 0.1% formic acid, were used as mobile phase. The flow rate was 4 or 5 mL/min, and detection was at 200 nm. Data acquisition and processing was performed using ChemStation software (Agilent Technologies). GC-MS was performed on a Hewlett-Packard GC/MS system (Agilent G1503A) equipped with a 5973 mass selective detector (MSD) and a 59864B ionization gauge controller (Agilent Technologies). A J&W DM-225 GC column (30 m; 0.25 mm i.d.; film thickness 0.25 μm; Agilent Technologies) was used. Injector temperature was 280 °C. Helium (0.7 mL/min) was used as a carrier gas. Transfer line temperature was 240 °C. The following temperature program was applied: 60 °C hold for 1 min, increase to 240 °C at 10 °C/min followed by 5 min at 240 °C. EI ionization was in positive ion mode (electron energy: 2040 V; full scan: m/z 50−700). Data acquisition was performed by MSD ChemStation D.03 software (Agilent Technologies), and data were processed with Spectrus Processor (ACD/Lab).

Optical rotations were measured on a JASCO P-2000 polarimeter (Brechbühler AG, Switzerland) equipped with a 10 cm temperature-controlled microcell. HRESIMS spectra were acquired on a LTQ Orbitrap XL hybrid ion trap−Orbitrap mass spectrometer (Thermo-Fisher Scientific). NMR spectra of **1**, **2**, and **3** were recorded on a Bruker Avance III spectrometer (Fällanden, Switzerland) operating at 500 MHz for ^{1}H and 126 MHz for ^{13}C. Spectra of **1** and **2** were obtained with a 1 mm TXI probe, and those of **3** with a BBI probe at 23 °C. ^{13}C NMR/DEPT spectra were recorded at 23 °C with a 5 mm BBO probe. NMR spectroscopic data for the remaining saponins were obtained on a Bruker Avance Neo 600 MHz NMR spectrometer, operating at 600 MHz for ^{1}H and 151 MHz for ^{13}C, and equipped with a QCI 5 mm Cryoprobe and a SampleJet automated sample changer (Rheinstetten, Germany). Spectra were measured in DMSO-d_6 (ARMAR Chemicals). Chemical shifts are reported in parts per million (δ) using the solvent signal (δ_H 2.50; δ_C 39.51) as internal reference; coupling constants (J) are given in Hz. Data were analyzed using Topspin (Bruker) and Spectrus Processor (ACD/Lab, Toronto, Canada) software.

TLC was performed on silica gel 60 F254-coated aluminum plates (Merck, Germany). Detection was with UV 254 nm and after spraying vanillin−sulfuric acid reagent followed by heating at 100 °C.

EtOH (96%) for extraction was from Brenntag Schweizerhall AG (Switzerland). Methyl *tert*-butyl ether (MTBE) and glacial HOAc were from Sigma-Aldrich (Germany). Ultrapure water was obtained from a Milli-Q water purification system (Merck Millipore, Darmstadt, Germany). HPLC-grade MeCN and MeOH were purchased from Avantor Performance Materials (Radnor Township, PA, USA). HPLC-grade *n*-BuOH, EtOAc, $CHCl_3$, DMSO, and formic acid were obtained from Scharlau (Scharlab S.L., Spain). Technical grade EtOAc was from

https://dx.doi.org/10.1021/acs.jnatprod.0c01220
J. Nat. Prod. 2021, 84, 630−645

Table 3. ^{1}H and ^{13}C NMR Spectroscopic Data of the Aglycone and Fatty Acid Residue in Compounds 7−10 (DMSO-d_6; 600 MHz for ^{1}H and 151 MHz for ^{13}C NMR; δ in ppm)

	7		8		9		10	
position	δ_C, type	δ_H (J in Hz)	δ_C, type	δ_H (J in Hz)	δ_C, type	δ_H (J in Hz)	δ_C, type	δ_H (J in Hz)
1	38.4, CH_2	0.90[a]	38.3, CH_2	0.90[a]	38.4, CH_2	0.89[a]	38.4, CH_2	0.89[a]
		1.52[a]		1.53[a]		1.52[a]		1.53[a]
2	25.4, CH_2	1.49[a]	25.5, CH_2	1.50[a]	25.5, CH_2	1.49[a]	25.5, CH_2	1.48[a]
		1.91[a]		1.84[a]		1.89[a]		1.83[a]
3	87.8, CH	3.01[a]	87.9, CH	3.02[a]	87.8, CH	3.02[a]	87.8, CH	3.01[a]
4	38.7, C		38.8, C		38.7, C		38.7, C	
5	55.1, CH	0.70[a]	55.2, CH	0.69[a]	55.1, CH	0.70[a]	55.2, CH	0.70[a]
6	18.0, CH_2	1.25[a]	17.8, CH_2	1.25[a]	18.0, CH_2	1.25[a]	17.9, CH_2	1.25[a]
		1.46[a]		1.46[a]		1.45[a]		1.45[a]
7	32.5, CH_2	1.31[a]	32.5, CH_2	1.31[a]	32.5, CH_2	1.33[a]	32.5, CH_2	1.33[a]
		1.39[a]		1.39[a]		1.38[a]		1.38[a]
8	39.1, C		39.1, C		39.1, C		39.1, C	
9	46.1, CH	1.52[a]	46.1, CH	1.51[a]	46.1, CH	1.52[a]	46.1, CH	1.52[a]
10	36.2, C		36.2, C		36.2, C		36.2, C	
11	22.9, CH_2	1.80[a]	22.9, CH_2	1.80[a]	22.9, CH_2	1.80[a]	22.9, CH_2	1.81[a]
12	121.5, CH	5.24	121.5, CH	5.24	121.5, CH	5.23[a]	121.4, CH	5.23[a]
13	143.1, C		143.1, C		143.1, C		143.1, C	
14	41.0, C		41.0, C		41.0, C		41.0, C	
15	34.7, CH_2	1.30[a]	34.7, CH_2	1.30[a]	34.7, CH_2	1.28[a]	34.7, CH_2	1.28[a]
		1.59[a]		1.58[a]		1.61[a]		1.61[a]
16	72.6, CH	4.32	72.6, CH	4.32	72.6, CH	4.32	72.6, CH	4.32
17	48.0, C		48.0, C		48.1, C		48.1, C	
18	40.4, CH	2.84, d (11.2)	40.4, CH	2.84, d (12.3)	40.3, CH	2.83, d (10.5)	40.4, CH	2.84, d (11.7)
19	46.5, CH_2	1.01[a]	46.5, CH_2	1.00[a]	46.5, CH_2	0.99[a]	46.5, CH_2	1.00[a]
		2.22, dd (13.5, 13.5)		2.23, dd (12.8, 12.8)		2.22, dd (12.5, 11.4)		2.24, dd (12.8, 12.0)
20	30.1, C		30.1, C		30.1, C		30.1, C	
21	35.0, CH_2	1.09[a]	35.0, CH_2	1.09[a]	35.0, CH_2	1.09[a]	35.0, CH_2	1.09[a]
		1.89[a]		1.89[a]		1.89[a]		1.89[a]
22	30.6, CH_2	1.63[a]	30.6, CH_2	1.63[a]	30.5, CH_2	1.65[a]	30.6, CH_2	1.67[a]
		1.80[a]		1.80[a]		1.83[a]		1.80[a]
23	27.7, CH_3	0.97[a]	27.7, CH_3	0.98[a]	27.7, CH_3	0.97[a]	27.7, CH_3	0.97[a]
24	16.5, CH_3	0.75, s	16.5, CH_3	0.76, s	16.5, CH_3	0.75, s	16.5, CH_3	0.75, s
25	15.4, CH_3	0.88[a]	15.4, CH_3	0.88[a]	15.4, CH_3	0.87[a]	15.4, CH_3	0.88[a]
26	16.7, CH_3	0.67[a]	16.8, CH_3	0.67[a]	16.8, CH_3	0.67[a]	16.8, CH_3	0.68[a]
27	26.2, CH_3	1.30[a]	26.2, CH_3	1.29[a]	26.2, CH_3	1.30[a]	26.2, CH_3	1.30[a]
28	175.0, C		175.0, C		175.1, C		175.3, C	
29	32.8, CH_3	0.83, s	32.8, CH_3	0.83, s	32.8, CH_3	0.83, s	32.8, CH_3	0.83, s
30	24.1, CH_3	0.89[a]	24.2, CH_3	0.89[a]	24.2, CH_3	0.90[a]	24.3, CH_3	0.90[a]
C1′	171.1, C		171.1, C		170.7, C		170.6, C	
C2′	42.6, CH_2	2.46[a]	42.6, CH_2	2.46[a]	38.3, CH_2	2.47[a]	38.3, CH_2	2.46[a]
						2.71, dd (14.5, 3.4)		2.72, dd (14.9, 3.9)
C3′	67.2, CH	3.82[a]	67.2, CH	3.82[a]	72.2, CH	3.91[a]	72.3, CH	3.91[a]
C4′	36.6, CH_2	1.37[a]	36.6, CH_2	1.37[a]	34.3, CH_2	1.53[a]	34.3, CH_2	1.54[a]
		1.44[a]		1.44[a]				
C5′	24.9, CH_2	1.27[a]	24.9, CH_2	1.26[a]	24.5, CH_2	1.33[a]	24.5, CH_2	1.34[a]
		1.37[a]		1.36[a]				
C6′	28.6, CH_2	1.22[a]	28.6, CH_2	1.20[a]	28.6, CH_2	1.22[a]	28.5, CH_2	1.24[a]
C7′	28.6, CH_2	1.23[a]	28.6, CH_2	1.24[a]	28.5, CH_2	1.24[a]	28.6, CH_2	1.22[a]
C8′	23.2, CH_2	1.44[a]	23.2, CH_2	1.43[a]	23.2, CH_2	1.43[a]	23.2, CH_2	1.44[a]
C9′	41.8, CH_2	2.38, t (7.3)	41.8, CH_2	2.38, t (7.3)	41.8, CH_2	2.38[a]	41.8, CH_2	2.38[a]
C10′	210.6, C		210.6, C		210.5, C		210.5, C	
C11′	41.8, CH_2	2.38, t (7.3)	41.8, CH_2	2.38, t (7.3)	41.8, CH_2	2.38[a]	41.8, CH_2	2.38[a]
C12′	23.3, CH_2	1.45[a]	23.3, CH_2	1.45[a]	23.2, CH_2	1.43[a]	23.2, CH_2	1.44[a]
C13′	28.6, CH_2	1.23[a]	28.6, CH_2	1.22[a]	28.7, CH_2	1.24[a]	28.6, CH_2	1.24[a]
C14′	25.6, CH_2	1.28[a]	25.6, CH_2	1.27[a]	25.6, CH_2	1.27[a]	25.6, CH_2	1.27[a]
C15′	29.0, CH_2	1.47[a]	29.0, CH_2	1.48[a]	29.0, CH_2	1.47[a]	29.0, CH_2	1.48[a]
C16′	66.3, CH_2	3.30[a]	66.3, CH_2	3.30[a]	66.3, CH_2	3.30[a]	66.3, CH_2	3.29[a]
		3.52, dt (9.7, 6.6)		3.52, dt (9.6, 6.7)		3.52[a]		3.52[a]

https://dx.doi.org/10.1021/acs.jnatprod.0c01220
J. Nat. Prod. 2021, 84, 630−645

Table 3. continued

[a]Overlapping signals. [b]Signal not visible.

Scharlau and was redistilled before use. Diaion HP-20 resin was purchased from Supelco Analytical (USA). Acetyl chloride, (*S*)-(+)-2-butanol, and trifluoroacetic anhydride (TFAA) were bought from TCI Chemicals (Japan). Reference sugars for sugar analysis were obtained from Sigma-Aldrich (L-arabinose, D-fucose, D-galactose, D-xylose) or from TCI Chemicals (D-galacturonic acid hydrate, D-glucuronic acid). DMSO (purity >99.5%) and hydrocortisone solution (50 μM, 0.2% v/v in EtOH) were purchased from Sigma-Aldrich. Human IL-8 and IL-6 ELISA kits, Dulbecco's modified Eagle's medium high glucose (1×), Dulbecco's phosphate-buffered saline without $CaCl_2$ and $MgCl_2$, trypsin-EDTA 0.5% (10×), 10.000 units/mL penicillin, 10.000 μg/mL streptomycin, and heat-inactivated calf serum (FCS) were provided by LubioScience (Lucerne, Switzerland). *E. coli*-derived recombinant human TNF-alpha (purity >98%), human MCP-1, and the RANTES ELISA kit were purchased from BioLegend (San Diego, CA, USA). CellTiter-Glo luminescent cell viability assay was obtained from Promega (Madison, WI, USA). Primer and TaqMan probe sets for IL-6 (Hs00985639_m1), IL-8 (Hs00174103_m1), MCP-1 (Hs00234140_m1), RANTES (Hs00982282_m1), and GAPDH (Hs02758991_m1) were obtained from Thermo Fisher (Reinach, Switzerland).

Plant Material. Corms of *C. sativus* used for activity profiling were obtained from Tagora (Aristau, Switzerland) in August 2017. Corms of *C. sativus* used for preparative isolation were purchased in September 2017 from Wyss Samen und Pflanzen (Zuchwil, Switzerland). Voucher specimens (No. 1232, Tagora, and No. 1016, Wyss) are deposited at the Division of Pharmaceutical Biology, University of Basel, Switzerland.

Activity Profiling. A portion (2.0 g) of SACE was dissolved in water (30 mL) and loaded onto a Diaion HP-20 cartridge (3.5 × 13 cm). The cartridge was eluted with water (1 L) followed by MeOH (800 mL). The H_2O fraction consisted of approximately 80% sucrose as revealed by NMR analysis (data not shown). A portion (40.0 mg) of the sugar-depleted MeOH fraction (155 mg) was separated by semipreparative HPLC by four injections of 10 mg each. The mobile phase consisted of water with 0.1% formic acid (A) and MeCN with 0.1% formic acid (B). A gradient of 5−100% B in 30 min followed by 100% B for 10 min was applied. The flow rate was 4 mL/min. Five fraction of 5 min each and a fraction of 10 min (25−35 min) were collected. All fractions were tested for their inhibition of TNF-α/IFN-γ-induced secretion of RANTES and MCP-1. In order to correlate the activity with additional chromatographic traces, the sugar-depleted MeOH fraction was analyzed by HPLC-UV-ELSD-ESIMS using the mobile phase and the gradient as described above. The flow rate was 0.4 mL/min. The sample was dissolved in DMSO at a concentration of 10 mg/mL, and 10 μL was injected.

Extraction and Isolation. Fresh corms (3.9 kg, including dry tunics) were shredded and macerated 4× with 5.4 L of EtOH (70%) for 16 h. The extract was dried under reduced pressure to yield a sticky residue (253 g). A portion of the residue (133 g) was suspended in water (1.2 L) and partitioned with EtOAc (5 × 1 L), followed by *n*-BuOH-saturated with H_2O (5 × 1 L) to provide an EtOAc-soluble fraction (5.5 g), an *n*-BuOH-soluble fraction (25.6 g), and a H_2O-soluble fraction (97.5 g).

For the purification of substances I−VI, a portion (5.3 g) of the *n*-BuOH-soluble fraction was separated by CPC utilizing a two-phase solvent system consisting of MTBE−*n*-BuOH−MeCN−H_2O (2:2:1:5). The sample was dissolved in a mixture of both phases (5 mL upper phase, 5 mL lower phase), and 10 mL was injected. Centrifugal rotation was 2000 rpm (333 g), and the flow rate 5 mL/min. One-minute fractions were collected in descending mode (69 fractions) followed by ascending mode (38 fractions). Based on TLC analysis the fractions were combined to 15 fractions (fractions A1−A15). The TLC was developed with $CHCl_3$−MeOH−H_2O (65:35:5).

A portion of fraction A2 (316 mg) was further separated by flash chromatography on a C_{18} Sepacore Flash cartridge. A gradient of 60−100% MeOH in 60 min was used at a flow rate of 10 mL/min. A total of 60 1 min fractions were collected and combined to eight fractions (fractions A2.1−A2.8) based on their TLC and HPLC profiles.

A part of fraction A2.3 (38 mg) was fractionated by flash chromatography using a Diol Sepacore Flash cartridge eluted with $CHCl_3$−MeOH (8:2). A total of 240 1 min fractions were collected and combined based on TLC analysis into seven fractions (fractions A2.3.1−A2.3.7). Final purification of Fr. A2.3.1 and Fr. A.2.3.2 by semipreparative HILIC-HPLC (90−75% MeCN in 30 min, flow rate of 4 mL/min) yielded substances I (t_R = 16.6 min; 0.4 mg) and II (t_R = 16.9 min; 0.5 mg). Final purification of Fr. A2.3.3−Fr. A2.3.7 by the same procedure (85−75% MeCN in 30 min) afforded substances III (t_R = 15.0 min; 1.3 mg), IV (t_R = 15.5 min; 1.0 mg), V (t_R = 19.5 min; 1.7 mg), and VI (t_R = 20.2 min; 1.4 mg) (Figure S2, Supporting Information).

For the isolation of **1**−**10** a larger portion of the *n*-BuOH-soluble fraction (20.0 g) was separated by CPC with the two-phase solvent system described above. The sample was dissolved in a mixture of both phases (30 mL upper phase, 30 mL lower phase) and injected in six portions of 10 mL each. Centrifugal rotation was 2000 rpm (333 g), and flow rate was 5 mL/min. Fractions were collected every minute. For each injection, 62 fractions were collected in descending mode. The fractions were combined to eight fractions (fractions B1−B8) based on TLC analysis using $CHCl_3$−MeOH−H_2O (65:35:5) as eluent. A part of Fr. B3 (3.3 g) was further separated by preparative HPLC (SunFire C_{18} column, UV detection at 210 nm) with a gradient of 70−100% MeOH in 30 min at a flow rate of 20 mL/min. A total of 11 fractions (Fr. B3.1−Fr. B3.11) were obtained. Separation of a portion of Fr. B3.4 (300 mg) by preparative HPLC on a HILIC column (85−75% MeCN in 30 min, detection at 198 nm) afforded crude **2** (t_R = 29.5 min, 47.5 mg), crude **1** (t_R = 30.6 min, 58.6 mg), and four fractions containing a saponin mixture (Fr. B3.4.1, t_R = 18.8 min, 10.7 mg; Fr. B3.4.2, t_R = 19.9 min, 10.4 mg; Fr. B3.4.3, t_R = 24.3 min, 40.8 mg; Fr. B3.4.4 t_R = 25.2 min, 33.0 mg). Final purification of **1** and **2** by preparative HPLC on a HILIC column (85−75% MeCN in 30 min) yielded pure **1** (47.1 mg) and **2** (29.8 mg). Fractions B3.4.3 and B3.4.4. were separated by preparative HPLC on a HILIC column (85−75% MeCN in 30 min). Further fractionation by semipreparative HPLC on a ReproSil-Pur 120 C_{18}-AQ column (39% MeCN, flow rate of 5 mL/min) afforded **4** (t_R = 22.4 min, 9.9 mg) and **6** (t_R = 26.1 min, 4.3 mg) from Fr. B3.4.3 and **3** (t_R = 21.0 min, 13.9 mg) and **5** (t_R = 23.5 min, 5.6 mg) from Fr. B3.4.4. Final purification by semipreparative HPLC on a HILIC column (90% MeCN, flow rate of 4 mL/min) yielded compounds **8** (t_R = 48.7 min, 4.2 mg) and **10** (t_R = 52.7 min, 2.0 mg) from Fr. B3.4.1 and compounds **7** (t_R = 48.4 min, 4.8 mg) and **9** (t_R = 52.9 min, 2.9 mg) from Fr B3.4.2 (Figure S3, Supporting Information). NMR and HPLC purity of the compounds was >95% except for **3** and **5** (approximately 85%) and for **9** and **10**, which contained about 40% of a further unidentified saponin.

Compounds **1** and **2** corresponded to the known substances VI and V, respectively. Substances I−IV were mixtures of compounds **8** and **10** (and minor amounts of **7** and **9**), **7** and **9** (and minor amounts of **8** and **10**), **4** and **6** (and minor amounts of **3** and **5**), and **3** and **5**, respectively.

*Azafrine 1 (**1**).* White amorphous powder; $[\alpha]^{25}_D$ −31 (*c* 0.1, MeCN−H_2O (1:1)); ^{1}H and ^{13}C NMR, see Tables S1 and S2, Supporting Information; HRESIMS *m*/*z* 1965.9411 $[M + Na]^+$ (calcd for $C_{92}H_{150}NaO_{43}^+$, 1965.9443).

*Azafrine 2 (**2**).* White amorphous powder; $[\alpha]^{25}_D$ −31 (*c* 0.1, MeCN−H_2O (1:1)); ^{1}H and ^{13}C NMR, see Tables S1 and S2, Supporting Information; HRESIMS *m*/*z* 1965.9493 $[M + Na]^+$ (calcd for $C_{92}H_{150}NaO_{43}^+$, 1965.9443).

*Azafrine 3 (**3**).* White amorphous powder; $[\alpha]^{25}_D$ −28 (*c* 0.1, MeCN−H_2O (1:1)); ^{1}H and ^{13}C NMR, see Tables 1 and 2; HRESIMS *m*/*z* 1803.8844 $[M + Na]^+$ (calcd for $C_{86}H_{140}NaO_{38}^+$, 1803.8915).

https://dx.doi.org/10.1021/acs.jnatprod.0c01220
J. Nat. Prod. 2021, 84, 630−645

Table 4. ^{1}H and ^{13}C NMR Spectroscopic Data of the Glycosidic Moiety in Compounds 7−10 (DMSO-d_6; 600 MHz for ^{1}H and 151 MHz for ^{13}C NMR; δ in ppm)

	7		8		9		10	
position	δ_C, type	δ_H (J in Hz)	δ_C, type	δ_H (J in Hz)	δ_C, type	δ_H (J in Hz)	δ_C, type	δ_H (J in Hz)
Sugar moiety at C-3								
GalA								
1			105.8, CH	4.10, d (6.3)			105.8, CH	4.08, d (6.8)
2			70.9, CH	3.30[a]			71.0, CH	3.30[a]
3			73.5, CH	3.22[a]			73.7, CH	3.19[a]
4			69.8, CH	3.75[a]			69.8, CH	3.73[a]
5			[b]	[b]			[b]	[b]
6			[b]				[b]	
GlcA								
1	105.4, CH	4.10, d (6.9)			105.4, CH	4.12, d (6.9)		
2	74.0, CH	2.93[a]			73.9, CH	2.93[a]		
3	77.0, CH	3.08[a]			76.9, CH	3.06[a]		
4	[b]	[b]			69.9, CH	3.75[a]		
5	[b]	[b]			74.7, CH	3.93[a]		
6	[b]				[b]			
Sugar moiety at C-28								
Fuc								
1	92.9, CH	5.32[a]	92.9, CH	5.32, d (8.2)	93.0, CH	5.32[a]	93.0, CH	5.32, d (7.8)
2	74.4, CH	3.47, dd (8.7, 8.7)	74.4, CH	3.48, dd (8.6, 8.6)	74.2, CH	3.50[a]	74.3, CH	3.51[a]
3	71.6, CH	3.80[a]	71.6, CH	3.80[a]	72.0, CH	3.80[a]	71.8, CH	3.80[a]
4	73.2, CH	4.91, d (2.8)	73.2, CH	4.91, d (2.8)	73.5, CH	4.91[a]	73.5, CH	4.92, br s
5	68.9, CH	3.85[a]	68.9, CH	3.85[a]	68.7, CH	3.85[a]	68.7, CH	3.85[a]
6	15.9, CH_3	0.94[a]	15.9, CH_3	0.94, d (6.3)	16.0, CH_3	0.92, d (5.8)	16.0, CH_3	0.93[a]
Rha3								
1	98.8, CH	5.26, br s	98.8, CH	5.26, br s	100.2, CH	5.07, d (2.9)	100.2, CH	5.06[a]
2	79.2, CH	3.84[a]	79.2, CH	3.84[a]	80.4, CH	3.78[a]	80.4, CH	3.78[a]
3	70.4, CH	3.71[a]	70.4, CH	3.71[a]	70.5, CH	3.62[a]	70.6, CH	3.62[a]
4	81.8, CH	3.38[a]	81.8, CH	3.38[a]	82.4, CH	3.38[a]	82.4, CH	3.38[a]
5	67.0, CH	3.57[a]	67.0, CH	3.57[a]	67.1, CH	3.57[a]	67.1, CH	3.57[a]
6	17.9, CH_3	1.17[a]	17.9, CH_3	1.18, d (5.9)	18.1, CH_3	1.17[a]	18.1, CH_3	1.17, d (5.6)
Xyl								
1	105.1, CH	4.41, d (7.6)	105.1, CH	4.41, d (7.5)	105.4, CH	4.35, d (7.5)	105.4, CH	4.35, d (7.5)
2	74.5, CH	3.02[a]	74.5, CH	3.01[a]	74.4, CH	3.01[a]	74.4, CH	3.02[a]
3	76.5, CH	3.13[a]	76.5, CH	3.13[a]	76.6, CH	3.10[a]	76.6, CH	3.11[a]
4	69.5, CH	3.27[a]	69.5, CH	3.27[a]	69.5, CH	3.25[a]	69.5, CH	3.26[a]
5	65.9, CH_2	3.04[a]	65.9, CH_2	3.04[a]	66.0, CH_2	3.03[a]	66.0, CH_2	3.03[a]
		3.69[a]		3.70[a]		3.68[a]		3.68[a]
Ara								
1	105.3, CH	4.28, d (6.7)	105.3, CH	4.28, d (6.5)				
2	71.0, CH	3.41[a]	71.0, CH	3.40[a]				
3	72.4, CH	3.33[a]	72.4, CH	3.33[a]				
4	67.5, CH	3.61	67.5, CH	3.61				
5	65.4, CH_2	3.37[a]	65.5, CH_2	3.37[a]				
		3.66[a]		3.66[a]				
Sugar moiety at C-3′								
Rha2								
1					98.7, CH	4.71, br s	98.7, CH	4.71, br s
2					70.8, CH	3.54[a]	70.7, CH	3.54[a]
3					70.7, CH	3.38[a]	70.7, CH	3.39[a]
4					72.1, CH	3.15[a]	72.0, CH	3.16[a]
5					68.7, CH	3.44, dd (8.7, 6.4)	68.9, CH	3.45
6					17.8, CH_3	1.12, d (6.5)	18.0, CH_3	1.12, d (5.6)
Sugar moiety at C-16′								
Rha1								
1	99.9, CH	4.51, br s	99.9, CH	4.51, br s	99.9, CH	4.51, br s	99.9, CH	4.51, br s
2	70.6, CH	3.57[a]	70.6, CH	3.57[a]	70.6, CH	3.57[a]	70.7, CH	3.58[a]
3	70.7, CH	3.40[a]	70.7, CH	3.39[a]	70.7, CH	3.38[a]	70.7, CH	3.39[a]
4	72.0, CH	3.16[a]	72.0, CH	3.16[a]	72.0, CH	3.17[a]	72.0, CH	3.18[a]

https://dx.doi.org/10.1021/acs.jnatprod.0c01220
J. Nat. Prod. 2021, 84, 630−645

Table 4. continued

	7		8		9		10	
position	δ_C, type	δ_H (J in Hz)	δ_C, type	δ_H (J in Hz)	δ_C, type	δ_H (J in Hz)	δ_C, type	δ_H (J in Hz)
5	68.4, CH	3.37[a]	68.4, CH	3.36[a]	68.4, CH	3.36[a]	68.4, CH	3.37[a]
6	17.9, CH_3	1.12, d (6.2)	17.9, CH_3	1.12, d (6.2)	17.9, CH_3	1.12, d (6.5)	18.0, CH_3	1.12, d (5.6)

[a]Overlapping signals. [b]Signal not visible.

*Azafrine 4 (**4**).* White amorphous powder; $[\alpha]^{25}_D$ −31 (c 0.1, MeCN−H_2O (1:1)); ^1H and ^{13}C NMR, see Tables 1 and 2; HRESIMS m/z 1803.8916 $[M + Na]^+$ (calcd for $C_{86}H_{140}NaO_{38}^+$, 1803.8915).

*Azafrine 5 (**5**).* White amorphous powder; $[\alpha]^{25}_D$ −19 (c 0.1, MeCN−H_2O (1:1)); ^1H and ^{13}C NMR, see Tables 1 and 2; HRESIMS m/z 1819.8827 $[M + Na]^+$ (calcd for $C_{86}H_{140}NaO_{39}^+$, 1819.8864).

*Azafrine 6 (**6**).* White amorphous powder; $[\alpha]^{25}_D$ −21 (c 0.1, MeCN−H_2O (1:1)); ^1H and ^{13}C NMR, see Tables 1 and 2; HRESIMS m/z 1819.8901 $[M + Na]^+$ (calcd for $C_{86}H_{140}NaO_{39}^+$, 1819.8864).

*Azafrine 7 (**7**).* White amorphous powder; $[\alpha]^{25}_D$ −24 (c 0.1, MeCN−H_2O (1:1)); ^1H and ^{13}C NMR, see Tables 3 and 4; HRESIMS m/z 1657.8340 $[M + Na]^+$ (calcd for $C_{80}H_{130}NaO_{34}^+$, 1657.8336).

*Azafrine 8 (**8**).* White amorphous powder; $[\alpha]^{25}_D$ −20 (c 0.1, MeCN−H_2O (1:1)); ^1H and ^{13}C NMR, see Tables 3 and 4; HRESIMS m/z 1657.8340 $[M + Na]^+$ (calcd for $C_{80}H_{130}NaO_{34}^+$, 1657.8336).

*Azafrine 9 (**9**).* White amorphous powder; $[\alpha]^{25}_D$ −37 (c 0.1, MeCN−H_2O (1:1)); ^1H and ^{13}C NMR, see Tables 3 and 4; HRESIMS m/z 1671.8415 $[M + Na]^+$ (calcd for $C_{81}H_{132}NaO_{34}^+$, 1671.8493).

*Azafrine 10 (**10**).* White amorphous powder; $[\alpha]^{25}_D$ −30.6 (c 0.08, MeCN−H_2O (1:1)); ^1H and ^{13}C NMR, see Tables 3 and 4; HRESIMS m/z 1671.8479 $[M + Na]^+$ (calcd for $C_{81}H_{132}NaO_{34}^+$, 1671.8493).

Acid Hydrolysis and Sugar Analysis. Each compound (1 mg, 0.5 mg for **9** and **10**) was hydrolyzed with 2 M HCl (1 mL) for 15 h at 100 °C. The hydrolysate was extracted with EtOAc (2 × 1 mL). The aqueous phase was lyophilized to give a residue that was treated with a mixture of (+)-2-butanol−acetyl chloride (10:0.5 (v/v); 1 mL) at 55 °C for 15 h. After drying under N_2 the residue was derivatized with TFAA−EtOAc (3:4 (v/v), 1 mL) at 55 °C for 10 min. Each sample (1 μL) was manually injected in split mode (1:10) into the gas chromatograph.[48] L-Arabinose, D-fucose, D-galactose, L-rhamnose, D-xylose, D-galacturonic acid, and D-glucuronic acid (1 mg each) derivatized in the same manner were used as references.

Cell Culture. All cell culture experiments were performed according to our previous protocols.[35,49] Human nontumorigenic HaCaT keratinocytes (Cell Line Services, Eppelheim, Germany) were maintained in Dulbecco's modified Eagle's medium high glucose 1× (DMEM) supplemented with 1% (v/v) penicillin 10.000 U/mL/streptomycin 10.000 μg/mL, and 10% (v/v) heat-inactivated FCS at 37 °C in a humidified atmosphere containing 5% CO_2.[50] Experiments were routinely conducted at approximately 80−90% confluency. Substances were individually applied in the same concentrations with a supplementation of 20 ng/mL TNF-α. This setup was used to simulate an in vitro inflammatory condition.[35,49] For RANTES determination, 20 ng/mL IFN-γ (R&D Systems, Minneapolis, MN, USA) was added in addition to TNF-α. The results of each experiment were compared to an untreated control signifying keratinocytes exposed to a treated control composed of medium with 20 ng/mL TNF-α. All compounds were tested in a final DMSO concentration of max. 0.1% (v/v), which has been proven harmless for this cell line (data not shown).[35,49]

ATP Assay. The CellTiter-Glo luminescent cell viability assay was carried out according to the manufacturer's protocol. The following alterations were made: cells were grown in a transparent, sterile 96-well plate at a density of 1.5×10^5 cells/mL. After an incubation period of 24 h (37 °C, 5% CO_2), cells were washed with PBS, subsequently treated accordingly with a 100 μL solution, and incubated for another 24 h. A 100 μL portion of CellTiter-Glo reagent was then added to each well, resulting in a 1:1 dilution. The sample plates were agitated for 2 min by an orbital shaker and incubated for 10 min. A 100 μL amount of each well was then transferred to a white, opaque sterile 96-well plate and immediately read by a microplate reader (SpectraMax L, Molecular Devices, Sunnyvale, CA, USA).

RNA and Real-Time Quantitative RT-PCR. After cell treatment and incubation in 12-well plates, mRNA was extracted using the RNEasy mini kit by Qiagen (Valencia, CA, USA). After extraction, RNA was treated with RNase-free DNase. Reverse transcription was performed using the Biometra T3000 thermocycler. RNA (5 μL) was incubated for 5 min at 70 °C with 0.24 μg of oligo-dT primers (Qiagen), followed by incubation for 1 h at 37 °C with 200 U of M-MLV reverse transcriptase, 1 × M-MLV reverse transcriptase buffer, and 2 mM of each dNTP. Quantitative real time PCR (qPCR) was performed using a Rotor-Gene Q PCR cycler (Qiagen) under the following conditions: 2 μL of the master mix for the respective gene was pipetted into a rotor gene tube for each reaction. In addition, 3 μL of the respective positive sample was added. The negative samples (without enzyme) from the Reverse Transcriptase PCR were only tested together with the GAPDH-Taqman assay to establish whether DNA was present in the samples or not. Biological duplicates were also measured for each sample. At the beginning of the PCR the temperature was 95 °C for 10 min. This was followed by 45 cycles of 15 s each at 95 °C and 1 min at 60 °C. Ct values were determined using the Rotor-Gene 6000 Series software connected to the real-time PCR device. A threshold line at 0.02619 was set for each measurement. The curve was set to "Dynamic Tube" and "Slope Correct". The Outlier Removal was set to 3%. The Ct values were then saved as an Excel table and transferred to a new Excel file for evaluation or data analysis. All values were normalized to the expression of the housekeeping gene glyceraldehyde-3-phosphate dehydrogenase (GAPDH).

Measurement of IL-6, IL-8, RANTES, and MCP-1 Secretion. The experimental setup including the TNF-α concentration was chosen according to Wedler et al.[35,49] For the samples and controls, cells were seeded into 12-well plates at a density of 1.5×10^5 cells/mL. After an incubation time of 24 h (37 °C, 5% CO_2), DMEM with 10% (v/v) serum was discarded, cells were washed with 1 mL/well PBS, and medium was exchanged to DMEM containing 0% FCS or the test solutions plus 20 ng/mL TNF-α. The second 24 h period happened under the same conditions. Protein levels obtained from the untreated control are regarded as the basal secretion of the designated target in keratinocytes. In the end, supernatants were aspirated, stored in sterile microcentrifuge tubes, and deep-frozen (−20 °C) immediately. Absorbance was measured at 450 nm using a microplate reader (Spectramax i3x Multimode detection platform, Molecular Devices). All ELISA assays were performed in triplicate on three independent days ($N = 3$).

Statistical Analysis. Data are shown as mean ± standard deviation (SD). ELISA experiments were performed in triplicates; each experiment was repeated at least three times (on different days). The protein levels were then calculated according to a standard curve. PCR experiments were executed in duplicates, a sample and one technical replicate; experiments were repeated at least five times (on different days). Results were processed according to the comparative Ct method (ΔΔCt method[51]) with the following equations using Microsoft Excel 2013:

$$\Delta Ct = Ct_{Target} - Ct_{Reference} \quad (1)$$

$$\Delta\Delta Ct = \Delta Ct_{test\ sample} - \Delta Ct_{calibrator\ sample} \quad (2)$$

$$SD(\Delta Ct) = SD(\Delta\Delta Ct) \quad (3)$$

$$\text{fold change} = 2^{-\Delta\Delta Ct} \quad (4)$$

$$\text{fold change range} = 2^{-(\Delta\Delta Ct \pm s)} \quad (5)$$

https://dx.doi.org/10.1021/acs.jnatprod.0c01220
J. Nat. Prod. 2021, 84, 630−645

To process the results by the comparative Ct method, the replication efficiency of the housekeeping gene and the targets have to be equal. The manufacturer of the TaqMan gene expression assays (Applied Biosciences) guarantees an amplification efficiency close to 100%.[52] The term "down-regulation" refers to a gene expression level below the untreated control (<1), whereas "up-regulation" describes a level >1.

Further statistical analysis was carried out by one-way analysis of variance (ANOVA) followed by Dunnett's multiple comparison test using the software package GraphPad Prism (version 6.01, GraphPad Software Inc.). In all cases, differences were considered significant if p was below 0.05.

■ ASSOCIATED CONTENT

Supporting Information

The Supporting Information is available free of charge at https://pubs.acs.org/doi/10.1021/acs.jnatprod.0c01220.

Additional information (PDF)

■ AUTHOR INFORMATION

Corresponding Authors

Veronika Butterweck − *School of Life Sciences, University of Applied Sciences, 4132 Muttenz, Switzerland;* orcid.org/0000-0001-7516-8789; Phone: +41-71-0466-447; Email: Veronika.Butterweck@ZellerAG.ch

Matthias Hamburger − *Pharmaceutical Biology, Pharmacenter, University of Basel, 4056 Basel, Switzerland;* orcid.org/0000-0001-9331-273X; Phone: +41-61-207-1425; Email: matthias.hamburger@unibas.ch

Authors

Morris Keller − *Pharmaceutical Biology, Pharmacenter, University of Basel, 4056 Basel, Switzerland*

Sarah Fankhauser − *School of Life Sciences, University of Applied Sciences, 4132 Muttenz, Switzerland*

Noreen Giezendanner − *School of Life Sciences, University of Applied Sciences, 4132 Muttenz, Switzerland*

Michelle König − *School of Life Sciences, University of Applied Sciences, 4132 Muttenz, Switzerland*

Franziska Keresztes − *Pharmaceutical Biology, Pharmacenter, University of Basel, 4056 Basel, Switzerland*

Ombeline Danton − *Pharmaceutical Biology, Pharmacenter, University of Basel, 4056 Basel, Switzerland*

Orlando Fertig − *Pharmaceutical Biology, Pharmacenter, University of Basel, 4056 Basel, Switzerland*

Laurence Marcourt − *School of Pharmaceutical Sciences and Institute of Pharmaceutical Sciences of Western Switzerland (ISPSW), University of Geneva, CMU, 1211 Geneva 4, Switzerland*

Olivier Potterat − *Pharmaceutical Biology, Pharmacenter, University of Basel, 4056 Basel, Switzerland;* orcid.org/0000-0001-5962-6516

Complete contact information is available at: https://pubs.acs.org/10.1021/acs.jnatprod.0c01220

Notes

The authors declare no competing financial interest.

■ ACKNOWLEDGMENTS

This project was supported by the Forschungsfonds Aargau (Project 20140831_09_Z_Safran Plus). Thanks are due to S. Bossard (Tagora, Aristau) for a sample of saffron corms and to Dr. A. Treyer (University of Basel, Division of Pharmaceutical Biology) for recording the HRESIMS spectra. We are grateful to Prof. J.-L. Wolfender and Dr. E. Ferreira Queiroz (Institute of Pharmaceutical Sciences of Western Switzerland, University of Geneva, Switzerland) for kindly providing access to their NMR spectrometer. We acknowledge the Swiss National Science Foundation for the support in the acquisition of the 600 MHz NMR spectrometer (SNF R'Equip Grant 316030_164095).

■ DEDICATION

Dedicated to Dr. A. Douglas Kinghorn, The Ohio State University, for his pioneering work on bioactive natural products.

■ REFERENCES

(1) Kumar, R.; Singh, V.; Devi, K.; Sharma, M.; Singh, M. K.; Ahuja, P. S. *Food Rev. Int.* **2008**, *25*, 44−85.

(2) Gresta, F.; Lombardo, G. M.; Siracusa, L.; Ruberto, G. *Agron. Sustainable Dev.* **2008**, *28*, 95−112.

(3) Srivastava, R.; Ahmed, H.; Dixit, R.; Dharamveer Saraf, S. *Pharmacogn. Rev.* **2010**, *4*, 200−208.

(4) Winterhalter, P.; Straubinger, M. *Food Rev. Int.* **2000**, *16*, 39−59.

(5) Manzo, A.; Panseri, S.; Bertoni, D.; Giorgi, A. *J. Mt. Sci.* **2015**, *12*, 1542−1550.

(6) Cardone, L.; Castronuovo, D.; Perniola, M.; Cicco, N.; Candido, V. *Sci. Hortic.* **2020**, *272*, 109560.

(7) Hosseinzadeh, H.; Nassiri-Asl, M. *Phytother. Res.* **2013**, *27*, 475−483.

(8) Lim, T. K. In *Edible Medicinal and Non Medicinal Plants, Flowers*, Vol. *8*; Lim, T. K., Ed.; Springer Netherlands: Dordrecht, 2014; pp 77−136.

(9) Mykhailenko, O.; Kovalyov, V.; Goryacha, O.; Ivanauskas, L.; Georgiyants, V. *Phytochemistry* **2019**, *162*, 56−89.

(10) Siracusa, L.; Gresta, F.; Ruberto, G. In *Carotenoids: Properties, Effects and Diseases*; Masayoshi, Y., Ed.; Nova Science Publishers, Inc., 2012; pp 145−178.

(11) Carmona, M.; Sánchez, A. M.; Ferreres, F.; Zalacain, A.; Tomás-Barberán, F.; Alonso, G. L. *Food Chem.* **2007**, *100*, 445−450.

(12) Culleré, L.; San-Juan, F.; Cacho, J. *Food Chem.* **2011**, *127*, 1866−1871.

(13) Li, C. Y.; Wu, T. S. *J. Nat. Prod.* **2002**, *65*, 1452−1456.

(14) Chrungoo, N. K.; Farooq, S. *Biochem. Physiol. Pflanz.* **1985**, *180*, 55−61.

(15) Bagri, J.; Yadav, A.; Anwar, K.; Dkhar, J.; Singla-Pareek, S. L.; Pareek, A. *Sci. Rep.* **2017**, *7*, 11904.

(16) Oda, Y.; Tatsumi, Y. *Biol. Pharm. Bull.* **1993**, *16*, 978−981.

(17) Escribano, J. *Biochim. Biophys. Acta, Gen. Subj.* **1999**, *1426*, 217−222.

(18) Escribano, J.; Rubio, A.; Alvarez-Orti, M.; Molina, A.; Fernandez, J. A. *J. Agric. Food Chem.* **2000**, *48*, 457−463.

(19) Loukis, A.; Al-Kofahi, A.; Philianos, S. *Plant. Med. Phytother.* **1983**, *17*, 89−91.

(20) Rubio-Moraga, A.; Trapero, A.; Ahrazem, O.; Gómez-Gómez, L. *Phytochemistry* **2010**, *71*, 1506−1513.

(21) Yu-Zhu; Ting-Han; Hou, T.-T.; Hu, Y.; Zhang, Q.-Y.; Rahman, K.; Qin, L.-P. *Chem. Nat. Compd.* **2008**, *44*, 666−667.

(22) Masuda, A.; Mori, K.; Miyazawa, M. *Chem. Nat. Compd.* **2012**, *48*, 319−321.

(23) Rubio-Moraga, Á.; Gerwig, G. J.; Castro-Díaz, N.; Jimeno, M. L.; Escribano, J.; Fernández, J. A.; Kamerling, J. P. *Ind. Crops Prod.* **2011**, *34*, 1401−1409.

(24) Liakopoulou-Kyriakides, M.; Sinakos, Z.; Kyriakidis, D. A. *Plant Sci.* **1985**, *40*, 117−120.

(25) Liakopoulou-Kyriakides, M.; Skubas, A. I. *Biochem. Int.* **1990**, *22*, 103−110.

(26) Escribano, J.; Diaz-Guerra, M. J.; Riese, H. H.; Alvarez, A.; Proenza, R.; Fernandez, J. A. *Planta Med.* **2000**, *66*, 157−162.

(27) Escribano, J.; Díaz-Guerra, M. J. M.; Riese, H. H.; Ontañón, J.; García-Olmo, D.; García-Olmo, D. C.; Rubio, A.; Fernández, J. A. L. *Cancer Lett.* **1999**, *144*, 107−114.
(28) Castro-Diaz, N.; Salaun, B.; Perret, R.; Sierro, S.; Romero, J. F.; Fernandez, J.-A.; Rubio-Moraga, A.; Romero, P. *Vaccine* **2012**, *30*, 388−397.
(29) Wang, Y.; Han, T.; Zhu, Y.; Zheng, C.-J.; Ming, Q.-L.; Rahman, K.; Qin, L.-P. *J. Nat. Med.* **2010**, *64*, 24−30.
(30) Goliaris, A. H. In *Medicinal and Aromatic Plants-Industrial Profiles*, Vol. *8*; Hardman, R., Negbi, M., Eds.; Harwood Academic Publishers: Amsterdam, 1999; pp 73−85.
(31) Sánchez-Vioque, R.; Rodríguez-Conde, M. F.; Reina-Ureña, J. V.; Escolano-Tercero, M. A.; Herraiz-Peñalver, D.; Santana-Méridas, O. *Ind. Crops Prod.* **2012**, *39*, 149−153.
(32) Ait-Oubahou, A.; El-Otmani, M. In *Medicinal and Aromatic Plants-Industrial Profiles*, Vol. *8*; Hardman, R., Negbi, M., Eds.; Harwood Academic Publishers: Amsterdam, 1999; pp 87−94.
(33) Wedler, J.; Rusanov, K.; Atanassov, I.; Butterweck, V. *Planta Med.* **2016**, *82*, 1000−1008.
(34) Uchi, H.; Terao, H.; Koga, T.; Furue, M. *J. Dermatol. Sci.* **2000**, *24*, 29−38.
(35) Wedler, J.; Weston, A.; Rausenberger, J.; Butterweck, V. *Fitoterapia* **2016**, *114*, 56−62.
(36) Pietrzak, A. T.; Zalewska, A.; Chodorowska, G.; Krasowska, D.; Michalak-Stoma, A.; Nockowski, P.; Osemlak, P.; Paszkowski, T.; Roliński, J. M. *Clin. Chim. Acta* **2008**, *394*, 7−21.
(37) Verjee, S.; Garo, E.; Pelaez, S.; Fertig, O.; Hamburger, M.; Butterweck, V. *Planta Med.* **2017**, *83*, 1176−1183.
(38) Kondo, S. *J. Invest. Dermatol. Symp. Proc.* **1999**, *4*, 177−183.
(39) Appay, V.; Rowland-Jones, S. L. *Trends Immunol.* **2001**, *22*, 83−87.
(40) Pivarcsi, A.; Nagy, I.; Kemeny, L. *Curr. Immunol. Rev.* **2005**, *1*, 29−42.
(41) Asada, Y.; Furuya, T. In *Saponins Used in Traditional and Modern Medicine*, Vol. *1*; Yamasaki, K., Waller, G. R., Eds.; Springer: USA, 1996; pp 459−469.
(42) Arican, O.; Aral, M.; Sasmaz, S.; Ciragil, P. *Mediators Inflammation* **2005**, *5*, 273−279.
(43) Nomura, I.; Gao, B.; Boguniewicz, M.; Darst, M. A.; Travers, J. B.; Leung, D. Y. M. *J. Allergy Clin. Immunol.* **2003**, *112*, 1195−1202.
(44) Nedoszytko, B.; Sokołowska-Wojdyło, M.; Ruckemann-Dziurdzińska, K.; Roszkiewicz, J.; Nowicki, R. J. *Postep. Dermatologii i Alergol.* **2014**, *31*, 84−91.
(45) Jiang, J. Z.; Ye, J.; Jin, G. Y.; Piao, H. M.; Cui, H.; Zheng, M. Y.; Yang, J. S.; Che, N.; Choi, Y. H.; Li, L. C.; Yan, G. H. *J. Agric. Food Chem.* **2017**, *65*, 8128−8135.
(46) Kimura, Y.; Sumiyoshi, M.; Samukawa, K.; Satake, N.; Sakanaka, M. *Eur. J. Pharmacol.* **2008**, *584*, 415−423.
(47) Cho, N.; Moon, E. H.; Kim, H. W.; Hong, J.; Beutler, J. A.; Sung, S. H. *Molecules* **2016**, *21*, 459.
(48) Nuevo, M.; Cooper, G.; Sandford, S. A. *Nat. Commun.* **2018**, *9*, 5276.
(49) Wedler, J.; Daubitz, T.; Schlotterbeck, G.; Butterweck, V. *Planta Med.* **2014**, *80*, 1678−1684.
(50) Boukamp, P.; Petrussevska, R. T.; Breitkreutz, D.; Hornung, J.; Markham, A.; Fusenig, N. E. *J. Cell Biol.* **1988**, *106*, 761−771.
(51) Applied Biosystems. Guide to Performing Relative Quantitation of Gene Expression Using Real-Time Quantitative PCR, 2008. https://assets.thermofisher.com/TFS-Assets/LSG/manuals/cms_042380.pdf (accessed Nov 5, 2020).
(52) Applied Biosystems. Amplification Efficiency of TaqMan® Gene Expression Assays, 2006. https://assets.thermofisher.com/TFS-Assets/LSG/Application-Notes/cms_040377.pdf (accessed Nov 5, 2020).

https://dx.doi.org/10.1021/acs.jnatprod.0c01220
J. Nat. Prod. 2021, 84, 630−645

3.3 Publication 3

Teucrium polium – wound healing potential, toxicity and polyphenolic profile

Sarra Chabane, Amel Boudjelal, **Morris Keller**, Sara Doubakh, Olivier Potterat

South African Journal of Botany **137**, 228−235 (2021)
doi: 10.1016/j.sajb.2020.10.017

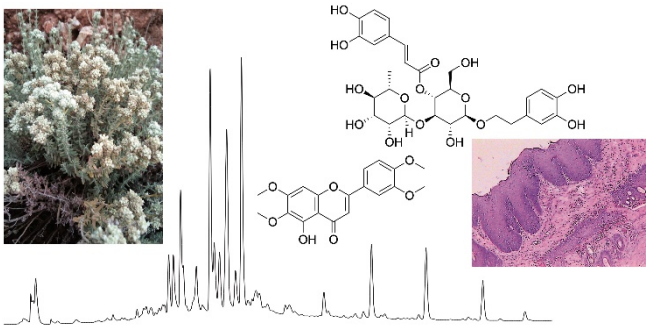

Teucrium polium L. is a plant used in traditional Algerian medicine for wound treatment. The wound healing properties of an ointment made from a methanolic extract of the aerial parts were studied using a wound excision model in rabbits. The ointment at both, 5% and 10% concentrations, showed a significant effect on wound closure compared to the allantoin and petroleum jelly treated groups. Toxicity was assessed in animal models, with no signs of toxicity observed in rabbits or mice following dermal or oral administration. HPLC-PDA-MS analysis identified 14 flavonoids and phenylethanoid glycosides as the main polyphenolic constituents of the extract. The findings support the traditional use of *T. polium* as a wound healing agent in traditional Algerian medicine.

The supporting information is available in the appendix

Contribution to this publication: Extraction, isolation, and structure elucidation of the compounds from *T. polium*

South African Journal of Botany 137 (2021) 228–235

Contents lists available at ScienceDirect

South African Journal of Botany

journal homepage: www.elsevier.com/locate/sajb

Teucrium polium - wound healing potential, toxicity and polyphenolic profile

Sarra Chabane[a,2,*], Amel Boudjelal[b], Morris Keller[c], Sara Doubakh[b], Olivier Potterat[c,1,*]

[a] Department of Life and Nature Science, Faculty of Sciences, Mohamed Boudiaf University, 28000 M'Sila, Algeria
[b] Department of Microbiology and Biochemistry, Faculty of Sciences, Mohamed Boudiaf University, 28000 M'Sila, Algeria
[c] Division of Pharmaceutical Biology, University of Basel, Klingelbergstrasse 50, CH-4056 Basel, Switzerland

ARTICLE INFO

Article History:
Received 11 May 2020
Revised 1 October 2020
Accepted 19 October 2020
Available online 1 November 2020

Edited by M Marrelli

Keywords:
Teucrium polium
Polyphenolic profile
Wound healing
Acute dermal and oral toxicity

ABSTRACT

The wound healing properties of *Teucrium polium* L., a plant used in the Algerian traditional medicine for the treatment of wounds, have been investigated using an excision wound model in rabbits. An ointment was prepared with two concentrations (5 and 10%) of a methanolic extract of the aerial parts. Both preparations showed significant effect on the wound contraction when compared to the control and the group treated with petroleum jelly. In addition, acute dermal and oral toxicity was assessed in animal models. The absence of signs of toxicity on the skin of rabbits indicated the safety of the ointment. After oral administration in mice at doses of 1000 and 2000 mg/kg b.wt, no signs of liver and kidney toxicity were detected by analysis of biochemical parameters and by histological examination. The composition of the methanolic extract was investigated by HPLC-PDA-MS analysis, and a comprehensive profile of phenolic compounds was established, with 14 flavonoids and phenylethanoid glycosides identified as the main polyphenolic constituents. Overall, the data support the use of *T. polium* as a wound healing agent in the Algerian traditional medicine.

1. Introduction

The genus *Teucrium* (family Lamiaceae) comprises approximately 300 species and is mainly distributed in Europe, North Africa and in the temperate parts of Asia (Bahramikia and Yazdanparast, 2012; Dehshiri and Azadbakht, 2012). Several species including *T. chamaedrys, T. montanum*, and *T. polium* are used in traditional medicinal systems (Stankovic et al., 2011). *T. polium* L., known popularly as felty germander (jâada or khayatit-lajrah in Arabic), is a deciduous shrub native to the western Mediterranean region abundantly growing in rocky places of the hills and deserts of Mediterranean countries up to South Western Asia (Bahramikia and Yazdanparast, 2012). The plant which includes many subspecies and varieties is very common in Algeria where it grows particularly in the Algerian and Oranian high plateaus and in the Oranian Saharian Atlas (Quézel and Santa, 1963). In Algerian traditional medicine, the aerial parts of the plant are used for the treatment of diabetes, hypertension and, in the form of a powder mixed with petroleum jelly or beeswax, as a wound healing agent (Boudjelal et al., 2013).

Extracts of *T. polium* have been shown to possess various biological activities including antioxidant, antibacterial, antiviral, antifungal, cytotoxic, antimutagenic, antiinflammatory, analgesic, antispasmodic, hypolipidemic, hypoglycemic, hepatoprotective, antiulcer, and anticonvulsant effects (Jaradat, 2015). Wound healing properties have been investigated in mice (Ansari et al., 2013) and rats (Meguellati et al., 2019; Huseini et al., 2020).

Flavonoids, phenylethanoid glycosides, and various terpenoids including neoclerodane diterpenes, sterols, and iridoids, have been isolated from the plant which also contains an essential oil rich in sesquiterpenes (Bahramikia and Yazdanparast, 2012; Basudan and Abu-Gabal, 2018; Elmasri et al., 2015).

The aim of the present study was to determine the polyphenolic composition of a methanolic extract of *T. polium* and to investigate its wound healing properties for the first time in rabbits. Furthermore, the acute cutaneous and oral toxicity were assessed. Wound excision was selected as a representative model to study the traditional use of the plant in the treatment of open wounds.

2. Materials and methods

2.1. Plant material and extraction

The flowering aerial parts of *Teucrium polium* (Subsp. *capitatum*) were collected in May 2018, in M'sila, Algeria, at 35° 12′ 36.97″ N

* Corresponding authors.
E-mail addresses: sarra.chabane@univ-msila.dz (S. Chabane), olivier.potterat@unibas.ch (O. Potterat).
[2] Orcid.org/0000-0002-2519-4900
[1] Orcid.org/0000-0001-5962-6516

https://doi.org/10.1016/j.sajb.2020.10.017

latitude and 4° 10′ 46.08″ E longitude. The plant was authenticated by Dr. Sarri Dj., Department SNV/M'sila University, and a specimen (AB-92) was deposited at the herbarium of the Department. The plant material was rinsed and dried in the shade at room temperature and finely ground into a powder with a grinder (sieve pore size 200 μm).

The methanolic extract was obtained with a Soxhlet extractor. The vegetable powder (50 g) was extracted with 500 ml of methanol for 6 h. The extract was filtered and evaporated under reduced pressure to yield an oily residue (17.5%).

2.2. General experimental procedures

Medium pressure liquid chromatography (MPLC) was performed on a Premium Flash-Prep LC system PuriFlash® 4100 (Interchim, Montluçon, France). The sample was prepared as a dry load and adsorbed on 25 g silica gel 60. Preparative HPLC was carried out on a Preparative LC/MSD System (Agilent Technologies, Santa Clara, CA, USA) consisting of a quaternary pump (1200 Series, 1290 Infinity II 1260 Prep Bin Pump), a PDA detector (1100 Series), and a 6120 Quadrupole LC/MS. A SunFire Prep C18 OBD column (5 μm, 30 × 150 mm i.d., Waters, Milford, MA, USA), equipped with a C18 Prep Guard Cartridge (10 × 30 mm i.d.) was used. The flow rate was 20 ml/min. Data acquisition and processing was performed using ChemStation software (Agilent Technologies). For injection a 1290 Infinity II 1290 Valve Drive manual injection system (Agilent Technologies) was used. Semi-preparative HPLC was carried out on an Agilent 1100 Series instrument equipped with a PDA detector. Separations were carried out on a SunFire C18 column (5 μm, 150 × 10 mm i.d., Waters) equipped with a guard column (10 × 10 mm i.d.). A flow rate of 4 ml/min was applied. Data acquisition and processing was performed using ChemStation software. NMR spectra were recorded on a Bruker Avance III spectrometer (Rheinstetten, Germany) operating at 500.13 MHz for ^{1}H and 125.77 MHz for ^{13}C. ^{1}H NMR and 2D NMR spectra were measured in DMSO-d6 or $CDCl_3$ (ARMAR Chemicals) with a 1 mm TXI probe at 23 °C. Data were analyzed using Topspin (Bruker) and Spectrus Processor (ACD/Lab, Toronto, Canada) softwares.

Silica gel 60 (0.040–0.063 mm) used for MPLC was from Merck KGaA (Darmstadt, Germany). TLC was performed on silica gel 60 F254 precoated plates (ALUGRAM Xtra Nano-SIL G, Macherey-Nagel, Düren, Germany); detection under UV 254 nm and after spraying with vanillin-sulfuric acid reagent followed by heating at 100 °C. Ultrapure water was obtained from a Milli-Q water purification system (Merck Millipore, Darmstadt, Germany). HPLC-grade acetonitrile was purchased from Avantor Performance Materials (Radnor Township, PA, USA). Methanol for extraction was from Honeywell (Offenbach, Germany). Solvents used for liquid/liquid partition and column chromatography were from Scharlau (Barcelona, Spain). Diosmin (Alexis Biochemicals, San Diego, CA, USA), luteolin (AdipoGen, San Diego, CA, USA), hyperoside (Carl Roth GmbH, Karlsruhe, Germany), isoquercitrin (Carl Roth), and luteolin 7-O-glucoside (Extrasynthèse, Gernay, France) were used as chromatographic reference substances.

2.3. Total phenolic and flavonoid contents

Total Phenolic Content (TPC) of the extract was determined using the Folin-Ciocalteu reagent according to the method of Singleton and Rossi (Singleton and Rossi, 1965), with gallic acid as a standard. 200 μl of each sample dissolved in methanol was added to 1 ml of Folin-Ciocalteu reagent (1:10 dilution in distilled water). The mixture was shaken and, after 4 min, 800 ml of Na_2CO_3 (75 mg/ml) solution were added. The mixture was kept for 2 h at room temperature and the absorbance measured at 760 nm. Total phenolic content was expressed in mg gallic acid equivalents per gram dry extract (mg GAE/g DE) using a calibration curve with gallic acid. All measurements were performed in triplicate.

Total Flavonoid Content (TFC) of the extract was measured according to the aluminum chloride colorimetric method based on the formation of a flavonoid-aluminum complex (Carocho et al., 2014) using a quercetin calibration curve: 1 ml of methanol extract was mixed with 1 ml of 2% $AlCl_3$ methanol solution. After 10 min, the absorbance was determined at 430 nm. The results were expressed as mg quercetin equivalent per gram of dry extract (mg QE/g DE). All measurements were performed in triplicate.

2.4. HPLC-PDA-MS analysis

HPLC-PDA-MS analysis was performed on a chromatographic system consisting of a degasser, quaternary pump (LC-20AD), a column oven (CTO-20AC), a PDA detector (SPD-M20A), and a triple quadrupole mass spectrometer (LCMS-8030) (Shimadzu, Kyoto, Japan). Separation was carried out on a SunFire C18 column (3.5 μm, 3.0 × 150 mm i.d., Waters) equipped with a guard column (3.0 × 10 mm). The mobile phase consisted of water + 0.1% formic acid (A) and acetonitrile + 0.1% formic acid (B). A gradient of 5–80% B in 30 min followed by 80–100% B in 5 min was applied. The flow rate was 0.4 ml/min. The extract was dissolved in DMSO at a concentration of 10 mg/ml and 10 μl were injected. The LabSolutions software (Shimadzu) was used for data acquisition and processing.

2.5. Compound isolation

The methanolic extract of *T. polium* (32 g) was suspended in 500 ml water and then successively partitioned with EtOAc (3 × 500 ml) and *n*-BuOH saturated with H_2O (4 × 500 ml) to provide a EtOAc-soluble fraction (8.2 g), a *n*-BuOH-soluble fraction (10.8 g), and the H_2O-soluble fraction (12.6 g). The EtOAc-soluble fraction was fractionated by MPLC on a silica column (47 × 5 cm, i.d.) with a *n*-hexane/EtOAc/MeOH gradient [*n*-hexane/EtOAc 98:2 (0–10 min), *n*-hexane/EtOAc 2–70% EtOAc (10–420 min), *n*-hexane/EtOAc 70–100% EtOAc (420–480 min), EtOAc/MeOH 0–20% MeOH (480–540 min), 100% MeOH (540–600 min)] at a flow rate of 20 ml/min. In total, 540 fractions were collected, which were combined based on TLC analysis into 22 fractions (Fr.1-Fr.22).

Fr. 11 (85 mg) afforded **14** (1.3 mg, t_R =29.3 min) after preparative HPLC with a gradient of 5–80% acetonitrile in water (both containing 0.1% formic acid) in 30 min. Compounds **10** (12.5 mg, t_R = 11.9 min), **11** (2.0 mg, t_R = 12.6 min), and **13** (16.9 mg, t_R = 19.3 min) were isolated from Fr. 14 (327 mg) by preparative HPLC with a gradient of 45–60% acetonitrile in water (both containing 0.1% formic acid) in 30 min. Separation of Fr. 21 (247 mg) by preparative HPLC with a gradient of 5–80% acetonitrile in water (both containing 0.1% formic acid) in 30 min afforded **9** (6.1 mg, t_R = 20.8 min) and **12** (3.0 mg, t_R = 23.9 min). Separation of Fr. 22 by preparative HPLC with a gradient of 15–50% acetonitrile in water (both containing 0.1% formic acid) in 30 min gave compound **2** (11.4 mg, t_R = 11.3 min) and a fraction (25.6 mg) which was further purified by semi-preparative HPLC with 16% aq. acetonitrile containing 0.1% formic acid to provide **3** (3.5 mg, t_R = 21.4 min), a mixture of **4** and **5** (4.8 mg, t_R = 23.4 min), and **6** (3.3 mg, t_R = 29.8 min). A portion (1.0 g) of the *n*-BuOH-soluble fraction was separated by preparative HPLC with a gradient of 5–80% acetonitrile in water (both containing 0.1% formic acid) in 30 min to give **1** (373 mg, t_R =11.6 min).

2.6. Animals

All animals (Swiss albino mice weighing 31–33 g and New Zealand albino rabbits weighing 1.9–2.1 kg) were obtained from Pasteur Institute of Algiers. They were fed *ad libitum* with water and kibble diet.

All experimental protocols were in accordance with the European Community Council Directive (86/609/EEC) and approved by the

National Committee for Evaluation and Programming of University Research of Algerian Ministry of Higher Education and Scientific Research (Registration N°: DO1N01UN280120150001).

2.7. Preparation of the ointment

The methanolic extract of *T. polium* was mixed with petroleum jelly (PJ) (Unilever, France) at a concentration of 5% and 10% to obtain the methanolic extract ointments OME 5% and OME 10%, respectively. Cicatryl-Bio (CIC) (Pierre Fabre, Paris, France) was used as reference drug.

2.8. Acute dermal irritation

The acute dermal irritation assay was carried out on New Zealand albino rabbits. The study was conducted according to the Organization for Economic Co-operation and Development (OECD) guidelines 404 (OECD 2002a). OME 5% and 10% were applied topically on the back of the animals at an amount of 0.5 g per rabbit. The animals were observed for mortality and any toxic or deleterious effects with special attention given to the first 4 hrs and then once daily for a period of 14 days following the topical application. At the application sites, the skin was observed for signs of erythema, edema and local injury. The body weight and food intake were also recorded.

2.9. Acute oral toxicity

The acute oral toxicity was assessed in healthy young adult female Swiss albino mice, nulliparous and non-pregnant. The study was conducted according to the Organization for Economic Co-operation and Development (OECD) guidelines 423 (OECD 2002b).

Twelve Swiss albino mice were divided into four groups of three animals and treated orally with different doses of *T. polium* extract for 14 days: Group I, control, received distilled water; Group II received 1000 mg/kg b.wt; Group III received 2000 mg/kg b.wt and Group IV received 5000 mg/kg b.wt as suspension by gavage. The treated mice were observed individually. The main observations and evaluations were external physical aspects (appearance and hair loss), behavioral changes (posture, scraping, aggressiveness, sensitivity to noise and light, hypersalivation) and measurable clinical signs (changes in heart and respiratory rhythms, abdominal contraction, diarrhea) (Hussain Mir et al., 2013).

At the end of the experiment, mice were sacrificed. Blood samples were collected to explore biochemical parameters (transaminases, alkaline phosphatase, serum total protein, creatinine, urea and uric acid). The parameters were measured by enzymatic colorimetric methods using commercially available kits (Spinreact, Girona, Spain). The livers and kidneys were excised from all experimental mice for histopathological examinations (Gandhare et al., 2013).

2.10. Evaluation of wound healing activity

An area of 500 mm^2 on the back of the New Zealand albino rabbit was shaved with an electric razor. The animals were left in their cages 24 h to verify the absence of irritation of the shaved zone (Hwisa et al., 2013). The animals were randomly divided into 5 groups of 4 rabbits as follows: first group was untreated (UT), second group treated with the reference drug (CIC), third group with OME 5%, fourth group with OME 10%, and fifth group with petroleum jelly (PJ).

2.10.1. Wound healing assay

Animals were anaesthetized using intraperitoneal injection of ketamine (90 mg/kg)-xylazine (10 mg/kg) (Mashreghi et al., 2013). A circle of 2.5 cm in diameter was drawn on the skin of the lumbar region which was then excised.

Excisional wounds were immediately treated after surgical operation and the animals placed in individual cages with clean litters. Preparations (CIC, OME 5%, OME 10% and PJ) were applied topically at an amount of 0.5 g per rabbit once per day till complete healing (Pipelzadeh et al., 2003).

The dimensions of excision wounds were measured every 4 days during the trial period by tracing the wounds on a transparent paper and measuring through the graph paper. The percentage of the evolution of wound contraction was calculated using the following formula (Tamri et al., 2014):

$$\%\text{wound contraction} = \frac{\text{Initial wound size} - \text{Specific day wound size}}{\text{Initial wound size}} \times 100$$

2.10.2. Histological sections

At the end of the experiment, the animals were sacrificed. The tissue slices (scarred skin and 0.5 cm of healthy skin) were fixed in formalin (10%) for 72 h. The samples were dehydrated by passing them through three successive baths of ethanol. Then they were thinned in two baths of xylene and embedded in paraffin by two successive baths at 60 °C each one. The paraffin blocks obtained were then cut with a microtome, rehydrated and stained with haematoxylin-eosin (Marck, 2010).

2.10.3. Statistical analysis

The data were subjected to one-way analysis of variance (ANOVA) for determining the significant difference (GraphPad, version 7). The results are presented as means ± SEM. The inter group significance was analyzed using by Dunnett's or Tukey test whenever applicable and differences were considered significant at $p \leq 0.05$.

3. Results

3.1. Polyphenolic profile

The methanolic extract of *T. polium* aerial parts had a total phenolic content of 86.63 ± 0.03 mg GAE/g DE, and a total flavonoid content of 24.43 ± 0.01 mg QE/g DE.

The polyphenolic profile of the extract was investigated by HPLC-UV-MS (Fig. 1), and revealed the presence of several peaks corresponding to flavonoids and caffeic acid derivatives. Compounds **7** and **8** were identified from their UV and MS data, and by chromatographic comparison with commercial reference samples as diosmin (Al Bahtiti, 2012) and luteolin (D'Abrosca et al., 2013; Elmasri et al., 2015), respectively. Further compounds were identified by ^{1}H and 2D NMR analysis after isolation. They included poliumoside (**1**) (De Marino et al., 2012; Oganesyan et al., 1991), acteoside (**2**) (Elmasri et al., 2015), hyperoside (**3**) (Rudakova et al., 2014), isoquercitrin (**4**) (Shammas and Verykokidou-Vitsaropoulou, 1987), luteolin 7-O-β-D-glucopyranoside (**5**) (D'Abrosca et al., 2013; De Marino et al., 2012), luteolin 7-O-(5-O-syringoyl-β-D-apiofuranosyl)-(1→2)-β-D-glucopyranoside (**6**) (D'Abrosca et al., 2013), cirsiliol (**9**), cirsimaritine (**10**) (Elmasri et al., 2015; Stefkov et al., 2011; Verykokidou-Vitsaropoulou and Vajias, 1986), cirsilineol (**11**) (Stefkov et al., 2011), eupatorin (**12**) (Verykokidou-Vitsaropoulou and Vajias, 1986), 5-desmethylsinensetin (**13**) (Alwahsh et al., 2015; Harborne et al., 1986; Kisiel et al., 2001; Topcu et al., 1996), and salvigenin (**14**) (Elmasri et al., 2014) (Fig. 2). All compounds had been previously reported in *T. polium* except flavonoid **13**. The latter compound had been previously described in other species of the genus *Teucrium*. To our knowledge, this study represents the first report of a detailed polyphenolic profile of *T. polium*.

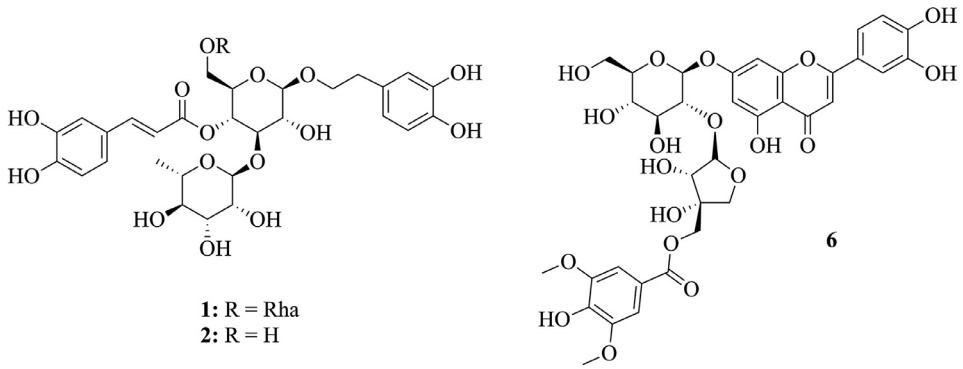

1: R = Rha
2: R = H

6

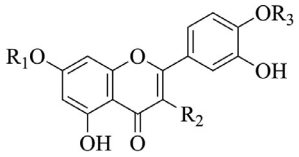

3: R_1 = H, R_2 = OGal, R_3 = H
4: R_1 = H, R_2 = OGlc, R_3 = H
5: R_1 = Glc, R_2 = H, R_3 = H
7: R_1 = Rha-(1→6)-Glc, R_2 = H, R_3 = CH_3
8: R_1 = H, R_2 = H, R_3 = H

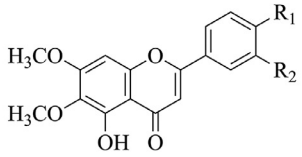

9: R_1 = OH, R_2 = OH
10: R_1 = OH, R_2 = H
11: R_1 = OH, R_2 = OCH_3
12: R_1 = OCH_3, R_2 = OH
13: R_1 = OCH_3, R_2 = OCH_3
14: R_1 = OCH_3, R_2 = H

Fig. 1. Structures of the compounds identified in the methanolic extract of *T. polium*.

3.2. Acute oral toxicity

Acute oral toxicity was tested in mice at doses of 1000 to 5000 mg/kg b.wt. Even at the highest dose no mortality or specific signs of toxicity were observed after oral administration of the extract. In addition, there were no respiratory, nervous, cutaneous or gastrointestinal symptoms. According to the toxicity scale of Hodge and Sterner (1949) for mice and rats, the extract of *T. polium* can be classified as a "practically nontoxic" substance (LD_{50} > 5000 mg/kg) (Lu, 1992).

As to the biochemical parameters (Table 1), the mice treated with the three doses showed non-significant differences compared to the control group. The extract appeared to be well tolerated, as it did not affect liver parameters and had no effect on transaminase protein levels. The extract did not induce any significant changes in the renal parameters (urea, uric acid and creatinine concentrations) in the treated mice compared to the control group.

The different histological sections of liver and kidney from the treated mice were compared to the section of the normal control (Fig 3). The extract did not induce any changes, and the observations revealed a typical normal kidney and hepatic lobule for all treated mice. Slight dilation of the portal vein was observed with the doses of 2000 and 5000 mg/kg b.wt. While the reasons for this histological peculiarity remain unclear, this should not be considered as a sign of toxicity in the absence of any other abnormalities.

3.3. Acute dermal irritation

The animals were observed frequently during the 14 days following the topical application of 0.5 g of OME 5% or OME 10%. No signs of toxicity or mortality were seen. The rabbits were normal and did not show any critical changes in behavior and breathing, or any disability in feeding and water utilization, or postural irregularities and loss of hair. There were no signs of cutaneous irritation, no erythema, eschar, edema, or any other reactions on the skin of all animals after topical application.

3.4. Wound healing

3.4.1. Evolution of the wound healing process

During the healing period, the wounds were measured every 4 days. The evolution of the surface of each wound excision was assessed in the treated and untreated animals. The results are presented in Table 2. The photographic documentation of the wound healing process is included as Supplementary Material. All treated animals (CIC, OME 5% and OME 10%) showed very significant and significant reduction in wound area when compared to untreated and PJ groups (p <0.001and p <0.01, respectively). There was no significant difference between groups treated with the ointment prepared with the two concentrations (5 and 10%) of the extract and the reference drug Cicatryl-Bio. The OME 10% ointment proved its effectiveness in the healing process with 92.00 ± 0.14% of contraction of excision wounds in rabbits, which was better than 85.25 ± 0.18% obtained with the reference drug Cicatryl-Bio.

The daily visual observations indicated the presence of signs of inflammation (redness and fever) around the wound in rabbits of the different groups the first days after the excision of the skin. These signs disappeared quickly in the treated groups (CIC, OME 5% and OME 10%) and persisted in the rest of the groups for a few days (UT and PJ).

3.4.2. Histological sections

Histopathological examination was performed at the end of the experiment. Cicatricial zones of rabbits (treated or not treated) were compared to a healthy zone on the same histological cut of the same sample (Fig. 4).

The histological sections showed better healing and complete re-epithelialization in animals treated with the reference drug (Cicatryl-Bio), OME 5% and OME 10% compared to the untreated group and the group treated with petroleum jelly. The healed skin showed normal epithelialization, with thick mature epidermis and granulation tissue, and also higher collagen deposition in treated groups with CIC, OME 5%, and OME 10%.

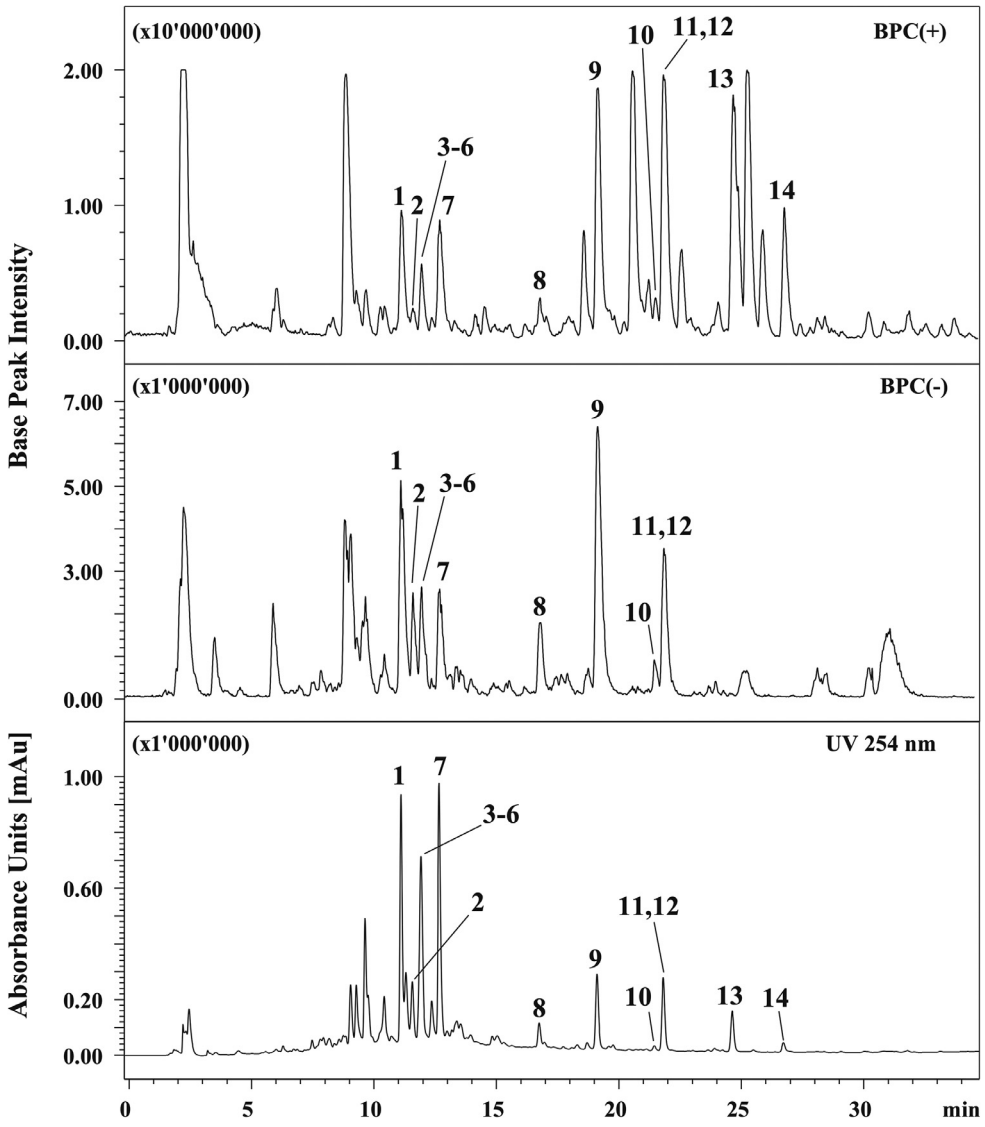

Fig. 2. HPLC-UV-MS analysis of the methanolic extract of *T. polium*. BPC: base peak chromatogram. Peak numbers refer to the identified compounds (Fig. 1).

Table 1
Biochemical parameters of the mice treated with the methanolic extract of *T. polium* at different doses.

Parameters	Treatment (mg/kg b.wt)			
	Control	1000	2000	5000
Urea (mg/l)	0.88 ± 0.02	0.91 ± 0.07	0.92 ± 0.03	0.93 ± 0.01
Creatinine (mg/l)	4.09 ± 0.15	5.43 ± 0.36	4.29 ± 0.47	4.05 ± 0.15
Uric Acid (mg/dl)	41.90 ± 4.49	42.32 ± 3.80	51.89 ± 7.63	25.98 ± 0.74
AST (IU/l)	40.66 ± 3.97	39.16 ± 3.83	43.16 ± 8.77	40.00 ± 2.31
ALT (IU/l)	11.00 ± 0.61	16.00 ± 1.00	15.66 ± 2.55	14.67 ± 1.02
ALP (IU/l)	54.67 ± 3.57	42.83 ± 3.51	53.20 ± 2.94	49.00 ± 1.29
Total Protein (g/dl)	60.00 ± 1.61	70.50 ± 3.43	72.00 ± 1.53	70.60 ± 2.50

Values are expressed as means ± SEM (n = 3).

The histological sections of the UT and PJ groups showed the presence of fleshy bud with more inflammatory cells, less collagen deposition and incomplete maturation of the dermis or epidermis. This indicates that, despite the contraction of the wound, petroleum jelly does not have therapeutic properties. Indeed, during the healing process, petroleum jelly is capable of inhibiting the evaporation of water from the wound. The formation of a wet physiological environment in the wound promotes skin repair and regeneration of damaged tissue. However, therapy with petroleum jelly can cause alteration and tissue maceration (Djerrou et al., 2011).

4. Discussion

Acute dermal toxicity corresponds to the adverse effects occurring within a short time of dermal application of a single dose of a test substance (OECD, 2017). Assessment of a single dermal dose toxicity

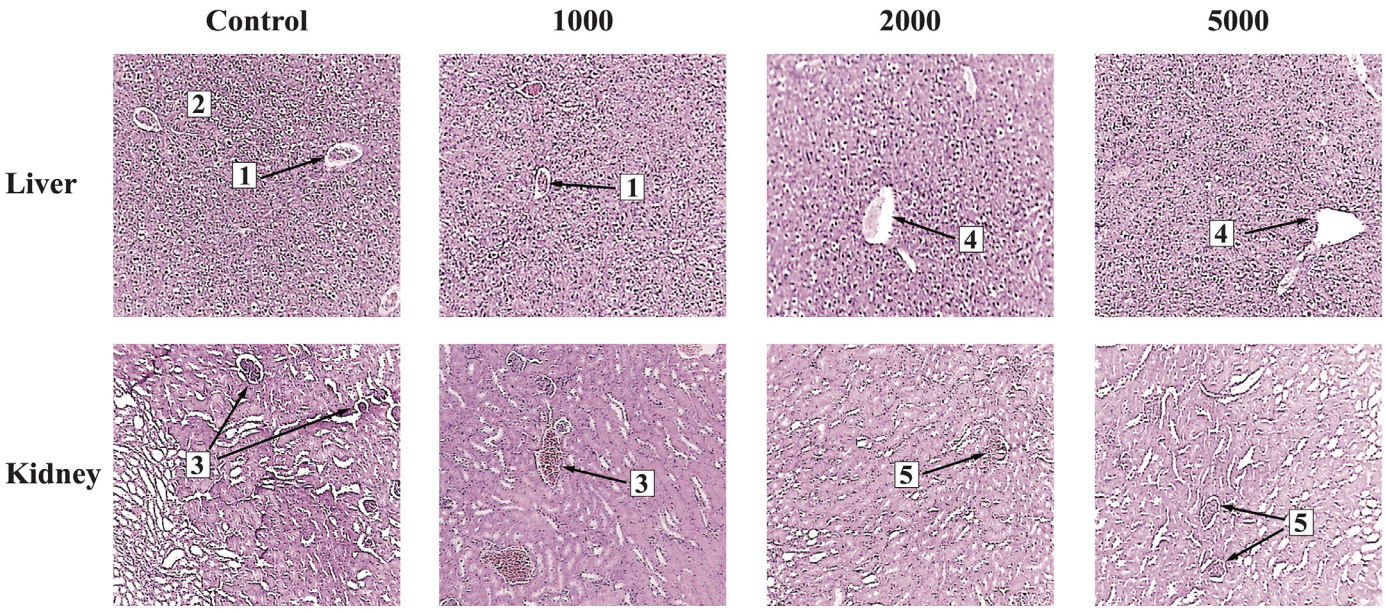

Fig. 3. Histopathological changes in liver and kidney of animals treated with *T. polium* methanolic extract at different doses (magnification x 10). 1: central vein; 2: surrounding hepatocytes; 3: glomerulus; 4: dilation of the portal vein; 5: tubular.

Table 2
Effect of different treatments on the evolution of the percentage of excision wound contraction in New Zealand albino rabbits.

Groups	Wound contraction (%)			
	Number of days			
	4	8	12	16
UT	15.73 ± 0.37	23.93 ± 0.24	25.57 ± 0.50	42.62 ± 0.38
CIC	19.87 ± 0.13	29.48 ± 0.28	58.33 ± 0.24**	85.25 ± 0.18***
OME 5%	11.33 ± 0.31	36.33 ± 0.64*	61.33 ± 0.70***	78.00 ± 0.95 ***
OME 10%	15.63 ± 0.85	38.18 ± 0.64*	81.81 ± 0.47***	92.00 ± 0.14***
PJ	17.91 ± 0.25	26.86 ± 0.17	32.83 ± 0.47*	65.16 ± 0.32**

Values are expressed as mean ± SEM, (n = 4), * p<0.05, **, p< 0.01, *** p< 0.001 when treated groups are compared to the UT group. UT: untreated group; CIC: group treated with Cicatryl-Bio; OME 5% / 10%: groups treated with methanolic extract ointment; PJ: group treated with petroleum jelly.

is an important part of any toxicology program for new pharmaceutical or cosmetic products to be applied on the skin (Vinardell and Mitjans, 2008). In our study, no signs of dermal toxicity were observed after application of the *T. polium* ointment. As to the oral acute toxicity, the methanolic extract of *T. polium* did not produce any signs of toxicity in mice even at the highest dose (5000 mg/kg b.wt), and none of the animals died after 14 days of observation. Also, no significant changes were observed in biochemical parameters or histological sections of liver or kidney except a slight dilation of the portal vein. Similar observations have been reported in the study of Meguellati et al. (2019). At the same time, it should be mentioned that hepatotoxic and nephrotoxic effects of *T. polium* have been shown in many case reports and experimental studies where vacuolization, destruction and degeneration of liver and kidney were the most frequently described events (Aktürk Esen et al., 2019; Rafieian-Kopaei and Baradaran, 2013). The absence of toxicity observed in our study may be explained by the relatively short duration of administration (2 weeks). Indeed, the toxic effects of *T. polium* have been related to the dose and duration of use (Bachtarzi et al., 2016; Dağ et al., 2014). Based on our data, short-term treatment with a *T. polium* extract appears safe.

The 5% and 10% ointments (OME 5% and OME 10%) prepared from the methanolic extract of *T. polium* significantly improved the wound healing process after excision in albino rabbits. On histological examination, the treated groups (Cicatryl-Bio, OME 5%, and OME 10%) showed higher collagen deposition and complete re-epithelialization. The best results were obtained with OME 10%. Cicatryl-Bio contains allantoin as active ingredient. In an open wound model, allantoin was able to ameliorate and accelerate the repair of the skin. The wound healing effect of allantoin occurred via the regulation of inflammatory response and stimulation of fibroblastic proliferation and extracellular matrix synthesis (Araújo et al., 2010). The treatment with the ointment produced a similar effect that the control drug and had a strong impact on the granulation and epithelialization of wounds, accelerated tissue repair and reduced the duration of this process. This may be due to the combined effects of the polyphenolic constituents, mainly flavonoids and caffeic acid derivatives. For example, the flavonoid fraction from *Ginkgo biloba* has been shown to enhance proliferation of normal human skin fibroblasts *in vitro* (Kim et al., 1997). Fibroblasts are responsible for the synthesis of collagen fibers and healing activity. The caffeic acid derivative acteoside (**2**) has been recently reported to increase the activation of promatrix metalloproteinase-2 and the expression of membrane type-1-matrix metalloproteinase, thereby possibly facilitating a remodeling of extracellular matrices (Si et al., 2018).

Our data confirm results obtained in previous studies performed in other animal models. Meguellati et al. (2019) reported that the treatment with an extract from callus tissue derived from *T. polium*

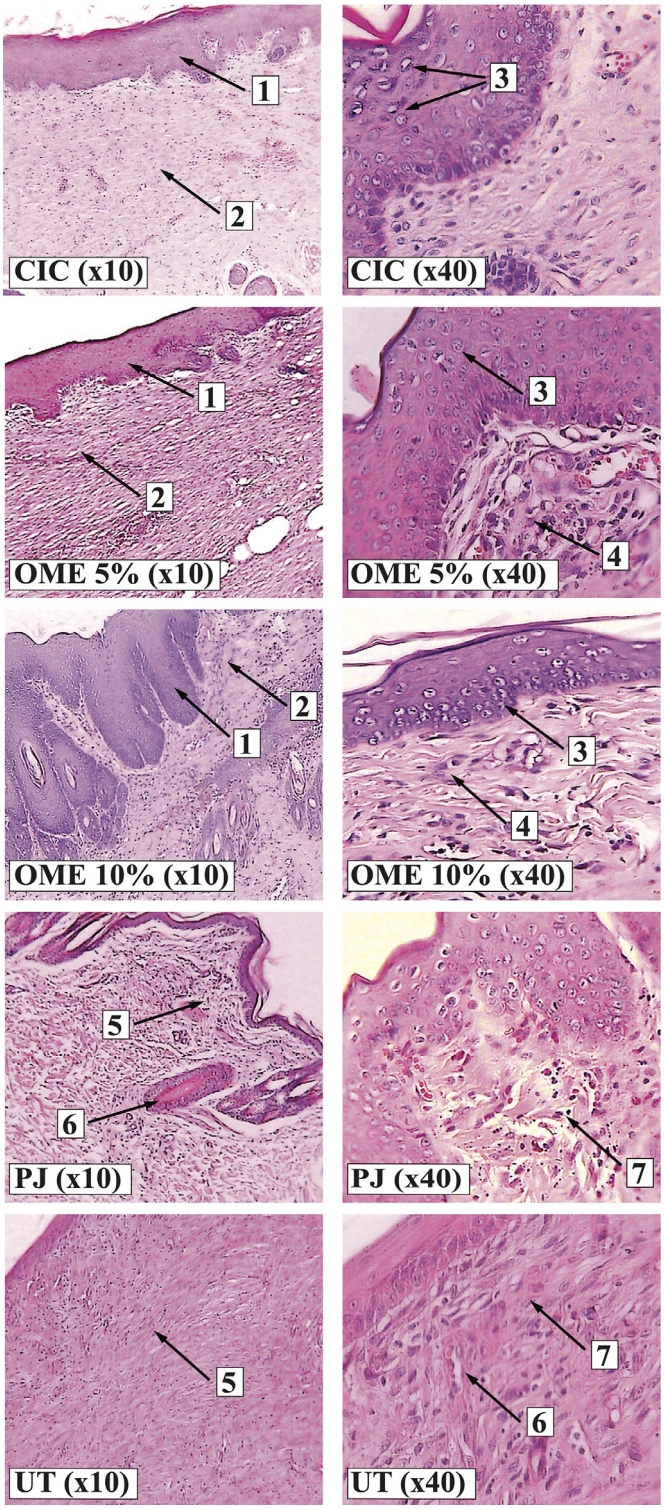

Fig. 4. Histological evaluation of wound skin sections stained with hematoxylin and eosin (10 and 40 x magnification) of various groups (CIC, OEM 5%, OEM 10%, PJ, and UT). UT: untreated group; CIC: group treated with Cicatryl-Bio; OME 5% / 10%: groups treated with methanolic extract ointment; PJ: group treated with petroleum jelly. 1: thick mature dermis; 2: collagen; 3: granulosa cells; 4: epidermis; 5: fleshy bud; 6: angiogenesis 7: incomplete epidermis.

had a strong impact on the granulation and epithelialization of wounds, accelerated tissue repair, and reduced the duration of wound healing process in an excision wound model in rats. Huseini et al., 2020 found that a 10% *T. polium* ointment accelerated the wound healing process in diabetic rats. Ansari et al. (2013) also demonstrated the effectiveness of a 2% *T. polium* extract with 91.5% of wound contraction against 75.3% for the reference drug silver sulfadiazine cream on experimental second degree burns in mice.

5. Conclusion

The 10% ointment obtained from the extract of *T. polium* showed significant wound healing properties in our wound excision model on rabbits, which were superior to those of the reference drug Cicatryl-Bio.

Moreover, acute oral toxicity studies in albino mice, and acute dermal toxicity assessment in albino rabbits indicated that the aerial

parts of *T. polium* are potentially safe over a two-week treatment period corresponding to a typical application time in the therapy of open wounds. Overall, our data confirm the potential of *T. polium* extract for the treatment of wounds and support the traditional use of this plant as a wound healing agent. Further investigations with *in vitro* models such as scratch assays are warranted to identify the active constituents and unravel the mechanism of action. In addition, the potential of *T. polium* for the treatment of other types of wounds such as closed wounds and diabetic ulcer wounds could also be explored.

Declaration of Competing Interest

The authors declare that they have no conflict of interest.

Acknowledgments

Prof. M. Hamburger (Division of Pharmaceutical Biology, University of Basel) is acknowledged for providing the infrastructure used for the analytical characterization, and for the critical proofreading of the manuscript.

Source of funding

This work was supported by the Algerian Ministry of Higher Education and Scientific Research through the National Committee for Evaluation and Programming of University Research (DO1N01UN280120150001).

Supplementary materials

Supplementary material associated with this article can be found, in the online version, at doi:10.1016/j.sajb.2020.10.017.

References

Aktürk Esen, S., Kahvecioğlu, S., Gül, C.B., Aktaş, N., Esen, İ., 2019. Toxic effects of herbal medicines: *Teucrium polium* and acute kidney injury. Eur. Research J. 5, 1028–1030 .

Al Bahtiti, N.H., 2012. "*Teucrium polium*" Extracts Jordanian Ja'adeh. Asian J. Agricult. Sci. 4, 379–382.

Alwahsh, M.A.A., Khairuddean, M., Chong, W.K., 2015. Chemical constituents and antioxidant activity of *Teucrium barbeyanum* Aschers. Records Natural Prod. 9, 159–163.

Ansari, R., Sahinfard, N., Namjou, A., Rafieian, M., Shirzad, H., Rafieian-kopaei, M., 2013. Ameliorative property of *Teucrium polium* on second degree burn. J. HerbMed Pharmacol. 2, 9–11.

Araújo, L.U., Grabe-Guimarães, A., Mosqueira, V.C.F., Carneiro, C.M., Silva-Barcellos, N.M., 2010. Profile of wound healing process induced by allantoin. Acta Cirurgica Brasileira 25 (5) doi.org/10.1590/S0102-86502010000500014.

Bachtarzi, K., Hilmi, S., Laouar, H., Belkheiri, A., Pacha, Y.H., 2016. The chronic toxic effect of *Teucrium polium* aqueous extract on some blood parameters in rat. Der Pharma Chemica 8, 384–387.

Bahramikia, S., Yazdanparast, R., 2012. Phytochemistry and medicinal properties of *Teucrium polium* L. (Lamiaceae). Phytother. Res. 26, 1581–1593.

Basudan, N., Abu-Gabal, N.S., 2018. Phytochemistry and biological properties investigation of *Teucrium polium* L. Int. J. Pharm. Biol. Sci. 8, 660–670.

Boudjelal, A., Henchiri, C., Sari, M., Sarri, D., Hendel, N., Benkhaled, A., Ruberto, G., 2013. Herbalists and wild medicinal plants in M'Sila (North Algeria): an ethnopharmacology survey. J. Ethnopharmacol. 148, 395–402.

Carocho, M., Barreiro, M.F., Morales, P., Ferreira, I.C.F.R., 2014. Adding molecules to food, pros and cons: a review on synthetic and natural food additives. Compr. Rev. Food Sci. Food Saf. 13, 377–399.

D'Abrosca, B., Pacifico, S., Scognamiglio, M., D'Angelo, G., Galasso, S., Monaco, P., Fiorentino, A., 2013. A new acylated flavone glycoside with antioxidant and radical scavenging activities from *Teucrium polium* leaves. Nat. Prod. Res. 27, 356–363.

Dağ, M., Özturk, Z., Aydinli, M., Koruk, I., Kadayifçi, A., 2014. Postpartum hepatotoxicity due to herbal medicine *Teucrium polium*. Ann. Saudi Med. 34, 541–543.

Dehshiri, M.M., Azadbakht, M., 2012. Anatomy of Iranian species *Teucrium polium* (Lamiaceae). J. Biol. Today's World 1, 48–52.

De Marino, S., Festa, C., Zollo, F., Incollingo, F., Raimo, G., Evangelista, G., Iorizzi, M., 2012. Antioxidant activity of phenolic and phenylethanoid glycosides from *Teucrium polium* L. Food Chem. 133, 21–28.

Djerrou, Z., Hamdi-Pacha, Y., Belkhiri, A.M., Djaalab, H., Riachi, F., Serakta, M., Boukeloua, A., Maameri, Z., 2011. Evaluation of *Pistacia lentiscus* fatty oil effects on glycemic index, liver functions and kidney functions of New Zealand rabbits. Afr. J. Tradit. Complement Altern. Med. 8, 214–219.

Elmasri, W.A., Hegazy, M.-E.F., Aziz, M., Koksal, E., Amor, W., Mechref, Y., Hamood, A.N., Cordes, D.B., Pare, P.W., 2014. Biofilm blocking sesquiterpenes from *Teucrium polium*. Phytochemistry 103, 107–113.

Elmasri, W.A., Yang, T., Tran, P., Hegazy, M.-E.F., Hamood, A.N., Mechref, Y., Pare, P.W., 2015. *Teucrium polium* phenylethanol and iridoid glycoside characterization and flavonoid inhibition of biofilm-forming *Staphylococcus aureus*. J. Nat. Prod. 78, 2–9.

Gandhare, B., Kavimani, S., Rajkapoor, B., 2013. Acute and subacute toxicity study of methanolic extract of *Ceiba pentandra* (Linn.) Gaertn. on rats. J. Sci. Res. 5, 315–324 .

Harborne, J.B., Tomas-Barberan, F.A., Williams, C.A., Gil, M.I., 1986. A chemotaxonomic study of flavonoids from European *Teucrium* species. Phytochemistry 25, 2811–2816.

Huseini, H.F., Abdolghaffari, A.H., Ahwazi, M., Jasemi, E., Yaghoobi, M., Ziaee, M., 2020. Topical application of *Teucrium polium* can improve wound healing in diabetic rats. Int. J. Low Extrem. Wounds 19, 132–138.

Hussain Mir, A., Sexena, M., Malla, M.Y., 2013. An acute oral toxicity study of methanolic extract from *Tridex procumbens* in Sprague Dawley's rats as per OECD guidelines 423. Asian J. Plant Sci. Res. 3, 16–20.

Hwisa, N.T., Katakam, P., Chandu, B.R., Abadi, E.G., Shefha, E.M., 2013. Comparative *in vivo* evaluation of three types of honey on topical wound healing activity in rabbits. J. Appl. Pharmaceut. Sci. 3, 139–143.

Jaradat, N.A., 2015. Review of the taxonomy, ethnobotany, phytochemistry, phytotherapy and phytotoxicity of germander plant (*Teucrium polium* L.). Asian J. Pharmaceut. Clin. Res. 8, 13–19.

Kim, S.J., Lim, M.H., Chun, I.K., Won, Y.H., 1997. Effects of flavonoids of *Ginkgo biloba* on proliferation of human skin fibroblast. Skin Pharmacol. Physiol. 10, 200–205.

Kisiel, W., Stojakowska, A., Piozzi, F., Rosselli, S., 2001. Flavonoids from *Teucrium fruticans* L. Acta Soc. Botanicorum Poloniae 70, 199–201.

Lu, F.C., 1992. Toxicologie : données Générales, Procédures d'Evaluation, Organes Cibles, Toxicologie : Données Générales, Procédures d'Evaluation, Organes Cibles, Evaluation du Risque. 1st ed. Elsevier Masson, Paris.

Marck, V., 2010. Manuel De Techniques D'anatomo-Cytopathologie, Manuel de Techniques d'Anatomo-Cytopathologie. 1st ed. Elsevier Masson, Paris.

Mashreghi, M., Rezazade Bazaz, M., Mahdavi Shahri, N., Asoodeh, A., Mashreghi, Mansour, Behnam Rassouli, M., Golmohammadzadeh, S., 2013. Topical effects of frog "Rana ridibunda" skin secretions on wound healing and reduction of wound microbial load. J. Ethnopharmacol. 145, 793–797.

Meguellati, H., Ouafi, S., Saad, S., Djemouai, N., 2019. Evaluation of acute, subacute oral toxicity and wound healing activity of mother plant and callus of *Teucrium polium* L. subsp. *geyrii* Maire from Algeria. S. Afr. J. Bot. 127, 25–34.

OECD (Organization of Economic Co-Operation and Development), 2002a. Test No. 404: Acute Dermal Irritation/Corrosion. OECD Publishing, Paris.

OECD (Organization of Economic Co-Operation and Development), 2002b. Test No. 423: Acute Oral Toxicity - Acute Toxic Class Method. OECD Guidelines for the Testing of Chemicals. OECD Publishing, Paris.

OECD (Organization of Economic Co-Operation and Development), 2017. Test No. 402: Acute Dermal Toxicity. OECD Publishing, Paris.

Oganesyan, G.B., Galstyan, A.M., Mnatsakanyan, V.A., Shashkov, A.S., Agababyan, R.V., 1991. Phenylpropanoid glycosides of *Teucrium polium*. Khimiya Prirodnykh Soedinenii 630.

Pipelzadeh, M.H., Pipelzadeh, M.R., Husseinzadeh, P., 2003. A study on the effects of modulation of intracellular calcium on excisional wound healing in rabbit. Iran. Biomed. J. 7, 161–166.

Quézel, P., Santa, S., 1963. Nouvelle Flore de l'Algérie et des Régions Désertiques Méridionales, 1st ed. Éditions CNRS, Paris, pp. 741–743.

Rafieian-Kopaei, M., Baradaran, A., 2013. *Teucrium polium* and kidney. J. Renal Inj. Prev. 2, 3–4.

Rudakova, Y.G., Senchenko, S.P., Popova, O.I., 2014. The study of phenolic compounds of herb *Teucrium polium* L. Vopr. Biol. Meditsinskoi i Farmatsevticheskoi Khimii 34–37.

Shammas, G., Verykokidou-Vitsaropoulou, E., 1987. Flavonoid heterosides of *Teucrium polium* L. Plantes Médicinales et Phytothérapie 21, 144–148.

Si, N., Kanazawa, H., Okuyama, K., Imada, K., Wang, H., Yang, J., Zhao, H., Bian, B., Ito, A., Sato, T., 2018. Involvement of catechols in acteoside in the activation of promatrix metalloproteinase-2 and membrane type-1-matrix metalloproteinase expression via a phosphatidylinositol-3-kinase pathway in human dermal fibroblasts. Biol. Pharm. Bull. 41, 1530–1536.

Singleton, V.L., Rossi, J.A.J., 1965. Colorimetry of total phenolics with phosphomolybdic-phosphotungstic acid reagents. Am. J. Enol. Vitic. 16, 144–158.

Stefkov, G., Kulevanova, S., Miova, B., Dinevska-Kjovkarovska, S., Moolgaard, P., Jaeaeger, A.K., Josefsen, K., 2011. Effects of *Teucrium polium* spp. *capitatum* flavonoids on the lipid and carbohydrate metabolism in rats. Pharm. Biol. 49, 885–892.

Tamri, P., Hemmati, A., Boroujerdnia, M.G., 2014. Wound healing properties of quince seed mucilage: *in vivo* evaluation in rabbit full-thickness wound model. Int. J. Surgery 12, 843–847.

Topcu, G., Eris, C., Kurucu, S., Ulubelen, A., 1996. A new flavanone from *Teucrium alyssifolium*. Turk. J. Chem. 20, 265–267.

Verykokidou-Vitsaropoulou, E., Vajias, C., 1986. Methylated flavones from *Teucrium polium*. Planta Med. 52, 401–402.

Vinardell, M.P., Mitjans, M., 2008. Alternative methods for eye and skin irritation tests: an overview. J. Pharm. Sci. 97, 46–59.

3.4 Publication 4

New neo-clerodane diterpenes from *Teucrium polium* subsp. *capitatum*

Morris Keller, Sarra Chabane, Amel Boudjelal, Ombeline Danton, Alessandro Prescimone, Matthias Hamburger, Olivier Potterat

Journal of Molecular Structure **1284**, 135447 (2023)
doi: 10.1016/j.molstruc.2023.135447

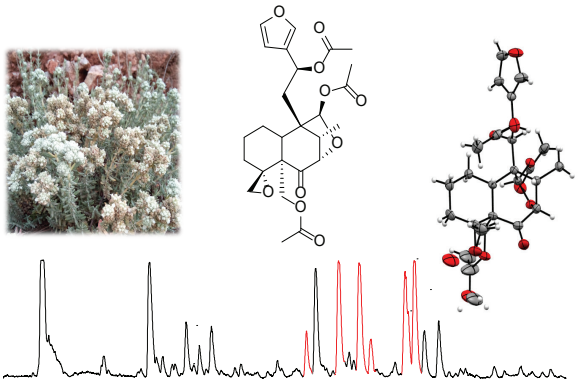

The methanolic extract of *Teucrium polium* subsp. *capitatum* was investigated for its chemical composition. Six acetoxylated neo-clerodane diterpenes, including 20-acetylauropolin and 6-acetylteucjaponin A, have been isolated along with four new congeners. Silica gel column chromatography and preparative HPLC-ESIMS were used to isolate the compounds, and their structures were determined using NMR and HRESIMS. The absolute configuration of 20-acetylauropolin was confirmed by X-ray crystallographic diffraction analysis. Some of the isolated diterpenes have unusual structural features not typically found in neo-clerodane diterpenes, such as a rare C-20 acetal function that forms an oxepane ring to C-7 of the *trans*-decalin core structure. Unfortunately, the acetal function was erroneously referred to as an hemiacetal function in the publication.

The supporting information is available in the appendix

Contribution to this publication: Extraction, isolation, and structure elucidation of the compounds from *T. polium*

Journal of Molecular Structure 1284 (2023) 135447

Contents lists available at ScienceDirect

Journal of Molecular Structure

journal homepage: www.elsevier.com/locate/molstr

New neo-clerodane diterpenes from *Teucrium polium* subsp. *capitatum*

Morris Keller[a], Sarra Chabane[b], Amel Boudjelal[c,d], Ombeline Danton[a], Alessandro Prescimone[e], Matthias Hamburger[a], Olivier Potterat[a,*]

[a] Division of Pharmaceutical Biology, University of Basel, Klingelbergstrasse 50, CH-4056 Basel, Switzerland
[b] Department of Life and Nature Science, Faculty of Sciences, Mohamed Boudiaf University, 28000 M'Sila, Algeria
[c] Department of Microbiology and Biochemistry, Faculty of Sciences, Mohamed Boudiaf University, 28000 M'Sila, Algeria
[d] Biology Laboratory: Applications in Health and Environment, Faculty of Sciences, Mohamed Boudiaf University, 28000 M'Sila, Algeria
[e] Department of Chemistry, University of Basel, Mattenstrasse 22, CH-4058 Basel, Switzerland

ARTICLE INFO

Article history:
Received 15 February 2023
Revised 24 March 2023
Accepted 26 March 2023
Available online 26 March 2023

Keywords:
Teucrium polium subsp. *capitatum*
Preparative HPLC-MS
Neo-clerodane type diterpenes
X-ray crystal structure
NMR spectroscopy

ABSTRACT

Phytochemical investigation of a methanolic extract from the aerial parts of *Teucrium polium* subsp. *capitatum* afforded six acetoxylated neo-clerodane diterpenes, including 20-acetylauropolin and 6-acetylteucjaponin A, along with four previously undescribed congeners. The compounds were isolated by a combination of silica gel column chromatography and preparative HPLC-ESIMS. Their structures were determined by extensive NMR analysis, HRESIMS, and by comparison with literature data of related compounds. The absolute configuration of 20-acetylauropolin was confirmed by X-ray crystallographic diffraction analysis. Some of the isolated diterpenes possess structural features unusual in the class of neo-clerodane diterpenes, such as a rare C-20 hemiacetal function which forms an oxepane ring to C-7 of the *trans*-decalin core structure.

1. Introduction

Teucrium polium subsp. *capitatum* (L.) Arcang (syn. *Teucrium capitatum* L.; Lamiaceae), also known as felty or golden germander, is a perennial subshrub that natively grows in Mediterranean regions of Europe, Northern Africa, and Southwestern Asia [1]. The aerial parts of the plant are traditionally used in Algeria as a decoction or ointment in the treatment of hypertension, diabetes, and wounds [2,3]. *T. polium* including subspecies and varieties is known to contain a wide variety of polyphenolic compounds including flavonoids and phenylethanoid glycosides, as well as various terpenoids, such as triterpenes, sterols, sesquiterpenoids, iridoids, and diterpenoids [2,4,5]. In particular, these plants are a source of neo-clerodane diterpenes [4–10], which are known for their antifeedant effects on insects and are thought to be responsible for the hepatotoxicity occasionally observed after the consumption of *Teucrium*-containing herbal products [11–16]. Recently, neo-clerodane diterpenes from *T. yemense* were shown to increase glucose-triggered release of insulin from murine pancreatic islets [17].

In a previous study we reported the wound healing properties of a methanolic extract from the aerial parts in a wound excision model in rabbits. A comprehensive analysis of the polyphenolic profile of this extract led to the isolation and identification of 12 flavonoids and two phenylethanoid glycosides [2]. Herein, we report on the further investigation of the methanolic extract leading to the isolation and structure elucidation of six furanoid neo-clerodane diterpenes including four new congeners.

2. Experimental

2.1. General procedures

Normal phase flash chromatography was performed on a Premium Flash-Prep LC system PuriFlash® 4100 equipped with an UV detector and a fraction collector (Interchim, Montluçon, France). Preparative HPLC was performed on a Preparative LC/MSD System (Agilent Technologies, Santa Clara, CA, USA) consisting of a 1260 binary pump, a 1100 diode array detector, and a 6120 single quadrupole MS detector. A SunFire Prep C18 OBD column (5 µm, 150 × 30 mm i.d., Waters, Milford, MA, USA), equipped with a C18 Prep Guard Cartridge (10 × 30 mm i.d.) was used. Water (A) and MeCN (B), both containing 0.1% formic acid, were used as mobile phase. A flow rate of 20 mL/min was applied. A 1290 Infinity II Valve Drive manual injection system (Agilent Technologies) was used for injection. Detection was with ESIMS in positive scan mode in combination with UV at 210 nm. For ESIMS detection a Quicksplit™ adjustable nano flow splitter (Analytical Scientific In-

* Corresponding author.
E-mail address: Olivier.potterat@unibas.ch (O. Potterat).

https://doi.org/10.1016/j.molstruc.2023.135447

struments Inc., Richmond, CA, USA) was used with a 1:100 flow split. A make-up flow of 0.4 mL/min (50% aqueous MeCN with 0.1% formic acid) generated by an Agilent 1290 Infinity II quaternary pump was added post-split. Data acquisition and processing was done by ChemStation software (Agilent Technologies).

Semi-preparative separations were carried out on an HP1100 Series HPLC instrument (Agilent Technologies) equipped with a binary pump, auto sampler, column oven, and a diode array detector. Chromatography was performed on a SunFire C18 column (5 µm, 150 × 10 mm i.d., Waters) equipped with a guard column (10 × 10 mm i.d.). The mobile phase consisted of A and B as described above at a flow rate of 4 mL/min. Data acquisition and processing was performed using ChemStation software (Agilent Technologies).

HPLC-PDA-ELSD-ESIMS was conducted on a LC-MS 8030 chromatographic system (Shimadzu, Kyoto, Japan) consisting of a degasser, auto-sampler, quaternary pump, a column oven, a diode array detector, a triple quadrupole MS, and an ELSD 3300 detector (Alltech, Deerfield, IL, USA). Analytical investigations were carried out on a SunFire C18 column (3.5 µm, 150 × 3 mm i.d., Waters) equipped with a guard column (10 × 3 mm i.d.). Solvents A and B (see above) were used as mobile phase. The gradient was 5–80% B in 30 min followed by 80–100% B from 30 to 35 min, and a final hold for 5 min at 100% B. The flow rate was 0.4 mL/min. The LabSolutions software (Shimadzu) was used for data acquisition and processing.

TLC was performed on silica gel 60 F254-coated aluminium plates (Macherey-Nagel, Düren, Germany). Detection was at UV 254 nm, and after spraying with 1% ethanolic vanillin and 10% sulfuric acid in EtOH followed by heating at 100 °C.

HRESIMS spectra were recorded on a LTQ Orbitrap XL hybrid ion trap–Orbitrap mass spectrometer (Thermo-Fisher Scientific, Massachusetts, MA, USA). Optical rotations were measured at 25 °C on a JASCO P-2000 polarimeter (Brechbühler, Schlieren, Switzerland) equipped with a 10 cm temperature-controlled microcell. UV and ECD spectra were recorded in MeOH (333 or 400 µg/mL) on a Chirascan CD spectrometer using 1 mm path precision cells (110 QS, Hellma Analytics, Müllheim, Germany). NMR spectra were recorded on a Bruker Avance III spectrometer (Bruker BioSpin, Rheinstetten, Germany) operating at 500.13 MHz for ^{1}H and 125.77 MHz for ^{13}C nuclei. ^{1}H NMR, ^{1}H,^{1}H-COSY, HSQC, HMBC, and ROESY spectra were recorded in $CDCl_3$ (ARMAR Chemicals, Döttingen, Switzerland) in a 1 mm TXI or a 5 mm BBO probe at 23 °C. Data were analysed using Bruker Topspin 3.5 and ACD/Labs NMR Workbook suites (Advanced Chemistry Development, Toronto, Canada) software. Chemical shifts are reported as δ values (ppm) using the solvent signal (δ_H 7.27; δ_C 77.00, $CDCl_3$) as internal reference; coupling constants (J) are given in Hz.

Silica gel 60 (0.040–0.063 mm) used for flash chromatography was from Merck (Darmstadt, Germany). Methanol for extraction was from Honeywell (Offenbach, Germany). HPLC-grade solvents MeCN, MeOH (Avantor, Radnor, PA, USA), and water from a Milli-Q water purification system (Merck Millipore, Billerica, USA) were used for HPLC separations. HPLC-grade *n*-BuOH, formic acid, and DMSO were obtained from Scharlau (Scharlab S.L., Barcelona, Spain). HPLC-grade isopropanol and EtOAc used for recrystallization were from Avantor and Scharlau, respectively. Technical grade EtOAc, MeOH, and *n*-hexane (Rheuss Chemie, Tägerig, Switzerland) were redistilled before use for preparative isolation.

2.2. Plant material

The flowering aerial parts of *Teucrium polium* subsp. *capitatum* L. were collected in May 2018, in M'Sila Algeria, at 35° 12′ 36.97″ N latitude and 4° 10′ 46.08″ E longitude. The taxonomic identity of the plant material was confirmed by Dr. Sarri Dj., botanist at the Department SNV/M'Sila, Mohamed Boudiaf University. A voucher specimen (AB-92) has been deposited at the department's herbarium of the University of M'Sila. The plant material was cleaned, dried at room temperature, and subsequently powdered.

2.3. Extraction and isolation

The powdered plant material was extracted in 50 g portions with MeOH (500 mL, each) by Soxhlet extraction for six hours to afford after filtration and evaporation under reduced pressure an oily residue (yield 17.5%). A portion of 32 g of the MeOH extract was suspended in water and partitioned with EtOAc (3 × 500 mL) to yield an EtOAc-soluble fraction (8.2 g). The EtOAc-soluble fraction was prepared as a dry load adsorbed on 25 g silica gel 60 for flash chromatography. The sample was loaded onto a self-packed silica gel 60 glass column (47 × 5 cm i.d.) and fractionated by applying a gradient of EtOAc in *n*-hexane [2% (0–10 min), 2–70% (10–420 min), 70–100% (420–480 min], followed by MeOH in EtOAc [0–20% (480–540 min), 20–100% (540–600 min)] at a flow rate of 20 mL/min. A total of 540 fractions were collected and combined based on TLC analysis into 22 fractions (F1-F22).

Further preparative purification of F15 (363 mg) by HPLC-PDA-ESIMS with a gradient of 35–70% B (see General procedures) in 30 min (ESIMS detection in positive mode at *m/z* 505–507) yielded **1** (19.0 mg, t_R 18.5 min) and **2** (4.7 mg, t_R 21.3 min). Compound **3** (9.1 mg, t_R 23.2 min) was obtained from F12 (120 mg) by preparative HPLC-PDA-ESIMS with a gradient of 15–90% B in 30 min, using ESIMS detection in positive mode at *m/z* 378–380. Compound **4** (1.8 mg, t_R 24.8 min) was isolated from fraction F13 (49.4 mg) by preparative HPLC-PDA-ESIMS using a gradient of 5–80% B in 30 min (ESIMS detection in positive mode at *m/z* 474–476). Compound **5** (9.6 mg, t_R 22.5 min) was isolated from F10 (192 mg) using preparative HPLC-PDA-ESIMS with a gradient of 5–80% B in 30 min, with ESIMS detection in positive mode at *m/z* 415–417. A second, later eluting peak (**5a**, t_R 27.6 min) was collected which yielded, however, after evaporation to dryness also **5** (10 mg). Preparative HPLC-PDA-ESIMS of F17 (79.4 mg) with a gradient from 5 to 80% B in 30 min and ESIMS detection in positive scan mode at *m/z* 402–405 afforded crude **6** (4.7 mg, t_R 20.6 min). Final purification by semi-preparative HPLC using a gradient of 5–80% B in 30 min (UV detection at 210 nm) yielded pure **6** (2.1 mg, t_R 17.7 min).

*((1′S,2R,2′R,4′S,5a'S,9a'R,10′S)–2′-Acetoxy-1′-((S)–2-acetoxy-2-(furan-3-yl)ethyl)–10′-methyl-5′-oxooctahydro-5a'H-spiro[oxirane-2,6′-[1,4]methanobenzo[d]oxepin]–5a'-yl)methyl acetate (20-Acetylauropolin, **1**).* White amorphous solid; $[\alpha]_D^{25}$ +55.0 (c 0.1, MeOH); UV (MeOH) λ_{max} (log ε) 195 (3.8), 270 (3.0) nm; ECD (MeOH, c 0.79 mM, 0.1 cm) $\Delta\varepsilon$ +3.13 (197 nm), −0.98 (214 nm), +0.54 (317 nm); ^{1}H and ^{13}C NMR data: Table 1 and Supplementary Materials Figs. S7-S12; HRESIMS *m/z* 527.1889 $[M+Na]^+$ (calcd for $C_{26}H_{32}NaO_{10}^+$, 527.1888).

*((2′R,3R,4′R,4a'R,5S,5′R,8a'S)–4′-Acetoxy-5-(furan-3-yl)–2′-methyl-2-oxooctahydro-2H-dispiro[furan-3,1′-naphthalene-5′,2′′-oxiran]–4a'(2′H)-yl)methyl acetate (6-Acetylteucjaponin A, **2**).* White amorphous solid; $[\alpha]_D^{25}$ −8.6 (c 0.06, MeOH); UV (MeOH) λ_{max} (log ε) 195 (3.9), 217 (3.6, sh), 270 (2.9) nm; ECD (MeOH, c 0.90 mM, 0.1 cm) $\Delta\varepsilon$ +2.21 (195 nm), −0.24 (254 nm); ^{1}H and ^{13}C NMR: Table 1 and Supplementary Materials Figs. S13-S18; HRESIMS *m/z* 469.1832 $[M+Na]^+$ (calcd for $C_{24}H_{30}NaO_8^+$, 469.1833).

*((1S,2R,4S,5aS,6R,9aR,10S)–2-Acetoxy-1-(2-acetoxy-2-(furan-3-yl)ethyl)–6-(chloromethyl)–6–hydroxy-10-methyl-5-oxooctahydro-1,4-methanobenzo[d]oxepin-5a(2H)-yl)methyl acetate (20-Acetylauropolin chlorohydrin, **3**).* White amorphous solid; $[\alpha]_D^{25}$ +20.0 (c 0.1, MeOH); UV (MeOH) λ_{max} (log ε) 195 (3.9), 208 (3.8, sh), 272 (2.9) nm; ECD (MeOH, c 0.74 mM, 0.1 cm) $\Delta\varepsilon$ +2.56

Table 1
^{1}H and ^{13}C NMR spectroscopic data of **1–3** ($CDCl_3$; 500 MHz for ^{1}H and 126 MHz for ^{13}C NMR; δ in ppm).

	1		**2**		**3**	
position	δ_C, type	δ_H, (J in Hz)	δ_C, type	δ_H, (J in Hz)	δ_C, type	δ_H, (J in Hz)
1	21.0, CH_2	1.70, qd (13.0, 13.0, 13.0, 4.1), (H_α) 2.17, m, (H_β)	23.0, CH_2	1.66, m, (H_α) 1.89[a], (H_β)	22.0, CH_2	1.46, qd (12.7, 12.7, 12.7, 3.6), (H_α) 2.04[a], (H_β)
2	24.5, CH_2	2.08, m, (H_α) 1.48[a], (H_β)	24.2, CH_2	2.05, m, (H_α) 1.58, m, (H_β)	22.6, CH_2	1.87, m, (H_α) 1.30, m, (H_β)
3	31.3, CH_2	2.48, m, (H_α) 1.09, dd (14.2, 4.7), (H_β)	32.7, CH_2	2.39, m, (H_α) 1.13, dt (14.1, 3.7), (H_β)	29.8, CH_2	1.69, td (15.0, 15.0, 5.0), (H_α) 2.24, dd (15.0, 4.0), (H_β)
4	62.3, C	–	61.4, C	–	76.8, C	–
4-OH	–	–	–	–	–	3.12, s
5	52.8, C	–	44.9, C	–	57.4, C	–
6	203.0, C	–	69.7, CH	5.14, t (2.1, 2.1)	208.1, C	–
7	91.0, CH	4.19, s	30.7, CH_2	2.21, m, (H_α) 1.85[a], (H_β)	90.1, CH	4.18, s
8	46.4, CH	2.02[a]	33.3, CH	1.87[a]	46.7, CH	2.03[a]
9	53.1, C	–	51.7, C	–	54.0, C	–
10	51.0, CH	2.02[a]	47.3, CH	2.25, m	46.8, CH	1.80, dd (12.7, 1.2)
11	31.1, CH_2	2.09[a] 2.28, dd (15.6, 7.6)	45.3, CH_2	2.43, dd (14.0, 8.8) 2.52, dd (14.0, 8.8)	31.2, CH_2	2.06[a] 2.32, dd (15.9, 8.2)
12	65.5, CH	5.85, dd (7.6, 4.9)	71.8, CH	5.40, t (8.8, 8.8)	65.8, CH	5.86, dd (8.2, 4.0)
13	125.1, C	–	125.1, C	–	125.6, C	–
14	108.5, CH	6.43, d (1.5)	108.0, CH	6.40, dd (1.6, 0.6)	108.7, CH	6.42, dd (1.7, 0.9)
15	143.8, CH	7.42, t (1.5, 1.5)	144.2, CH	7.45, t (1.6, 1.6)	144.3, CH	7.42, t (1.7, 1.7)
16	140.1, CH	7.44, s	139.5, CH	7.47, d (0.6)	140.3, CH	7.45, t (0.9, 0.9)
17	14.7. CH_3	1.16, d (7.0)	16.2, CH_3	1.00, d (6.7)	15.2, CH_3	1.22, d (7.0)
18	48.8, CH_2	2.38, d (5.2) 3.04, dd (5.2, 1.8)	51.6, CH_2	2.28, m 2.98, dd (5.0, 2.0)	48.3, CH_2	3.80, d (11.6) 3.92, dd (11.6, 1.8)
19	62.5, CH_2	4.82, d (11.3) 5.24, d (11.3)	62.4, CH_2	4.97, d (13.1) 5.04, d (13.1)	64.8, CH_2	4.42, d (11.3) 4.85, d (11.3)
20	97.7, CH	6.11, s	176.9, C	–	98.3	6.31, s
6-OAc-1′	–	–	169.1, C	–	–	–
6-OAc-2′	–	–	21.6, CH_3	2.10, s[a]	–	–
12-OAc-1′	170.0, C	–	–	–	170.6, C	–
12-OAc-2′	21.5, CH_3	2.05, s	–	–	21.9, CH_3	2.07,s[a]
19-OAc-1′	170.8, C	–	170.9, C	–	170.2, C	–
19-OAc-2′	20.9, CH_3	2.09, s[a]	21.1, CH_3	2.10, s[a]	21.3, CH_3	1.98, s
20-OAc-1′	169.5, C	–	–	–	169.7, C	–
20-OAc-2′	21.2, CH_3	2.10, s[a]	–	–	21.6, CH_3	2.09, s

[a] Overlapping signals.

(196 nm), −0.77 (217 nm), +0.38 (311 nm); ^{1}H and ^{13}C NMR: Table 1 and Supplementary Materials Figs. S19-S24; HRESIMS *m/z* 563.1653 $[M+Na]^+$ (calcd for $C_{26}H_{33}ClNaO_{10}^+$, 563.1654).

((1S,2R,4S,5aR,6R,9aS,10S)−2-Acetoxy-1-(2-acetoxy-2-(furan-3-yl)ethyl)−6–hydroxy-10-methyl-5-oxodecahydro-1,4-methanobenzo[d]oxepin-6-yl)methyl acetate (Teupocapin A, ***4****).* white amorphous solid; $[\alpha]_D^{25}$ +2.8 (c 0.07, MeOH); UV (MeOH) λ_{max} (log ε) 195 (3.9), 268 (3.1, sh) nm; ECD (MeOH, c 0.81 mM, 0.1 cm) $\Delta\varepsilon$ +0.08 (195 nm), −0.85 (207 nm), +0.42 (311 nm); ^{1}H and ^{13}C NMR: Table 2 and Supplementary Materials Figs. S25-S30; HRESIMS *m/z* 515.1887 $[M+Na]^+$ (calcd for $C_{25}H_{32}NaO_{10}^+$, 515.1888).

(5aR,6S,7R,9S,10S)−6-(2-Acetoxy-2-(furan-3-yl)ethyl)−9a–hydroxy-10-methyl-3,4,5,5a,6,7,9,9a-octahydro-2H-6,9-methanooxepino[3,4,5-cd]isobenzofuran-7-yl acetate (Teupocapin B, ***5****).* Slightly yellow amorphous solid; $[\alpha]_D^{25}$ +58.0 (c 0.1, MeOH); UV (MeOH) λ_{max} (log ε) 195 (4.0), 240 (3.4, sh), nm; ECD (MeOH, c 0.77 mM, 0.1 cm) $\Delta\varepsilon$ +9.46 (201 nm); ^{1}H and ^{13}C NMR: Table 2 and Supplementary Materials Figs. S31-S36; HRESIMS *m/z* 455.1676 $[M+Na]^+$ (calcd for $C_{23}H_{28}NaO_8^+$, 455.1676).

2-((3R,5S,5aS,7aR,11R,11aS,12S,13S)−5a,7a-Dihydroxy-13-methyloctahydro-1H-3,11,5-(epiethane[1,1,2]triyl)[1,3]dioxepino[5,6-c]isobenzofuran-12-yl)−1-(furan-3-yl)ethyl acetate (Teupocapin C, ***6****).* White amorphous solid; $[\alpha]_D^{25}$ −22.0 (c 0.1, MeOH); UV (MeOH) λ_{max} (log ε) 195 (3.8), 215 (3.5, sh) nm; ECD (MeOH, c 0.95 mM, 0.1 cm) $\Delta\varepsilon$ −0.97 (198 nm), +0.01 (218 nm), −0.33 (241 nm); ^{1}H and ^{13}C NMR: Table 2 and Supplementary Materials Figs. S37-S42; HRESIMS *m/z* 443.1675 $[M+Na]^+$ (weak, calcd for $C_{22}H_{28}NaO_8^+$, 443.1676), 403.1758 $[M+H-H_2O]^+$ (calcd for $C_{22}H_{27}O_7^+$, 403.1757).

2.4. Single-crystal X-ray crystallographic analysis of ***1***

X-ray diffraction data were collected on a Stoe StadiVari diffractometer (STOE & Cie GmbH, Darmstadt, Germany) equipped with an Oxford Cryosystems low-temperature device operating at T = 150 K (OxfordCryosystems, Oxford, United Kingdom). Data were measured using rotation method, ω scans using a metaljet source with GaK_α radiation (λ = 1.34143 Å).

Single colorless block-shaped crystals of **1** were recrystallized from a mixture of EtOAc and *i*-PrOH by solvent layering. A suitable crystal 0.13 × 0.09 × 0.06 mm was selected and the crystal was mounted on a mylar loop in perfluoroether oil. The crystal was kept at a steady T = 150 K during data collection. The structure was solved with the ShelXT [18,19] structure solution program using the Intrinsic Phasing solution method and by using Olex2 [20] as the graphical interface. The model was refined with version 2018/3 of ShelXL [18,19] using Least Squares minimization.

Crystallographic data for the structure of 20-acetylauropolin (**1**) were deposited at the Cambridge Crystallographic Data center (CCDC) as supplementary crystallographic data with number CCDC 2,236,028.

20-Acetylauropolin (**1**): $C_{26}H_{32}O_{10}$, M_r = 504.51, orthorhombic, $P2_12_12$ (No. 18), a = 17.3203(7) Å, b = 17.4805(9) Å, c = 8.3553(3) Å, $\alpha = \beta = \gamma$ = 90°, V = 2529.71(19) Å^3, T = 150 K, Z = 4, Z' = 1, $\mu(GaK_\alpha)$ = 0.547, 52,085 reflections measured, 5209 unique (R_{int} = 0.1141) which were used in all calculations. The final wR_2 was 0.1418 (all data) and R_1 was 0.0557 ($I > 2(I)$). The Flack parameter was refined to 0.02(12). Additional information is available in Supplementary Materials.

Table 2
^{1}H and ^{13}C NMR spectroscopic data of **4–6** ($CDCl_3$; 500 MHz for ^{1}H and 126 MHz for ^{13}C NMR; δ in ppm).

	4		5		6	
position	δ_C, type	δ_H, (J in Hz)	δ_C, type	δ_H, (J in Hz)	δ_C, type	δ_H, (J in Hz)
1	22.4, CH_2	1.37[a] (H_α) 1.89[a], (H_β)	24.0, CH_2	1.31, m, (H_α) 2.28, m, (H_β)	22.8, CH_2	1.44[a], (H_α) 1.98[a], (H_β)
2	28.1, CH_2	2.25[a], (H_α) 1.36[a], (H_β)	22.1, CH_2	2.00[a], (H_α) 1.55, m, (H_β)	24.7, CH_2	1.95[a], (H_α) 1.22, m, (H_β)
3	35.0, CH_2	1.94, m, (H_α) 1.39[a], (H_β)	22.2, CH_2	2.09[a], (H_α, H_β)	29.5, CH_2	1.63, m, (H_α) 1.91[a], (H_β)
4	73.4, C	–	140.4, C	–	80.3, C	–
4-OH	–	2.63, s	–	–	–	3.69, s
5	55.3, CH	2.79, d (11.9)	132.2, C	–	51.4, C	–
6	208.8, C	–	108.7, C	–	109.1, C	–
6-OH	–	–	–	n.d.	–	3.95, s
7	89.2, CH	4.08, s	86.8, CH	4.05, s	86.5, CH	3.81, s
8	44.7, CH	2.13[a]	41.4, CH	2.57[a]	46.4, CH	2.26, q (7.0, 7.0, 7.0)
9	52.9, C	–	53.2, C	–	49.4, C	–
10	43.4, CH	1.86[a]	37.9, CH	2.54[a]	45.5, CH	1.44[a]
11	31.0, CH_2	2.05, dd (15.9, 3.4) 2.29, dd (15.9, 8.9)	30.9, CH_2	1.94, dd (15.4, 3.1) 2.10[a]	34.7, CH_2	1.82, dd (15.5, 3.1) 2.46, dd (15.5, 10.1)
12	66.2, CH	5.91, dd (8.9, 3.4)	66.4, CH	5.93, dd (8.5, 3.1)	66.3, CH	6.01, dd (10.1, 3.1)
13	125.2, C	–	125.8, C	–	125.9, C	–
14	108.8, CH	6.43, dd (1.5, 0.9)	108.6, CH	6.42, dd (1.5, 0.9)	108.9, CH	6.41, dd (1.8, 0.9)
15	144.0, CH	7.41, t (1.5, 1.5)	143.6, CH	7.39, t (1.5, 1.5)	143.8, CH	7.39, t (1.8, 1.8)
16	140.4, CH	7.49, t (0.9, 0.9)	140.1, CH	7.47, t (0.9, 0.9)	140.5, CH	7.46, t (0.9, 0.9)
17	14.8, CH_3	1.18, d (7.0)	14.6, CH_3	1.10, d (7.0)	15.0, CH_3	1.01, d (7.0)
18	64.5, CH_2	4.25, d (11.9) 4.50, d (11.9)	75.4, CH_2	4.49, dd (13.1, 3.3) 4.73, dd (13.1, 3.3)	79.2, CH_2	4.14, d (10,1) 4.31, d (10,1)
19	–	– –	–	– –	59.0, CH_2	3.91, d (11.3) 4.11, d (11.3)
20	98.2, CH	6.21, s	98.9, CH	5.87, s	106.8, CH	5.18, s
12-OAc-1′	170.4, C	–	170.1, C	–	170.2, C	–
12-OAc-2′	21.6, CH_3[a]	2.09, s[a]	21.3, CH_3	2.03, s[a]	21.7, CH_3	2.03, s
18-OAc-1′	171.6, C	–	–	–	–	–
18-OAc-2′	21.3, CH_3	2.09, s[a]	–	–	–	–
20-OAc-1′	170.1, C	–	169.9, C	–	–	–
20-OAc-2′	21.6, CH_3[a]	2.11, s[a]	21.4, CH_3	2.04, s[a]	–	–

[a] Overlapping signals, n.d. not detected.

3. Results and discussion

HPLC-PDA-ESIMS analysis of the MeOH extract of *T. polium* subsp. *capitatum* L. revealed, besides the previously reported flavonoids and caffeic acid derivatives [2], the presence of a series of compounds that strongly ionized in the positive ESIMS mode but did not show any signals in the UV (254 nm) trace (Fig. 1). Their MS data in conjunction with chemotaxonomic information suggested that these compounds were diterpenes.

Targeted isolation of the corresponding peaks afforded six neo-clerodane type diterpenes (Fig. 2), including four previously undescribed compounds (**3**–**6**). Compound **1** was identified as 20-acetylauropolin. This compound has been reported as an acetylation product of auropolin, which has previously been isolated from several *T. polium* subspecies and *T. asiaticum*, but has never been directly isolated from plant material [12,21,22]. Optical rotation and NMR data of **1** were identical to those described in literature [21,22]. The absolute configuration of **1** was determined by X ray diffraction analysis (Fig. 3 and Supplementary Materials).

Compound **2** was identified as 6-acetylteucjaponin A based on NMR analysis and comparison with literature data (Supporting Material Fig. S19). It was originally obtained by acetylation of teucjaponin A and later isolated from *T. polium* [23–25]. The structures of the previously undescribed neo-clerodanes **3**–**6** were established by extensive 1D and 2D NMR analysis and by comparison with the NMR data recorded for **1**.

Compound **3** had a molecular formula of $C_{26}H_{33}ClO_{10}$ deduced from the sodium adduct ion peak in HRESIMS at *m/z* 563.1653 (calcd for $C_{26}H_{33}ClNaO_{10}^{+}$, 563.1654). The presence of a chlorine atom was confirmed by the isotopic pattern. Comparison of the NMR data of compounds **1** and **3** revealed that ^{1}H and ^{13}C NMR chemical shifts and coupling constants of both compounds were very similar. The main difference was observed for C-4, which was more downfield shifted in **3** (δ_C 76.8) compared to **1** (δ_C 62.3). Additionally, while the ^{13}C NMR chemical shifts for C-18 were very similar in both compounds (δ_C 48.8 in **1** *vs* δ_C 48.3 in **3**) a clear difference was observed in the H-18 chemical shifts [δ_H 2.38 (*d*, J = 5.2 Hz, H_a-18) and δ_H 3.04 (*dd*, J = 5.2, 1.8 Hz, H_b-18) in **1**, and δ_H 3.80 (*d*, J = 11.6 Hz, H_a-18) and δ_H 3.92 (*dd*, J = 11.6, 1.8 Hz, H_b-18) in **3**]. The H-18 proton signals in **1** displayed the typical chemical shifts and coupling constants for a α,α-disubstituted oxirane ring system [21,26]. This pattern was not found in **3**, thereby indicating a different substitution at C-4. ^{1}H and ^{13}C NMR shifts were in full agreement with the replacement of the oxirane ring in **1** by a chlorohydrin in **3** (Table 1 and Supplementary Materials). The presence of the hydroxyl group at C-4 of the chlorohydrin could be clearly confirmed by ^{2}J, ^{3}J, and ^{4}J HMBC correlations between the hydroxyl proton (δ_H 3.12, *s*) and C-2 (δ_C 22.6), C-3 (δ_C 29.8), C-4 (δ_C 76.8), and C-5 (δ_C 57.4) (Fig. 4). Chlorinated neo-clerodane diterpenes have already been reported several times and were either described as artifacts resulting from the use of chlorinated solvents in the isolation procedure, or as naturally occurring compounds [26–33]. Indeed, the chlorohydrin **3** was detected by HPLC-ESIMS analysis in the crude methanolic extract, which was obtained by Soxhlet extraction. However, in a freshly prepared methanolic extract obtained by maceration of the same dried plant material the chlorohydrin was only detected in minute amounts (data not shown). Although no chlorinated chemicals were used in the isolation procedure, we assume that the chlorohydrin **3** is likely to be an artifact formed by the opening of the oxirane in **1**,

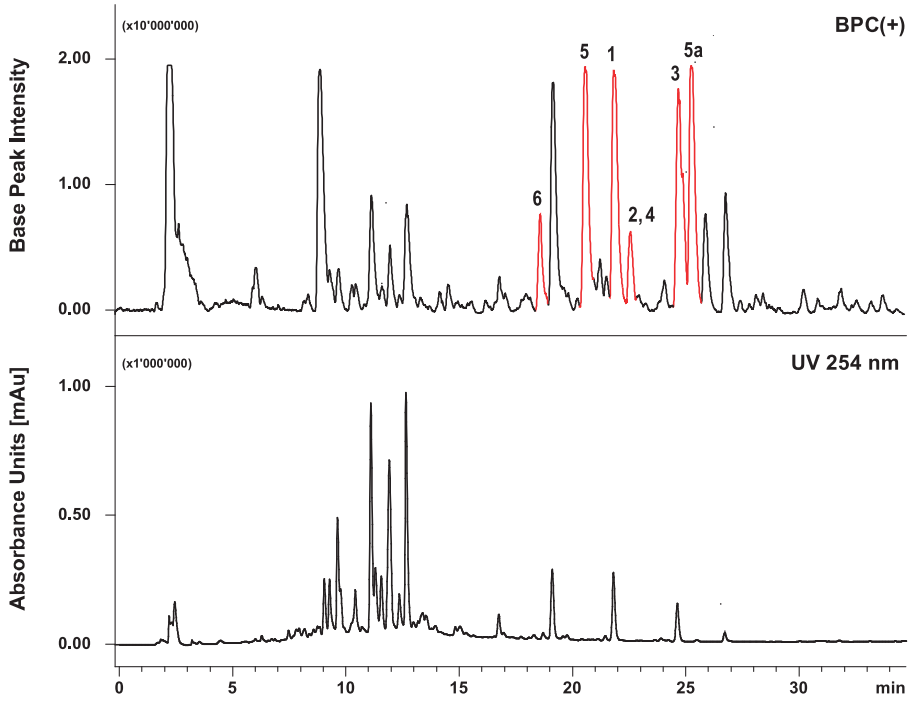

Fig. 1. HPLC profile of the methanolic *T. polium* subsp. *capitatum* extract. The profile was obtained on a SunFire C18 column (3.5 µm, 150 × 3 mm i.d) applying a gradient of 5–80% MeCN in water containing 0.1% formic acid in 30 min at a flow rate of 0.4 mL/min. The upper trace shows the base peak chromatogram (BPC) recorded with ESIMS in positive mode. The lower trace shows the PDA chromatogram at 254 nm. Peak numbers refer to neo-clerodane diterpenes **1–6**. The black peaks correspond to polyphenolic compounds [2].

probably due to the presence of traces of chlorinated contaminants in the solvent used for Soxhlet extraction. Such oxirane opening reactions in the presence of traces of chloroform and/or hydrochloric acid have been reported in 4α,18-epoxy-neo-clerodanes from *Teucrium* species and in epoxy-sesquiterpene lactones from *Centaurea solstitialis* [34,35].

Compound **4** had a molecular formula of $C_{25}H_{32}O_{10}$ (HRESIMS *m/z* 515.1887 $[M+Na]^+$; calcd for $C_{25}H_{32}NaO_{10}^+$, 515.1888). As in **1**–**3**, the NMR data of **4** showed ^1H and ^{13}C NMR resonances of a β-substituted furan ring [(δ_H 6.43, *dd*, J = 1.5, 0.9 Hz, H-14; δ_H 7.41, *t*, J = 1.5, 1.5 Hz, H-15; δ_H 6.49, *t*, J = 0.9, 0.9 Hz H-16), (δ_C 125.2 (C-13), 108.8 (C-14), 144.0 (C-15), 140.4 (C-16))]. The furan ring was linked to an acetoxylated methine (δ_H 5.91 *dd*, J = 8.9, 3.4 Hz, H-12; δ_C 66.2, C-12) further connected via a methylene carbon to C-9 (δ_C 52.9) of the decalin core. The one-proton singlet at δ_H 6.21 (H-20) could be assigned to an acetal function containing an acetoxy group (δ_C 98.2) without vicinally connected protons. The ring closure of this acetal function was corroborated by a ^2J HMBC correlation between H-20 and C-9, and a ^3J HMBC correlation from H-20 to C-7 (δ_C 89.2). Compared to the spectra of compounds **1**–**3** differences were observed at positions C-4 (δ_C 73.4) and C-5 (δ_C 55.3). The ^{13}C NMR chemical shift of C-4 (δ_C 73.4) indicated the presence of a hydroxyl group at this position. Furthermore, ^2J HMBC correlations between the methylene H-18 protons (δ_H 4.25, *d*, J = 11.9 Hz, H_a-18; δ_H 4.50, *d*, J = 11.9 Hz, H_b-18) and C-4, in conjunction with ^3J HMBC correlations from these protons to the acetyl carbonyl at δ_C 171.6, suggested an acetoxymethylene group attached to C-4. The relative configuration at C-4 was indicated by a ROESY correlation between the methylene protons H_2–18 and H_β–10 (δ_H 1.86). HSQC correlations from C-5 (δ_C 55.3) to H-5 (δ_H 2.79, *d*, J = 11.9 Hz), and ^1H,^1H-COSY correlations of H-5 to H-10 revealed C-5 as a sp^3 methine group with the proton in axial orientation. Compound **4** was thus a 19-nor-neo-clerodane diterpene (Fig. 5). The presence of a hydroxyl group together with an acetoxymethylene group at C-4 is quite rare in neo-clerodane diterpenes and has been described so far only in picropolinol from *T. polium* subsp. *capitatum,* in alysin B and its 3-deacetyl derivative identified in *T. alyssifolium*, and in a neo-clerodane diterpene found in *Ajuga decumbens* [33,36,37]. Compound **4** was named teupocapin A in reference to the name of the species and subspecies.

Compound **5** had a molecular formula of $C_{23}H_{28}O_8$ (HRESIMS *m/z* 455.1676 $[M+Na]^+$; calcd for $C_{23}H_{28}NaO_8^+$, 455.1676). The ^1H and ^{13}C NMR spectra of **5** showed also the typical pattern of a β-substituted furan ring [(δ_H 6.42, *dd*, J = 1.5, 0.9 Hz, H-14; δ_H 7.39, *t*, J = 1.5, 1.5 Hz, H-15; δ_H 7.47, *t*, J = 0.9, 0.9 Hz, H-16), (δ_C 125.8 (C-13), 108.6 (C-14), 143.6 (C-15), 140.1 (C-16))]. As for **1, 3**, and **4,** ^3J HMBC correlations from H-12 (δ_H 5.93 (*dd*, J = 8.5, 3.1 Hz) to C-14 and C-16 revealed that the furan ring was linked to an acetoxylated methine group at C-12 (δ_C 66.4) further connected to C-9 (δ_C 53.2) of the decalin moiety via a methylene group. Furthermore, the cyclic acetoxylated acetal function at C-20 was also present in **5**, as indicated by a ^2J HMBC correlation between H-20 (δ_H 5.87, *s*) and C-9, and a ^3J HMBC correlation from H-7 (δ_H 4.05, *s*) to C-20 (δ_C 98.9). Compared to the neo-clerodane diterpenes **1**–**4**, the resonances of C-4 (δ_C 140.4) and C-5 (δ_C 132.2) were observed at lower field. Diterpene **5** thus had a double bond at this position and consequently a 19-nor-neo-clerodane diterpene scaffold. Furthermore, the NMR data revealed the presence of an allylic hemiketal function ranging from C-4 (δ_C 140.4) to C-6 (δ_C 108.7) with cyclization via the C-18 methylene group [(δ_H 4.49 (*dd*, J = 13.1, 3.3 Hz, H_a-18); δ_H 4.73 (*dd*, J = 13.1, 3.3 Hz, H_b-18); (δ_C 75.4)]. The partial structure was supported by ^2J and ^3J HMBC correlations (Fig. 7). Such a hemiketal has so far only been reported from the chemical transformation of eriocephalin into a series of 19-nor-neo-clerodane derivatives [38]. Initially, two well separated peaks (**5** and **5a**) were collected after preparative HPLC separation of fraction F10 from the initial fractionation on a silica gel column. However, after evaporation to dryness, both peaks afforded the same compound **5** as confirmed by HPLC and NMR analysis. We hypothesize that the acidic mobile phase used during isolation

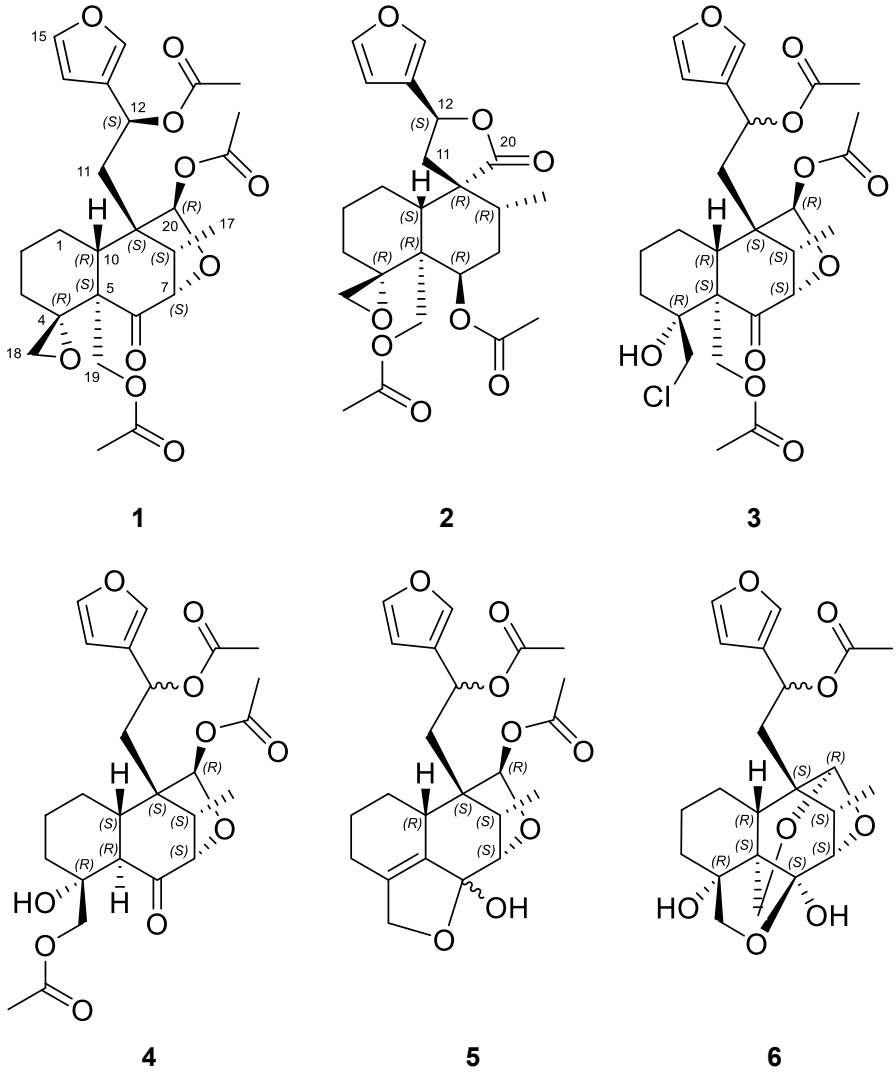

Fig. 2. Structures of neo-clerodane diterpenes **1–6**.

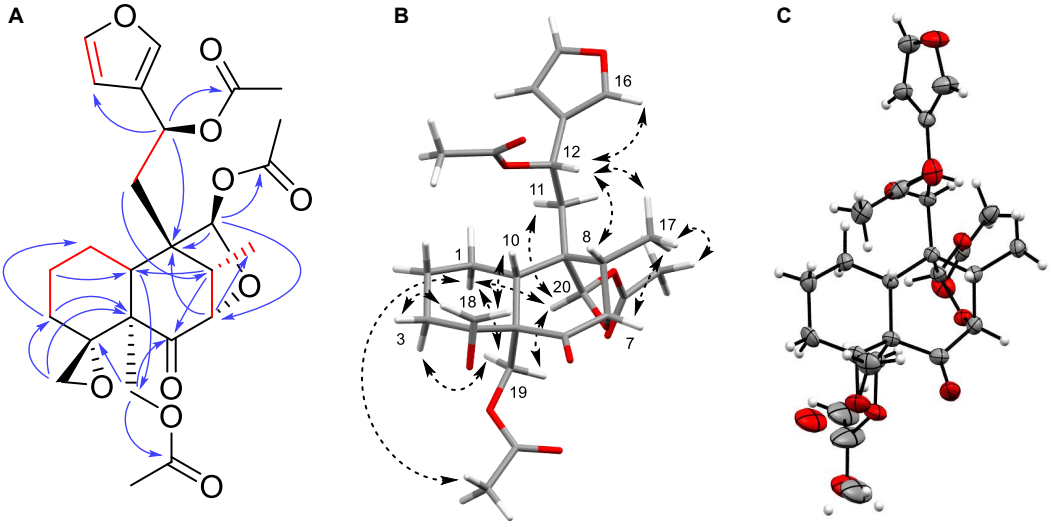

Fig. 3. (A) COSY (red) and key HMBC correlations (blue arrows), (B) key ROESY correlations (black dotted arrows), and (C) ORTEP drawing obtained by single crystal X-ray diffraction (ellipsoids at 50% probability) of **1**.

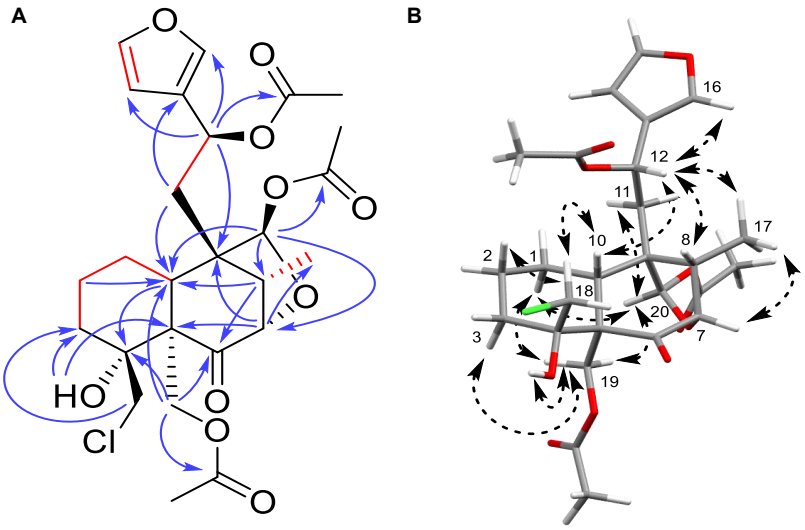

Fig. 4. (A) COSY (red) and key HMBC correlations (blue arrows), (B) key ROESY correlations of **3** (structure depicted as (12*S*) isomer).

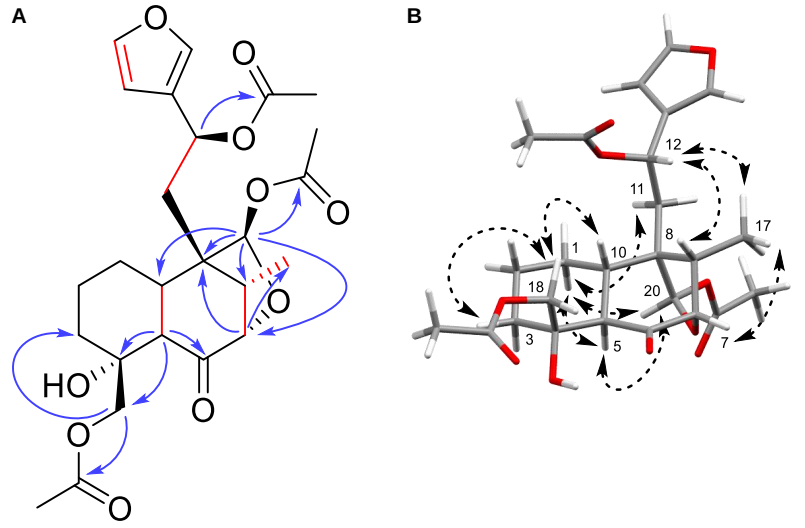

Fig. 5. (A) COSY (red) and key HMBC correlations (blue arrows), (B) key ROESY correlations of **4** (structure depicted as (12*S*) isomer).

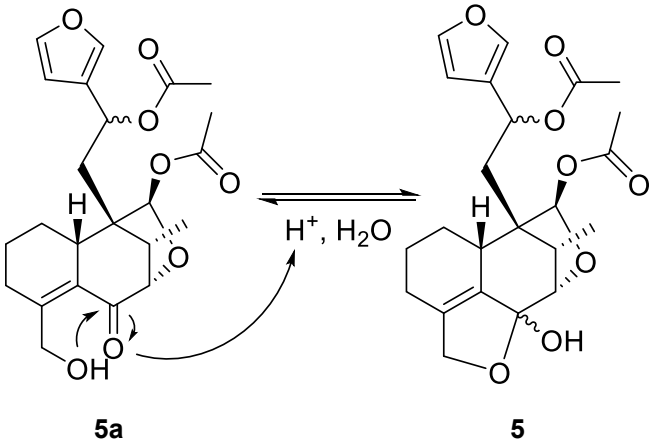

Fig. 6. Putative formation of **5** from **5a** under the acidic conditions used during isolation.

catalyzed an intramolecular hemiketal formation by reaction of the hydroxyl group at position C-18 with the carbonyl group at C-6 in **5a** to form **5** (Fig. 6). The structure of **5** was named as teupocapin B.

Compound **6** had a molecular formula of $C_{22}H_{28}O_8$ as revealed by a minor HRESIMS peak at *m/z* 443.1675 $[M+Na]^+$ (calcd for $C_{22}H_{28}NaO_8^+$, 443.1676) and further supported by an intense fragment ion peak at *m/z* 403.1758 ($[M+H-H_2O]^+$; calcd for $C_{22}H_{27}O_7^+$, 403.1757). Compound **6** also showed the chemical shifts for a β-substituted furan ring attached at the C-12 acetoxylated methine group [(δ_H 6.01, *dd*, *J* = 10.1, 3.1 Hz, H-12); (δ_C 66.3 (C-12)] and the C-11 methylene group [(δ_H 1.82, *dd*, *J* = 15.5, 3.1 Hz, H_a-11 and δ_H 2.46, *dd*, *J* = 15.5, 10.1 Hz, H_b-11); (δ_C 34.7 (C-11))] connected to C-9 (δ_C 49.4) of the decalin core structure. In addition, **6** also contained an acetal function at C-20 (δ_C 106.8), with a ring closure to C-7, as revealed by the ^3J HMBC correlation from H-20 (δ_H 5.18, *s*) to C-7 (δ_C 86.5) (Fig. 8). However, in contrast to the neo-clerodane diterpenes **1** and **3**–**5**, the C-20 acetal function did not include an acetoxyl group, but showed a further ring closure to C-19 (δ_C 59.0). The linkage was corroborated by ^3J HMBC correlations from the C-19 oxo-methylene protons (δ_H 3.91, *d*, *J* = 11.3 Hz, H_a-19 and δ_H 4.11, *d*, *J* = 11.3 Hz, H_b-11) to C-20 (δ_C 106.8), C-4 (δ_C 80.3), C-5 (δ_C 51.4), C-6 (δ_C 109.1), and C-10 (δ_C 45.5). Such a C-20/C-19 and C-20/C-7 bridged acetal function

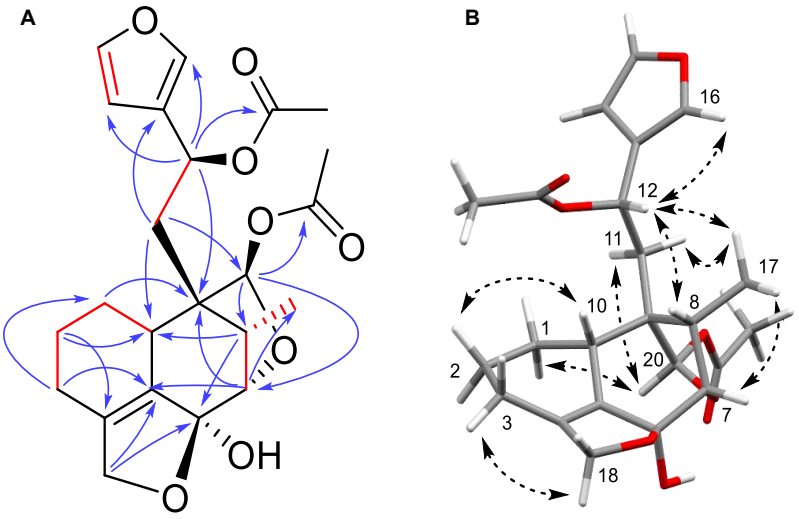

Fig. 7. (A) COSY (red) and key HMBC correlations (blue arrows), (B) key ROESY correlations of **5** (structure depicted as (6*S*,12*S*) isomer).

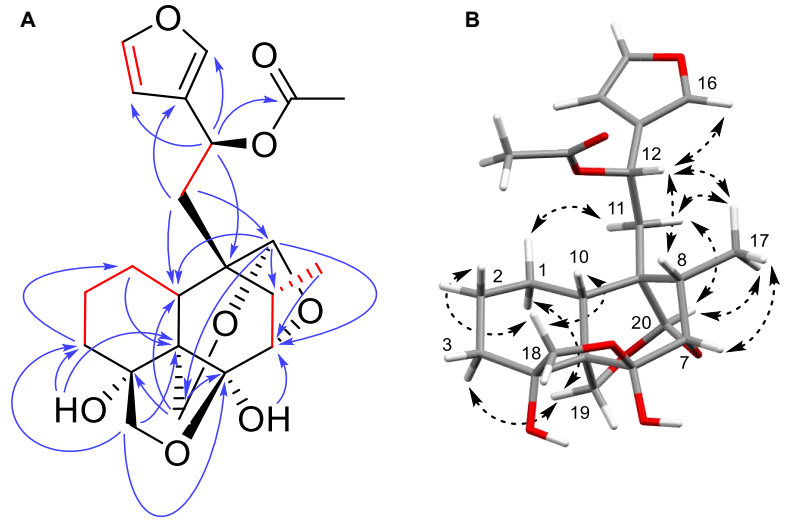

Fig. 8. (A) COSY (red) and key HMBC correlations (blue arrows), (B) key ROESY correlations of **6** (structure depicted as (12*S*) isomer).

is a rare structural feature in neo-clerodane diterpenes and has so far only been described in a diterpene isolated from *Salvia minata* [39]. As in compound **5**, ^{2}J and ^{3}J HMBC correlations in **6** revealed a hemiketalic ring closure from C-6 (δ_C 109.1) to C-4 (δ_C 80.3) via the C-18 methylene group [(δ_H 4.14, *d*, J = 10.1 Hz, H_a-18 and δ_H 4.31, *d*, J = 10.1, H_b-18); (δ_C 79.2 (C-18))]. The relative configuration at C-4 was established by a ROESY cross-peak between the methylene proton H_b-18 and H_β−10 (δ_H 1.44). The same structural feature with an oxolane ring and a tertiary hydroxy group at C-4 has been found in teulanigerin, teupolin V, teugnaphalodin and its derivatives, and teulepicephin [40–44]. Compound **6** was named as teupocapin C.

Except compound **2**, all isolated neo-clerodanes contain a rarely occurring axial oxy-function at C-7 that forms a hemiacetalic bridge to C-20 [12,45]. Compound **2** possesses instead a five-membered lactone ring connecting C-20 to C-12, a structural feature that is very often found in neo-clerodane diterpenes from *Teucrium* species [7–9,45].

The absolute configuration of compounds **2**–**6** could not be ascertained from the data above. Attempts at obtaining crystals suitable for single X-ray diffraction analysis were not successful. However, clerodane diterpenes found in the genus *Teucrium* so far all belonged to the neo-clerodane series [6,7,45]. Additionally, given that the absolute configuration of **1** could be established by X-ray crystallographic analysis it can be reasonably assumed that diterpenes **2**–**6** are also neo-clerodanes.

The vast majority of neo-clerodane diterpenes from *Teucrium* has been shown to possess the *S* configuration at C-12 [7,46]. Since the crystal structure of **1** revealed the *S*-configuration at C-12, it is likely that diterpenes **2**–**6** possess the same configuration at this position. Moreover, a method based on NOESY spectroscopy in combination with molecular mechanics calculations of different conformers has been developed by Jiménez-Barbero for establishing the absolute configuration at C-12 in neo-clerodanes bearing a furanyl ethyl side chain with a hydroxyl or acetoxyl substituent at C-12, as found in **1** and in **3**–**6** [47]. Thus, an *S* configuration at C-12 leads to conformers in which H-12 shows strong NOE signals with H-8 and H-17, while NOE cross-peaks with H_β−1 and H-10 are weak or not detectable. An *R* configuration at C-12, in contrast, leads to strong NOESY cross-peaks of H-12 with H_β−1 and H-10, while signals with H-8 and H-17 are rather weak or absent. In the ROESY spectrum of **1**, a strong cross-peak was detected between H-12 and H-17, and between H-12 and H-8, while the signal with H_β−1 was much weaker, in accord with the *S* configuration established by X-ray diffraction analysis. ROESY cross-peak intensities observed in **3**–**6** were similar to those detected in **1,** thereby

supporting the *S* configuration at C-12 in these compounds. However, confirmation by X-ray diffraction analysis will be needed for a definitive configurational assignment. As for neo-clerodanes containing a lactone ring, the absence of an NOE cross-peak between H-12 and H-17 has been found indicative of the *S* configuration at C-12, since H-12 is located on the other face of the plane which is spanned by the C-12/C-20 lactone [7,48,49]. This was also the case for compound **2**, confirming the *S* configuration at C-12.

4. Conclusion

The genus *Teucrium* is a rich source of neo-clerodane diterpenoids, and the occurrence of this type of compounds is considered as a chemotaxonomic marker [8]. Even though the phytochemistry of *Teucrium* species has been extensively investigated it was shown in several studies that the composition in neo-clerodane diterpenes can significantly vary depending on geographic origin and environmental conditions [6–10]. This is confirmed by the present study given that most diterpenes detected in the methanolic extract of *T. polium* subsp. *capitatum* collected in Algeria were previously undescribed compounds, while 20-acetylauropolin was known up to now only as a natural product derivative. X ray crystallographic data of 20-acetylauropolin support the validity of a previously reported method based on molecular mechanic calculations and NOESY correlations for the determination of the absolute configuration at C-12 in neo-clerodanes bearing a furanyl ethyl side chain. Taken together, the compounds described here extend the structural diversity of neo-clerodane diterpenoids, as they combine common structural characteristics with features that are rare in naturally occurring neo-clerodanes.

Declaration of Competing Interest

The authors declare the following financial interests/personal relationships which may be considered as potential competing interests:

Matthias Hamburger reports financial support, administrative support, article publishing charges, and equipment, drugs, or supplies were provided by University of Basel, Department of Pharmaceutical Sciences. Amel Boudjelal reports financial support, administrative support, equipment, drugs, or supplies, and travel were provided by Algerian Ministry of Higher Education and Scientific Research.

CRediT authorship contribution statement

Morris Keller: Methodology, Software, Validation, Formal analysis, Investigation, Resources, Data curation, Writing – original draft, Writing – review & editing, Visualization. **Sarra Chabane:** Methodology, Software, Validation, Formal analysis, Investigation, Resources, Data curation, Writing – review & editing. **Amel Boudjelal:** Conceptualization, Methodology, Validation, Resources, Writing – review & editing, Project administration. **Ombeline Danton:** Methodology, Software, Validation, Formal analysis, Investigation, Resources, Data curation, Writing – review & editing, Visualization. **Alessandro Prescimone:** Methodology, Software, Validation, Formal analysis, Investigation, Resources, Data curation, Writing – review & editing, Visualization. **Matthias Hamburger:** Resources, Writing – review & editing, Funding acquisition. **Olivier Potterat:** Conceptualization, Methodology, Software, Validation, Formal analysis, Investigation, Resources, Data curation, Writing – review & editing, Supervision, Project administration.

Data availability statement

The datasets generated for this study are available on request.

Funding

This work was supported by the Algerian Ministry of Higher Education and Scientific Research through the PRFU (D01N01UN280120200002).

Acknowledgements

Thanks are due to Dr. Sarri Dj. (botanist at Department SNV/M'Sila, Mohamed Boudiaf University, M'Sila) for the taxonomic identification of the plant material. ECD spectra were measured at the Biophysics Facility, Biocenter, University of Basel. We thank also Mr. Merzok Yahia for the picture of *Teucrium polium* included in the graphical abstract.

Supplementary materials

Supplementary material associated with this article can be found, in the online version, at doi:10.1016/j.molstruc.2023.135447.

References

[1] M.S. Stanković, N.M. Zlatić, Ethnobotany of *Teucrium* species, in: J.L. Martinez, A. Muñoz-Acevedo, M. Rai (Eds.), Ethnobotany, 1st ed., CRC Press, Boca Raton, FL, 2019, pp. 214–231, doi:10.1201/9780429424069-11.
[2] S. Chabane, A. Boudjelal, M. Keller, S. Doubakh, O. Potterat, *Teucrium polium* - wound healing potential, toxicity and polyphenolic profile, South Afr. J. Bot. 137 (2021) 228–235, doi:10.1016/j.sajb.2020.10.017.
[3] A. Boudjelal, C. Henchiri, M. Sari, D. Sarri, N. Hendel, A. Benkhaled, G. Ruberto, Herbalists and wild medicinal plants in M'Sila (North Algeria): an ethnopharmacology survey, J. Ethnopharmacol. 148 (2013) 395–402, doi:10.1016/j.jep.2013.03.082.
[4] F.O. Abdullah, F.H.S. Hussain, A.S. Sardar, G. Gilardoni, Z.M. Thu, G. Vidari, Bio-active compounds from *Teucrium* plants used in the traditional medicine of Kurdistan region, Iraq, Molecules 27 (2022) 3116, doi:10.3390/molecules27103116.
[5] A.S. Tepe, M. Ozaslan, I.H. Kilic, S.B. Oguzkan, A. History, Traditional uses, phytochemistry, and toxic potential of *Teucrium polium* L.: a comprehensive review, Int. J. Plant Based Pharm. 1 (2021) 1–41.
[6] F. Piozzi, The diterpenoids of *Teucrium* species, Heterocycles 15 (1981) 1489–1503, doi:10.3987/s-1981-02-1489.
[7] F. Piozzi, B. Rodriguez, G. Savona, Advances in the chemistry of the furanoditerpenoids from *Teucrium* species, Heterocycles 25 (1987) 807–841, doi:10.3987/s-1987-01-0807.
[8] F. Piozzi, Further researches on the furoclerodanes from *Teucrium* species, Heterocycles 37 (1994) 603–626, doi:10.3987/REV-93-SR3.
[9] F. Piozzi, M. Bruno, S. Rosselli, Further furoclerodanes from *Teucrium* genus, Heterocycles 48 (1998) 2185–2203, doi:10.3987/REV-98-503.
[10] F. Piozzi, M. Bruno, S. Rosselli, A. Maggio, Advances on the chemistry of furanoditerpenoids from *Teucrium* genus, Heterocycles 65 (2005) 1221–1234, doi:10.3987/REV-04-593.
[11] E.A. Klein Gebbinck, B.J.M. Jansen, A. de Groot, Insect antifeedant activity of clerodane diterpenes and related model compounds, Phytochemistry 61 (2002) 737–770, doi:10.1016/S0031-9422(02)00174-7.
[12] M. Bruno, A.M. Maggio, F. Piozzi, S. Puech, S. Rosselli, M.S.J. Simmonds, Neoclerodane diterpenoids from *Teucrium polium* subsp. *polium* and their antifeedant activity, Biochem. Syst. Ecol. 31 (2003) 1051–1056, doi:10.1016/S0305-1978(03)00042-5.
[13] E. Mazokopakis, S. Lazaridou, M. Tzardi, J. Mixaki, I. Diamantis, E. Ganotakis, Acute cholestatic hepatitis caused by *Teucrium polium* L., Phytomedicine 11 (2004) 83–84, doi:10.1078/0944-7113-00337.
[14] I. Starakis, D. Siagris, L. Leonidou, E. Mazokopakis, A. Tsamandas, C. Karatza, Hepatitis caused by the herbal remedy *Teucrium polium* L., Eur., J. Gastroenterol. Hepatol. 18 (2006) 681–683, doi:10.1097/00042737-200606000-00016.
[15] A. Fiorentino, B. D'Abrosca, S. Pacifico, M. Scognamiglio, G. D'Angelo, M. Gallicchio, A. Chambery, P. Monaco, Structure elucidation and hepatotoxicity evaluation against HepG2 human cells of neo-clerodane diterpenes from *Teucrium polium* L., Phytochemistry 72 (2011) 2037–2044, doi:10.1016/j.phytochem.2011.07.006.
[16] S. Pacifico, B. D'Abrosca, M. Scognamiglio, G. D'Angelo, M. Gallicchio, S. Galasso, P. Monaco, A. Fiorentino, NMR-based metabolic profiling and in vitro antioxidant and hepatotoxic assessment of partially purified fractions from golden germander (*Teucrium polium* L.) methanolic extract, Food Chem. 135 (2012) 1957–1967, doi:10.1016/j.foodchem.2012.06.071.
[17] M. Nur-e-Alam, I. Parveen, B. Wilkinson, S. Ahmed, R.M. Hafizur, A. Bari, T.J. Woodman, M.D. Threadgill, A.J. Al-Rehaily, A neoclerodane orthoester and other new neoclerodane diterpenoids from *Teucrium yemense* chemistry and effect on secretion of insulin, Sci. Rep. 11 (2021) 1–17, doi:10.1038/s41598-021-87513-3.

[18] G.M. Sheldrick, Crystal structure refinement with SHELXL, Acta Crystallogr. Sect. C C71 (2015) 3–8, doi:10.1107/S2053229614024218.
[19] G.M. Sheldrick, SHELXT - integrated space-group and crystal-structure determination, Acta Crystallogr. Sect. A A71 (2015) 3–8, doi:10.1107/S2053273314026370.
[20] O.V. Dolomanov, L.J. Bourhis, R.J. Gildea, J.A.K. Howard, H. Puschmann, OLEX2: a complete structure solution, refinement and analysis program, J. Appl. Crystallogr. 42 (2009) 339–341, doi:10.1107/S0021889808042726.
[21] L. Eguren, A. Perales, J. Fayos, G. Savona, M. Paternostro, F. Piozzi, B. Rodriguez, New clerodane diterpenoid from *Teucrium polium* subsp. *aureum*. X-ray structure determination, J. Org. Chem. 46 (1981) 3364–3367, doi:10.1021/jo00329a053.
[22] F. Camps, J. Coll, O. Dargallo, J. Rius, C. Miravitlles, Clerodane diterpenoids from *Teucrium* and *Ajuga* plants, Phytochemistry 26 (1987) 1475–1479, doi:10.1016/S0031-9422(00)81838-5.
[23] T. Miyase, H. Kawasaki, T. Noro, A. Ueno, S. Fukushima, T. Takemoto, Studies on the furanoid diterpenes from *Teucrium japonicum* Houtt., Chem. Pharm. Bull. 29 (1981) 3561–3564, doi:10.1248/cpb.29.3561.
[24] G. Papanov, P. Malakov, Clerodane diterpenoids from *Teucrium montanum* subsp. *skorpilii*, Phytochemistry 22 (1983) 2787–2789, doi:10.1016/s0031-9422(00)97697-0.
[25] A.A. Omar, New neoclerodanes from *Teucrium polium*, Alex. J. Pharm. Sci. 1 (1987) 100–102.
[26] M.C. Carreiras, B. Rodriguez, F. Piozzi, G. Savona, M.R. Torres, A. Perales, A chlorine-containing and two 17β-neo-clerodane diterpenoids from T*eucrium polium* subsp. *vincentinum*, Phytochemistry 28 (1989) 1453–1461, doi:10.1016/s0031-9422(00)97764-1.
[27] J.R. Hanson, D.E.A. Rivett, S.V. Ley, D.J. Williams, The X-ray structure and absolute configuration of insect antifeedant clerodane diterpenoids from *Teucrium africanum*, J. Chem. Soc. Perkin Trans. 1 (1982) 1005–1008, doi:10.1039/p19820001005.
[28] H. Shimomura, Y. Sashida, K. Ogawa, Y. Iitaka, The chemical constituents of *Ajuga* plants. I. Neo-clerodanes from the leaves of *Ajuga nipponensis* Makino, Chem. Pharm. Bull. 31 (1983) 2192–2199, doi:10.1248/cpb.31.2192.
[29] N. Xie, Z. Min, S. Zhao, Y. Lu, Q. Zheng, C. Wang, M. Mizuno, M. Iinuma, T. Tanaka, A chlorine-containing neo-clerodane diterpene from *Teucrium pernyi*, Chem. Pharm. Bull. 40 (1992) 2193–2195, doi:10.1248/cpb.40.2193.
[30] M. Bruno, C. Fazio, F. Piozzi, G. Savona, B. Rodríguez, M.C. de la Torre, Neo-clerodane diterpenoids from *Teucrium racemosum*, Phytochemistry 40 (1995) 505–507, doi:10.1016/0031-9422(95)00286-G.
[31] P. Guo, Y. Li, J. Xu, C. Liu, Y. Ma, Y. Guo, Bioactive neo-clerodane diterpenoids from the whole plants of *Ajuga ciliata* Bunge, J. Nat. Prod. 74 (2011) 1575–1583, doi:10.1021/np2001557.
[32] P. Guo, Y. Li, J. Xu, Y. Guo, D.-.Q. Jin, J. Gao, W. Hou, T. Zhang, Neo-clerodane diterpenes from *Ajuga ciliata* Bunge and their neuroprotective activities, Fitoterapia 82 (2011) 1123–1127, doi:10.1016/j.fitote.2011.07.010.
[33] Z. Sun, Y. Li, D. Jin, P. Guo, H. Song, J. Xu, Y. Guo, L. Zhang, Neo-clerodane diterpenes from *Ajuga decumbens* and their inhibitory activities on LPS-induced NO production, Fitoterapia 83 (2012) 1409–1414, doi:10.1016/j.fitote.2012.08.003.
[34] B. Rodríguez, M.C. de la Torre, A. Perales, P.Y. Malakov, G.Y. Papanov, M.S.J. Simmonds, W.M. Blaney, Oxirane-opening reactions of some 6,19-oxygenated 4α,18-epoxy-neo-clerodanes isolated from *Teucrium*. Biogenesis and antifeedant activity of their derivatives, Tetrahedron 50 (1994) 5451–5468, doi:10.1016/S0040-4020(01)80701-8.
[35] M. Hamburger, J.L. Wolfender, K. Hostettmann, Search for chlorinated sesquiterpene lactones in the neurotoxic thistle *Centaurea solstitialis* by liquid chromatography-mass spectrometry, and model studies on their possible artifactual formation, Nat. Toxins 1 (1993) 315–327, doi:10.1002/nt.2620010602.
[36] P. Fernández, B. Rodríguez, G. Savona, F. Piozzi, Neo-clerodane diterpenoids from *Teucrium polium* subsp. *capitatum*, Phytochemistry 25 (1986) 181–184, doi:10.1016/S0031-9422(00)94525-4.
[37] G. Topcu, C. Eriş, A. Ulubelen, M. Krawiec, W.H. Watson, New rearranged neo-clerodane diterpenoids from *Teucrium alyssifolium*, Tetrahedron 51 (1995) 11793–11800, doi:10.1016/0040-4020(95)00740-Y.
[38] G. Dominguez, M.C. De la Torre, B. Rodriguez, Transformation of neoclerodane diterpenoids into 19-norneoclerodane derivatives, J. Org. Chem. 56 (1991) 6595–6600, doi:10.1021/jo00023a027.
[39] A. Bisio, G. Damonte, D. Fraternale, E. Giacomelli, A. Salis, G. Romussi, S. Cafaggi, D. Ricci, N. De Tommasi, Phytotoxic clerodane diterpenes from *Salvia miniata* Fernald (Lamiaceae), Phytochemistry 72 (2011) 265–275, doi:10.1016/j.phytochem.2010.11.011.
[40] J.A. Hueso-Rodriguez, F. Fernandez-Gadea, C. Pascual, B. Rodriguez, G. Savona, F. Piozzi, Neo-clerodane diterpenoids from *Teucrium lanigerum*, Phytochemistry 25 (1986) 175–180, doi:10.1016/s0031-9422(00)94524-2.
[41] P.Y. Malakov, G.Y. Papanov, Furanoid diterpenes from *Teucrium polium*, Phytochemistry 22 (1983) 2791–2793, doi:10.1016/S0031-9422(00)97698-2.
[42] M.C. de la Torre, B. Rodríguez, G. Savona, F. Piozzi, Teugnaphalodin, a neo-clerodane diterpenoid from *Teucrium gnaphalodes*, Phytochemistry 25 (1986) 171–173, doi:10.1016/S0031-9422(00)94523-0.
[43] M.José Sexmero Cuadrado, M.C. De La Torre, B. Rodríguez, M. Bruno, F. Piozzi, G. Savona, Neo-clerodane diterpenoids from *Teucrium oxylepis* subsp. *marianum*, Phytochemistry 30 (1991) 4079–4082, doi:10.1016/0031-9422(91)83471-V.
[44] G. Savona, F. Piozzi, O. Servettaz, B. Rodriguez, J.A. Hueso-Rodriguez, M.C. De La Torre, Neo-clerodane diterpenoids from *Teucrium lepicephalum* and *Teucrium buxifolium*, Phytochemistry 25 (1986) 2569–2572, doi:10.1016/S0031-9422(00)84512-4.
[45] R. Li, S.L. Morris-Natschke, K.H. Lee, Clerodane diterpenes: sources, structures, and biological activities, Nat. Prod. Rep. 33 (2016) 1166–1226, doi:10.1039/c5np00137d.
[46] A. Lourenço, M.C. dela Torre, B. Rodríguez, N. Harada, H. Ono, H. Uda, M. Bruno, F. Piozzi, G. Savona, The absolute stereoschemistry at C-12 in 12-hydroxylated neo-clerodane diterpenoids, Tetrahedron 48 (1992) 3925–3934, doi:10.1016/S0040-4020(01)88472-6.
[47] J. Jiménez-Barbero, ^{1}H NMR spectroscopy as a tool for establishing the C-12 stereochemistry and the conformation of the side chain in 12-hydroxylated neo-clerodanes isolated from *Teucrium* species, Tetrahedron 49 (1993) 6921–6930, doi:10.1016/S0040-4020(01)80434-8.
[48] J. Fayos, F. Fernandez-Gadea, C. Pascual, A. Perales, F. Piozzi, M. Rico, B. Rodriguez, G. Savona, Correct structures of montanin C, teupolin I, and 12-*epi*-teucvin, three (12*R*)-neoclerodan-20,12-olides isolated from the *Teucrium* species, J. Org. Chem. 49 (1984) 1789–1793, doi:10.1021/jo00184a023.
[49] C. Pascual, P. Fernández, M.C. García-Alvarez, J.L. Marco, F. Fernández-Gadea, M.C. de la Torre, J.A. Hueso-Rodríguez, B. Rodríguez, M. Bruno, M. Paternostro, F. Piozzi, G. Savona, The C-12 and C-20 configurations of some neo-clerodane diterpenoids isolated from *Teucrium* species, Phytochemistry 25 (1986) 715–718, doi:10.1016/0031-9422(86)88030-X.

4. Discussion, Conclusion, and Outlook

Despite their excellent efficacy, classic immunosuppressive small molecules like cyclosporine are accompanied by various limitations, such as unwanted side effects, gradual loss of efficacy over time, providing no long-lasting relief of symptoms, non-responding, and high treatment costs. Unwanted side effects include increased susceptibility for infections and malignancies, direct organ-specific toxicities caused by off-target effects, sensitization that may lead to hypersensitivity reactions, and high risk for drug-drug interactions. Therefore, during therapy the dose of immunosuppressive drugs are regularly monitored and adapted. This makes the treatment of autoimmune diseases quite challenging, and is therefore usually made in experienced institutions[1,145–149].

In this regard, the development of biologics like monoclonal antibodies and fusion proteins has revolutionized the treatment of systemic inflammatory autoimmune diseases. These types of drugs stand out due to their remarkable target specificity towards specific immune cells and cytokines. This target specificity significantly improved patient outcomes and reduced adverse events caused by off-target effects. The success achieved with existing biologic agents has sparked significant research interest in the identification of novel biologic agents that can target alternative pathways implicated in autoimmunity. Nevertheless, biologic agents have been shown to cause a variety of other types of adverse effects such as, cytokine release syndrome, hypersensitivity reactions, or anti-drug antibodies[1,145–149].

In the field of wound treatment the incidence of non-healing chronic wounds is increasing worldwide and impact tremendously the life quality of patients. Effective management of such wounds requires multiple clinic or hospital visits, which result in high cost treatments that have a large economic impact on health system budgets. Unfortunately, current available wound healing therapies are only partially effective, and thus more efficacious and cost-effective therapies are needed to decrease this burden[50,166,215,216].

Therefore, continued research into new therapies for both, autoimmunity and wound treatment is needed[145–147,166]. Considering that inflammation, autoimmunity,

and wound healing are complex and multifactorial conditions with diverse pathophysiological mechanisms, recent efforts are focused on discovering novel therapeutic interventions that can address these conditions more systemically. The goal is to target multiple modes of action simultaneously, with the intention of enhancing clinical outcomes by impacting several targets[151,164–166,168]. Plant extracts as complex mixtures of various phytochemical substances are known to have a beneficial impact in diseases with complex etiology and pathophysiology by acting in a synergistic manner on multiple targets[93,168,169,217–220]. Furthermore, certain treatment strategies that use a combination of different compounds can offer greater therapeutic effectiveness while reducing the likelihood of disease resistance and severe side effects compared to single drug treatments[164,221–225]. In this context, multicomponent plant extracts are assumend to improve the outcome of multifactorial conditions including autoimmunity or non-healing wounds by simultaneously targeting different cell types at different stages of disease progression.

This is the approach that has also been followed during this work. Plant extracts have been investigated for possible beneficial effects in different *in vitro* and *in vivo* test systems of T-cell mediated autoimmunity and wound healing. Inhibitory effects on T cell activation, proliferation, and cytokine secretion caused by plant extracts and isolated phytochemical substances have been studied in a T cell proliferation assay using human PBMCs. PBMCs have been stimulated with soluble CD3 and CD28 monoclonal antibodies, stained with carboxyfluorescein diacetate succinimidyl ester (CFSE), and incubated with the extracts and isolated compounds. The influence on T cell proliferation was assessed with a FACS analysis. Among the tested extracts, a strong inhibitory effect was observed for an ethyl acetate extract derived from the aerial parts of *H. brachiata*. A subsequent HPLC-based activity profiling approach resulted in the isolation of aryltetralin lignans that significantly inhibited T cell proliferation in a concentration-dependent manner. To gain a better understanding of the mechanism of action, investigations into cell cycle arrest revealed an inhibition of dividing T cells in G2/M phase. Additionally, a

multi-fluorescence panel was used to examine the production of inflammatory cytokines by effector T cells. The extract and the isolated triterpenes weakly reduced the secretion of cytokines like IL-2 and TNF-α. In this work we could show that a plant extract can exert inhibitory effects on T cells by affecting different modes of action, simultaneously. The observed effect of the ethyl acetate extract from *H. brachiata* could be traced back to a complementary synergistic effect between structurally different substance classes. Aryltetralin lignans showed an antimitotic effect, while the triterpenes reduced the secretion of inflammatory cytokines. This makes herbal preparations of *H. brachiata* potentially interesting for future developments in the field of T cell-mediated autoimmune diseases and should encourage further investigations in additional test systems.

In a further project, we looked at a sugar-depleted methanolic fraction of an EtOH extract from saffron corms that significantly inhibited the TNF-α/IFN-γ-induced gene expression and secretion of the inflammatory chemokines IL-8, MCP-1, and RANTES in human HaCaT keratinocytes. HaCaT cells represent an *in vitro* model to study wound healing and inflammatory skin diseases like psoriasis and atopic dermatitis. During innate immunity and wound healing keratinocytes get activated to migrate, proliferate, and produce inflammatory cytokines like MCP-1 and RANTES, which attract monocytes and effector T cells into the skin. Therefore, activated keratinocytes play a crucial role in autoimmune diseases, like for example in psoriasis, by sustaining an inflammatory environment, which can ultimately result in excessive keratinocyte proliferation and the formation of plaques. The effects of the sugar-depleted MeOH fraction on the TNF-α/IFN-γ-induced gene expression and secretion of the chemokines IL-6, IL-8, MCP-1, and RANTES in human HaCaT keratinocytes could be linked to a series of complex bidesmosidic triterpenoid saponins with a fatty acid residue attached to the glycosidic moiety at C-28. Activity-guided isolation procedures afforded azafrines 1 and 2, and eight new congeners named as azafrines 3−10. Saffron saponins significantly inhibited expression and secretion of RANTES more potently than the positive control hydrocortisone. Additionally, saffron saponins inhibited the expression but not

secretion of MCP-1. To summarize, *in vitro* data indicates that saffron saponins exhibit anti-inflammatory properties by influencing the expression and secretion of chemotactic cytokines. Therefore, saffron corm extracts and saponins have the potential to be further developed as topical agents for the treatment of inflammatory skin diseases like atopic dermatitis and psoriasis.

Finally, the wound healing properties of a methanolic extract from the aerial parts of *Teucrium polium* subsp. *capitatum*, a traditional medicinal plant used in Algeria to treat wounds, have been investigated using a wound excision model in rabbits. For this purpose, the *in vivo* wound healing effect of an ointment made out of the methanolic extract was compared to a commercially available allantoin-containing ointment. Wound assessment after treatment showed that the *Teucrium*-containing ointment significantly improved the wound healing process after excision. Histological examination showed faster granulation and re-epithelization of the wound, as well as higher collagen deposition compared to the positive control. Thus, the duration of tissue repair and wound closure was shorter with the *Teucrium*-containing ointment. A comprehensive phytochemical analysis of the extract led to the identification of flavonoids, phenylethanoid glycosides, and neo-clerodane type diterpenes as major components. Superior wound healing effects compared to the single drug treatment with allantoin might be explained due to the combined effects of the various polyphenolic constituents, which may act synergistically on different cell types and processes involved in tissue repair[92,226–228]. The overall data confirm the potential of the *T. polium* extract for wound treatment, and support the traditional use of this plant as a wound healing agent.

In conclusion, within the scope of this work we demonstrated by applying different approaches that plant extracts as complex mixtures of phytochemical substances may have the potential to exert beneficial effects in the treatment of multifactorial conditions, such as autoimmunity and non-healing wounds. Compared to single drug treatments, the different secondary metabolites in an herbal preparation may act synergistically on different target cells and mechanisms that are involved in the pathogenesis of such diseases. The ethyl acetate extract obtained from *H. brachiata*,

along with the isolated aryltetralin lignans, demonstrated inhibition of T cell proliferation by directly disrupting spindle formation during mitosis. Additionally, the same extract and the identified triterpenes reduced the secretion of pro-inflammatory cytokines by effector T cells. This demonstrated that different phytochemical substances of a single extract interact with different targets simultaneously, which may be beneficial in T cell-mediated autoimmune diseases. An additive synergistic effect is also assumed by a mixture of different saponins obtained from a sugar-depleted saffron corm extract. The sugar-depleted extract influenced the expression and secretion of various cytokines in keratinocytes more efficiently than the individual saponins alone. Moreover, it is assumed that these benefical *in vitro* effects on cytokines could affect leukocyte infiltration into the skin *in vivo* and mitigate the development of inflammation. And finally, the favorable outcomes observed *in vivo* from the *T. polium* extract in wound treatment, in comparison to the single drug treatment of allantoin, suggest that the enriched composition of diverse polyphenolic compounds likely plays a significant role in its beneficial wound healing properties.

The results of our studies support the benefits of utilizing phenotype-based testing systems for studying complex substance mixtures like plant extracts. Such testing systems take into account the complexity associated with multifactorial diseases, offering a more natural environment. In many cases, the specific targets involved in the development of such diseases are unknown, and the underlying pathophysiological mechanisms are not fully understood. As a result, employing phenotype-based assays to investigate complex substance mixtures enables the identification of molecules or combinations of molecules that exhibit beneficial effects by interacting with novel potential targets and modes of action[229,230]. Therefore, adhering to this approach holds the potential to discover herbal preparations or phytochemicals that exert effects on different biological processes, associated with autoimmunity and wound healing, concomitantly, including cell activation, cell migration, angiogenesis, or apoptosis. Even the identification of

previously unknown mechanisms of action may be possbile, as it was the case with the discovery of fingolimod[39].

Nevertheless, additional investigations using supplementary *in vitro* and *in vivo* models are necessary to identify the specific targets and mechanisms of action that may underlie the observed effects of the plant extracts studied in this work. In the case of *H. brachiata*, an *in vivo* study using an animal model for chronic allograft rejection to assess long-term immunosuppression could be a follow-up possibility to investigate systemic effects of the extract[174]. In addition, disease-specific animal models, for example for rheumatoid arthritis or multiple sclerosis, could provide a opportunity to explore beneficial synergistic effects of *H. brachiata* in specific autoimmune diseases[175,176].Saffron corm extracts or saponin-enriched fractions could be further studied in specific 2D and 3D *in vitro* skin models for inflammatory skin diseases[177,178]. Since the corm extracts are intended to be applied topically, cutaneous penetration and distribution could be examined *ex vivo* in porcine ear skin using the cutaneous biodistribution method (CBM) in combination with mass spectrometry imaging (MSI)[231,232]. If such investigations confirm beneficial effects for inflammatory skin diseases, next steps could include the testing of corm extracts and saffron saponins in mouse models for psoriasis, as it has been done for extracts and acetyl-11-keto-β-boswellic acid obtained from *Boswellia carteri* [87,197]. The methanolic extract of *T. polium* and the isolated compounds should initially be further investigated in *in vitro* and *ex vivo* models of wound healing, because animal skin does not precisely replicate the structural characteristics of human skin. The combination of various 2D and 3D *in vitro* models, such as scratch assays to investigate cell migration of keratinocytes and fibroblasts, along with *ex vivo* human skin models to examine angiogenesis, can offer a greater understanding of the mode of action and aid in identifying the active compounds of the extract[212,214]. As a subsequent step, the evaluation of the wound healing effect of *T. polium* could include the consideration of small-scale clinical studies involving individuals with non-healing wounds as an additional possibility[206,212–214].

References

1. Parham, P. *The Immune System*. (W.W. Norton & Company, New York, 2021).
2. Kumar, V., Abbas, A. K. & Aster, J. C. *Robbins & Cotran Pathologic Basis of Disease*. (Elsevier, Philadelphia, 2020).
3. Murphy, K. & Weaver, C. *Janeway's Immunobiology*. (Garland Science, New York, 2016).
4. Abbas, A., Lichtmann, A. H. & Pillai, S. *Cellular and Molecular Immunology*. (Elsevier Saunders, Philadelphia, 2014).
5. Esmaeili, A., Biazar, E., Ebrahimi, M., Keshel, S. H., Kheilnezhad, B. & Landi, F. S. Acellular fish skin for wound healing. *Int. Wound J.* 1–18 (2023).
6. van der Laan, S. & Meijer, O. C. Pharmacology of glucocorticoids: beyond receptors. *Eur. J. Pharmacol.* **585**, 483–491 (2008).
7. Mann, J. Natural products as immunosuppressive agents. *Nat. Prod. Rep.* **18**, 417–430 (2001).
8. Stuetz, A., Baumann, K., Grassberger, M., Wolff, K. & Meingassner, J. G. Discovery of topical calcineurin inhibitors and pharmacological profile of pimecrolimus. *Int. Arch. Allergy Immunol.* **141**, 199–212 (2006).
9. Gupta, A. K. & Chow, M. Pimecrolimus: a review. *J. Eur. Acad. Dermatology Venereol.* **17**, 493–503 (2003).
10. Yoo, Y. J., Kim, H., Park, S. R. & Yoon, Y. J. An overview of rapamycin: from discovery to future perspectives. *J. Ind. Microbiol. Biotechnol.* **44**, 537–553 (2017).
11. Li, Z., Nie, L., Chen, L., Sun, Y. & Li, G. Rapamycin relieves inflammation of experimental autoimmune encephalomyelitis by altering the balance of Treg/Th17 in a mouse model. *Neurosci. Lett.* **705**, 39–45 (2019).
12. Suto, T. & Karonitsch, T. The immunobiology of mTOR in autoimmunity. *J. Autoimmun.* **110**, 102373 (2020).
13. Tedesco-Silva, H., Saliba, F., Barten, M. J., De Simeone, P., Potena, L., Gottlieb, J., Gawai, A., Bernhardt, P. & Pascual, J. An overview of the efficacy and safety of everolimus in adult solid organ transplant recipients. *Transplant. Rev.* **36**, 100655 (2022).
14. Hasskarl, J. Everolimus. in *Small Molecules in Oncology. Recent Results in Cancer Research* **211**, 101–123 (Springer, Cham, 2018).
15. Chatenoud, L. & Bluestone, J. A. CD3-specific antibodies: a portal to the treatment of autoimmunity. *Nat. Rev. Immunol.* **7**, 622–632 (2007).

16. Kuhn, C. & Weiner, H. L. Therapeutic anti-CD3 monoclonal antibodies: from bench to bedside. *Immunotherapy* **8**, 889–906 (2016).

17. Vincenti, F. Costimulation blockade in autoimmunity and transplantation. *J. Allergy Clin. Immunol.* **121**, 299–306 (2008).

18. Schwarz, C., Mahr, B., Muckenhuber, M. & Wekerle, T. Belatacept/CTLA4Ig: an update and critical appraisal of preclinical and clinical results. *Expert Rev. Clin. Immunol.* **14**, 583–592 (2018).

19. Creed, T. J., Probert, C. S. J., Norman, M. N., Moorghen, M., Shepherd, N. A., Hearing, S. D. & Dayan, C. M. Basiliximab for the treatment of steroid-resistant ulcerative colitis: further experience in moderate and severe disease. *Aliment. Pharmacol. Ther.* **23**, 1435–1442 (2006).

20. Kiskaddon, A. L., Wilsey, M., Gonzalez-Gomez, I., Laks, J., Miles, A., Carapellucci, J. & Asante-Korang, A. Basiliximab therapy for immune-mediated bowel disease in a pediatric heart transplant patient. *Pediatr. Transplant.* **27**, e14443 (2023).

21. Rebora, A., Parodi, A. & Murialdo, G. Basiliximab is effective for erosive lichen planus. *Arch. Dermatol.* **138**, 1100–1101 (2002).

22. Dhillon, S. Intravenous tocilizumab: a review of its use in adults with rheumatoid arthritis. *BioDrugs* **28**, 75–106 (2014).

23. Jones, S. A. Directing transition from innate to acquired immunity: defining a role for IL-6. *J. Immunol.* **175**, 3463–3468 (2005).

24. Patel, A. A., Swerlick, R. A. & McCall, C. O. Azathioprine in dermatology: the past, the present, and the future. *J. Am. Acad. Dermatol.* **55**, 369–389 (2006).

25. Nielsen, O. H., Vainer, B. & Rask-Madsen, J. The treatment of inflammatory bowel disease with 6-mercaptopurine or azathioprine. *Aliment. Pharmacol. Ther.* **15**, 1699–1708 (2001).

26. Bedoui, Y., Guillot, X., Sélambarom, J., Guiraud, P., Giry, C., Jaffar-Bandje, M. C., Ralandison, S. & Gasque, P. Methotrexate an old drug with new tricks. *Int. J. Mol. Sci.* **20**, 5023 (2019).

27. Broen, J. C. A. & van Laar, J. M. Mycophenolate mofetil, azathioprine and tacrolimus: mechanisms in rheumatology. *Nat. Rev. Rheumatol.* **16**, 167–178 (2020).

28. Leban, J. & Vitt, D. Human dihydroorotate dehydrogenase inhibitors, a novel approach for the treatment of autoimmune and inflammatory diseases. *Arzneimittelforschung* **61**, 66–72 (2011).

29. Ahlmann, M. & Hempel, G. The effect of cyclophosphamide on the immune system: implications for clinical cancer therapy. *Cancer Chemother. Pharmacol.* **78**, 661–671 (2016).

30. Melsheimer, R., Geldhof, A., Apaolaza, I. & Schaible, T. Remicade® (infliximab): 20 years of contributions to science and medicine. *Biol. Targets Ther.* **13**, 139–178 (2019).

31. Bellinvia, S., Cummings, J. R. F., Ardern-Jones, M. R. & Edwards, C. J. Adalimumab biosimilars in europe: an overview of the clinical evidence. *BioDrugs* **33**, 241–253 (2019).

32. Azevedo, V. F., Galli, N., Kleinfelder, A., D'Ippolito, J. & Urbano, P. C. M. Etanercept biosimilars. *Rheumatol. Int.* **35**, 197–209 (2015).

33. Mohty, M. Mechanisms of action of antithymocyte globulin: T-cell depletion and beyond. *Leukemia* **21**, 1387–1394 (2007).

34. Pan, P., Chen, C., Hong, J. & Gu, Y. Autoimmune pathogenesis, immunosuppressive therapy and pharmacological mechanism in aplastic anemia. *Int. Immunopharmacol.* **117**, 110036 (2023).

35. Young, N. S., Calado, R. T. & Scheinberg, P. Current concepts in the pathophysiology and treatment of aplastic anemia. *Blood* **108**, 2509–2519 (2006).

36. Dzuris, J. L., Bloy, C., Ruzek, M. & Williams, J. M. Transplantation immunotherapy with antithymocyte globulin (ATG). in *Immunotherapy in Transplantation: Principles and Practice* 330–345 (Wiley-Blackwell, New Jersey, 2012).

37. Chung, D. T., Korn, T., Richard, J., Ruzek, M., Kohm, A. P., Miller, S., Nahill, S. & Oukka, M. Anti-thymocyte globulin (ATG) prevents autoimmune encephalomyelitis by expanding myelin antigen-specific Foxp3+ regulatory T cells. *Int. Immunol.* **19**, 1003–1010 (2007).

38. Willis, M. D. & Robertson, N. P. Alemtuzumab for multiple sclerosis. *Curr. Neurol. Neurosci. Rep.* **16**, 84 (2016).

39. Adachi, K. & Chiba, K. FTY720 story. Its discovery and the following accelerated development of sphingosine 1-phosphate receptor agonists as immunomodulators based on reverse pharmacology. *Perspect. Medicin. Chem.* **1**, 11–23 (2007).

40. Wyant, T., Fedyk, E. & Abhyankar, B. An overview of the mechanism of action of the monoclonal antibody vedolizumab. *J. Crohn's Colitis* **10**, 1437–1444 (2016).

41. Brandstadter, R. & Sand, I. K. The use of natalizumab for multiple sclerosis. *Neuropsychiatr. Dis. Treat.* **13**, 1691–1702 (2017).

42. Nirk, E. L., Reggiori, F. & Mauthe, M. Hydroxychloroquine in rheumatic autoimmune disorders and beyond. *EMBO Mol. Med.* **12**, e12476 (2020).

43. Plosker, G. L. & Croom, K. F. Sulfasalazine: a review of its use in the management of rheumatoid arthritis. *Drugs* **65**, 1825–1849 (2005).

44. Mushtaq, S. & Sarkar, R. Sulfasalazine in dermatology: a lesser explored drug with broad therapeutic potential. *Int. J. Women's Dermatology* **6**, 191–198 (2020).

45. Jakimovski, D., Kolb, C., Ramanathan, M., Zivadinov, R. & Weinstock-Guttman, B. Interferon β for multiple sclerosis. *Cold Spring Harb. Perspect. Med.* **8**, a032003 (2018).

46. Aharoni, R. The mechanism of action of glatiramer acetate in multiple sclerosis and beyond. *Autoimmun. Rev.* **12**, 543–553 (2013).

47. Montes Diaz, G., Hupperts, R., Fraussen, J. & Somers, V. Dimethyl fumarate treatment in multiple sclerosis: recent advances in clinical and immunological studies. *Autoimmun. Rev.* **17**, 1240–1250 (2018).

48. Ayaz, F. *Fumaria officinalis* L. in *Novel Drug Targets With Traditional Herbal Medicines* 301–315 (Springer, Cham, 2022).

49. Brück, J., Dringen, R., Amasuno, A., Pau-Charles, I. & Ghoreschi, K. A review of the mechanisms of action of dimethylfumarate in the treatment of psoriasis. *Exp. Dermatol.* **27**, 611–624 (2018).

50. Frykberg, R. G. & Banks, J. Challenges in the treatment of chronic wounds. *Adv. Wound Care* **4**, 560–582 (2015).

51. Tottoli, E. M., Dorati, R., Genta, I., Chiesa, E., Pisani, S. & Conti, B. Skin wound healing process and new emerging technologies for skin wound care and regeneration. *Pharmaceutics* **12**, 1–30 (2020).

52. Kramer, A., Dissemond, J., Kim, S., Willy, C., Mayer, D., Rapke, R., Tuchmann, F. & Assadian, O. Consensus on wound antisepsis: update 2018. *Skin Pharmacol. Physiol.* **31**, 28–58 (2018).

53. Sherman, R. A., Mumcuoglu, K. Y., Grassberger, M. & Tantawi, T. I. Maggot therapy. in *Biotherapy - History, Principles and Practice* 5–29 (Springer, Dordrecht, 2013).

54. Babalska, Z. Ł., Korbecka-Paczkowska, M. & Karpiński, T. M. Wound antiseptics and European guidelines for antiseptic application in wound treatment. *Pharmaceuticals* **14**, 1253 (2021).

55. Rezvani Ghomi, E., Khalili, S., Nouri Khorasani, S., Esmaeely Neisiany, R. & Ramakrishna, S. Wound dressings: current advances and future directions. *J. Appl. Polym. Sci.* **136**, 47738 (2019).

56. Lansdown, A. B. G., Mirastschijski, U., Stubbs, N., Scanlon, E. & Ågren, M. S. Zinc in wound healing: theoretical, experimental, and clinical aspects. *Wound Repair Regen.* **15**, 2–16 (2007).

57. Tashkandi, H. Honey in wound healing: an updated review. *Open Life Sci.* **16**, 1091–1100 (2021).

58. Draelos, Z. D. New treatments for restoring impaired epidermal barrier permeability: skin barrier repair creams. *Clin. Dermatol.* **30**, 345–348 (2012).

59. Short, R. W., Chan, J. L., Choi, J. M., Egbert, B. M., Rehmus, W. E. & Kimball A. B. Effects of moisturization on epidermal homeostasis and differentiation. *Clin. Exp. Dermatol.* **32**, 88–90 (2007).

60. Läuchli, S., Vannotti, S., Hafner, J., Hunziker, T. & French, L. A plant-derived wound therapeutic for cost-effective treatment of post-surgical scalp wounds with exposed bone. *Forsch. Komplementmed.* **21**, 88–93 (2014).

61. Mainetti, S. & Carnevali, F. An experience with paediatric burn wounds treated with a plant-derived wound therapeutic. *J. Wound Care* **22**, 681–689 (2013).

62. Del Missier, A., La Torre, F. & Toma, E. Treatment of peristomal granulomatosis with a neem and red *Hypericum* oil application: case studies. *Clin. Ter.* **170**, e86-92 (2019).

63. Eaglstein, W. H. & Falanga, V. Tissue engineering and the development of Apligraf®, a human skin equivalent. *Clin. Ther.* **19**, 894–905 (1997).

64. Chen, H., Yin, B., Hu, B., Zhang, B., Liu, J., Jing, Y., Fan, Z., Tian, Y., Wei, X. & Zhang, W. Acellular fish skin enhances wound healing by promoting angiogenesis and collagen deposition. *Biomed. Mater.* **16**, 045011 (2021).

65. Agarwal, P., Kukrele, R. & Sharma, D. Vacuum assisted closure (VAC)/negative pressure wound therapy (NPWT) for difficult wounds: a review. *J. Clin. Orthop. Trauma* **10**, 845–848 (2019).

66. Shih, R., Waltzman, J. & Evans, G. R. D. Review of over-the-counter topical scar treatment products. *Plast. Reconstr. Surg.* **119**, 1091–1095 (2007).

67. Chen, M. A. & Davidson, T. M. Scar management: prevention and treatment strategies. *Curr. Opin. Otolaryngol. Head Neck Surg.* **13**, 242–247 (2005).

68. Olczyk, P., Mencner, Ł. & Komosinska-Vassev, K. Diverse roles of heparan sulfate and heparin in wound repair. *Biomed Res. Int.* **2015**, (2015).

69. Proksch, E., de Bony, R., Trapp, S. & Boudon, S. Topical use of dexpanthenol: a 70th anniversary article. *J. Dermatolog. Treat.* **28**, 766–773 (2017).

70. Fujiwara, S. & Noguchi, T. Degradation of purines: only ureidoglycollate lyase out of four allantoin-degrading enzymes is present in mammals. *Biochem. J.* **312**, 315–318 (1995).

71. Dinica, R. M., Sandu, C., Dediu Botezatu, A. V., Cazanevscaia Busuioc, A., Balanescu, F., Ionica Mihaila, M. D., Dumitru, C. N., Furdui, B. & Iancu, A. V. Allantoin from valuable Romanian animal and plant sources with promising anti-inflammatory activity as a nutricosmetic ingredient. *Sustainability* **13**, 10170 (2021).

72. Araújo, L. U., Grabe-Guimarães, A., Mosqueira, V. C. F., Carneiro, C. M. & Silva-Barcellos, N. M. Profile of wound healing process induced by allantoin. *Acta Cir. Bras.* **25**, 460–466 (2010).

73. Wai, S. H., Shun, Y. Y., Pik, C. C. & Chan, H. H. Use of onion extract, heparin, allantoin gel in prevention of scarring in Chinese patients having laser removal of tattoos: a prospective randomized controlled trial. *Dermatol. Surg.* **32**, 891–896 (2006).

74. Jenwitheesuk, K., Surakunprapha, P., Jenwitheesuk, K., Kuptarnond, C., Prathanee, S. & Intanoo, W. Role of silicone derivative plus onion extract gel in presternal hypertrophic scar protection: a prospective randomized, double blinded, controlled trial. *Int. Wound J.* **9**, 397–402 (2012).

75. Jeannin, J.-M. Phyto- und Mykotoxine (3). *Schweiz. Z. Ganzheitsmed.* **25**, 151–152 (2013).

76. Pfirrmann, R. W. & Wicki, O. Method and composition for the treatment of scars. *United States Patent* (1980).

77. Chittoria, R. & Padi, T. A prospective, randomized, placebo controlled, double blind study of silicone gel in prevention of hypertrophic scar at donor site of skin grafting. *J. Cutan. Aesthet. Surg.* **6**, 12–16 (2013).

78. Yang, H., Song, L., Zou, Y., Sun, D., Wang, L., Yu, Z. & Guo, J. Role of hyaluronic acids and potential as regenerative biomaterials in wound healing. *ACS Appl. Bio Mater.* **4**, 311–324 (2021).

79. Mathew-Steiner, S. S., Roy, S. & Sen, C. K. Collagen in wound healing. *Bioengineering* **8**, 63 (2021).

80. Sinno, S., Lee, D. S. & Khachemoune, A. Vitamins and cutaneous wound healing. *J. Wound Care* **20**, 287–293 (2011).

81. Bikle, D. D. Role of vitamin D and calcium signaling in epidermal wound healing. *J. Endocrinol. Invest.* **46**, 205–212 (2023).

82. Dingermann, T. & Loew, D. *Phytopharmakologie.* (Wissenschaftliche Verlagsgesellschaft mbH, Stuttgart, 2003).

83. Teuscher, E., Melzig, M. F. & Lindequist, U. *Biogene Arzneimittel.* (Wissenschaftliche Verlagsgesellschaft mbH, Stuttgart, 2012).

84. Sticher, O., Heilmann, J. & Zündorf, I. *Hänsel / Sticher Pharmakognosie - Phytopharmazie.* (Wissenschaftliche Verlagsgesellschaft mbH, Stuttgart, 2015).

85. Miller, M. R., Abshirini, M., Wolber, F. M., Tuterangiwhiu, T. R. & Kruger, M. C. Greenshell mussel products: a comprehensive review of sustainability, traditional use, and efficacy. *Sustainability* **15**, 3912 (2023).

86. Abdel-Tawab, M., Werz, O. & Schubert-Zsilavecz, M. *Boswellia serrata* an overall assessment of *in vitro*, preclinical, pharmacokinetic and clinical data. *Clin. Pharmacokinet.* **50**, 349–369 (2011).

87. Wang, H., Syrovets, T., Kess, D., Büchele, B., Hainzl, H., Lunov, O., Weiss, J. M., Scharffetter-Kochanek, K. & Simmet, T. Targeting NF-κB with a natural triterpenoid alleviates skin inflammation in a mouse model of psoriasis. *J. Immunol.* **183**, 4755–4763 (2009).

88. Zamolodchikova, T. S., Tolpygo, S. M. & Svirshchevskaya, E. V. Cathepsin G–not only inflammation: the immune protease can regulate normal physiological processes. *Front. Immunol.* **11**, 411 (2020).

89. Zimmermann-Klemd, A. M., Reinhardt, J. K., Nilsu, T., Morath, A., Falanga, C. M., Schamel, W. W., Huber, R., Hamburger, M. & Gründemann, C. *Boswellia carteri* extract and 3-O-acetyl-alpha-boswellic acid suppress T cell function. *Fitoterapia* **146**, 104694 (2020).

90. Gruenwald, J., Uebelhack, R. & Moré, M. I. *Rosa canina* – Rose hip pharmacological ingredients and molecular mechanics counteracting osteoarthritis – a systematic review. *Phytomedicine* **60**, 152958 (2019).

91. Gündling, P. W. Einsatzmöglichkeiten der Phytotherapie bei Hautkrankheiten. *Schweiz. Z. Ganzheitsmed.* **29**, 208–213 (2017).

92. Ghosh, P. K. & Gaba, A. Phyto-extracts in wound healing. *J. Pharm. Pharm. Sci.* **16**, 760–820 (2013).

93. Tsioutsiou, E. E., Giachetti, D., Miraldi, E., Governa, P., Magnano, A. R. & Biagi, M. Phytotherapy and skin wound healing. *Acta Vulnologica* **14**, 126–139 (2016).

94. Vitale, S., Colanero, S., Placidi, M., Di Emidio, G., Tatone, C., Amicarelli, F. & D'Alessandro, A. M. Phytochemistry and biological activity of medicinal plants in wound healing: an overview of current research. *Molecules* **27**, 3566 (2022).

95. Simatupang, M. H., Dietrichs, H. H. & Gottwald, H. Über die hautreizenden Stoffe in *Vatairea guianensis* Aubl. *Holzforschung* **21**, 89–94 (1967).

96. Steger, J. W. Anthralin and chrysarobin: a reexamination of the origins and early use. *Arch. Dermatol.* **118**, 625–626 (1982).

97. Mahrle, G. Dithranol. *Clin. Dermatol.* **15**, 723–737 (1997).

98. Lee, H.-S. & Jeong, G.-S. Chrysophanol attenuates manifestations of immune bowel diseases by regulation of colorectal cells and T cells activation *in vivo*. *Molecules* **26**, 1682 (2021).

99. Song, G., Zhang, Y., Yu, S., Lv, W., Guan, Z., Sun, M. & Wang, J. Chrysophanol attenuates airway inflammation and remodeling through nuclear factor-kappa B signaling pathway in asthma. *Phyther. Res.* **33**, 2702–2713 (2019).

100. Jeong, H.-J., Kim, H.-Y. & Kim, H.-M. Molecular mechanisms of anti-inflammatory effect of chrysophanol, an active component of AST2017-01 on atopic dermatitis *in vitro* models. *Int. Immunopharmacol.* **54**, 238–244 (2018).

101. Lee, H.-S. & Jeong, G.-S. Chrysophanol mitigates T cell activation by regulating the expression of CD40 ligand in activated T cells. *Int. J. Mol. Sci.* **21**, 1–13 (2020).

102. Galle, K., Bladt, S. & Wagner, H. DC- und HPLC-Analyse der Rinde von *Mahonia aquifolium* und anderer *Mahonia*-Arten. *Dtsch. Apoth. Ztg.* **134**, 35–44 (1994).

103. Hellinger, R., Koehbach, J., Fedchuk, H., Sauer, B., Huber, R., Gruber, C. W. & Gründemann, C. Immunosuppressive activity of an aqueous *Viola tricolor* herbal extract. *J. Ethnopharmacol.* **151**, 299–306 (2014).

104. Piana, M., Silva, M. A., Trevisan, G., de Brum, T. F., Silva, C. R., Boligon, A. A., Oliveira, S. M., Zadra, M., Hoffmeister, C., Rossato, M. F., Tonello, R., Laporta, L. V., de Freitas, R. B., Belke, B. V., da Silva Jesus, R., Ferreira, J. & Athayde, M. L. Antiinflammatory effects of *Viola tricolor* gel in a model of sunburn in rats and the gel stability study. *J. Ethnopharmacol.* **150**, 458–465 (2013).

105. Olejnik, M., Adamski, Z. & Dorocka-Bobkowska, B. Psoriasis: from antiquity to the present. *Indian J. Dermatol. Venereol. Leprol.* **89**, 149–153 (2022).

106. Chularojanamontri, L., Wongpraparut, C., Silpa-archa, N. & Pongparit, K. A guide to the ingredients of over-the-counter moisturizers for psoriasis. *Psoriasis Forum* **20**, 24–30 (2014).

107. Niederle, S. *Cardiospermum halicacabum* (L.) – Die Ballonrebe. *Z. Phyther.* **17**, 61–66 (1996).

108. Elangovan, A., Ramachandran, J., Lakshmanan, D. K., Ravichandran, G. & Thilagar, S. Ethnomedical, phytochemical and pharmacological insights on an Indian medicinal plant: the balloon vine (*Cardiospermum halicacabum* Linn.). *J. Ethnopharmacol.* **291**, 115143 (2022).

109. Fai, D., Fai, C., Di Vito, M., Martini, C., Zilio, G. & De Togni, H. *Cardiospermum halicacabum* in atopic dermatitis: clinical evidence based on phytotherapic approach. *Dermatol. Ther.* **33**, 1–5 (2020).

110. Biswas, D., Mandal, S., Chatterjee Saha, S., Tudu, C. K., Nandy, S., Batiha, G. E., Shekhawat, M. S., Pandey, D. K. & Dey, A. Ethnobotany, phytochemistry, pharmacology, and toxicity of *Centella asiatica* (L.) Urban: a comprehensive review. *Phyther. Res.* **35**, 6624–6654 (2021).

111. Bylka, W., Znajdek-Awizeń, P., Studzińska-Sroka, E., Dańczak-Pazdrowska, A. & Brzezińska, M. *Centella asiatica* in dermatology: an overview. *Phyther. Res.* **28**, 1117–1124 (2014).

112. Kukula, O., Kırmızıkan, S., Tiryaki, E. S., Çiçekli, M. N. & Günaydın, C. Asiatic acid exerts an anti-psoriatic effect in the imiquimod-induced psoriasis model in mice. *Immunopharmacol. Immunotoxicol.* **44**, 367–372 (2022).

113. OuYang, Q., Pan, Y., Luo, H., Xuan, C., Liu, J. & Liu, J. MAD ointment ameliorates imiquimod-induced psoriasiform dermatitis by inhibiting the IL-23/IL-17 axis in mice. *Int. Immunopharmacol.* **39**, 369–376 (2016).

114. Scheffler, A. The wound healing properties of betulin from birch bark from bench to bedside. *Planta Med.* **85**, 524–527 (2019).

115. Orra, S., Boyajian, M. K., Bryant, J. R., Talbet, J. H., Mulliken, J. B., Rogers, G. F. & Oh, A. K. Balsam of Peru: history and utility in plastic surgery. *J. Craniofac. Surg.* **32**, 1209–1210 (2021).

116. Forrest, R. D. Early history of wound treatment. *J. R. Soc. Med.* **75**, 198–205 (1982).

117. Aguiar, A. T. C., Barcellos-Silva, I.-G. C., de Oliveira Habib-Pereira, N R., Antonio, A. S. & da Veiga-Junior, V. F. Chemistry, biological activities, and uses of balsams. in *Gums, Resins and Latexes of Plant Origin. Reference Series in Phytochemistry* 399–432 (Springer, Cham, 2022).

118. Jokinen, J. J. & Sipponen, A. Refined spruce resin to treat chronic wounds: rebirth of an old folkloristic therapy. *Adv. Wound Care* **5**, 198–207 (2016).

119. Goels, T., Eichenauer, E., Langeder, J., Hoeller, F., Sykora, C., Tahir, A., Urban, E., Heiss, E. H., Saukel, J. & Glasl, S. Norway spruce balm: phytochemical composition and ability to enhance re-epithelialization *in vitro*. *Planta Med.* **86**, 1080–1088 (2020).

120. Goels, T., Eichenauer, E., Tahir, A., Prochaska, P., Hoeller, F., Heiss, E. H. & Glasl, S. Exudates of *Picea abies*, *Pinus nigra*, and *Larix decidua*: chromatographic comparison and pro-migratory effects on keratinocytes *in vitro*. *Plants* **11**, 599 (2022).

121. Sipponen, A., Kuokkanen, O., Tiihonen, R., Kauppinen, H. & Jokinen, J. J. Natural coniferous resin salve used to treat complicated surgical wounds: pilot clinical trial on healing and costs. *Int. J. Dermatol.* **51**, 726–732 (2012).

122. Sipponen, A., Jokinen, J. J., Sipponen, P., Papp, A., Sarna, S. & Lohi, J. Beneficial effect of resin salve in treatment of severe pressure ulcers: a prospective, randomized and controlled multicentre trial. *Br. J. Dermatol.* **158**, 1055–1062 (2008).

123. Martinotti, S. & Ranzato, E. Propolis: A new frontier for wound healing? *Burn. Trauma* **3**, 1–7 (2015).

124. Oryan, A., Alemzadeh, E. & Moshiri, A. Potential role of propolis in wound healing: biological properties and therapeutic activities. *Biomed. Pharmacother.* **98**, 469–483 (2018).

125. Amirghofran, Z. Herbal medicines for immunosuppression. *Iran. J. Allergy, Asthma Immunol.* **11**, 111–119 (2012).

126. Sahoo, B. M. & Banik, B. K. Medicinal plants: source for immunosuppressive agents. *Immunol. Curr. Res.* **2**, 106 (2018).

127. Saurin, S., Meineck, M., Erkel, G., Opatz, T., Weinmann-Menke, J. & Pautz, A. Drug candidates for autoimmune diseases. *Pharmaceuticals* **15**, 503 (2022).

128. Asadi-Samani, M., Bagheri, N., Rafieian-Kopaei, M. & Shirzad, H. Inhibition of Th1 and Th17 cells by medicinal plants and their derivatives: a systematic review. *Phyther. Res.* **31**, 1128–1139 (2017).

129. Venkatesha, S. H., Astry, B., Nanjundaiah, S. M., Kim, H. R., Rajaiah, R., Yang, Y., Tong, L., Yu, H., Berman, B. M. & Moudgil, K. D. Control of autoimmune arthritis by herbal extracts and their bioactive components. *Asian J. Pharm. Sci.* **11**, 301–307 (2016).

130. Marton, L. T., Barbalho, S. M., Sloan, K. P., Sloan, L. A., de Alvares Goulart, R., Araújo, A. C. & Bechara, M. D. Curcumin, autoimmune and inflammatory diseases: going beyond conventional therapy – a systematic review. *Crit. Rev. Food Sci. Nutr.* **62**, 2140–2157 (2022).

131. Zeng, L., Yang, T., Yang, K., Yu, G., Li, J., Xiang, W. & Chen, H. Curcumin and *Curcuma longa* extract in the treatment of 10 types of autoimmune diseases: a systematic review and meta-analysis of 31 randomized controlled trials. *Front. Immunol.* **13**, 896476 (2022).

132. Ranjan, D., Chen, C., Johnston, T. D., Jeon, H. & Nagabhushan, M. Curcumin inhibits mitogen stimulated lymphocyte proliferation, NFκB activation, and IL-2 signaling. *J. Surg. Res.* **121**, 171–177 (2004).

133. Xie, L., Li, X.-K., Funeshima-Fuji, N., Kimura, H., Matsumoto, Y., Isaka, Y. & Takahara S. Amelioration of experimental autoimmune encephalomyelitis by curcumin treatment through inhibition of IL-17 production. *Int. Immunopharmacol.* **9**, 575–581 (2009).

134. Bao, J. & Dai, S.-M. A Chinese herb *Tripterygium wilfordii* Hook F in the treatment of rheumatoid arthritis: mechanism, efficacy, and safety. *Rheumatol. Int.* **31**, 1123–1129 (2011).

135. Tang, W. & Zuo, J.-P. Immunosuppressant discovery from *Tripterygium wilfordii* Hook f: the novel triptolide analog (5*R*)-5-hydroxytriptolide (LLDT-8). *Acta Pharmacol. Sin.* **33**, 1112–1118 (2012).

136. Qiu, D. & Kao, P. N. Immunosuppressive and anti-inflammatory mechanisms of triptolide, the principal active diterpenoid from the Chinese medicinal herb *Tripterygium wilfordii* Hook. f. *Drugs R D* **4**, 1–18 (2003).

137. Chen, S.-R., Dai, Y., Zhao, J., Lin, L., Wang, Y. & Wang, Y. A mechanistic overview of triptolide and celastrol, natural products from *Tripterygium wilfordii* Hook F. *Front. Pharmacol.* **9**, 104 (2018).

138. Zhang, Y., Mao, X., Li, W., Chen, W., Wang, X., Ma, Z. & Lin, N. *Tripterygium wilfordii*: an inspiring resource for rheumatoid arthritis treatment. *Med. Res. Rev.* **41**, 1337–1374 (2021).

139. Sundrud, M. S., Koralov, S. B., Feuerer, M., Calado, D. P., Kozhaya, A. E., Rhule-Smith, A., Lefebvre, R. E., Unutmaz, D., Mazitschek, R., Waldner, H., Whitman, M., Keller, T. & Rao, A. Halofuginone inhibits TH17 cell differentiation by activating the amino acid starvation response. *Science* **324**, 1334–1338 (2009).

140. Park, M.-K., Park, J.-S., Park, E.-M., Lim, M.-A., Kim, S.-M., Lee, D.-G., Baek, S.-Y., Yang, E.-J., Woo, J.-W., Lee, J., Kwok, S.-K., Kim, H.-Y., Cho, M.-L. & Park, S.-H. Halofuginone ameliorates autoimmune arthritis in mice by regulating the balance between Th17 and Treg cells and inhibiting osteoclastogenesis. *Arthritis Rheumatol.* **66**, 1195–1207 (2014).

141. Pines, M. & Spector, I. Halofuginone – the multifaceted molecule. *Molecules* **20**, 573–594 (2015).

142. Carlson, T. J., Pellerin, A., Djuretic I. M., Trivigno, C., Koralov, S. B., Rao, A. & Sundrud, M. S. Halofuginone-induced amino acid starvation regulates Stat3-dependent Th17 effector function and reduces established autoimmune inflammation. *J. Immunol.* **192**, 2167–2176 (2014).

143. Giorgi, V., Marotto, D., Batticciotto, A., Atzeni, F., Bongiovanni, S. & Sarzi-Puttini, P. Cannabis and autoimmunity: possible mechanisms of action. *ImmunoTargets Ther.* **10**, 261–271 (2021).

144. Katz, D., Katz, I., Porat-Katz, B. S. & Shoenfeld, Y. Medical cannabis: another piece in the mosaic of autoimmunity? *Clin. Pharmacol. Ther.* **101**, 230–238 (2017).

145. Rosenblum, M. D., Remedios, K. A. & Abbas, A. K. Mechanisms of human autoimmunity. *J. Clin. Invest.* **125**, 2228–2233 (2015).

146. Chandrashekara, S. The treatment strategies of autoimmune disease may need a different approach from conventional protocol: a review. *Indian J. Pharmacol.* **44**, 665–671 (2012).

147. Feldmann, M. & Steinman, L. Design of effective immunotherapy for human autoimmunity. *Nature* **435**, 612–619 (2005).

148. Her, M. & Kavanaugh, A. Alterations in immune function with biologic therapies for autoimmune disease. *J. Allergy Clin. Immunol.* **137**, 19–27 (2016).

149. Samotij, D. & Reich, A. Biologics in the treatment of lupus erythematosus: a critical literature review. *Biomed Res. Int.* **2019**, 8142368 (2019).

150. Balagué, C., Kunkel, S. L. & Godessart, N. Understanding autoimmune disease: new targets for drug discovery. *Drug Discov. Today* **14**, 926–934 (2009).

151. Ramsay, R. R., Popovic-Nikolic, M. R., Nikolic, K., Uliassi, E. & Bolognesi, M. L. A perspective on multi-target drug discovery and design for complex diseases. *Clin. Transl. Med.* **7**, 3 (2018).

152. T. Virtanen, A., Haikarainen, T., Raivola, J. & Silvennoinen, O. Selective JAKinibs: prospects in inflammatory and autoimmune diseases. *BioDrugs* **33**, 15–32 (2019).

153. Perry, M. W. D., Abdulai, R., Mogemark, M., Petersen, J., Thomas, M. J., Valastro, B. & Westin Eriksson, A. Evolution of PI3Kγ and δ inhibitors for inflammatory and autoimmune diseases. *J. Med. Chem.* **62**, 4783–4814 (2019).

154. Brzezicka, K. A. & Paulson, J. C. Impact of siglecs on autoimmune diseases. *Mol. Aspects Med.* **90**, 101140 (2023).

155. Fugger, L., Jensen, L. T. & Rossjohn, J. Challenges, progress, and prospects of developing therapies to treat autoimmune diseases. *Cell* **181**, 63–80 (2020).

156. Qing, C. The molecular biology in wound healing & non-healing wound. *Chinese J. Traumatol.* **20**, 189–193 (2017).

157. Ellis, S., Lin, E. J. & Tartar, D. Immunology of wound healing. *Curr. Dermatol. Rep.* **7**, 350–358 (2018).

158. Kaplani, K., Koutsi, S., Armenis, V., Skondra, F. G., Karantzelis, N., Champeris Tsaniras, S. & Taraviras, S. Wound healing related agents: ongoing research and perspectives. *Adv. Drug Deliv. Rev.* **129**, 242–253 (2018).

159. Sorg, H., Tilkorn, D. J., Hager, S., Hauser, J. & Mirastschijski, U. Skin wound healing: an update on the current knowledge and concepts. *Eur. Surg. Res.* **58**, 81–94 (2017).

160. Han, G. & Ceilley, R. Chronic wound healing: a review of current management and treatments. *Adv. Ther.* **34**, 599–610 (2017).

161. Dong, R. & Guo, B. Smart wound dressings for wound healing. *Nano Today* **41**, 101290 (2021).

162. Dreifke, M. B., Jayasuriya, A. A. & Jayasuriya, A. C. Current wound healing procedures and potential care. *Mater. Sci. Eng. C* **48**, 651–662 (2015).

163. Nicholas, M. N. & Yeung, J. Current status and future of skin substitutes for chronic wound healing. *J. Cutan. Med. Surg.* **21**, 23–30 (2017).

164. Proschak, E., Stark, H. & Merk, D. Polypharmacology by design: a medicinal chemist's perspective on multitargeting compounds. *J. Med. Chem.* **62**, 420–444 (2019).

165. Hou, M., Wei, Y., Zhao, Z., Han, W., Zhou, R., Zhou, Y., Zheng, Y. & Yin, L. Immuno-engineered nanodecoys for the multi-target anti-inflammatory treatment of autoimmune diseases. *Adv. Mater.* **34**, 2108817 (2022).

166. Meier, K. & Nanney, L. B. Emerging new drugs for wound repair. *Expert Opin. Emerg. Drugs* **11**, 23–37 (2006).

167. Wainwright, C. L., Teixeira, M. M., Adelson, D. L., Buenz, E. J., David, B., Glaser, K, B., Harata-Lee, Y., Howes, M.-J. R., Izzo, A. A., Maffia, P., Mayer, A. M. S., Mazars, C., Newman, D. J., Lughadha, E. N., Pimenta, A. M. C., Parra, J. A. A., Qu, Z., Shen, H., Spedding, M. & Wolfender, J.-L. Future directions for the discovery of natural product-derived immunomodulating drugs: an IUPHAR positional review. *Pharmacol. Res.* **177**, 106076 (2022).

168. Tian, X. & Liu, L. Drug discovery enters a new era with multi-target intervention strategy. *Chin. J. Integr. Med.* **18**, 539–542 (2012).

169. Rather, M. A., Bhat, B. A. & Qurishi, M. A. Multicomponent phytotherapeutic approach gaining momentum: is the "one drug to fit all" model breaking down? *Phytomedicine* **21**, 1–14 (2013).

170. Comino-Sanz, I. M., López-Franco, M. D., Castro, B. & Pancorbo-Hidalgo, P. L. The role of antioxidants on wound healing: a review of the current evidence. *J. Clin. Med.* **10**, 3558 (2021).

171. Newman, D. J. & Cragg, G. M. Natural products as sources of new drugs over the nearly four decades from 01/1981 to 09/2019. *J. Nat. Prod.* **83**, 770–803 (2020).

172. Atanasov, A. G., Zotchev, S. B., Dirsch, V. M. & Supuran, C. T. Natural products in drug discovery: advances and opportunities. *Nat. Rev. Drug Discov.* **20**, 200–216 (2021).

173. Holt, C. D. Overview of immunosuppressive therapy in solid organ transplantation. *Anesthesiol. Clin.* **35**, 365–380 (2017).

174. Bedi, D. S., Riella, L. V., Tullius, S. G. & Chandraker, A. Animal models of chronic allograft injury: contributions and limitations to understanding the mechanism of long-term graft dysfunction. *Transplantation* **90**, 935–944 (2010).

175. Choudhary, N., Bhatt, L. K. & Prabhavalkar, K. S. Experimental animal models for rheumatoid arthritis. *Immunopharmacol. Immunotoxicol.* **40**, 193–200 (2018).

176. Kipp, M., van der Star, B., Vogel, D. Y. S., Puentes, F., van der Valk, P., Baker, D. & Amor, S. Experimental *in vivo* and *in vitro* models of multiple sclerosis: EAE and beyond. *Mult. Scler. Relat. Disord.* **1**, 15–28 (2012).

177. Niehues, H. & van den Bogaard, E. H. Past, present and future of *in vitro* 3D reconstructed inflammatory skin models to study psoriasis. *Exp. Dermatol.* **27**, 512–519 (2018).

178. Sarama, R., Matharu, P. K., Abduldaiem, Y., Corrêa, M, P., Gil, C. D. & Greco, K. V. *In vitro* disease models for understanding psoriasis and atopic dermatitis. *Front. Bioeng. Biotechnol.* **10**, 251 (2022).

179. Potterat, O. & Hamburger, M. Concepts and technologies for tracking bioactive compounds in natural product extracts: generation of libraries, and hyphenation of analytical processes with bioassays. *Nat. Prod. Rep.* **30**, 546–564 (2013).

180. Potterat, O. & Hamburger, M. Combined use of extract libraries and HPLC-based activity profiling for lead discovery: potential, challenges, and practical considerations. *Planta Med.* **80**, 1171–1181 (2014).

181. Hubert, J., Nuzillard, J.-M. & Renault, J.-H. Dereplication strategies in natural product research: how many tools and methodologies behind the same concept? *Phytochem. Rev.* **16**, 55–95 (2017).

182. Hell, T., Rutz, A., Dürr, L., Dobrzyński, M., Reinhardt, J. K., Lehner, T., Keller, M., John, A., Gupta, M., Pertz, O., Hamburger, M., Wolfender, J.-L. & Garo, E. Combining activity profiling with advanced annotation to accelerate the discovery of natural products targeting oncogenic signaling in melanoma. *J. Nat. Prod.* **2022**, 1540–1554 (2022).

183. Allard, P.-M., Péresse, T., Bisson, J., Gindro, K., Marcourt, L., Pham, V. C., Roussi, F., Litaudon, M. & Wolfender, J.-L. Integration of molecular networking and *in-silico* MS/MS fragmentation for natural products dereplication. *Anal. Chem.* **88**, 3317–3323 (2016).

184. Nothias, L.-F., Nothias-Esposito, M., da Silva, R., Wang, M., Protsyuk, I., Zhang, Z., Sarvepalli, A., Leyssen. P., Touboul, D., Costa, J., Paolini, J., Alexandrov, T., Litaudon, M. & Dorrestein, P. C. Bioactivity-based molecular networking for the discovery of drug leads in natural product bioassay-guided fractionation. *J. Nat. Prod.* **81**, 758–767 (2018).

185. Wolfender, J.-L., Litaudon, M., Touboul, D. & Queiroz, E. F. Innovative omics-based approaches for prioritisation and targeted isolation of natural products – new strategies for drug discovery. *Nat. Prod. Rep.* **36**, 855–868 (2019).

186. Wolfender, J.-L., Nuzillard, J.-M., van der Hooft, J. J. J., Renault, J.-H. & Bertrand, S. Accelerating metabolite identification in natural product research: toward an ideal combination of liquid chromatography-high-resolution tandem mass spectrometry and NMR profiling, *in silico* databases, and chemometrics. *Anal. Chem.* **91**, 704–742 (2019).

187. Falanga, C. M., Steinborn C., Muratspahić, E., Zimmermann-Klemd, A. M., Winker, M., Krenn, L., Huber, R., Gruber, C. W. & Gründemann, C. Ipecac root extracts and isolated circular peptides differentially suppress inflammatory immune response characterised by proliferation, activation and degranulation capacity of human lymphocytes *in vitro*. *Biomed. Pharmacother.* **152**, 113120 (2022).

188. Reinhardt, J. K., Klemd, A. M., Danton, O., De Mieri, M., Smieško, M., Huber, R., Bürgi, T., Gründemann, C. & Hamburger, M. Sesquiterpene lactones from *Artemisia argyi*: absolute configuration and immunosuppressant activity. *J. Nat. Prod.* **82**, 1424–1433 (2019).

189. Zimmermann-Klemd, A. M., Reinhardt, J. K., Morath, A., Schamel, W. W., Steinberger, P., Leitner, J., Huber, R., Hamburger, M. & Gründemann, C. Immunosuppressive activity of *Artemisia argyi* extract and isolated compounds. *Front. Pharmacol.* **11**, 402 (2020).

190. von Schönfeld, C., Huber, R., Trittler, R., Kammerer, B., Garcia-Käufer, M. & Gründemann, C. Rosemary has immunosuppressant activity mediated through the STAT3 pathway. *Complement. Ther. Med.* **40**, 165–170 (2018).

191. Chilczuk, T., Steinborn, C., Breinlinger S., Zimmermann-Klemd, A. M., Huber, R., Enke, H., Enke, D., Niedermeyer, T. H. J. & Gründemann, C. Hapalindoles from the cyanobacterium *Hapalosiphon* sp. inhibit T cell proliferation. *Planta Med.* **86**, 96–103 (2020).

192. Syafni, N., Devi, S., Zimmermann-Klemd, A. M., Reinhardt, J. K., Danton, O., Gründemann, C. & Hamburger, M. Immunosuppressant flavonoids from *Scutellaria baicalensis*. *Biomed. Pharmacother.* **144**, 112326 (2021).

193. Reinhardt, J. K., Zimmermann-Klemd, A. M., Danton, O., Smieško, M., Gründemann, C. & Hamburger, M. Compounds from *Toddalia asiatica*: immunosuppressant activity and absolute configurations. *J. Nat. Prod.* **83**, 3012–3020 (2020).

194. Devi, S., Zimmermann-Klemd, A. M., Fiebich, B. L., Heinrich, M., Gründemann, C., Steinberger, P., Kowarschik, S. & Huber, R. Immunosuppressive activity of non-psychoactive *Cannabis sativa* L. extract on the function of human T lymphocytes. *Int. Immunopharmacol.* **103**, 108448 (2022).

195. Gründemann, C., Stenberg, K. G. & Gruber, C. W. T20K: an immunomodulatory cyclotide on its way to the clinic. *Int. J. Pept. Res. Ther.* **25**, 9–13 (2019).

196. Gründemann, C. *Viola tricolor* as phytomedicine for treating ulcerative colitis. Available at: https://pharma.unibas.ch/de/research/research-groups/translational-complementary-medicine/research/viola-tricolor-as-phytomedicine-for-treating-ulcerative-colitis/. (Accessed: 1st May 2023)

197. Bochénska, K., Smolińska, E., Moskot, M., Jakóbkiewicz-Banecka, J. & Gabig-Cimińska, M. Models in the research process of psoriasis. *Int. J. Mol. Sci.* **18**, 2514 (2017).

198. Saelee, C., Thongrakard, V. & Tencomnao, T. Effects of Thai medicinal herb extracts with anti-psoriatic activity on the expression on NF-κB signaling biomarkers in HaCat keratinocytes. *Molecules* **16**, 3908–3932 (2011).

199. Wedler, J., Rusanov, K., Atanassov, I. & Butterweck, V. A polyphenol-enriched fraction of rose oil distillation wastewater inhibits cell proliferation, migration and TNF-α-induced VEGF secretion in human immortalized keratinocytes. *Planta Med.* **82**, 1000–1008 (2016).

200. Gendrisch, F., Haarhaus, B., Krieger, N., Quirin, K.-W., Schempp C. M. & Wölfle, U. The effect of herbal medicinal products on psoriasis-like keratinocytes. *Biomolecules* **11**, 371 (2021).

201. Herman, A. & Herman, A. P. Topically used herbal products for the treatment of psoriasis – mechanism of action, drug delivery, clinical studies. *Planta Med.* **82**, 1447–1455 (2016).

202. Rasool, R., Ullah, I., Shahid, S., Mubeen, B., Imam, S. S., Alshehri, S., Ghoneim, M. M., Alzarea, S. I., Murtaza, B. N., Nadeem, M. S. & Kazmi, I. *In vivo* assessment of the ameliorative impact of some medicinal plant extracts on lipopolysaccharide-induced multiple sclerosis in wistar rats. *Molecules* **27**, 1608 (2022).

203. Stojanović, I., Šavikin, K., Đedović, N., Živković, J., Saksida, T., Momčilović, M., Koprivica, I., Vujičić, M., Stanisavljević, S., Miljković, Đ. & Menković, N. Pomegranate peel extract ameliorates autoimmunity in animal models of multiple sclerosis and type 1 diabetes. *J. Funct. Foods* **35**, 522–530 (2017).

204. Furgiuele, A., Cosentino, M., Ferrari, M. & Marino, F. Immunomodulatory potential of cannabidiol in multiple sclerosis: a systematic review. *J. Neuroimmune Pharmacol.* **16**, 251–269 (2021).

205. Deligiannidou, G.-E., Gougoula, V., Bezirtzoglou, E., Kontogiorgis, C. & Constantinides, T. K. The role of natural products in rheumatoid arthritis: current knowledge of basic *in vitro* and *in vivo* research. *Antioxidants* **10**, 599 (2021).

206. Krishnan, P. The scientific study of herbal wound healing therapies: current state of play. *Curr. Anaesth. Crit. Care* **17**, 21–27 (2006).

207. Ab Rahman, M. R., Abdul Razak, F. & Mohd Bakri, M. Evaluation of wound closure activity of *Nigella sativa*, *Melastoma malabathricum*, *Pluchea indica*, and *Piper sarmentosum* extracts on scratched monolayer of human gingival fibroblasts. *Evidence-based Complement. Altern. Med.* **2014**, (2014).

208. Zimmermann-Klemd, A. M., Konradi, V., Steinborn, C., Ücker, A., Falanga, C. M., Woelfle, U., Huber, R., Jürgenliemk, G., Rajbhandari, M. & Gründemann, C. Influence of traditionally used Nepalese plants on wound healing and immunological properties using primary human cells *in vitro*. *J. Ethnopharmacol.* **235**, 415–423 (2019).

209. Wedler, J., Daubitz, T., Schlotterbeck, G. & Butterweck, V. *In vitro* anti-inflammatory and wound-healing potential of a *Phyllostachys edulis* leaf extract – identification of isoorientin as an active compound. *Planta Med.* **80**, 1678–1684 (2014).

210. Verjee, S., Garo, E., Pelaez, S., Fertig, O., Hamburger, M. & Butterweck, V. Saffron flower extract promotes scratch wound closure of keratinocytes and enhances VEGF production. *Planta Med.* **83**, 1176–1183 (2017).

211. Kimura, Y., Sumiyoshi, M., Samukawa, K., Satake, N. & Sakanaka, M. Facilitating action of asiaticoside at low doses on burn wound repair and its mechanism. *Eur. J. Pharmacol.* **584**, 415–423 (2008).

212. Ud-Din, S. & Bayat, A. Non-animal models of wound healing in cutaneous repair: *in silico*, *in vitro*, *ex vivo*, and *in vivo* models of wounds and scars in human skin. *Wound Repair Regen.* **25**, 164–176 (2017).

213. Wilhelm, K.-P., Wilhelm, D. & Bielfeldt, S. Models of wound healing: an emphasis on clinical studies. *Ski. Res. Technol.* **23**, 3–12 (2017).

214. Masson-Meyers, D. S., Andrade, T. A. M., Caetano, G. F., Guimaraes, F. R., Leite, M. N., Leite, S. N. & Frade, M. A. C. Experimental models and methods for cutaneous wound healing assessment. *Int. J. Exp. Pathol.* **101**, 21–37 (2020).

215. Graves, N., Phillips, C. J. & Harding, K. A narrative review of the epidemiology and economics of chronic wounds. *Br. J. Dermatol.* **187**, 141–148 (2022).

216. Whittam, A. J., Maan, Z. N., Duscher, D., Wong, V. W., Barrera, J. A., Januszyk, M. & Gurtner, G. C. Challenges and opportunities in drug delivery for wound healing. *Adv. Wound Care* **5**, 79–88 (2016).

217. Zhang, J., Zhou, Y. & Ma, Z. Multi-target mechanism of *Tripteryguim wilfordii* Hook for treatment of ankylosing spondylitis based on network pharmacology and molecular docking. *Ann. Med.* **53**, 1090–1098 (2021).

218. Li, J.-W. Multi-target therapy for autoimmune hemolytic anemia under the guidance of traditional Chinese medicine pharmacology. *TMR Theory Hypoth.* **4**, 505–510 (2021).

219. Wang, Y., Fan, X., Qu, H., Gao, X. & Cheng, Y. Strategies and techniques for multi-component drug design from medicinal herbs and traditional Chinese medicine. *Curr. Top. Med. Chem.* **12**, 1356–1362 (2012).

220. Makhoba, X. H., Viegas, C., Mosa, R. A., Viegas, F. P. D. & Pooe, O. J. Potential impact of the multi-target drug approach in the treatment of some complex diseases. *Drug Des. Devel. Ther.* **14**, 3235–3249 (2020).

221. Zhou, X., Seto, S. W., Chang, D., Kiat, H., Razmovski-Naumovski, V., Chan, K. & Bensoussan, A. Synergistic effects of Chinese herbal medicine: a comprehensive review of methodology and current research. *Front. Pharmacol.* **7**, 201 (2016).

222. Bhuyan, D. J., Perera, S., Kaur, K., Alsherbiny, M. A., Low, M., Seto, S.-W., Li, C.-G. & Zhou, X. Synergistic effects of Chinese herbal medicine and biological networks. in *Approaching Complex Diseases, Human Perspectives in Health Sciences and Technology* 393–436 (Springer, Cham, 2020).

223. Caesar, L. K. & Cech, N. B. Synergy and antagonism in natural product extracts: when 1 + 1 does not equal 2. *Nat. Prod. Rep.* **36**, 869–888 (2019).

224. Wagner, H. & Ulrich-Merzenich, G. Synergy research: approaching a new generation of phytopharmaceuticals. *Phytomedicine* **16**, 97–110 (2009).

225. Ulrich-Merzenich, G., Panek, D., Zeitler, H., Wagner, H. & Vetter, H. New perspectives for synergy research with the "omic"-technologies. *Phytomedicine* **16**, 495–508 (2009).

226. Zulkefli, N., Che Zahari, C. N. M., Sayuti, N. H., Kamarudin, A. A., Saad, N., Hamezah, H. S., Bunawan, H., Baharum, S. N., Mediani, A., Ahmed, Q. U., Ismail, A. F. H. & Sarian, M. N. Flavonoids as potential wound-healing molecules: emphasis on pathways perspective. *Int. J. Mol. Sci.* **24**, 4607 (2023).

227. Aslam, M. S., Ahmad, M. S., Riaz, H., Raza, S. A., Hussain, S., Qureshi, O. S., Maria, P., Hamzah, Z. & Javed, O. Role of flavonoids as wound healing agent. in *Phytochemicals - Source of Antioxidants and Role in Disease Prevention* 95–102 (InTech, London, 2018).

228. Carvalho, M. T. B., Araújo-Filho, H. G., Barreto, A. S., Quintans-Júnior, L. J., Quintans, J. S. S. & Barreto, R. S. S. Wound healing properties of flavonoids: a systematic review highlighting the mechanisms of action. *Phytomedicine* **90**, 153636 (2021).

229. Croston, G. E. The utility of target-based discovery. *Expert Opin. Drug Discov.* **12**, 427–429 (2017).

230. Swinney, D. C. Phenotypic *vs.* target-based drug discovery for first-in-class medicines. *Clin. Pharmacol. Ther.* **93**, 299–301 (2013).

231. Quartier, J., Capony, N., Lapteva, M. & Kalia, Y. N. Cutaneous biodistribution: a high-resolution methodology to assess bioequivalence in topical skin delivery. *Pharmaceutics* **11**, (2019).

232. Quartier, J., Rao, W., Slade, S., Métral, F., Lapteva, M. & Kalia, Y. N. DESI-MS imaging to visualize spatial distribution of xenobiotics and endogenous lipids in the skin. *Int. J. Pharm.* **607**, 120967 (2021).

Appendix

Aryltetralin lignans from *Hyptis brachiata* inhibiting T lymphocyte proliferation

Morris Keller[1#], Moritz Winker[2#], Amy Marisa Zimmermann-Klemd[2], Nino Sperisen[1], Mahabir P. Gupta[3], Pablo N. Solis[3], Matthias Hamburger[1], Olivier Potterat[1*], Carsten Gründemann[2*]

1 Division of Pharmaceutical Biology, University of Basel, Klingelbergstrasse 50, CH-4056 Basel, Switzerland

2 Translational Complementary Medicine, Department of Pharmaceutical Sciences, University of Basel, Campus Rosental – Mattenstrasse 22, CH-4058 Basel, Switzerland

3 Centro de Investigaciones Farmacognosticas de la Flora Panamena (CIFLORPAN), Facultad de Farmacia, Universidad de Panama, Panama City, Republic of Panama

# These authors contributed equally to the work

Corresponding authors:

Prof. Olivier Potterat
olivier.potterat@unibas.ch
Tel. +41 612071534
Fax. +41 612071474
Orcid.org/0000-0001-5962-6516

Prof. Carsten Gründemann
carsten.gruendemann@unibas.ch
Tel.: +41 61 207 61 84
Orcid.org/ 0000-0003-0240-0342

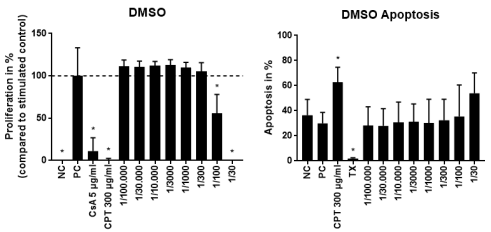

Figure S 1. Evaluation of DMSO vehicle control.

Effect of the DMSO vehicle control on T lymphocyte proliferation and apoptosis induction. In the experiments primary human lymphocytes were stained either with CFSE or Annexin V-FITC stainings. Lymphocytes were stimulated with anti-CD3 and anti-CD28 mAbs (except the unstimulated control) and incubated for 72 h in the presence of medium (unstimulated (unstim), stimulated (stim)), cyclosporine A (CsA), camptothecin (CPT) or triton-x100 (TX), or different dilutions of DMSO. Viability was assessed by microplate reader; proliferation and apoptosis/necrosis induction were analyzed by flow cytometry. Only the viability and proliferation results were normalized to stimulated control. Results are depicted as mean ± standard deviation. *$p < 0.05$. The Shapiro-Wilk test was used to test for a normal distribution. A multiple group comparison was performed with the Brown-Forsythe and Welch ANOVA, followed by Dunnet´s T3 post-hoc test.

Table S 2. Physicochemical data of **1**.

4'-demethyldeoxypodophyllotoxin

$C_{21}H_{20}O_7$, M = 384.38 g/mol, white amorphous powder

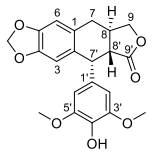

ESIMS (pos. & neg. mode): *m/z* 384.7 $[M+H]^+$, 383.2 $[M-H]^-$

$[\alpha]_D^{25}$ -112 (c 0.1, $CHCl_3$) [1,2]

^1H and ^{13}C NMR Spectroscopic Data (DMSO-d_6; 500 MHz for ^1H and 126 MHz for ^{13}C NMR; δ in ppm) [2,3]

position	δ_C, type	δ_H (*J* in Hz)
1	129.0, C	-
2	131.0, C	-
3	110.0, CH	6.50, s
4	146.2, C	-
4,5-OCH_2	100.9, CH_2	5.95, s 5.97, s
5	145.8, C	-
6	108.5, CH[a]	6.80, s
7	32.0, CH_2	2.73, dd (15.8, 12.5) 3.01, dd (15.8, 5.0)
8	32.5, CH	2.60, m
9	71.5, CH_2	3.94, dd (10.2, 8.7) 4.40, t (7.6, 7.6)
1'	131.4, C	-
2'	108.5, CH[a]	6.25, s[a]
3'	147.1, C[a]	-
3'-OMe	56.0, CH_3[a]	3.62, s[a]
4'	134.6, C	-
4'-OH	-	8.27, br s
5'	147.1, C[a]	-
5'-OMe	56.0, CH_3[a]	3.62, s[a]
6'	108.5, CH[a]	6.25, s[a]
7'	42.8, CH	4.46, d (4.9)
8'	46.3, CH	2.93, dd (13.7, 4.9)
9'	175.1, C	-

[a]Overlapping signals.

Table S 3. Physicochemical data of **2**.

***β*-peltatin,** $C_{22}H_{22}O_8$, M = 414.41 g/mol, white amorphous powder

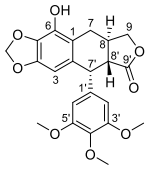

ESIMS (pos. & neg. mode): *m/z* 414.7 $[M+H]^+$, 413.0 $[M-H]^-$

$[\alpha]_D^{25}$ -31 (c 0.1, $CHCl_3$) [4,5]

^1H and ^{13}C NMR Spectroscopic Data ($CDCl_3$; 500 MHz for ^1H and 126 MHz for ^{13}C NMR; δ in ppm) [6,7]

position	δ_C, type	δ_H (*J* in Hz)
1	118.3, C	-
2	132.0, C	-
3	103.8, CH	6.25, s
4	147.4, C	-
4,5-OCH_2	101.9, CH_2	5.96, dd (5.0, 1.4)
5	133.2, C	-
6	137.0, C	-
7	27.1, CH_2	2.52, dd (16.2, 10.4) 3.22, dd (16.2, 5.0)
8	32.4, CH	2.69, dtdd (13.4, 10.4, 10.4, 6.7)[a]
9	72.6, CH_2	3.97, dd (10.4, 8.8) 4.50, dd (8.8, 6.7)
1’	136.5, C	-
2’	108.4, CH[a]	6.37, s[a]
3’	152.7, C[a]	-
3’-OMe	56.5, CH_3[a]	3.77, s[a]
4’	137.3, C	-
4’-OMe	61.0, CH_3	3.81, s
5’	152.7, C[a]	-
5’-OMe	56.5, CH_3[a]	3.77, s[a]
6’	108.4, CH[a]	6.37, s[a]
7’	44.1, CH	4.61, d (4.3)
8’	47.6, CH	2.71, dd (13.4, 4.3)[a]
9’	175.3, C	-

[a]Overlapping signals.

Table S 4. Physicochemical data of **3**.

deoxypicropodophyllin

$C_{22}H_{22}O_7$, M = 398.41 g/mol, white amorphous powder

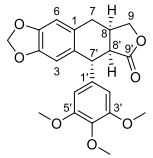

ESIMS (pos. mode): *m/z* 398.7 $[M+H]^+$, 420.7 $[M+Na]^+$

$[\alpha]_D^{25}$ +24 (c 0.1, $CHCl_3$) [8]

^1H and ^{13}C NMR Spectroscopic Data ($CDCl_3$; 500 MHz for ^1H and 126 MHz for ^{13}C NMR; δ in ppm) [8]

position	δ_C, type	δ_H (*J* in Hz)
1	128.5, C	-
2	130.7, C	-
3	110.1, CH	6.59, s
4	147.0, C	-
4,5-OCH_2	101.2, CH_2	5.93, d (1.5) 5.96, d (1.5)
5	147.1, C	-
6	109.0, CH	6.68, s
7	32.3, CH_2	2.50, dd (15.3, 5.5) 2.87, dd (15.3, 6.3)
8	33.2, CH	3.03, ddddd (9.8, 7.3, 6.3, 5.5, 3.2)
9	73.0, CH_2	3.98, dd (9.3, 3.2) 4.46, dd (9.3, 7.3)
1’	138.4, C	-
2’	105.1, CH[a]	6.34, s[a]
3’	153.6, C[a]	-
3’-OMe	56.4, CH_3[a]	3.79, s[a]
4’	136.9, C	-
4’-OMe	61.1, CH_3	3.84, s
5’	153.6, C[a]	-
5’-OMe	56.4, CH_3[a]	3.79, s[a]
6’	105.1, CH[a]	6.34, s[a]
7’	45.5, CH	4.38, d (3.1)
8’	46.6, CH	3.35, dd (9.8, 3.1)
9’	178.6, C	-

[a]Overlapping signals.

Table S 5. Physicochemical data of **4**.

(-)-isodeoxypodophyllotoxin

$C_{22}H_{22}O_7$, M = 398.41 g/mol, white amorphous powder

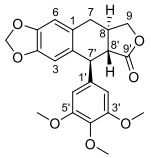

ESIMS (pos. mode): *m/z* 398.7 $[M+H]^+$, 420.7 $[M+Na]^+$

$[\alpha]_D^{25}$ -39 (c 0.1, $CHCl_3$) [9,10]

^1H and ^{13}C NMR Spectroscopic Data ($CDCl_3$; 500 MHz for ^1H and 126 MHz for ^{13}C NMR; δ in ppm) [9,11–13]

position	δ_C, type	δ_H (*J* in Hz)
1	128.0, C	-
2	132.5, C	-
3	110.2, CH	6.35, s
4	146.9, C	-
4,5-OCH_2	101.3, CH_2	5.90, d (6.7)
5	146.7, C	-
6	108.7, CH	6.61, s
7	33.2, CH_2	2.96, tdd (15.0, 15.0, 11.6, 5.2)
8	40.3, CH	2.61, ddddd (13.4, 11.6, 10.0, 7.0, 5.2)
9	71.2, CH_2	4.00, dd (10.0, 8.0) 4.53, dd (8.0, 7.0)
1’	138.9, C	-
2’	106.7, CH[a]	6.42, s[a]
3’	153.4, C[a]	-
3’-OMe	56.4, CH_3[a]	3.83, s[a]
4’	137.1, C	-
4’-OMe	61.1, CH_3	3.86, s
5’	153.4, C[a]	-
5’-OMe	56.4, CH_3[a]	3.83, s[a]
6’	106.7, CH[a]	6.42, s[a]
7’	46.9, CH	4.06, d (11.0)
8’	48.9, CH	2.54, dd (13.4, 11.0)
9’	175.6, C	-

[a]Overlapping signals.

Table S 6. Physicochemical data of **5**.

(-)-podophyllotoxin

$C_{22}H_{22}O_8$, M = 414.41 g/mol, white-yellowish amorphous powder

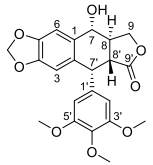

ESIMS (pos. & neg. mode): *m/z* 414.8 $[M+H]^+$, 396.7 $[M-H_2O]^+$, 395.0 $[M-H_2O-H]^-$, 459.0 $[M+FA-H]^-$ [14]

$[\alpha]_D^{25}$ -75 (c 0.1, $CHCl_3$) [8]

^1H and ^{13}C NMR Spectroscopic Data (DMSO-d_6; 500 MHz for ^1H and 126 MHz for ^{13}C NMR; δ in ppm) [15]

position	δ_C, type	δ_H (*J* in Hz)
1	135.0, C	-
2	130.7, C	-
3	109.1, CH	6.47, s
4	146.5, C	-
4,5-OCH_2	101.0, CH_2	5.99, dd (11.0, 0.6)
5	146.6, C	-
6	106.4, CH	7.10, s
7	70.6, CH	4.62, d (9.8)
8	40.4, CH	2.60, m
9	71.1, CH_2	4.09, dd (10.6, 8.2) 4.48, t (8.2, 8.2)[a]
1’	136.6, C	-
2’	108.4, CH[a]	6.33, s[a]
3’	151.9, C[a]	-
3’-OMe	55.9, CH_3[a]	3.64, s[a]
4’	136.4, C	-
4’-OMe	59.9, CH_3	3.62, s
5’	151.9, C[a]	-
5’-OMe	55.9, CH_3[a]	3.64, s[a]
6’	108.4, CH[a]	6.33, s[a]
7’	43.4, CH	4.49, d (5.0)[a]
8’	44.1, CH	3.15, dd (14.3, 5.0)
9’	174.7, C	-

[a]Overlapping signals.

Table S 7. Physicochemical data of **6**.

6-methoxyepipodophyllotoxin

$C_{23}H_{24}O_9$, M = 444.44 g/mol, white-yellowish amorphous powder

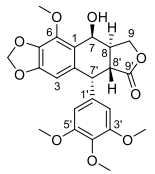

ESIMS (pos. & neg. mode): *m/z* 444.7 $[M+H]^+$, 426.7 $[M-H_2O]^+$, 443.1 $[M-H]^-$

$[\alpha]_D^{25}$ -15 (c 0.1, $CHCl_3$) [16]

^1H and ^{13}C NMR Spectroscopic Data (DMSO-d_6; 500 MHz for ^1H and 126 MHz for ^{13}C NMR; δ in ppm) [16]

position	δ_C, type	δ_H (*J* in Hz)
1	125.8, C	-
2	132.4, C	-
3	104.2, CH	6.25, s
4	148.8, C	-
4,5-OCH_2	101.2, CH_2	5.99, dd (4.9, 0.6)
5	135.4, C	-
6	141.3, C	-
6-OMe	59.8, CH_3	3.98, s
7	59.4, CH	5.03, br s
7-OH	-	[b]
8	38.5, CH	2.69, dddd (14.3, 10.5, 8.2, 3.3)
9	67.7, CH_2	4.16, dd (10.5, 8.2) 4.32, t (8.2, 8.2)
1’	136.0, C	-
2’	108.1, CH[a]	6.24, s[a]
3’	151.9, C[a]	-
3’-OMe	55.8, CH_3[a]	3.63, s[a]
4’	136.3, C	-
4’-OMe	59.9, CH_3	3.61, s
5’	151.9, C[a]	-
5’-OMe	55.8, CH_3[a]	3.63, s[a]
6’	108.1, CH[a]	6.24, s[a]
7’	43.3, CH	4.51, d (5.7)
8’	39.5, CH	3.27, dd (14.3, 5.7)
9’	175.0, C	-

[a]Overlapping signals. [b]Signal not visible

Table S 8. Physicochemical data of **7**.

***β*-apopicropodophyllin**

$C_{22}H_{20}O_7$, M = 396.40 g/mol, white amorphous powder

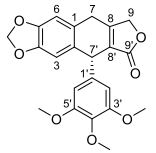

ESIMS (pos. & neg. mode): *m/z* 396.7 $[M+H]^+$, 418.7 $[M+Na]^+$, 395.1 $[M-H]^-$

$[\alpha]_D^{25}$ +60 (c 0.1, $CHCl_3$) [17]

^1H and ^{13}C NMR Spectroscopic Data ($CDCl_3$; 500 MHz for ^1H and 126 MHz for ^{13}C NMR; δ in ppm) [17]

position	δ_C, type	δ_H (*J* in Hz)
1	123.7, C	-
2	129.6, C	-
3	109.5, CH	6.64, s
4	147.2, C	-
4,5-OCH_2	101.3, CH_2	5.96, d (4.3)
5	147.0, C	-
6	107.7, CH	6.73, s
7	29.2, CH_2	3.67, dd (22.0, 3.7) 3.87, dd (22.0, 3.7)
8	157.3, C	-
9	71.0, CH_2	4.83, m[a] 4.90, d (17.1)
1’	138.3, C	-
2’	105.6, CH[a]	6.38, s[a]
3’	153.2, C[a]	-
3’-OMe	56.1, CH_3[a]	3.79, s[a]
4’	137.0, C	-
4’-OMe	60.8, CH_3	3.80, s
5’	153.2, C[a]	-
5’-OMe	56.1, CH_3[a]	3.79, s[a]
6’	105.6, CH[a]	6.38, s[a]
7’	42.7, CH	4.82, m[a]
8’	128.1, C	-
9’	172.2, C	-

[a]Overlapping signals.

Table S 9. Physicochemical data of **8**.

dehydropodophyllotoxin

$C_{22}H_{18}O_8$, M = 410.38 g/mol, white amorphous powder

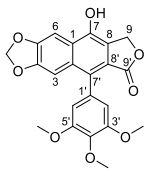

ESIMS (pos. & neg. mode): *m/z* 410.7 $[M+H]^+$, 409.1 $[M-H]^-$, 819.0 $[2M-H]^-$

^1H and ^{13}C NMR Spectroscopic Data (DMSO-d_6; 500 MHz for ^1H and 126 MHz for ^{13}C NMR; δ in ppm) [18,19]

position	δ_C, type	δ_H (*J* in Hz)
1	124.6, C	-
2	130.9, C[a]	-
3	102.6, CH	6.86, s
4	148.8, C	-
4,5-OCH_2	102.0, CH_2	6.17, s
5	148.4, C	-
6	98.1, CH	7.62, s
7	145.4, C	-
7-OH	-	10.44, s
8	122.3, C	-
9	66.6, CH_2	5.36, s
1’	130.9, C[a]	-
2’	107.8, CH[a]	6.53, s[a]
3’	152.4, C[a]	-
3’-OMe	55.9, CH_3[a]	3.73, s[a]
4’	136.8, C	-
4’-OMe	60.1, CH_3	3.77 s
5’	152.4, C[a]	-
5’-OMe	55.9, CH_3[a]	3.73, s[a]
6’	107.8, CH[a]	6.53 s[a]
7’	130.3, C	-
8’	119.1, C	-
9’	169.4, C	-

[a]Overlapping signals.

Table S 10. Physicochemical data of **9**.

dehydro-*β*-peltatin methyl ether

$C_{23}H_{20}O_8$, M = 424.41 g/mol, white amorphous powder

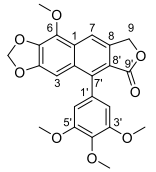

ESIMS (pos. mode): *m/z* 424.7 $[M+H]^+$

^1H and ^{13}C NMR Spectroscopic Data ($CDCl_3$; 500 MHz for ^1H and 126 MHz for ^{13}C NMR; δ in ppm) [9,20]

position	δ_C, type	δ_H (*J* in Hz)
1	129.0, C	-
2	130.4, C	-
3	98.4, CH	6.87, s
4	149.6, C	-
4,5-OCH_2	101.7, CH_2	6.07, s
5	136.1, C	-
6	135.7, C	-
6-OMe	60.1, CH_3	4.23, s
7	114.0, CH	8.17, s
8	139.1, C	-
9	68.3, CH_2	5.40, s
1’	130.5, C	-
2’	107.2, CH[a]	6.54, s[a]
3’	152.9, C[a]	-
3’-OMe	56.1, CH_3[a]	3.85, s[a]
4’	137.7, C	-
4’-OMe	61.0, CH_3	3.97 s
5’	152.9, C[a]	-
5’-OMe	56.1, CH_3[a]	3.85, s[a]
6’	107.2, CH[a]	6.54 s[a]
7’	140.0, C	-
8’	119.2, C	-
9’	169.8, C	-

[a]Overlapping signals.

Table S 11. Physicochemical data of **10**.

6-methoxydehydropodophyllotoxin

$C_{23}H_{20}O_9$, M = 440.40 g/mol, white amorphous powder

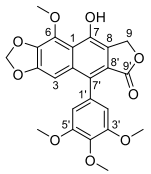

ESIMS (pos. & neg. mode): *m/z* 440.7 $[M+H]^+$, 439.1 $[M-H]^-$

^1H and ^{13}C NMR Spectroscopic Data ($CDCl_3$; 500 MHz for ^1H and 126 MHz for ^{13}C NMR; δ in ppm) [9]

position	δ_C, type	δ_H (*J* in Hz)
1	116.1, C	-
2	132.9, C	-
3	100.1, CH	6.88, s
4	149.1, C	-
4,5-OCH_2	102.0, CH_2	6.08, s
5	135.7, C	-
6	136.5, C	-
6-OMe	61.3, CH_3	4.29, s
7	147.6, C	-
7-OH	-	9.58, s
8	123.3, C	-
9	66.7, CH_2	5.35, s
1’	130.6, C	-
2’	107.6, CH[a]	6.49, s[a]
3’	152.9, C[a]	-
3’-OMe	56.1, CH_3[a]	3.83, s[a]
4’	137.5, C	-
4’-OMe	61.0, CH_3	3.96, s
5’	152.9, C[a]	-
5’-OMe	56.1, CH_3[a]	3.83, s[a]
6’	107.6, CH[a]	6.49, s[a]
7’	130.8, C	-
8’	120.7, C	-
9’	169.8, C	-

[a]Overlapping signals.

Table S 12. Physicochemical data of **11**.

dehydrodesoxypodophyllotoxin

$C_{22}H_{18}O_7$, M = 394.38 g/mol, white amorphous powder

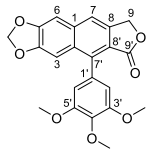

ESIMS (pos. mode): *m/z* 395.6 $[M+H]^+$, 416.6 $[M+Na]^+$

^1H and ^{13}C NMR Spectroscopic Data (DMSO-d_6; 500 MHz for ^1H and 126 MHz for ^{13}C NMR; δ in ppm) [21]

position	δ_C, type	δ_H (*J* in Hz)
1	134.5, C	-
2	129.5, C	-
3	102.7, CH	6.91, s
4	148.7, C	-
4,5-OCH_2	102.5, CH_2	6.19, s
5	150.0, C	-
6	104.1, CH	7.53, s
7	120.0, CH	7.96, s
8	140.5, C	-
9	68.4, CH_2	5.44, d (0.5)
1’	130.6, C	-
2’	107.7, CH[a]	6.59, s[a]
3’	152.9, C[a]	-
3’-OMe	56.4, CH_3[a]	3.74, s[a]
4’	137.4, C	-
4’-OMe	60.5, CH_3	3.78 s
5’	152.9, C[a]	-
5’-OMe	56.4, CH_3[a]	3.74, s[a]
6’	107.7, CH[a]	6.59 s[a]
7’	139.4, C	-
8’	118.8, C	-
9’	169.5, C	-

[a]Overlapping signals.

Table S 13. Physicochemical data of **12**.

4'-demethyldehydropodophyllotoxin

$C_{21}H_{16}O_8$, M = 396.35 g/mol, white-brownish amorphous powder

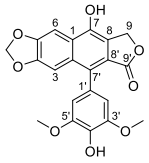

ESIMS (pos. & neg. mode): *m/z* 396.7 $[M+H]^+$, 395.1 $[M-H]^-$, 790.9 $[2M-H]^-$

^1H and ^{13}C NMR Spectroscopic Data (DMSO-d_6; 500 MHz for ^1H and 126 MHz for ^{13}C NMR; δ in ppm) [15,22,23]

position	δ_C, type	δ_H (*J* in Hz)
1	125.6, C	-
2	131.3, C[a]	-
3	102.6, CH	6.86, s
4	148.0, C[a]	-
4,5-OCH_2	101.7, CH_2	6.12, s
5	148.1, C[a]	-
6	98.7, CH	7.67, s
7	147.6, C	-
7-OH	-	8.49, br s
8	119.3, C	-
9	67.0, CH_2	5.33, s
1'	128.5, C	-
2'	108.1, CH[a]	6.47, s[a]
3'	147.5, C[a]	-
3'-OMe	56.0, CH_3[a]	3.71, s[a]
4'	134.9, C	-
4'-OH	-	[b]
5'	147.5, C[a]	-
5'-OMe	56.0, CH_3[a]	3.71, s[a]
6'	108.1, CH[a]	6.47 s[a]
7'	125.7, C	-
8'	122.2, C	-
9'	170.1, C	-

[a]Overlapping signals. [b]Signal not visible

Table S 14. Physicochemical data of **13**.

corosolic acid

$C_{30}H_{48}O_4$, M = 472.71 g/mol, white amorphous powder

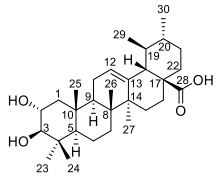

ESIMS (pos. & neg. mode): *m/z* 472.9 $[M+H]^+$, 495.0 $[M+Na]^+$, 945.4 $[2M+H]^+$, 454.9 $[M-H_2O]^+$, 436.9 $[M-2H_2O]^+$, 943.1 $[2M-H]^-$, 471.2 $[M-H]^-$

$[\alpha]_D^{25}$ +43 (c 0.1, MeOH) [24]

^{1}H and ^{13}C NMR Spectroscopic Data (DMSO-d_6; 500 MHz for ^{1}H and 126 MHz for ^{13}C NMR; δ in ppm) [25]

position	δ_C, type	δ_H (*J* in Hz)
1	47.0, CH_2	0.79, m[a] 1.79, d (4.3)
2	67.1, CH	3.42, m
2-OH	-	[b]
3	82.2, CH	2.74, d (9.5)
3-OH	-	[b]
4	38.9, C	-
5	54.7, CH	0.75, m[a]
6	18.0, CH_2	1.32, m[a] 1.47, m[a]
7	32.6, CH_2	1.26, m[a] 1.45, m[a]
8	39.1, C	-
9	46.8, CH	1.49, m[a]
10	37.6, C	-
11	22.9, CH_2	1.86, dd (8.5, 2.8)
12	124.5, CH	5.14, t (2.8, 2.8)
13	138.2, C	-
14	41.7, C	-
15	27.5, CH_2	0.99, dd (13.4, 4.0) 1.80, m
16	23.8, CH_2	1.52, m[a] 1.93, td (13.4, 13.4, 4.0)
17	46.8, C	-
18	52.4, CH	2.11, d (11.3)
19	38.4, CH	1.31, m[a]
20	38.5, CH	0.94, m[a]
21	30.2, CH_2	1.27, m[a] 1.43, m[a]
22	36.3, CH_2	1.51, m[a] 1.57, t (4.0, 4.0)
23	28.8, CH_3	0.92, m[a]
24	17.2, CH_3	0.70, s
25	16.4, CH_3	0.92, m[a]
26	16.9, CH_3	0.74, s
27	23.3, CH_3	1.04, s
28	178.3, C	-
28-OH	-	11.96, br s
29	17.0, CH_3	0.82, d (6.4)
30	21.1, CH_3	0.92, m[a]

[a]Overlapping signals. [b]Signal not visible

Table S 15. Physicochemical data of **14**.

tormentic acid

$C_{30}H_{48}O_5$, M = 488.71 g/mol, white amorphous powder

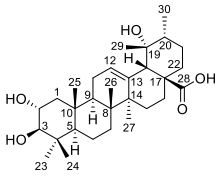

ESIMS (pos. & neg. mode): *m/z* 488.9 $[M+H]^+$, 470.9 $[M-H_2O]^+$, 452.9 $[M-2H_2O]^+$ 487.3 $[M-H]^-$

$[\alpha]_D^{25}$ +15 (c 0.1, MeOH) [26]

^{1}H and ^{13}C NMR Spectroscopic Data (DMSO-d_6; 500 MHz for ^{1}H and 126 MHz for ^{13}C NMR; δ in ppm) [27]

position	δ_C, type	δ_H (*J* in Hz)
1	47.0, CH_2	0.77, m[a] 1.77, dd (11.9, 3.7)
2	67.1, CH	3.42, m
2-OH	-	[b]
3	82.3, CH	2.74, d (9.5)
3-OH	-	[b]
4	39.0, C	-
5	54.8, CH	0.76, m[a]
6	18.2, CH_2	1.33, m[a] 1.46, m[a]
7	32.6, CH_2	1.23, m[a] 1.46, m[a]
8	39.5, C	-
9	46.7, CH	1.62, m[a]
10	37.6, C	-
11	23.2, CH_2	1.89, m
12	126.6, CH	5.16, br s
13	138.8, C	-
14	41.1, C	-
15	28.1, CH_2	0.88, m[a] 1.70, m
16	25.2, CH_2	1.38, m[a] 2.46, m
17	46.9, C	-
18	53.2, CH	2.38, s
19	71.7, C	-
19-OH	-	3.73, br s
20	41.4, CH	1.25, m[a]
21	26.0, CH_2	1.12, m 1.61, m[a]
22	37.3, CH_2	1.50, m[a] 1.58, m[a]
23	28.8, CH_3	0.92, s
24	17.2, CH_3	0.70, m[a]
25	16.3, CH_3	0.90, s[a]
26	16.7, CH_3	0.69, m[a]
27	24.0, CH_3	1.28, s
28	179.1, C	-
28-OH	-	[b]
29	26.5, CH_3	1.08, s
30	16.3, CH_3	0.84, d (6.4)

[a]Overlapping signals. [b]Signal not visible

Table S 16. Physicochemical data of **15**.

euscaphic acid

$C_{30}H_{48}O_5$, M = 488.71 g/mol, white amorphous powder

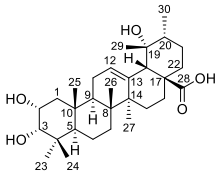

ESIMS (pos. & neg. mode): *m/z* 489.0 $[M+H]^+$, 470.9 $[M-H_2O]^+$, 452.9 $[M-2H_2O]^+$ 487.3 $[M-H]^-$

$[\alpha]_D^{25}$ +15 (c 0.1, MeOH) [28]

^{1}H and ^{13}C NMR Spectroscopic Data (DMSO-d_6; 500 MHz for ^{1}H and 126 MHz for ^{13}C NMR; δ in ppm) [28]

position	δ_C, type	δ_H (*J* in Hz)
1	41.6, CH_2	1.13, m[a]
		1.39, m[a]
2	64.7, CH	3.77, m[a]
2-OH	-	4.12, d (6.1)
3	77.9, CH	3.15, t (3.1, 3.1)
3-OH	-	4.01, d (3.1)
4	38.0, C	-
5	47.7, CH	1.14, m[a]
6	17.7, CH_2	1.29, m[a]
		1.37, m[a]
7	32.6, CH_2	1.22, m[a]
		1.44, m[a]
8	39.5, C	-
9	46.5, CH	1.67, m[a]
10	37.8, C	-
11	23.2, CH_2	1.89, m
12	126.8, CH	5.17, t (3.7, 3.7)
13	138.6, C	-
14	41.2, C	-
15	28.0, CH_2	0.89, m[a]
		1.68, m[a]
16	25.2, CH_2	1.37, m[a]
		2.50, m[a]
17	46.9, C	-
18	53.2, CH	2.37, s
19	71.6, C	-
19-OH	-	3.79, s[a]
20	41.4, CH	1.25, m[a]
21	25.9, CH_2	1.13, m[a]
		1.61, m[a]
22	37.3, CH_2	1.51, dd (12.8, 4.6)
		1.59, m[a]
23	28.9, CH_3	0.88, m[a]
24	21.9, CH_3	0.78, s
25	16.1, CH_3	0.89, m[a]
26	16.6, CH_3	0.68, s
27	24.1, CH_3	1.29, m[a]
28	179.0, C	-
28-OH	-	11.89, br s
29	26.4, CH_3	1.08, s
30	16.3, CH_3	0.84, d (6.4)

[a]Overlapping signals

Table S 17. Physicochemical data of **16**.

sideritoflavone

$C_{18}H_{16}O_8$, M = 360.32 g/mol, yellow amorphous powder

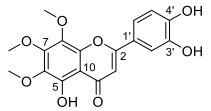

ESIMS (pos. & neg. mode): *m/z* 360.7 $[M+H]^+$, 359.0 $[M-H]^-$, 719.0 $[2M-H]^-$

^{1}H and ^{13}C NMR Spectroscopic Data (DMSO-d_6; 500 MHz for ^{1}H and 126 MHz for ^{13}C NMR; δ in ppm) [29]

position	δ_C, type	δ_H (*J* in Hz)
2	164.5, C	-
3	102.4, CH	6.76, s
4	182.4, C	-
5	145.2, C	-
5-OH	-	12.80, br s
6	135.8, C	-
6-OMe	60.6, CH_3	3.81, s
7	152.4, C	-
7-OMe	61.5, CH_3	4.01, s
8	132.6, C	
8-OMe	62.0, CH_3	3.92, s
9	[b]	-
10	106.3, C	-
1'	120.8, C	-
2'	113.2, CH	7.45, s[a]
3'	146.1, C	-
3'-OH	-	[b]
4'	150.9, C	-
4'-OH	-	[b]
5'	116.2, CH	6.89, d (7.9)
6'	119.2, CH	7.44, m[a]

[a]Overlapping signals. [b]Signal not visible

Table S 18. Physicochemical data of **17**.

8-methoxycirsilineol

$C_{19}H_{18}O_8$, M = 374.35 g/mol, yellow amorphous powder

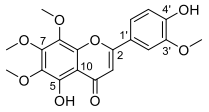

ESIMS (pos. & neg. mode): *m/z* 374.7 $[M+H]^+$, 373.1 $[M-H]^-$

^1H and ^{13}C NMR Spectroscopic Data (DMSO-d_6; 500 MHz for ^1H and 126 MHz for ^{13}C NMR; δ in ppm) [30]

position	δ_C, type	δ_H (*J* in Hz)
2	[b]	-
3	101.1, CH	6.84, s
4	[b]	-
5	[b]	-
5-OH	-	12.99, br s
6	135.4, C	-
6-OMe	60.4, CH_3	3.80, s
7	151.9, C	-
7-OMe	61.3, CH_3	4.00, s
8	132.2, C	
8-OMe	61.6, CH_3	3.91, s
9	[b]	-
10	[b]	-
1'	[b]	-
2'	109.2, CH	7.47, s
3'	148.6, C	-
3'-OMe	55.4, CH_3	3.84, s
4'	[b]	-
4'-OH	-	[b]
5'	116.4, CH	6.79, br s
6'	121.1, CH	7.54, d (8.2)

[a]Overlapping signals. [b]Signal not visible

^{13}C NMR data derived from HSQC and HMBC spectra

Table S 19. Physicochemical data of **18**.

cinnamyl cinnamate

$C_{18}H_{16}O_2$, M = 264.32 g/mol, white amorphous powder

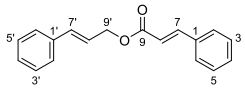

ESIMS (pos. mode): *m/z* 380.8 [2M-cinnamate]

^1H and ^{13}C NMR Spectroscopic Data (DMSO-d_6; 500 MHz for ^1H and 126 MHz for ^{13}C NMR; δ in ppm) [31]

position	δ_C, type	δ_H (*J* in Hz)
1	134.0, C	-
2	128.5, CH[a]	7.71, m[a]
3	129.0, CH[a]	7.43, m[a]
4	130.6, CH	7.43, m[a]
5	129.0, CH[a]	7.43, m[a]
6	128.5, CH[a]	7.71, m[a]
7	144.9, CH	7.70, m[a]
8	117.9, CH	6.66, d (16.2)
9	166.0, C	-
1'	136.0, C	-
2'	126.6, CH[a]	7.47, d (7.6)[a]
3'	128.7, CH[a]	7.35, m[a]
4'	128.1, CH	7.27, m
5'	128.7, CH[a]	7.35, m[a]
6'	126.6, CH[a]	7.47 d (7.6)[a]
7'	133.3, CH	6.74, d (15.9)
8'	123.8, CH	6.42 dt (15.9, 6.1, 6.1)
9'	64.6, CH_2	4.84, dd (6.1, 1.0)

[a]Overlapping signals.

References

[1] A. Jutiviboonsuk, H. Zhang, G.T. Tan, C. Ma, N. Van Hung, N.M. Cuong, N. Bunyapraphatsara, D.D. Soejarto, H.H.S. Fong, Bioactive constituents from roots of *Bursera tonkinensis*, Phytochemistry. 66 (2005) 2745–2751. https://doi.org/10.1016/j.phytochem.2005.09.025.

[2] T. Terada, K. Fujimoto, M. Nomura, J. Yamashita, T. Kobunai, S. Takeda, K. Wierzba, Y. Yamada, H. Yamaguchi, Antitumor agents. I. DNA topoisomerase II inhibitory activity and the structural relationship of podophyllotoxin derivatives as antitumor agents, Chem. Pharm. Bull. 40 (1992) 2720–2727. https://doi.org/10.1248/cpb.40.2720.

[3] E. Kim, H.J. Kim, S.S. Cho, J.H. Shim, G. Yoon, Isolation, semisynthesis, and molecular modeling of deoxypodophyllotoxin analogs for an anti-oral cancer agent, Bull. Korean Chem. Soc. 41 (2020) 472–475. https://doi.org/10.1002/bkcs.11979.

[4] S. Hasegawa, Y. Hirose, A diterpene glycoside and lignans from seed of *Thujopsis dolabrata*, Phytochemistry. 19 (1980) 2479–2481. https://doi.org/10.1016/S0031-9422(00)91060-4.

[5] J.L. Hartwell, W.E. Detty, Components of podophyllin. III. Isolation of α- and β-peltatin. Structure studies, J. Am. Chem. Soc. 72 (1950) 246–253. https://doi.org/10.1021/ja01157a068.

[6] B. Konuklugil, Aryltetralin lignans from *Linum cariense*, Chem. Nat. Compd. 41 (2005) 306–307. https://doi.org/10.1007/s10600-005-0136-5.

[7] J.P. David, E.F. Da Silva, D.L. De Moura, M.L.D.S. Guedes, R.D.J. Assunção, J.M. David, Lignanas e triterpenos do extrato citotóxico de *Eriope blanchetii*, Quim. Nova. 24 (2001) 730–733. https://doi.org/10.1590/S0100-40422001000600004.

[8] J. Xiao, X.W. Cong, G.Z. Yang, Y.W. Wang, Y. Peng, Divergent asymmetric syntheses of podophyllotoxin and related family members via stereoselective reductive Ni-catalysis, Org. Lett. 20 (2018) 1651–1654. https://doi.org/10.1021/acs.orglett.8b00408.

[9] M. Novelo, J.G. Cruz, L. Hernández, R. Pereda-Miranda, H. Chai, W. Mar, J.M. Pezzuto, Cytotoxic constituents from *Hyptis verticillata*, J. Nat. Prod. 56 (1993) 1728–1736. https://doi.org/10.1021/np50100a011.

[10] M. Kuhn, A. Von Wartbung, Podophyllum-Lignane: Struktur und Absolutkonfiguration von Podorhizol-β-D-glucosid (= Lignan F), Helv. Chim. Acta. 50 (1967) 1546–1565. https://doi.org/10.1002/hlca.19670500614.

[11] J.P. Robin, R. Dhal, E. Brown, Syntheses totales et etudes de lignanes biologiquement actifs-II. Application de l'α-hydroxyalkylation de β-benzyl γ-butyrolactone a la creation des squelettes phenyl tetraline et bisbenzocyclooctadienes. Synthese totale du (±) podorhizol, de la (±) podorhizone et de la (±) isodesoxypodophyllotoxine, Tetrahedron. 38 (1982) 3667–3671. https://doi.org/10.1016/0040-4020(82)80075-6.

[12] E. Brown, A. Daugan, Lignanes. 10. Preparation des (*R*)-(+) et (*S*)-(-)-β-piperonyl et β-veratryl-γ-butyrolactones et leur utilisation dans la synthèse totale de lignanes optiquement actifs, Tetrahedron. 45 (1989) 141–154. https://doi.org/10.1016/0040-4020(89)80041-9.

[13] T. Itoh, J. ichi Chika, Y. Takagi, S. Nishiyama, An efficient enantioselective total synthesis of antitumor lignans: synthesis of enantiomerically pure 4-hydroxyalkanenitriles via an enzymatic reaction, J. Org. Chem. 58 (1993) 5717–5723. https://doi.org/10.1021/jo00073a034.

[14] S.P. Forsey, D. Rajapaksa, N.J. Taylor, R. Rodrigo, Comprehensive synthetic route to eight diastereomeric *Podophyllum* lignans, J. Org. Chem. 54 (1989) 4280–4290. https://doi.org/10.1021/jo00279a011.

[15] Z. Yang, P. Guo, R. Han, J.M. Gao, Preparative separation of flavone dimers from *Dysosma versipellis* by counter-current chromatography: trifluoroacetic acid as a solvent system modifier, J. Sep. Sci. 41 (2018) 3631–3643. https://doi.org/10.1002/jssc.201800530.

[16] Y.J. Zhang, M. Litaudon, H. Bousserouel, M.T. Martin, O. Thoison, S. Léonce, V. Dumontet, T. Sévenet, F. Guéritte, Sesquiterpenoids and cytotoxic lignans from the bark of *Libocedrus chevalieri*, J. Nat. Prod. 70 (2007) 1368–1370. https://doi.org/10.1021/np070124q.

[17] K. Maeda, T. Hamada, S. Onitsuka, H. Okamura, Total synthesis of the claimed structure of (±)-hyptinin and structural revision of natural hyptinin, J. Nat. Prod. 80 (2017) 1446–1449. https://doi.org/10.1021/acs.jnatprod.6b01116.

[18] T. Ogiku, S.-ichi Yoshida, H. Ohmizu, T. Iwasaki, Efficient syntheses of 1-arylnaphthalene lignan lactones and related compounds from cyanohydrins, J. Org. Chem. 60 (1995) 4585–4590. https://doi.org/10.1021/jo00119a041.

[19] C. Ito, T. Matsui, T.S. Wu, H. Furukawa, T.S. Wu, Isolation of 6,7-demethylenedesoxypodophyllotoxin from *Hernandia ovigera*, Chem. Pharm. Bull. 40 (1992) 1318–1321. https://doi.org/10.1248/cpb.40.1318.

[20] M. Tanoguchi, M. Arimoto, H. Saika, H. Yamaguchi, Studies on the constituents of the seeds of *Hernandia ovigera* L. VI. Isolation and structural determination of three lignans, Chem. Pharm. Bull. 35 (1987) 4162–4168. https://doi.org/10.1248/cpb.35.4162.

[21] J. Xiao, G. Nan, Y.W. Wang, Y. Peng, Concise synthesis of (+)-*β*- and *γ*-apopicropodophyllins, and dehydrodesoxypodophyllotoxin, Molecules. 23 (2018) 3037. https://doi.org/10.3390/molecules23113037.

[22] S.A. Beers, Y. Imakura, H.J. Dai, D.H. Li, Y.C. Cheng, K.H. Lee, Antitumor agents, 99. Synthetic ring C aromatized podophyllotoxin analogues as potential inhibitors of human DNA topoisomerase II, J. Nat. Prod. 51 (1988) 901–905. https://doi.org/10.1021/np50059a014.

[23] Atta-ur-Rahman, M. Ashraf, M. Iqbal Choudhary, Habib-ur-Rehman, M.H. Kazmi, Antifungal aryltetralin lignans from leaves of *Podophyllum hexandrum*, Phytochemistry. 40 (1995) 427–431. https://doi.org/10.1016/0031-9422(95)00195-D.

[24] P.T. Thuong, B.S. Min, W.Y. Jin, M.K. Na, J.P. Lee, R.S. Seong, Y.M. Lee, K.S. Song, Y.H. Seong, H.K. Lee, K.H. Bae, S.S. Kang, Anti-complementary activity of ursane-type triterpenoids from *Weigela subsessilis*, Biol. Pharm. Bull. 29 (2006) 830–833. https://doi.org/10.1248/bpb.29.830.

[25] D.A. Torres-Ortiz, R. de L. Eloy, B. Moustapha, I.A. César, M.S. Edmundo, C.R. Jesús Eduardo, R.P. Dulce María, Vasorelaxing effect and possible chemical markers of the flowers of the Mexican *Crataegus gracilior*, Nat. Prod. Res. 34 (2020) 3522–3525. https://doi.org/10.1080/14786419.2019.1577833.

[26] N. Hirai, M. Sugie, M. Wada, E.H. Lahlou, T. Kamo, R. Yoshida, M. Tsuda, H. Ohigashi, Triterpene phytoalexins from strawberry fruit, Biosci. Biotechnol. Biochem. 64 (2000) 1707–1712. https://doi.org/10.1271/bbb.64.1707.

[27] G. da G. Rocha, M. Simões, K.A. Lúcio, R.R. Oliveira, M.A. Coelho Kaplan, C.R. Gattass, Natural triterpenoids from *Cecropia lyratiloba* are cytotoxic to both sensitive and multidrug resistant leukemia cell lines, Bioorganic Med. Chem. 15 (2007) 7355–7360. https://doi.org/10.1016/j.bmc.2007.07.020.

[28] L. Apaza T, F. Antognoni, G. Potente, Á. Rumbero Sánchez, Triterpenoids isolated from *Jatropha macrantha* (Müll. Arg.) inhibit the NF-κB and HIF-1α pathways in tumour cells, Nat. Prod. Res. (2020) 1–5. https://doi.org/10.1080/14786419.2020.1795851.

[29] M.L. Li, L.Y. Xu, Z.L. Li, S.H. Qian, M.J. Qin, Flavonoids from *Mentha haplocalyx*, Chem. Nat. Compd. 50 (2014) 124–125. https://doi.org/10.1007/s10600-014-0884-1.

[30] C.O. Van Den Broucke, R.A. Dommisse, E.L. Esmans, J.A. Lemli, Three methylated flavones from *Thymus vulgaris*, Phytochemistry. 21 (1982) 2581–2583. https://doi.org/10.1016/0031-9422(82)85261-8.

[31] A.B. Lutjen, M.A. Quirk, A.M. Barbera, E.M. Kolonko, Synthesis of (*E*)-cinnamyl ester derivatives via a greener Steglich esterification, Bioorg. Med. Chem. 26 (2018) 5291–5298. https://doi.org/10.1016/j.bmc.2018.04.007.

Saponins from Saffron Corms Inhibit the Gene Expression and Secretion of Pro-Inflammatory Cytokines

Morris Keller[1], Sarah Fankhauser[2], Noreen Giezendanner[2], Michelle König[2], Franziska Keresztes[1], Ombeline Danton[1], Orlando Fertig[1], Laurence Marcourt[3], Matthias Hamburger[1,*], Veronika Butterweck[2,*], Olivier Potterat[1]

[*]**Corresponding Authors**

Veronika Butterweck – School of Life Sciences, University of Applied Sciences, Northwestern Switzerland, Muttenz, Switzerland; Current address: Max Zeller Söhne AG, 8590 Romanshorn, Switzerland; Phone: +41-71-0466-447; Email: Veronika.Butterweck@ZellerAG.ch; orcid.org/0000-0001-7516-8789

Matthias Hamburger – Pharmaceutical Biology, Pharmacenter, University of Basel, 4056 Basel, Switzerland; Phone: +41-61-207-1425; Email: matthias.hamburger@unibas.ch; orcid.org/0000-0001-9331-273X

[1] Pharmaceutical Biology, Pharmacenter, University of Basel, 4056 Basel, Switzerland

[2] School of Life Sciences, University of Applied Sciences, Northwestern Switzerland, Muttenz, Switzerland

[3] School of Pharmaceutical Sciences and Institute of Pharmaceutical Sciences of Western Switzerland (ISPSW), University of Geneva, CMU, 1211 Geneva 4, Switzerland

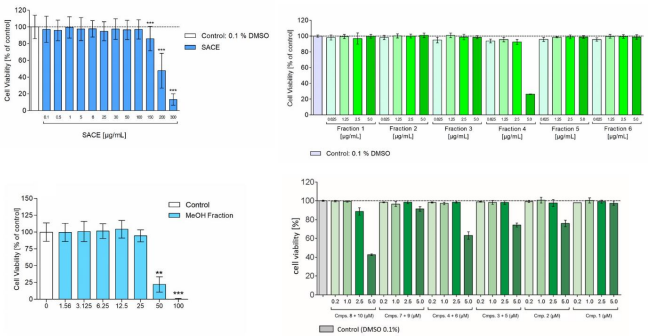

Figure S 1. Effect of the compounds **1-10** on cell viability of HaCaT cells compared to the control (DMEM incl. 0.1% DMSO). The results represent three independent experiments (n=3) and are presented as mean ± standard deviation. *$p \leq 0.05$ vs. control, **$p \leq 0.01$ vs. control, ***$p \leq 0.001$ vs. control

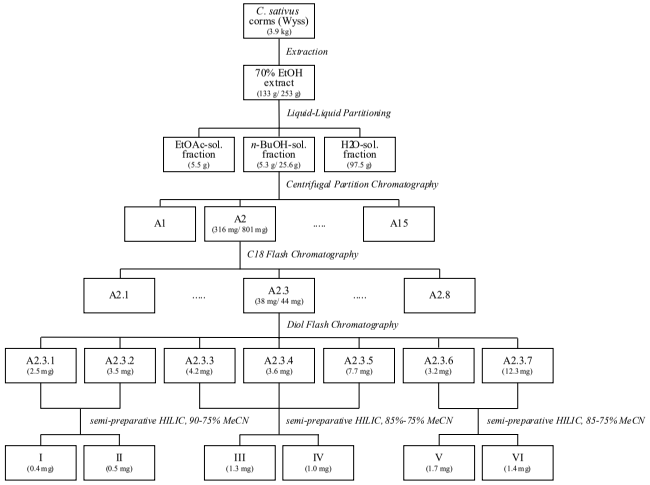

Figure S2. Isolation scheme for the isolation of substances I-VI.

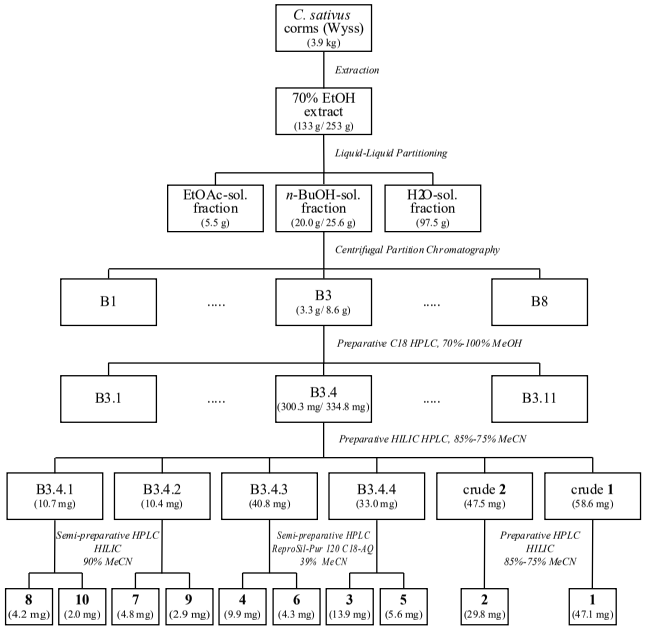

Figure S3. Isolation scheme for the isolation of compounds **1-10**.

Table S1. ^{1}H and ^{13}C NMR Spectroscopic Data of the Aglycone and Fatty Acid Residue in Compounds **1-2** (DMSO-d_6; 500 MHz for ^{1}H and 126 MHz for ^{13}C NMR; δ in ppm)

	1		**2**	
position	δ_C, type	δ_H (*J* in Hz)	δ_C, type	δ_H (*J* in Hz)
1	38.3, CH_2	0.89[a] 1.52[a]	38.4, CH_2	0.89[a] 1.54[a]
2	25.7, CH_2	1.53[a] 1.69[a]	25.6, CH_2	1.55[a] 1.88[a]
3	88.1, CH	3.05[a]	88.2, CH	3.04[a]
4	38.8, C		38.8, C	
5	55.1, CH	0.69[a]	55.2, CH	0.69[a]
6	18.0, CH_2	1.26[a] 1.46[a]	17.9, CH_2	[b] 1.47[a]
7	32.6, CH_2	1.30[a] 1.37[a]	32.6, CH_2	1.31[a] 1.38[a]
8	39.1, C		39.1, C	
9	46.1, CH	1.51[a]	46.2, CH	1.51, m
10	36.3, C		36.3, C	
11	23.0, CH_2	1.79[a]	23.0, CH_2	1.80[a]
12	121.4, CH	5.24, m	121.5, CH	5.24, m
13	143.3, C		143.3, C	
14	41.1, C		41.1, C	
15	34.7, CH_2	1.28[a] 1.57[a]	34.7, CH_2	1.30[a] 1.58[a]
16	72.7, CH	4.30, m	72.7, CH	4.31, m
17	48.1, C		48.1, C	
18	40.4, CH	2.83, d (10.7)	40.4, CH	2.83, d (12.5)
19	46.6, CH_2	0.99[a] 2.22, dd (11.6, 10.4)	46.7, CH_2	0.99[a] 2.22, dd (11.9, 11.9)
20	30.2, C		30.2, C	
21	35.1, CH_2	1.09[a] 1.88[a]	35.1, CH_2	1.09[a] 1.89[a]
22	30.7, CH_2	1.63[a] 1.81[a]	30.7, CH_2	1.64[a] 1.81[a]
23	27.6, CH_3	0.97[a]	27.7, CH_3	0.97[a]
24	16.5, CH_3	0.75, s	16.5, CH_3	0.77, s
25	15.5, CH_3	0.86[a]	15.5, CH_3	0.88[a]
26	16.9, CH_3	0.67[a]	16.9, CH_3	0.68[a]
27	26.3, CH_3	1.30[a]	26.3, CH_3	1.30[a]
28	175.1, C		175.1, C	
29	32.9, CH_3	0.82, s	32.9, CH_3	0.82, s
30	24.2, CH_3	0.90[a]	24.2, CH_3	0.89[a]
C1'	170.8, C		170.8, C	
C2'	38.3, CH_2	2.48[a] 2.70, dd (15.6, 3.7)	38.3, CH_2	2.49[a] 2.71, dd (15.6, 4.3)
C3'	72.4, CH	3.90, tt (5.2, 5.2)	72.3, CH	3.90, tt (5.5, 5.5)
C4'	34.4, CH_2	1.53[a]	34.3, CH_2	1.53[a]
C5'	24.5, CH_2	1.32[a]	24.5, CH_2	1.33[a]
C6'	28.6, CH_2	1.21[a]	28.6, CH_2	1.22[a]
C7'	28.6, CH_2	1.22[a]	28.6, CH_2	1.24[a]
C8'	23.3, CH_2	1.43[a]	23.3, CH_2	1.43[a]
C9'	41.8, CH_2	2.37, t (6.9)	41.8, CH_2	2.37, t (7.3)
C10'	210.6, C		210.6, C	
C11'	41.8, CH_2	2.37, t (6.9)	41.8, CH_2	2.37, t (7.3)
C12'	23.3, CH_2	1.43[a]	23.3, CH_2	1.43[a]
C13'	28.7, CH_2	1.20[a]	28.7, CH_2	1.21[a]
C14'	25.6, CH_2	1.25[a]	25.6, CH_2	1.26[a]
C15'	29.1, CH_2	1.47[a]	29.1, CH_2	1.47[a]
C16'	66.4, CH_2	3.30[a] 3.52[a]	66.4, CH_2	3.30[a] 3.51[a]

[a] Overlapping signals, [b] Signal not visible.

Table S2. ^{1}H and ^{13}C NMR Spectroscopic Data of the Glycosidic Moiety in Compounds **1-2** (DMSO-d_6; 500 MHz for ^{1}H and 126 MHz for ^{13}C NMR; δ in ppm)

	1		**2**	
position	δ_C, type	δ_H (*J* in Hz)	δ_C, type	δ_H (*J* in Hz)
Sugar moiety at 3				
GalA				
1	—		105.5, CH	4.16, d (4.9)
2	—		70.6, CH	3.31[a]
3	—		73.1, CH	3.32[a]
4	—		70.0, CH	3.87[a]
5	—		73.8, CH	3.96, br s
6	—		170.5, C	
GlcA				
1	105.6, CH	4.24, d (7.0)	—	
2	73.7, CH	2.99[a]	—	
3	76.2, CH	3.14[a]	—	
4	71.6, CH	3.27[a]	—	
5	75.5, CH	3.56[a]	—	
6	170.8, C		—	
Sugar moiety at 28				
Fuc				
1	93.0, CH	5.30[a]	93.0, CH	5.31[a]
2	74.7, CH	3.47[a]	74.7, CH	3.47[a]
3	71.6, CH	3.81[a]	71.6, CH	3.81[a]
4	73.5, CH	4.92, br s	73.5, CH	4.92, br s
5	68.8, CH	3.85[a]	68.8, CH	3.85[a]
6	16.0, CH_3	0.92, d (5.8)	16.0, CH_3	0.92[a]
Rha3				
1	98.5, CH	5.31[a]	98.5, CH	5.32[a]
2	78.2, CH	3.83[a]	78.2, CH	3.83[a]
3	70.3, CH	3.71[a]	70.3, CH	3.70[a]
4	82.1, CH	3.36[a]	82.0, CH	3.36[a]
5	67.0, CH	3.55[a]	67.0, CH	3.56[a]
6	18.0, CH_3	1.18[a]	18.0, CH_3	1.18, d (6.1)
Xyl				
1	104.7, CH	4.48, d (7.6)	104.7, CH	4.48, d (7.6)
2	74.6, CH	2.99[a]	74.6, CH	2.99[a]
3	76.3, CH	3.17[a]	76.3, CH	3.17[a]
4	69.7, CH	3.24[a]	69.7, CH	3.24[a]
5	65.7, CH_2	3.15[a] 3.65[a]	65.8, CH_2	3.17[a] 3.65[a]
Ara				
1	102.0, CH	4.57, d (4.3)	102.0, CH	4.57, d (4.9)
2	78.2, CH	3.68[a]	78.2, CH	3.68[a]
3	71.2, CH	3.63[a]	71.2, CH	3.63[a]
4	66.2, CH	3.70[a]	66.2, CH	3.70[a]
5	63.8, CH_2	3.35[a] 3.66[a]	63.8, CH_2	3.35[a] 3.67[a]
Gal				
1	104.0, CH	4.33, d (7.6)	104.0, CH	4.33, d (7.3)
2	71.1, CH	3.35[a]	71.1, CH	3.35[a]
3	73.4, CH	3.31[a]	73.4, CH	3.31[a]
4	67.8, CH	3.67[a]	67.7, CH	3.67[a]
5	75.4, CH	3.37[a]	75.4, CH	3.38[a]
6	60.0, CH_2	3.50[a] 3.58[a]	60.0, CH_2	3.50[a] 3.59[a]
Sugar moiety at C3'				
Rha2				
1	98.8, CH	4.70, br s	98.8, CH	4.70, br s
2	70.9, CH	3.54[a]	70.9, CH	3.54[a]
3	70.8, CH	3.40[a]	70.8, CH	3.40[a]
4	71.9, CH	3.18[a]	71.9, CH	3.18[a]
5	69.0, CH	3.44[a]	69.0, CH	3.44[a]
6	17.8, CH_3	1.12, d (5.8)	17.8, CH_3	1.12, d (6.1)
Sugar moiety at C16'				
Rha1				
1	100.0, CH	4.50, br s	100.0, CH	4.51, d (0.9)[a]
2	70.6, CH	3.57[a]	70.6, CH	3.57[a]
3	70.8, CH	3.39[a]	70.8, CH	3.38[a]
4	72.0, CH	3.16[a]	72.0, CH	3.16[a]
5	68.4, CH	3.36[a]	68.4, CH	3.36[a]
6	18.0, CH_3	1.12, d (5.8)	17.8, CH_3	1.12, d (6.1)

[a] Overlapping signals, [b] Signal not visible.

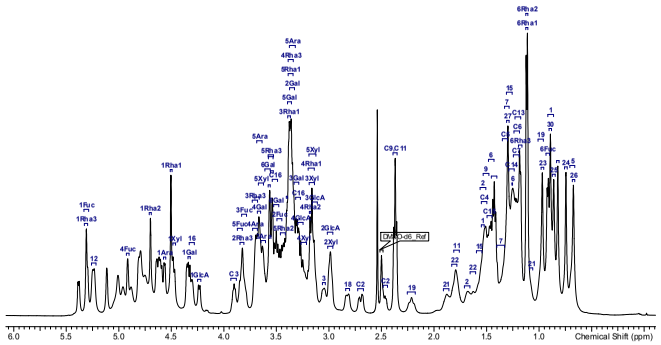

Figure S4. ^{1}H-NMR spectrum of compound **1** (500 MHz, DMSO-d_6).

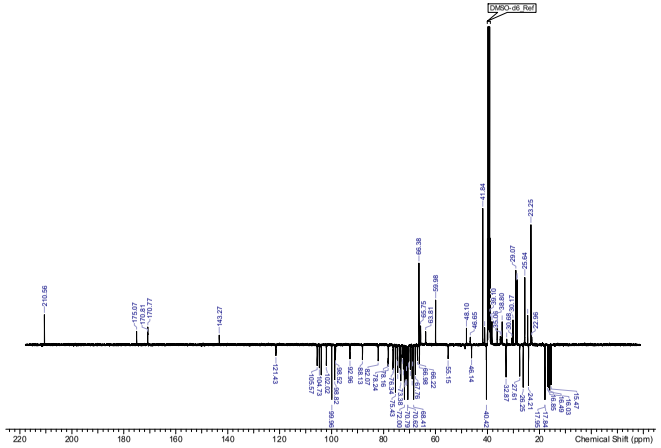

Figure S5. ^{13}C-DEPTq spectrum of compound **1** (126 MHz, DMSO-d_6).

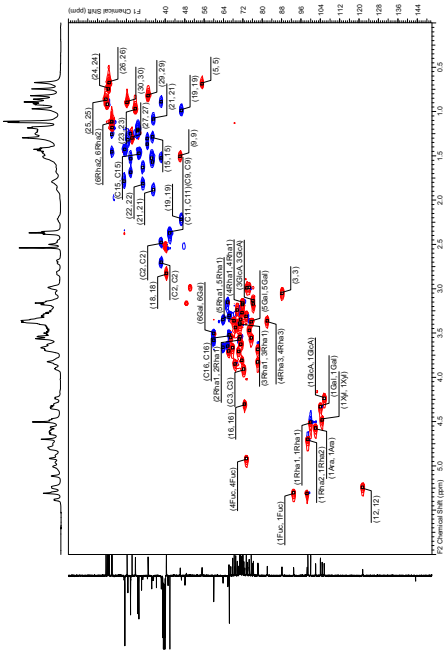

Figure S8. HSQC-DEPT spectrum of compound **1** (500 MHz, DMSO-d_6).

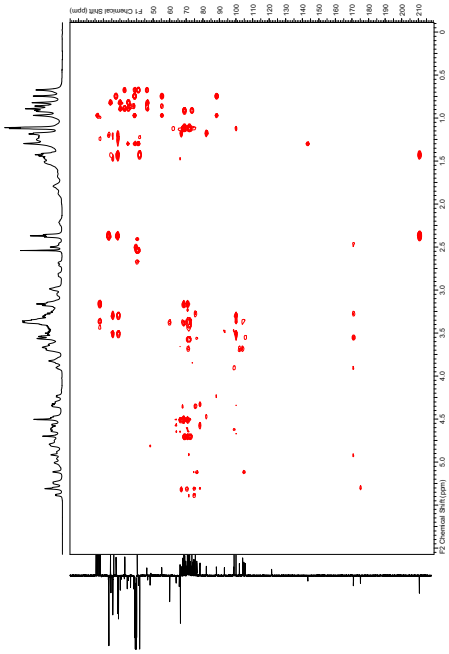

Figure S9. HMBC spectrum of compound **1** (500 MHz, DMSO-d_6).

10

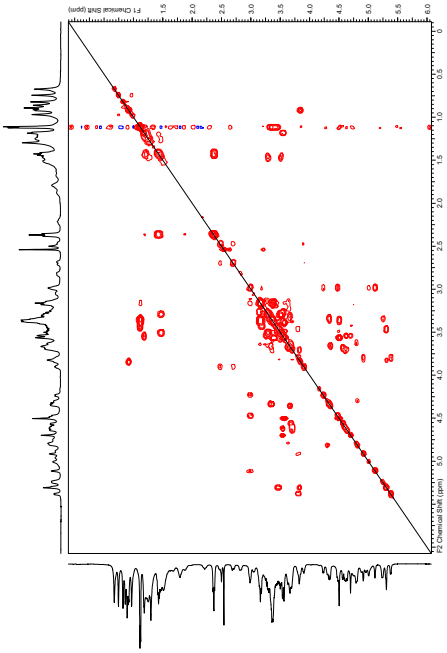

Figure S6. ^{1}H-^{1}H COSY spectrum of compound **1** (500 MHz, DMSO-d_6).

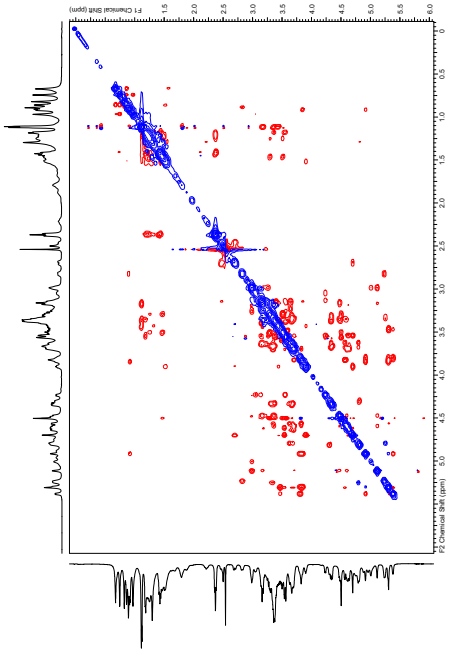

Figure S7. ^{1}H-^{1}H ROESY spectrum of compound **1** (500 MHz, DMSO-d_6).

9

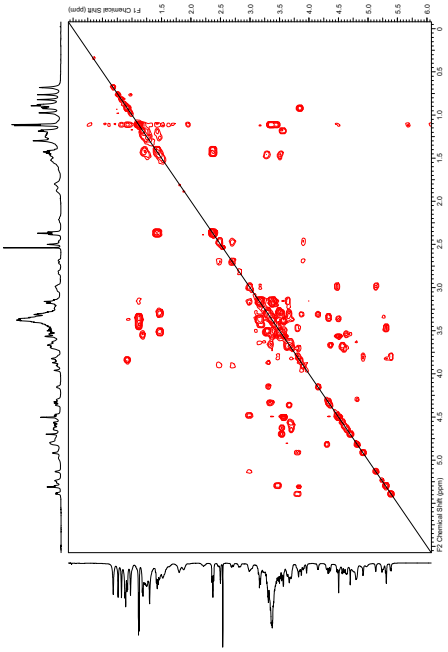

Figure S12. ^{1}H-^{1}H COSY spectrum of compound **2** (500 MHz, DMSO-d_6).

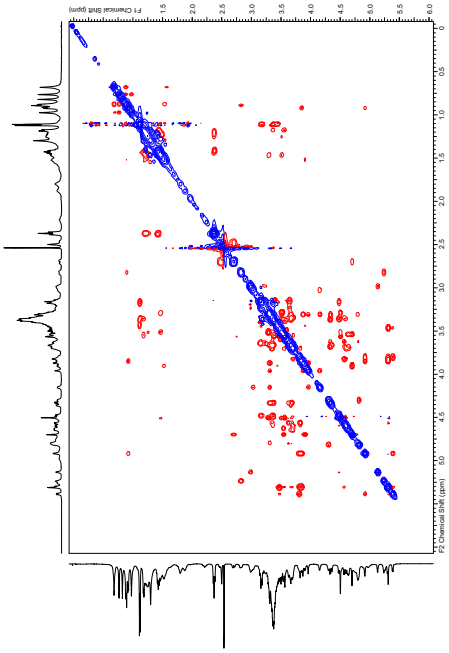

Figure S13. ^{1}H-^{1}H ROESY spectrum of compound **2** (500 MHz, DMSO-d_6).

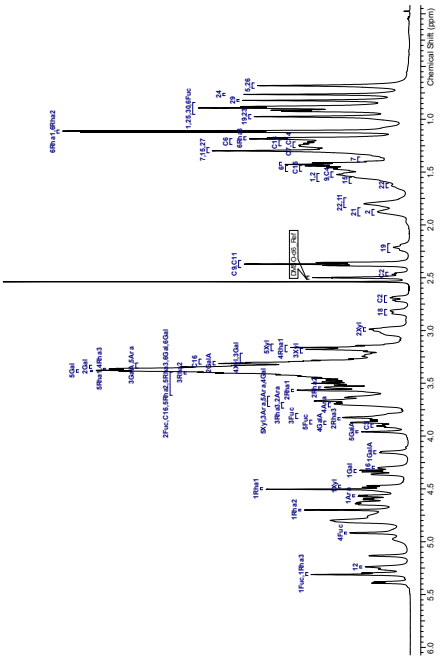

Figure S10. ^{1}H-NMR spectrum of compound **2** (500 MHz, DMSO-d_6).

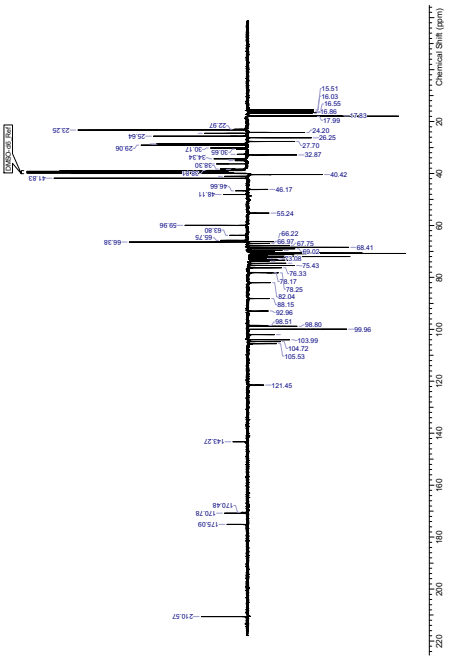

Figure S11. ^{13}C-DEPTq spectrum of compound **2** (126 MHz, DMSO-d_6).

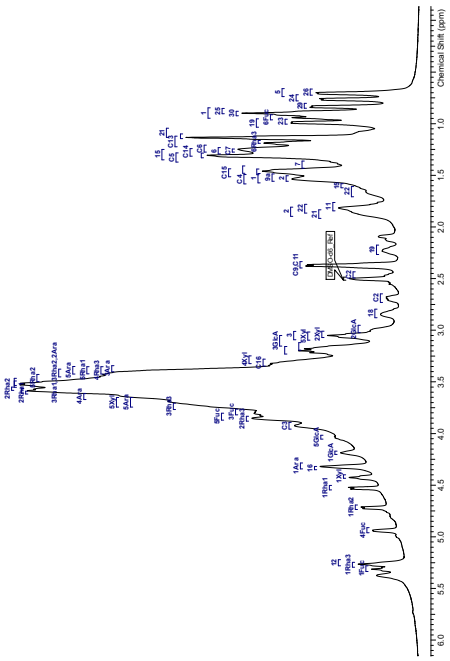

Figure S16. ^{1}H-NMR spectrum of compound **3** (500 MHz, DMSO-d_6).

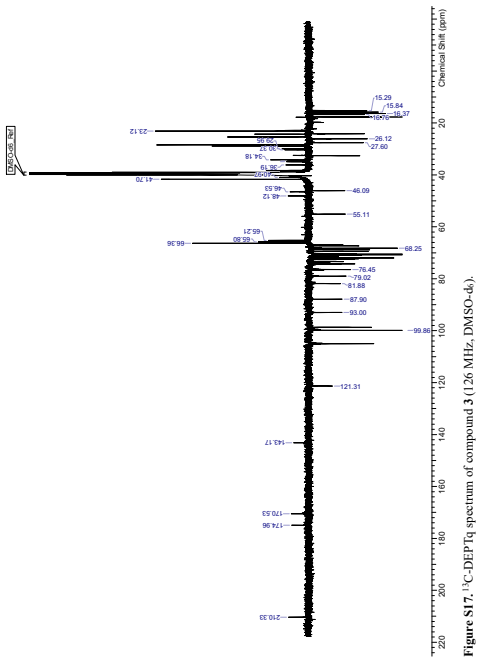

Figure S17. ^{13}C-DEPTq spectrum of compound **3** (126 MHz, DMSO-d_6).

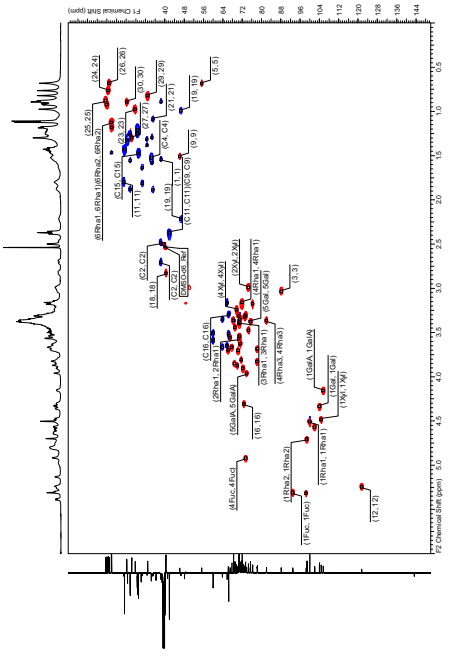

Figure S14. HSQC-DEPT spectrum of compound **2** (500 MHz, DMSO-d_6).

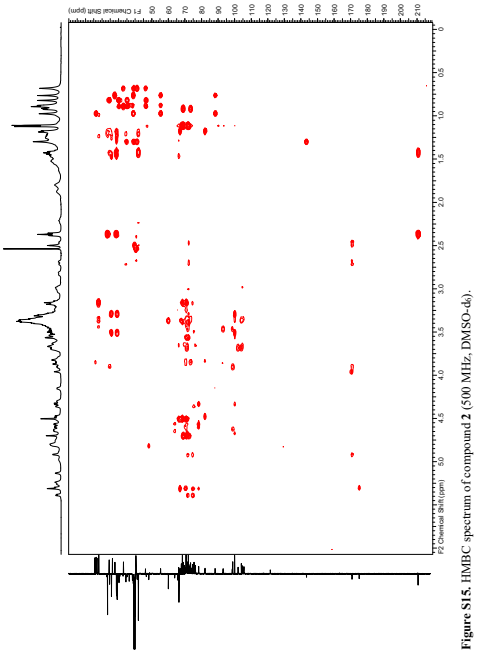

Figure S15. HMBC spectrum of compound **2** (500 MHz, DMSO-d_6).

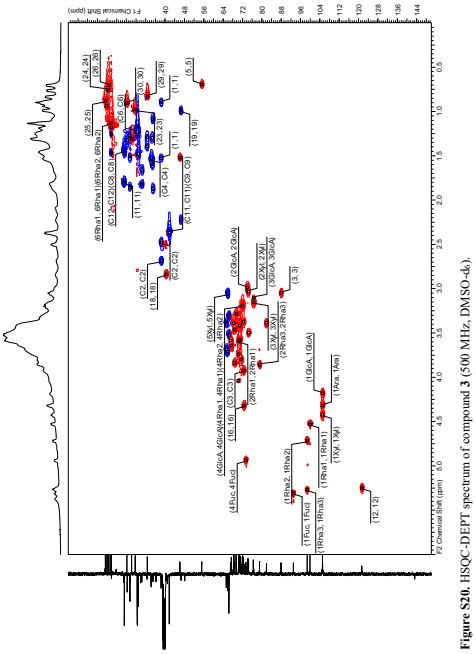

Figure S20. HSQC-DEPT spectrum of compound **3** (500 MHz, DMSO-d_6).

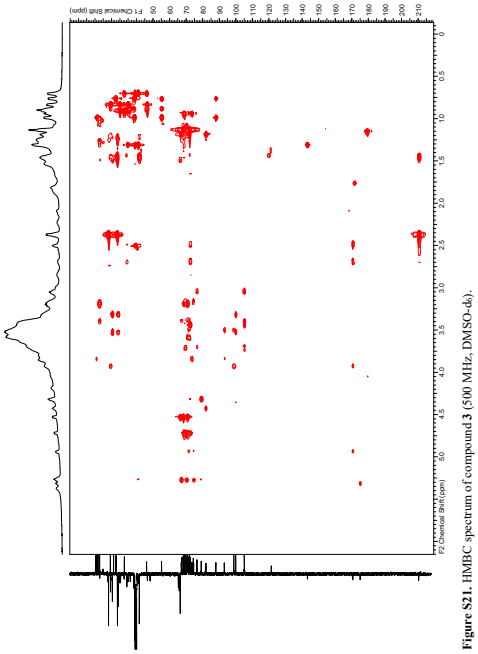

Figure S21. HMBC spectrum of compound **3** (500 MHz, DMSO-d_6).

16

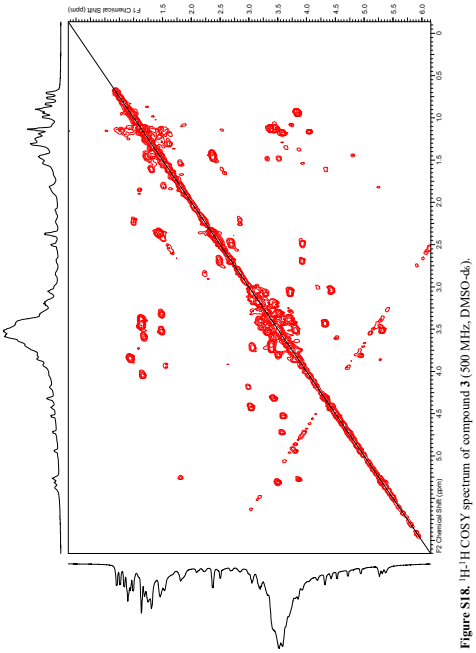

Figure S18. ^{1}H-^{1}H COSY spectrum of compound **3** (500 MHz, DMSO-d_6).

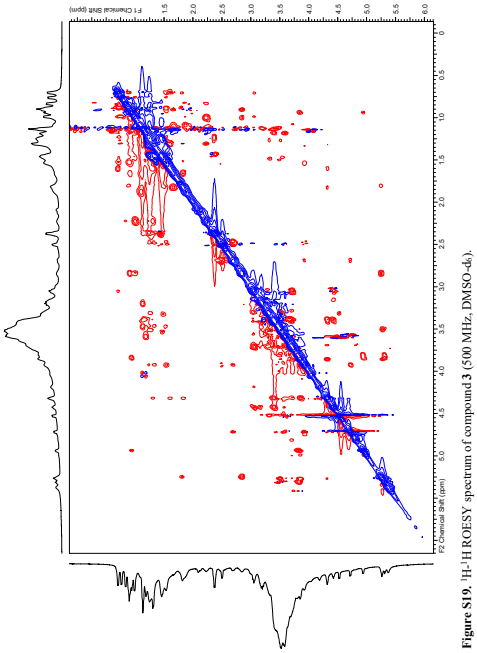

Figure S19. ^{1}H-^{1}H ROESY spectrum of compound **3** (500 MHz, DMSO-d_6).

15

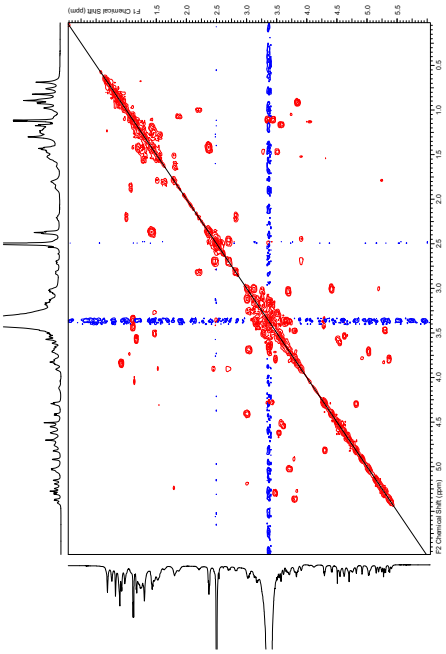

Figure S24. ^{1}H-^{1}H COSY spectrum of compound **4** (600 MHz, DMSO-d_6).

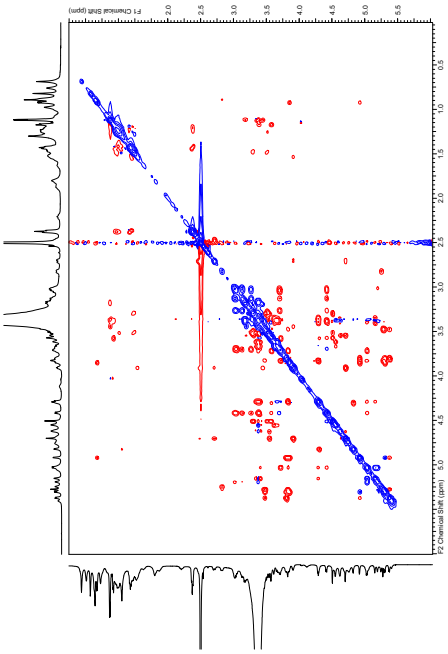

Figure S25. ^{1}H-^{1}H ROESY spectrum of compound **4** (600 MHz, DMSO-d_6).

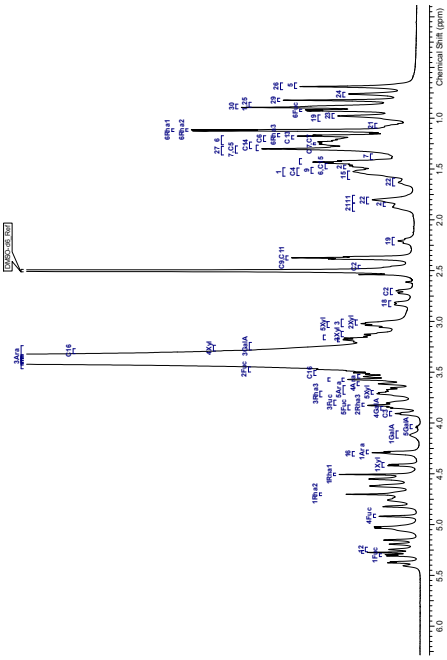

Figure S22. ^{1}H-NMR spectrum of compound **4** (600 MHz, DMSO-d_6).

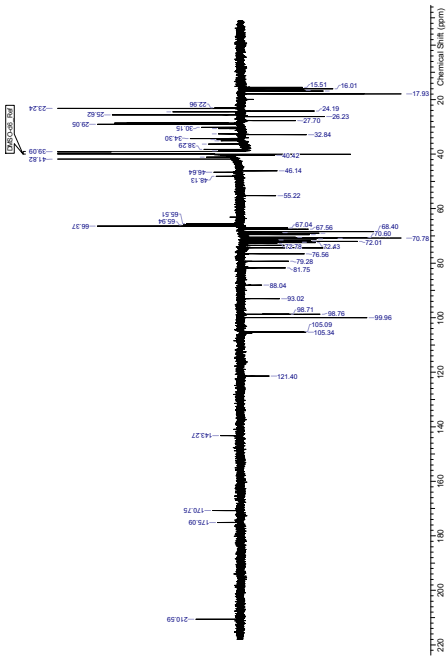

Figure S23. ^{13}C-DEPTq spectrum of compound **4** (151 MHz, DMSO-d_6).

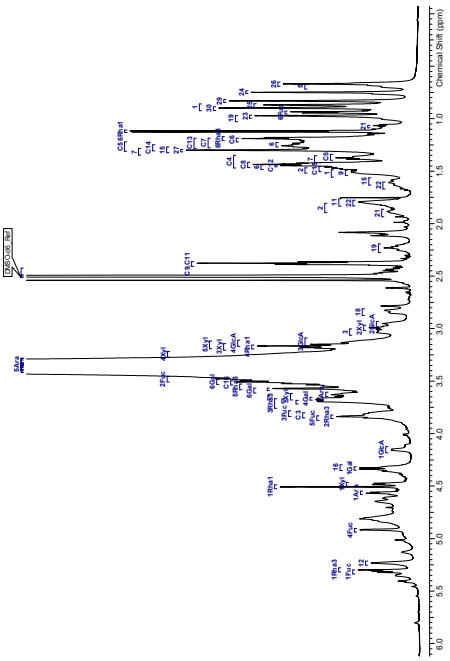

Figure S28. ^{1}H-NMR spectrum of compound **5** (600 MHz, DMSO-d_6).

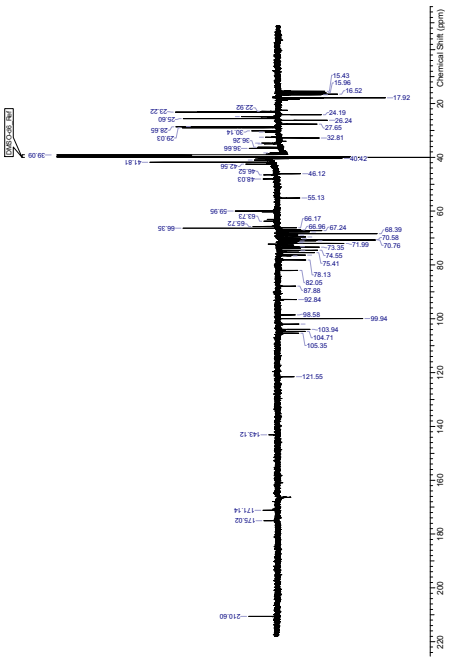

Figure S29. ^{13}C-DEPTq spectrum of compound **5** (151 MHz, DMSO-d_6).

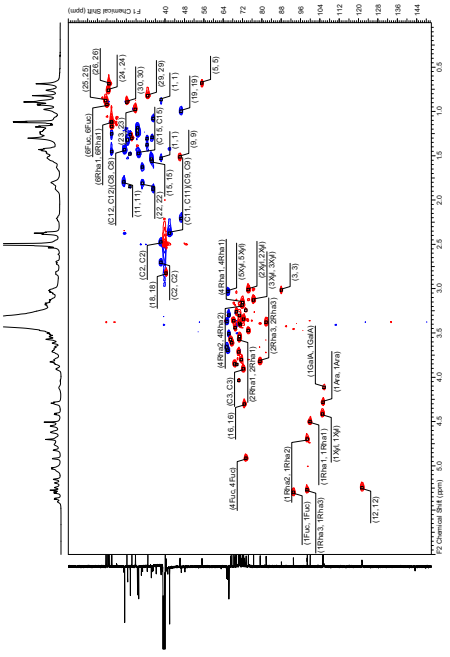

Figure S26. HSQC-DEPT spectrum of compound **4** (600 MHz, DMSO-d_6).

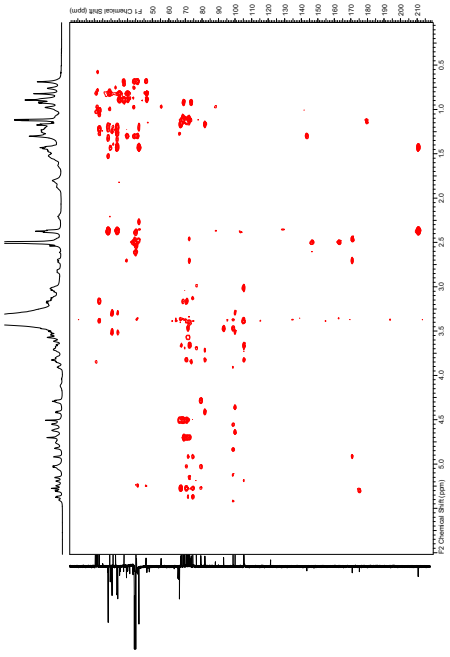

Figure S27. HMBC spectrum of compound **4** (600 MHz, DMSO-d_6).

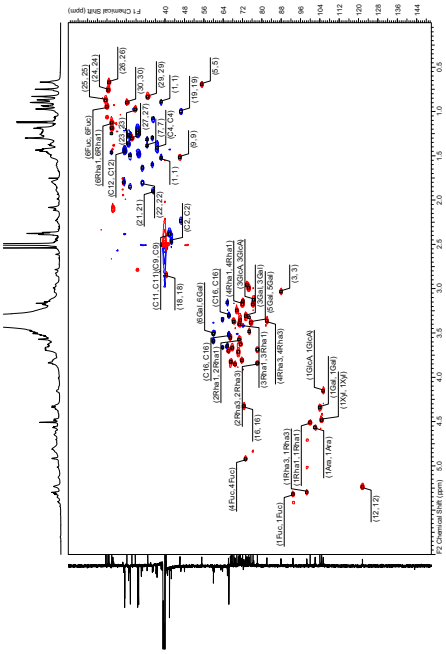

Figure S32. HSQC-DEPT spectrum of compound **5** (600 MHz, DMSO-d_6).

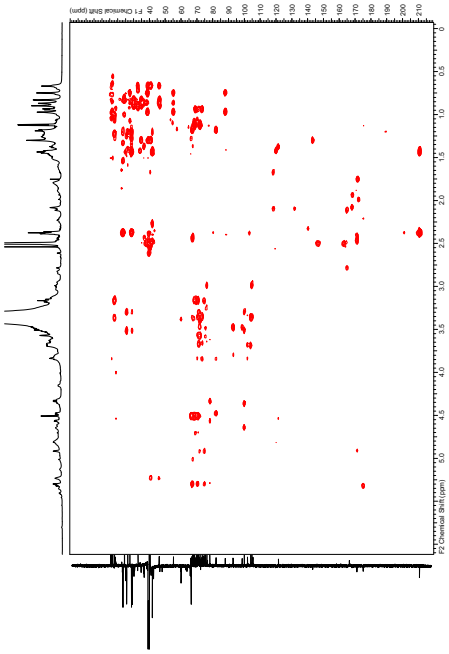

Figure S33. HMBC spectrum of compound **5** (600 MHz, DMSO-d_6).

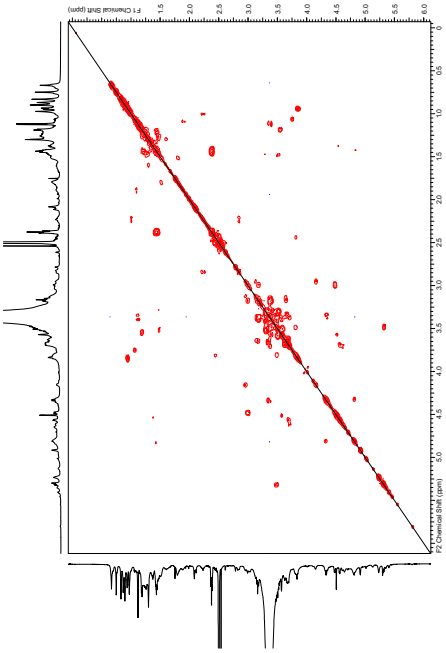

Figure S30. ^{1}H-^{1}H COSY spectrum of compound **5** (600 MHz, DMSO-d_6).

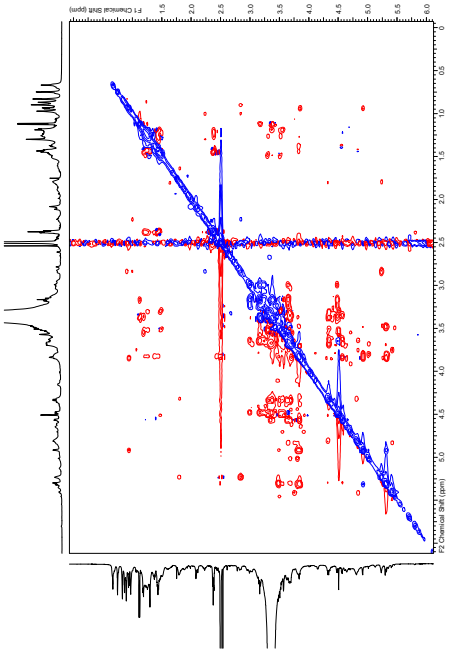

Figure S31. ^{1}H-^{1}H ROESY spectrum of compound **5** (600 MHz, DMSO-d_6).

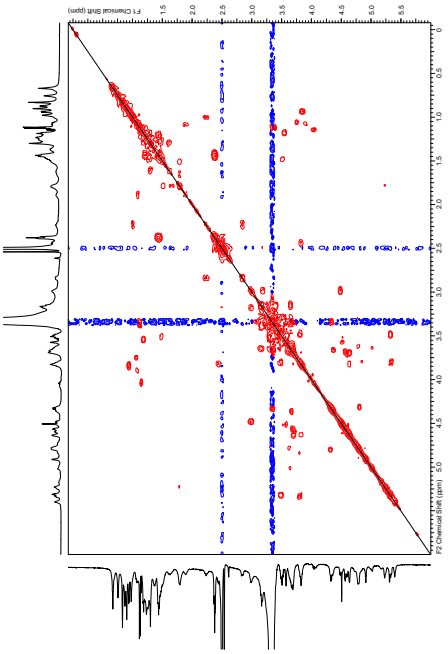

Figure S36. ^{1}H-^{1}H COSY spectrum of compound **6** (600 MHz, DMSO-d_6).

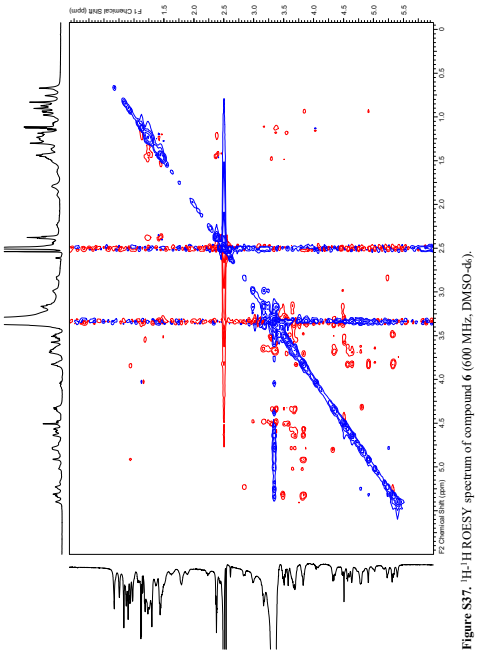

Figure S37. ^{1}H-^{1}H ROESY spectrum of compound **6** (600 MHz, DMSO-d_6).

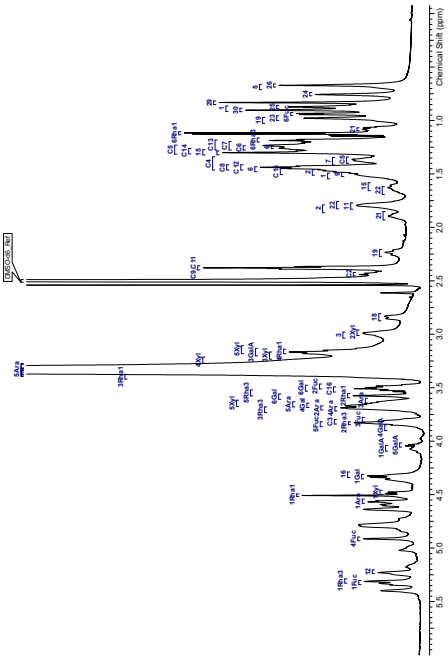

Figure S34. ^{1}H-NMR spectrum of compound **6** (600 MHz, DMSO-d_6).

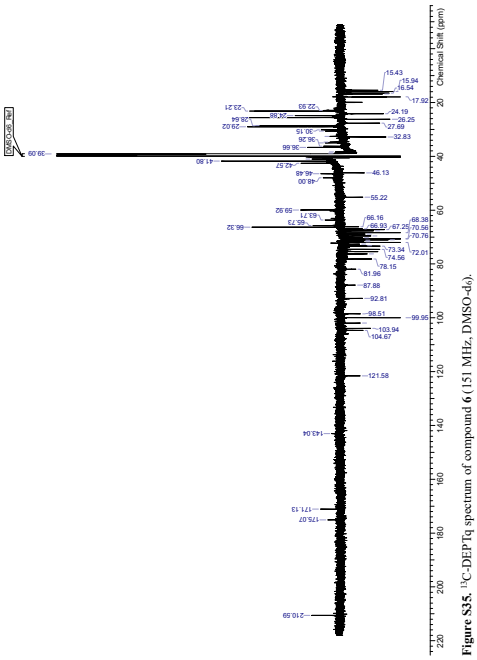

Figure S35. ^{13}C-DEPTq spectrum of compound **6** (151 MHz, DMSO-d_6).

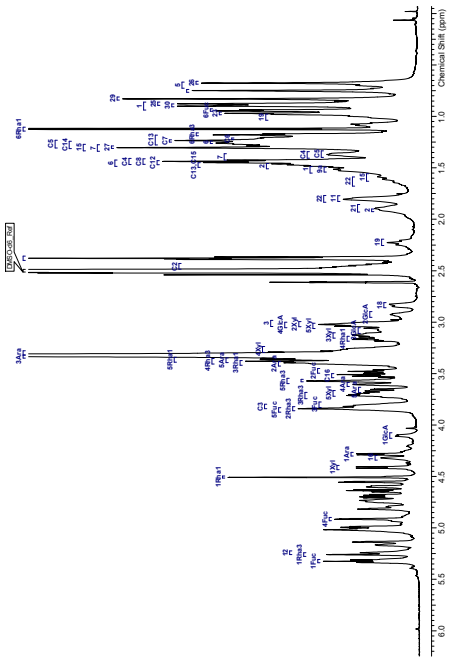

Figure S40. ^{1}H-NMR spectrum of compound **7** (600 MHz, DMSO-d_6).

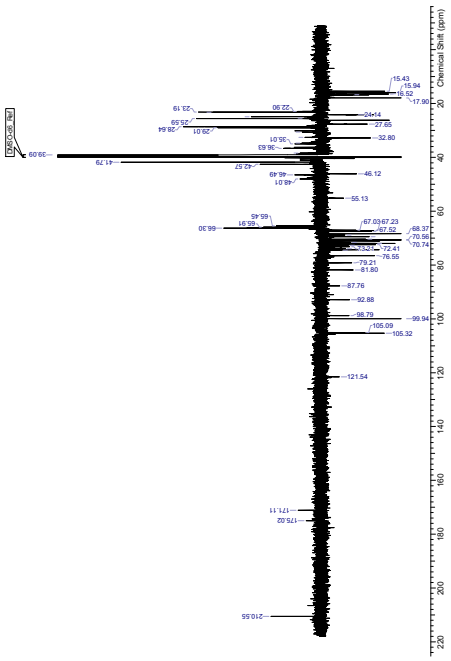

Figure S41. ^{13}C-DEPTq spectrum of compound **7** (151 MHz, DMSO-d_6).

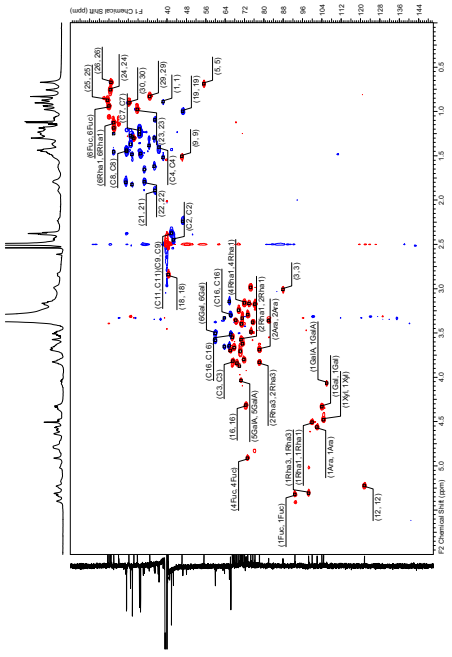

Figure S38. HSQC-DEPT spectrum of compound **6** (600 MHz, DMSO-d_6).

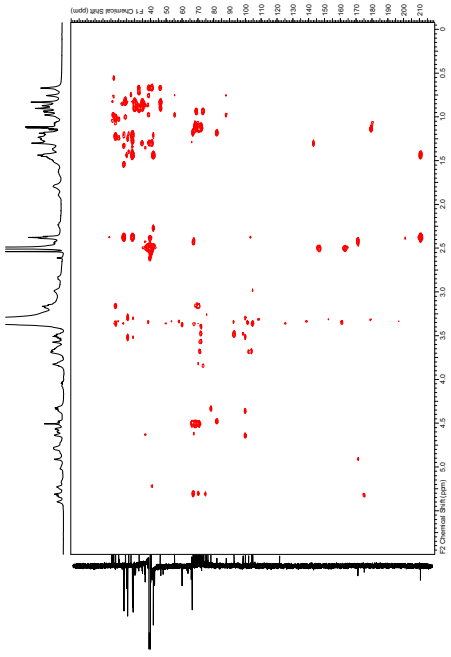

Figure S39. HMBC spectrum of compound **6** (600 MHz, DMSO-d_6).

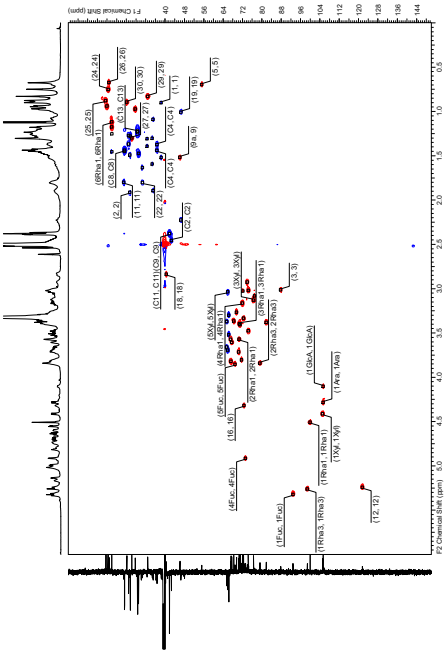

Figure S44. HSQC-DEPT spectrum of compound **7** (600 MHz, DMSO-d_6).

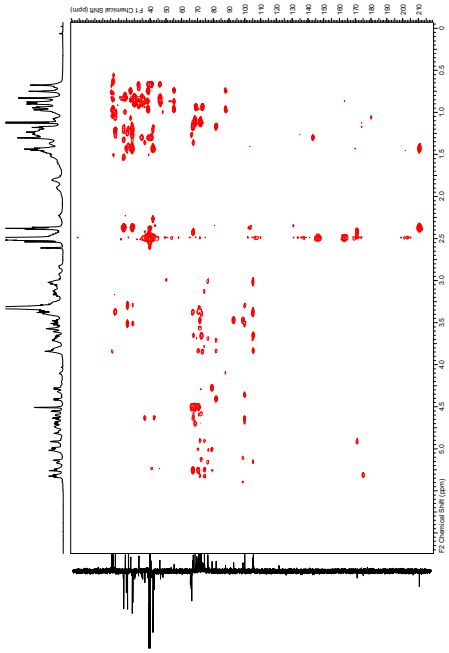

Figure S45. HMBC spectrum of compound **7** (600 MHz, DMSO-d_6).

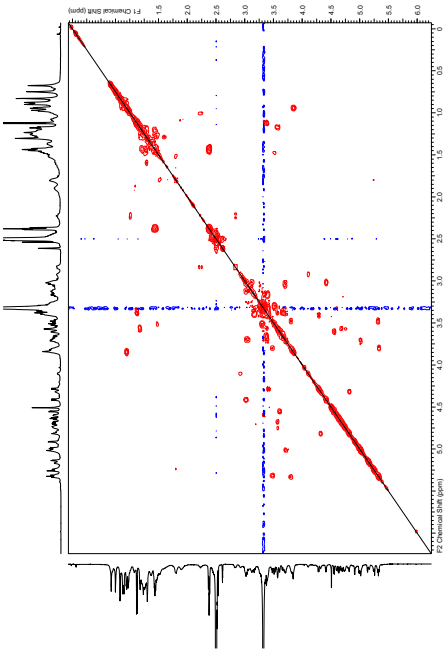

Figure S42. ^{1}H-^{1}H COSY spectrum of compound **7** (600 MHz, DMSO-d_6).

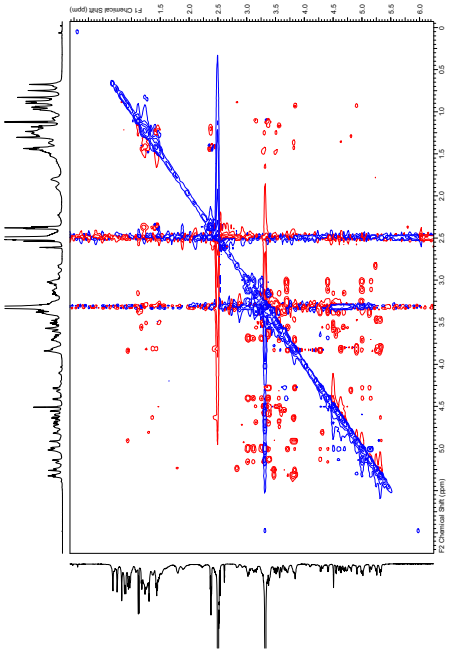

Figure S43. ^{1}H-^{1}H ROESY spectrum of compound **7** (600 MHz, DMSO-d_6).

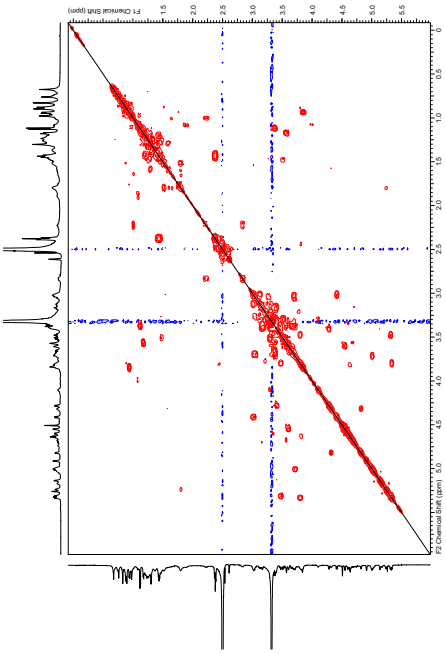

Figure S48. ^{1}H-^{1}H COSY spectrum of compound **8** (600 MHz, DMSO-d_6).

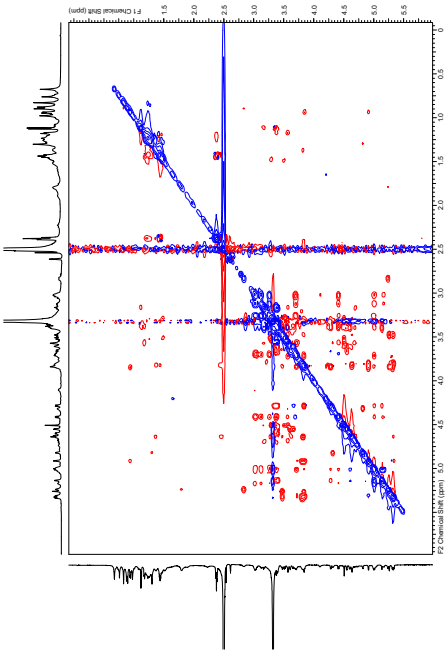

Figure S49. ^{1}H-^{1}H ROESY spectrum of compound **8** (600 MHz, DMSO-d_6).

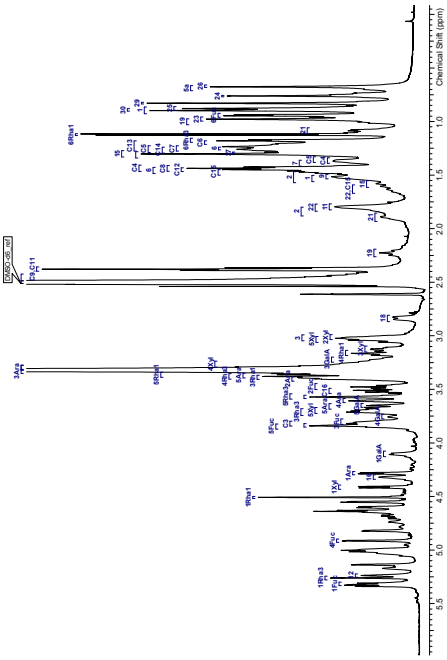

Figure S46. ^{1}H-NMR spectrum of compound **8** (600 MHz, DMSO-d_6).

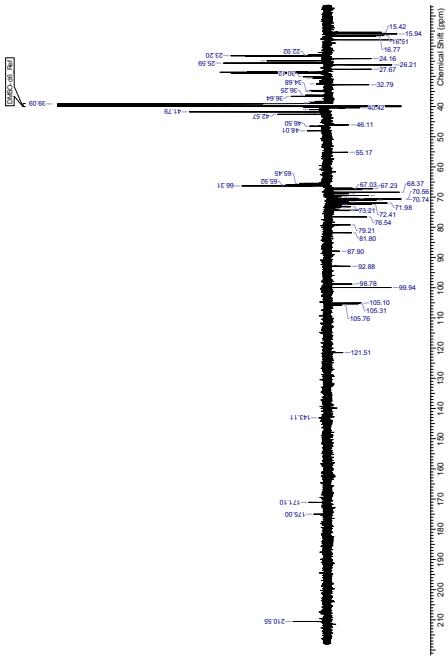

Figure S47. ^{13}C-DEPTq spectrum of compound **8** (151 MHz, DMSO-d_6).

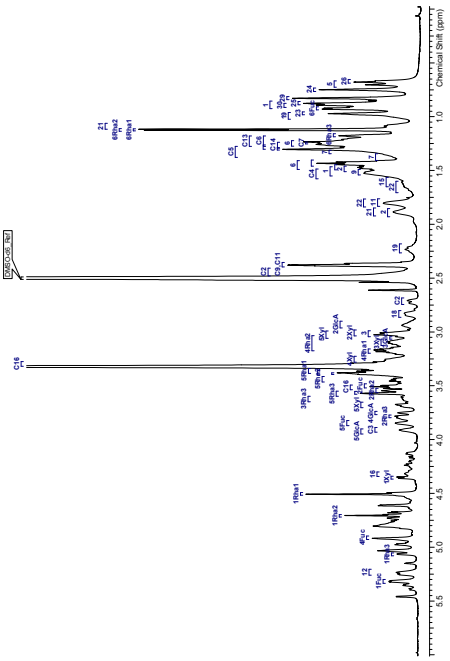

Figure S52. ^{1}H-NMR spectrum of compound **9** (600 MHz, DMSO-d_6).

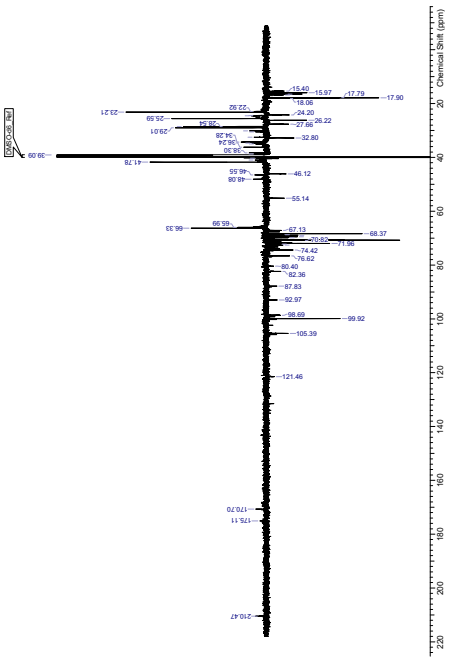

Figure S53. ^{13}C-DEPTq spectrum of compound **9** (151 MHz, DMSO-d_6).

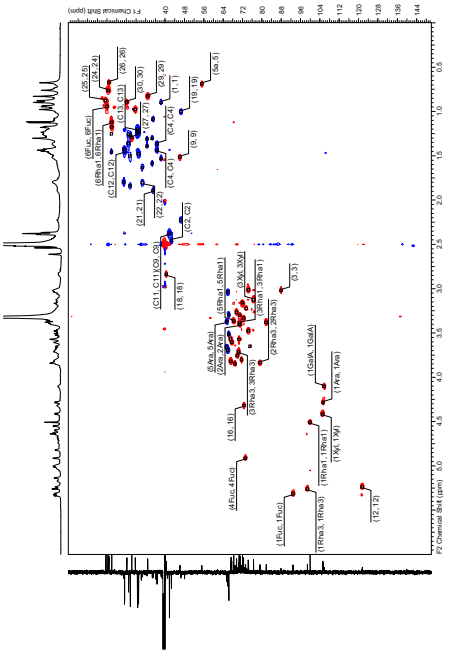

Figure S50. HSQC-DEPT spectrum of compound **8** (600 MHz, DMSO-d_6).

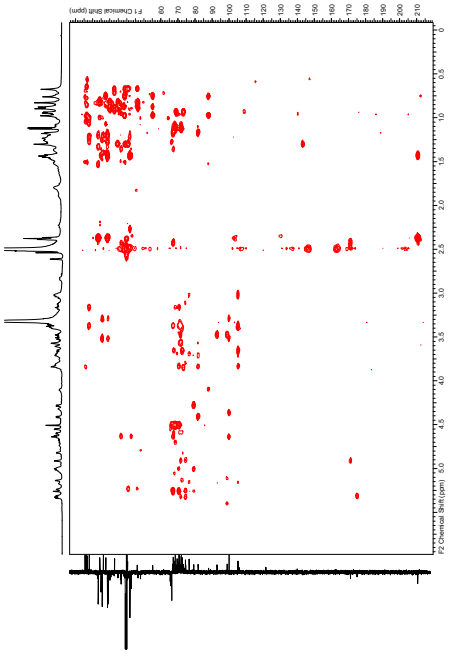

Figure S51. HMBC spectrum of compound **8** (600 MHz, DMSO-d_6).

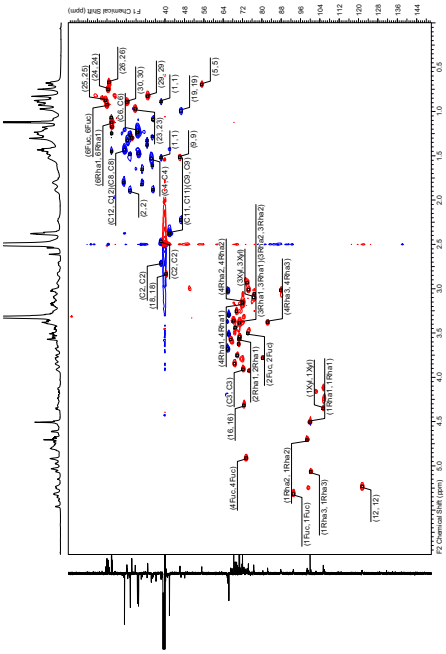

Figure S54. ^{1}H-^{1}H COSY spectrum of compound **9** (600 MHz, DMSO-d_6).

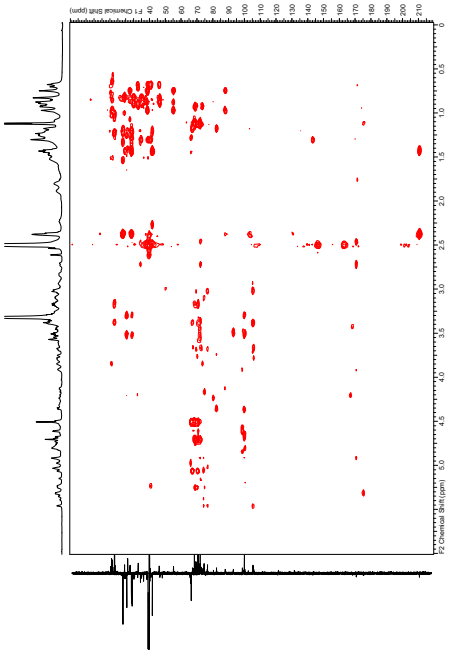

Figure S55. ^{1}H-^{1}H ROESY spectrum of compound **9** (600 MHz, DMSO-d_6).

Figure S56. HSQC-DEPT spectrum of compound **9** (600 MHz, DMSO-d_6).

Figure S57. HMBC spectrum of compound **9** (600 MHz, DMSO-d_6).

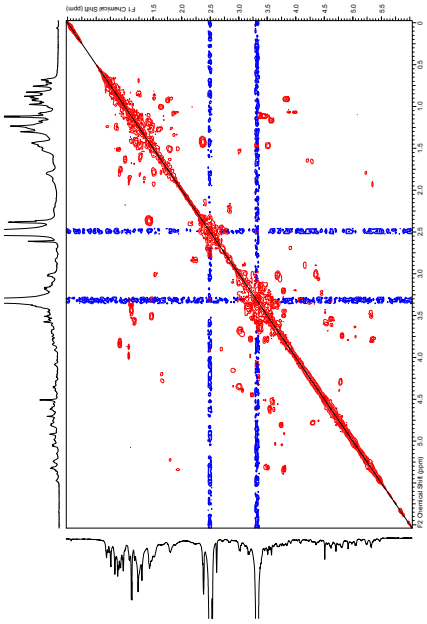

Figure S60. ^{1}H-^{1}H COSY spectrum of compound **10** (600 MHz, DMSO-d_6).

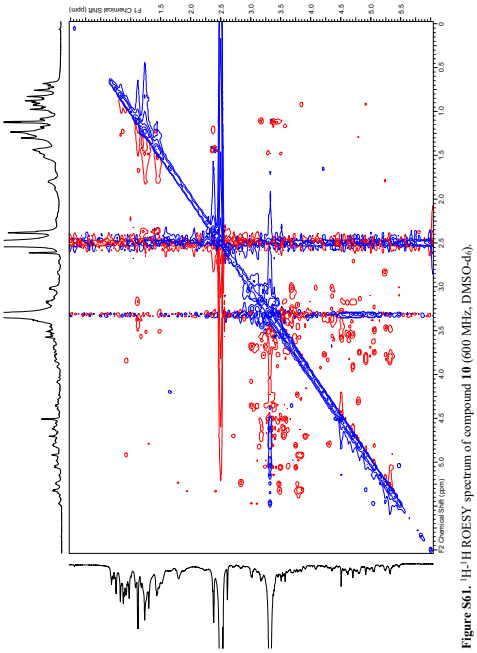

Figure S61. ^{1}H-^{1}H ROESY spectrum of compound **10** (600 MHz, DMSO-d_6).

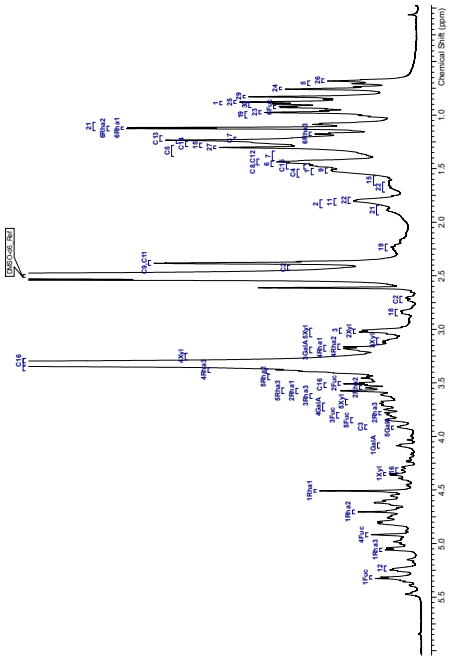

Figure S58. ^{1}H-NMR spectrum of compound **10** (600 MHz, DMSO-d_6).

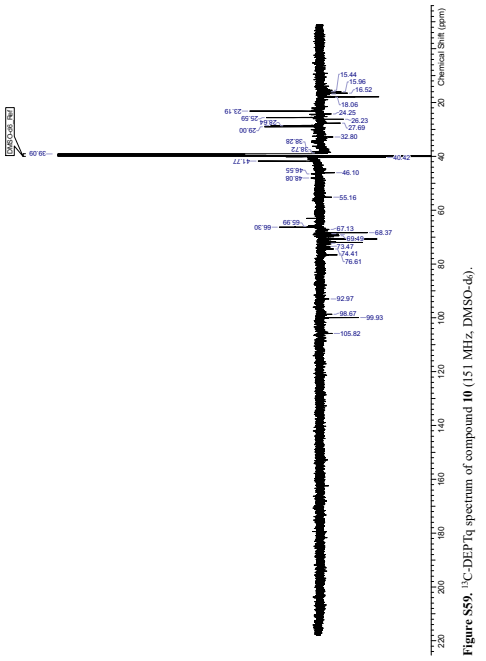

Figure S59. ^{13}C-DEPTq spectrum of compound **10** (151 MHz, DMSO-d_6).

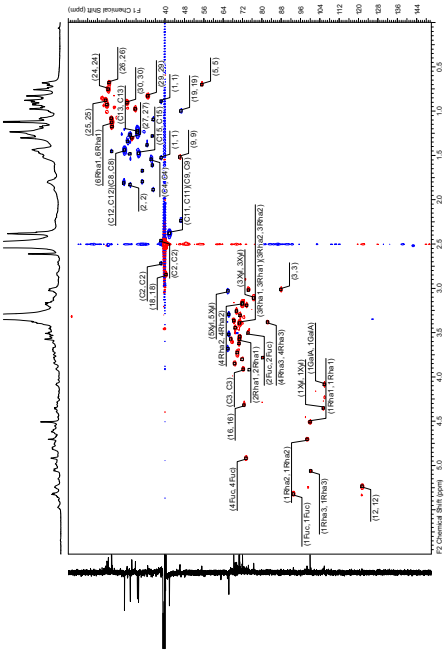

Figure S62. HSQC-DEPT spectrum of compound **10** (600 MHz, DMSO-d_6).

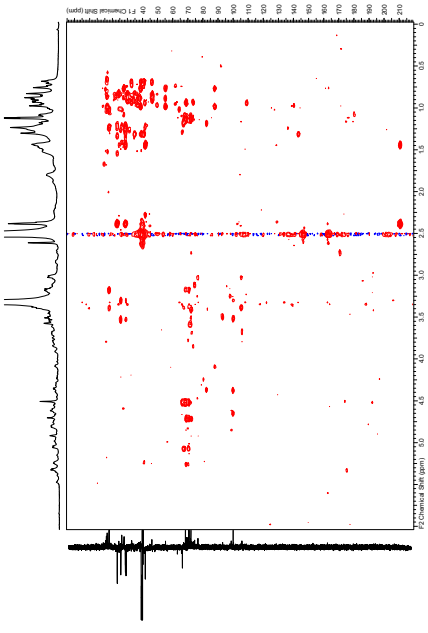

Figure S63. HMBC spectrum of compound **10** (600 MHz, DMSO-d_6).

SUPPLEMENTARY MATERIALS

Teucrium polium - Wound healing potential, toxicity and polyphenolic profile

Sarra Chabane[1*], Amel Boudjelal[2], Morris Keller[3], Sara Doubakh[2], Olivier Potterat[3*]

1. Department of Life and Nature Science, Faculty of Sciences, Mohamed Boudiaf University, 28000 M'Sila, Algeria.
2. Department of Microbiology and Biochemistry, Faculty of Sciences, Mohamed Boudiaf University, 28000 M'Sila, Algeria.
3. Division of Pharmaceutical Biology, University of Basel, Klingelbergstrasse 50, CH-4056 Basel, Switzerland

Corresponding authors:

Prof. Olivier Potterat
Olivier.potterat@unibas.ch
Tel. +41 612071534
Orcid.org/0000-0001-5962-6516

Sarra Chabane
sarra.chabane@univ-msila.dz
Tel. +21 3658858923
Orcid.org/0000-0002-2519-4900

Content:

Table 1. ^{1}H and ^{13}C NMR Spectroscopic Data for Poliumoside (**1**) (DMSO-d6; 500.13 Hz; δ in ppm)

		1
Position	δ_C	δ_H (mult *J* in Hz)
1	126.3, C	-
2	115.4,CH	7.07 d (1.8)
3	146.0, C	-
4	149.1, C	-
5	116.5, CH	6.81 d (8.3)
6	122.1, CH	7.01 dd (8.3, 2.0)
7	146.3, CH	7.54 d (16.2)
8	114.2, CH	6.22 d (16.2)
9	166.2, C	-
1'	130.0, C	-
2'	116.3, CH	6.68 br d[a]
3'	145.6, C	-
4'	144.2, C	-
5'	117.0, CH	6.67 br d[a]
6'	120.2, CH	6.54 dd (8.1, 2.0)
7'	35.7, CH_2	2.75 m
8'	71.0, CH_2	3.89 m 3.69 m[a]
Glc 1	103.1 CH	4.41 br d (7.9)
Glc 2	75.1, CH	3.28 m
Glc 3	79.7, CH	3.77 m[a]
Glc 4	69.8, CH	4.79 t (9.6, 9.6)
Glc 5	73.6, CH	3.70 br d (1.8)[a]
Glc 6	66.7, CH_2	3.58 br dd (9.8) 3.39 m[a]
Rha(1) 1	101.2, CH	4.55 br d (0.9)
Rha(1) 2	71.1, CH	3.65 m[a]
Rha(1) 3	71.4, CH	3.46 m[a]
Rha(1) 4	72.6, CH	3.20 m[a]
Rha(1) 5	69.2, CH	3.43 m[a]
Rha(1) 6	18.4, CH_3	1.10 d (6.1)
Rha(2) 1	101.8, CH	5.09 br d (0.9)
Rha(2) 2	71.2, CH	3.75 m[a]
Rha(2) 3	71.2, CH	3.35 m[a]
Rha(2) 4	72.5, CH	3.17 m[a]
Rha(2) 5	69.2, CH	3.43 m[a]
Rha(2) 6	18.7, CH_3	1.02 br d (0.9)

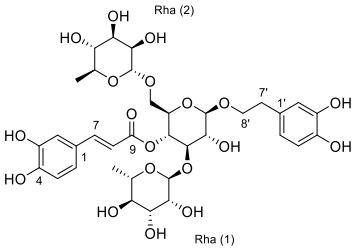

[a]Overlapping signals.
nd: not detected signals
Assignments based on COSY, HSQC, and HMBC data
^{13}C NMR data extracted from HSQC and HMBC spectra

Table 2. ^{1}H and ^{13}C NMR Spectroscopic Data for Acteoside (**2**) (DMSO-d6; 500.13 Hz; δ in ppm)

		2
Position	δ_C	δ_H (mult *J* in Hz)
1	125.6, C	-
2	114.8,CH	7.03 br s
3	145.5, C	-
4	148.6, C	-
5	116.0, CH	6.77 d (6.4)
6	121.5, CH	6.97 d (6.4)
7	145.7, CH	7.46 br d (15.9)
8	113.9, CH	6.19 br d (15.9)
9	165.7, C	-
1'	129.4, C	-
2'	115.7, CH	6.64 br s[a]
3'	145.0, C	-
4'	143.6, C	-
5'	116.4, CH	6.65 m[a]
6'	119.7, CH	6.50 d (6.4)
7'	35.1, CH_2	2.71 m
8'	70.3, CH_2	3.63 br d 3.89 br d[a]
Glc 1	102.5 CH	4.35 br d (5.5)
Glc 2	74.7, CH	3.23 m[a]
Glc 3	79.3, CH	3.70 m[a]
Glc 4	69.4, CH	4.72 br t
Glc 5	74.6, CH	3.48 m[a]
Glc 6	61.0, CH_2	3.42 m[a] 3.35 m[a]
Rha 1	101.3, CH	5.05 br d
Rha 2	70.6, CH	3.71 br s[a]
Rha 3	70.7, CH	3.32 m[a]
Rha 4	71.9, CH	3.13 m[a]
Rha 5	68.8, CH	3.38 m[a]
Rha 6	18.1, CH_3	0.97 br d

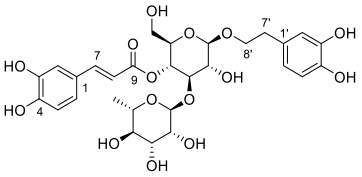

[a]Overlapping signals.
nd: not detected signals
Assignments based on COSY, HSQC, and HMBC data
^{13}C NMR data extracted from HSQC and HMBC spectra

Table 3. ^{1}H and ^{13}C NMR Spectroscopic Data for Hyperoside (**3**) (DMSO-d6; 500.13 Hz; δ in ppm)

		3
Position	δ_C	δ_H (mult *J* in Hz)
2	157.4, C	-
3	134.6, C	-
4	nd	-
5	nd	-
5-OH	-	12.60 br
6	99.7, CH	6.22 br s
7	nd	-
8	94.5, CH	6.43 br s
9	nd	-
10	nd	-
1'	122.1, C	-
2'	117.1, CH	7.61 br s[a]
3'	145.6, C	-
4'	149.3, C	-
5'	116.2, CH	6.86 br d (8.2)
6'	122.8, CH	7.65 br d (8.2)[a]
Gal 1	103.2, CH	5.34 d (7.9)
Gal 2	72.2, CH	3.63 m[a]
Gal 3	74.2, CH	3.43 m[a]
Gal 4	68.9, CH	3.72 m
Gal 5	76.6, CH	3.38 m[a]
Gal 6	61.1, CH_2	3.51 m[a] 3.53 m[a]

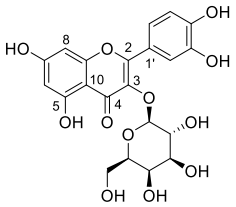

[a]Overlapping signals.
nd: not detected signals
Assignments based on COSY, HSQC, and HMBC data
^{13}C NMR data extracted from HSQC and HMBC spectra

Table 4. ^{1}H and ^{13}C NMR Spectroscopic Data for Isoquercitrin (**4**) (DMSO-d6; 500.13 Hz; δ in ppm)

		4
Position	δ_C	δ_H (mult *J* in Hz)
2	156.8, C	-
3	134.1, C	-
4	nd	-
5	nd	-
5-OH	-	nd
6	99.5, CH	6.24 br s
7	nd	-
8	94.2, CH	6.44 br s
9	nd	-
10	104.5, C	-
1'	121.7, C	-
2'	116.9, CH	7.65 br s
3'	145.5, C	-
4'	149.2, C	-
5'	115.9, CH	6.90 br d (8.2)
6'	122.1, CH	7.61 br d (8.2)
Glc 1	101.8, CH	5.47 d (7.0)
Glc 2	74.8, CH	3.31 m[a]
Glc 3	77.2 CH	3.31 m[a]
Glc 4	70.7, CH	3.18 m[a]
Glc 5	78.0, CH	3.16 m[a]
Glc 6	61.7, CH_2	3.63 br d (11.3) 3.41 m[a]

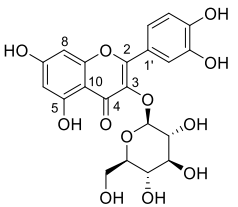

[a]Overlapping signals
nd: not detected
Assignments based on COSY, HSQC, and HMBC data
^{13}C NMR data extracted from HSQC and HMBC spectra

Table 5. ^{1}H and ^{13}C NMR Spectroscopic Data for Luteolin-7-O- β-D-glucopyranoside (**5**) (DMSO-d6; 500.13 Hz; δ in ppm)

		5
Position	δ_C	δ_H (mult *J* in Hz*)*
2	165.1, C	-
3	103.7, CH	6.74 s
4	nd	-
5	nd	-
5-OH	-	12.80 br
6	100.2, CH	6.49 s
7	163.5, C	-
8	95.4, CH	6.83 s
9	157.6, C	-
10	106.0, C	-
1'	121.9, C	-
2'	114.1, CH	7.47 br s[a]
3'	145.5, C	-
4'	150.8, C	-
5'	116.7, CH	6.95 br d
6'	119.8, CH	7.46 br d[a]
Glc 1	100,7 CH	5.12 d (7.6)
Glc 2	73.8, CH	3.35 m[a]
Glc 3	77.1, CH	3.39 m[a]
Glc 4	70.4, CH	3.27 m[a]
Glc 5	77.8, CH	3.50 m[a]
Glc 6	61.3, CH_2	3.78 m 3.56 m[a]

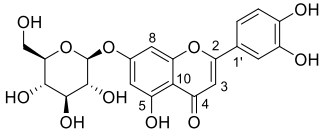

Overlapping signals.
nd: not detected signals
Assignments based on COSY, HSQC, and HMBC data
^{13}C NMR data extracted from HSQC and HMBC spectra

Table 6. ^{1}H and ^{13}C NMR Spectroscopic Data for Luteolin 7-O-(5-O-syringoyl-β-D-apiofuranosyl)-(1→2)-β-D-glucopyranoside (**6**) (DMSO-d6; 500.13 Hz; δ in ppm)

		6
Position	δ_C	δ_H (mult *J* in Hz*)*
2	166.6, C	-
3	105.1, CH	6.60 s
4	183.7, C	-
5	nd	-
5-OH	-	nd
6	101.2, CH	6.32 s
7	164.5, C	-
8	96.3, CH	6.65 d
9	158.9, C	-
10	107.4, C	-
1'	123.8, C	-
2'	115.7, CH	7.40 br s[a]
3'	147.0, C	-
4'	151.9, C	-
5'	118.1, CH	6.93 br d (7.7)
6'	121.2, CH	7.37 br d (7.7)[a]
1''	120.9, C	-
2''	109.3, CH	7.04 s[a]
3''	149.7, C	-
3''-OMe	58.0, CH_3	3.71 s[a]
4''	142.9, C	-
4''-OH	nd	-
5''	149.4, C	-
5''-OMe	58.0, CH_3	3.71 s[a]
6''	109.3, CH	7.04 s[a]
7''	167.3, C	-
Glc 1	100.1 CH	5.17 br d (7.1)
Glc 2	78.2, CH	3.57 m[a]
Glc 3	79.1, CH	3.46 m[a]
Glc 4	72.0, CH	3.25 br t
Glc 5	78.9, CH	3.55 m[a]
Glc 6	62.7, CH_2	3.51 m[a] 3.73 m[a]
Api 1	110.6, CH	5.42 s
Api 2	79.0, CH	3.89 s
Api 3	79.5, C	-
Api 4	69.1, CH_2	4.22 d (11.0) 4.14 d (11.0)
Api 5	75.8, CH_2	3.85 br d (9.3) 4.08 br d (9.3)

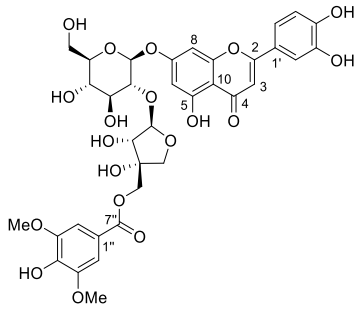

[a]Overlapping signals.
nd: not detected signals
Assignments based on COSY, HSQC, and HMBC data
^{13}C NMR data extracted from HSQC and HMBC spectra

Table 7. ^{1}H and ^{13}C NMR Spectroscopic Data for Cirsiliol (**9**) (DMSO-d6; 500.13 Hz; δ in ppm)

		9
Position	δ_C	δ_H (mult *J* in Hz)
2	164.4, C	-
3	102.7, CH	6.65 s
4	182.0, C	-
5	nd	-
5-OH	-	12.90 br s
6	132.2, C	-
6-OMe	60.0, CH_3	3.75 s
7	158.6, C	-
7-OMe	56.3, CH_3	3.92 s
8	91.4, CH	6.80 s
9	152.7, C	-
10	105.4, C	-
1'	121.9, C	-
2'	113.6, CH	7.43 br s[a]
3'	145.8, C	-
4'	150.1, C	-
5'	116.1, C	6.91 br d (7.9)
6'	118.9, CH	7.41, d (7.9)[a]

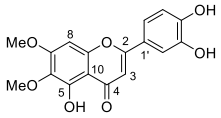

[a]Overlapping signals.
nd: not detected signals
Assignments based on COSY, HSQC, and HMBC data
^{13}C NMR data extracted from HSQC and HMBC spectra

Table 8. ^{1}H and ^{13}C NMR Spectroscopic Data for Cirsimaritine (**10**) (DMSO-d6; 500.13 Hz; δ in ppm)

		10
Position	δ_C	δ_H (mult *J* in Hz)
2	161.2, C	-
3	103.2, CH	6.83 s
4	179.2, C	-
5	nd	-
5-OH	-	12.90 br s
6	129.5, C	-
6-OMe	60.6, CH_3	3.78 s
7	155.6, C	-
7-OMe	57.0, CH_3	3.96 s
8	92.1, CH	6.93 s
9	149.7, C	-
10	102.1, C	-
1'	122.6, C	-
2'	129.1, CH	7.99 br s
3'	116.7, CH	6.98 br s
4'	158.5, C	-
5'	116.7, CH	6.96 br s
6'	118.2, CH	7.56, br s

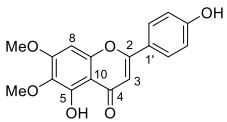

[a]Overlapping signals.
nd: not detected signals
Assignments based on COSY, HSQC, and HMBC data
^{13}C NMR data extracted from HSQC and HMBC spectra

Table 9. ^{1}H and ^{13}C NMR Spectroscopic Data for Cirsilineol (**11**) (DMSO-d6; 500.13 Hz; δ in ppm)

		11
Position	δ_C	δ_H (mult *J* in Hz)
2	163.7, C	-
3	102.4, CH	6.85[a]
4	181.7, C	-
5	nd	-
5-OH	-	13.00 br
6	131.6, C	-
6-OMe	59.6, CH_3	3.75 br s
7	158.2, C	-
7-OMe	56.0, CH_3	3.93 br s[a]
8	91.0, CH	6.88[a]
9	152.3, C	-
10	104.7, C	-
1'	120.8, C	-
2'	110.1, CH	7.55[a]
3'	147.9, C	-
3'-OMe	55.7, CH_3	3.91 br s[a]
4'	151.1, C	-
5'	115.6, CH	6.97 br d[a]
6'	120.2, CH	7.56, br d[a]

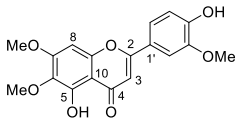

[a]Overlapping signals.
nd: not detected signals
Assignments based on COSY, HSQC, HMBC, and NOESY data
^{13}C NMR data extracted from HSQC and HMBC spectra

Table 10. ^{1}H and ^{13}C NMR Spectroscopic Data for Eupatorin (**12**) (DMSO-d6; 500.13 Hz; δ in ppm)

		12
Position	δ_C	δ_H (mult *J* in Hz)
2	163.5, C	-
3	102.9, CH	6.75 br s
4	181.6, C	-
5	nd	-
5-OH	-	12.90 br
6	131.6, C	-
6-OMe	59.5, CH_3	3.75 br s
7	158.2, C	-
7-OMe	56.0, CH_3	3.93 br s
8	91.1, CH	6.88 br s
9	152.1, C	-
10	104.7, C	-
1'	122.6, C	-
2'	112.8, CH	7.49 br s
3'	146.5, C	-
4'	150.8, C	-
4'-OMe	55.4, CH_3	3.88 br s
5'	111.8, CH	7.09 br d (8.5)
6'	118.2, CH	7.56, br d (8.5)

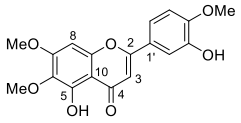

[a]Overlapping signals.
nd: not detected signals
Assignments based on COSY, HSQC, HMBC, and NOESY data
^{13}C NMR data extracted from HSQC and HMBC spectra

Table 11. ^{1}H and ^{13}C NMR Spectroscopic Data for 5-Desmethylsinesetin (**13**) ($CDCl_3$; 500.13 Hz; δ in ppm)

		13
Position	δ_C	δ_H (mult *J* in Hz)
2	164.0, C	-
3	104.3, CH	6.51 s
4	182.6, C	-
5	153.1, C	-
5-OH	-	12.94 s
6	132.9, C	-
6-OMe	60.6, CH_3	3.89 s
7	158.8, C	-
7-OMe	56.0, CH_3	3.93 br s[a]
8	90.6, CH	6.49 s
9	153.3, C	-
10	106.2, C	-
1'	122.6, C	-
2'	109.3, CH	7.29 s
3'	149.6, C	-
3'-OMe	56.0, CH_3	3.94 br s[a]
4'	152.6, C	-
4'-OMe	56.2, CH_3	3.93 br s[a]
5'	111.5, CH	6.93 d (8.2)
6'	120.0, CH	7.45, br d (8.2)

[a]Overlapping signals.
nd: not detected signals
Assignments based on COSY, HSQC, and HMBC data
^{13}C NMR data extracted from HSQC and HMBC spectra

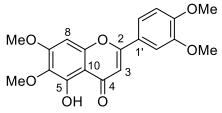

Table 12. ^{1}H and ^{13}C NMR Spectroscopic Data for Salvigenin (**14**) (DMSO-d6; 500.13 Hz; δ in ppm)

		14
Position	δ_C	δ_H (mult *J* in Hz)
2	160.8, C	-
3	104.0, CH	6.88 s
4	179.2, C	-
5	149.6, C	-
5-OH	-	12.83 br
6	128.6, C	-
6-OMe	60.8, CH_3	3.78 s
7	155.7, C	-
7-OMe	57.2, CH_3	3.97 s
8	92.3, CH	6.95 s
9	155.2, C	-
10	102.2, C	-
1'	119.8, C	-
2'	129.1, CH	8.06 br s
3'	115.4, CH	7.14 br s
4'	159.5, C	-
4'-OMe	56.3, CH_3	3.90 s
5'	115.4, CH	7.16 br s
6'	129.1, CH	8.08 br s

[a]Overlapping signals.
nd: not detected signals
Assignments based on COSY, HSQC, and HMBC data
^{13}C NMR data extracted from HSQC and HMBC spectra

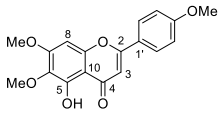

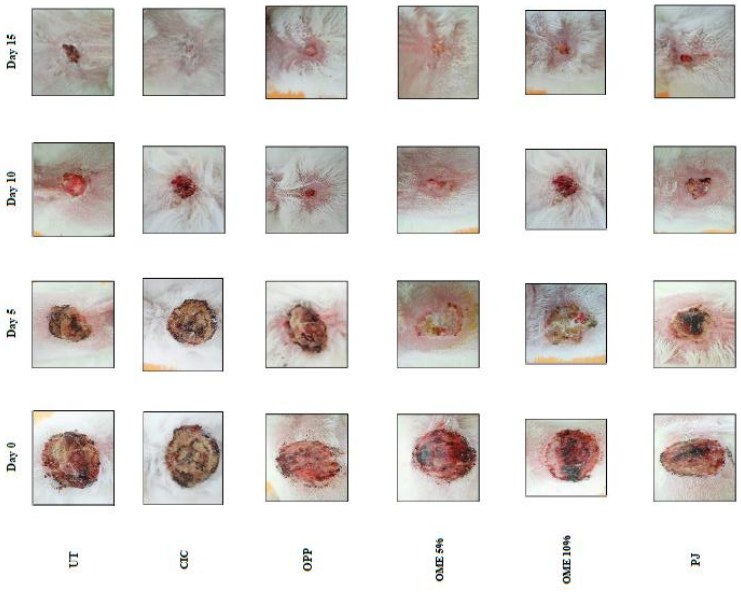

Fig. 1 Pictures of chronological evolution of wound healing in the various groups. UT: untreated group; CIC: group treated with Cicatryl-Bio; OME 5% / 10%: groups treated with the methanolic extract ointment; PJ: group treated with petroleum jelly.

Publication 4

New neo-clerodane diterpenes from *Teucrium polium* subsp. *capitatum*

Morris Keller[1], Sarra Chabane[2], Amel Boudjelal[3,4], Ombeline Danton[1], Alessandro Prescimone[5], Matthias Hamburger[1], Olivier Potterat[1,*]

1 Division of Pharmaceutical Biology, University of Basel, Klingelbergstrasse 50, CH-4056 Basel, Switzerland;

2 Department of Life and Nature Science, Faculty of Sciences, Mohamed Boudiaf University, 28000 M'Sila, Algeria

3 Department of Microbiology and Biochemistry, Faculty of Sciences, Mohamed Boudiaf University, 28000 M'Sila, Algeria

4 Biology Laboratory: Applications in Health and Environment, Faculty of Sciences, Mohamed Boudiaf University, 28000 M'Sila, Algeria

5 Department of Chemistry, University of Basel, Mattenstrasse 22, CH-4058 Basel, Switzerland

Corresponding authors:
Prof. Olivier Potterat
Olivier.potterat@unibas.ch
Tel. +41 612071534
Fax. +41 612071474
Orcid.org/0000-0001-5962-6516

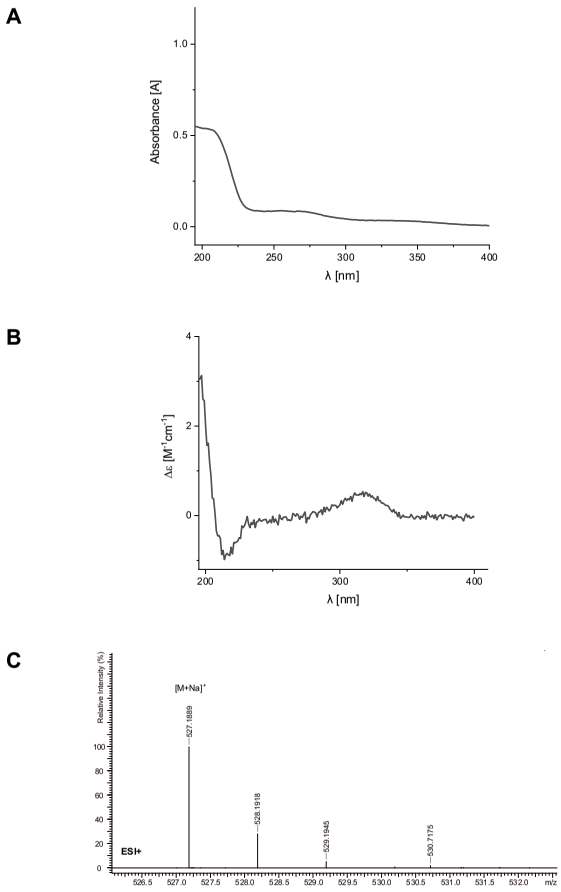

Figure S1. A) UV and **B)** ECD spectrum of **1** in MeOH, **C)** HRESIMS spectrum of **1**.

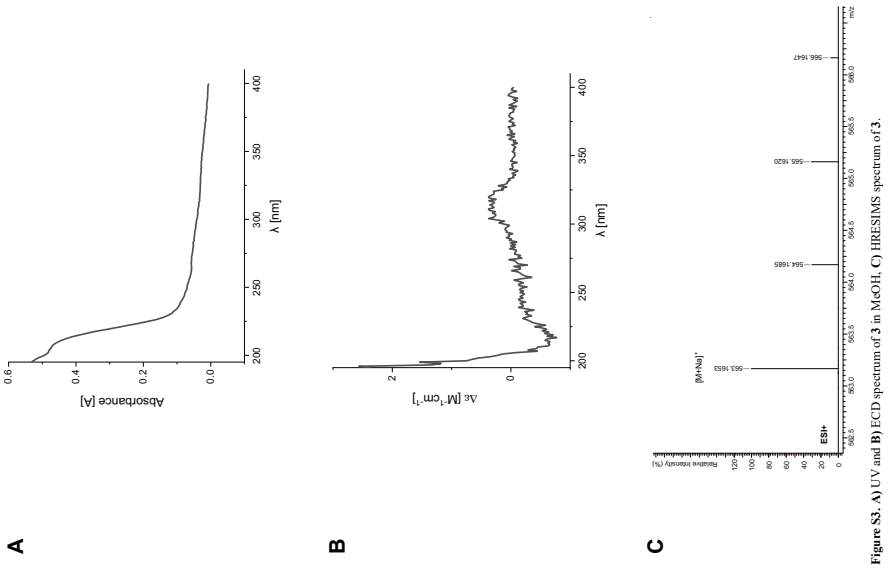

Figure S3. **A)** UV and **B)** ECD spectrum of **3** in MeOH, **C)** HRESIMS spectrum of **3**.

3

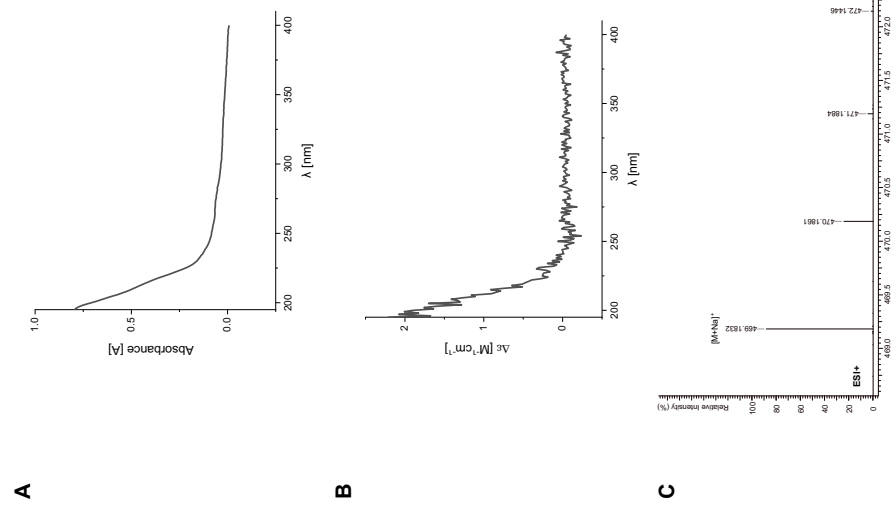

Figure S2. **A)** UV and **B)** ECD spectrum of **2** in MeOH, **C)** HRESIMS spectrum of **2**.

2

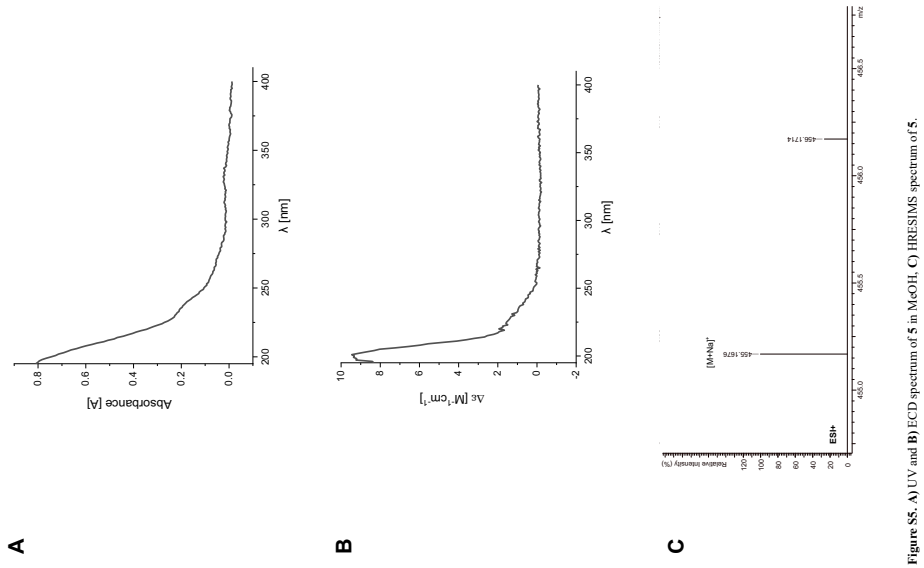

Figure S5. **A)** UV and **B)** ECD spectrum of **5** in MeOH, **C)** HRESIMS spectrum of **5**.

5

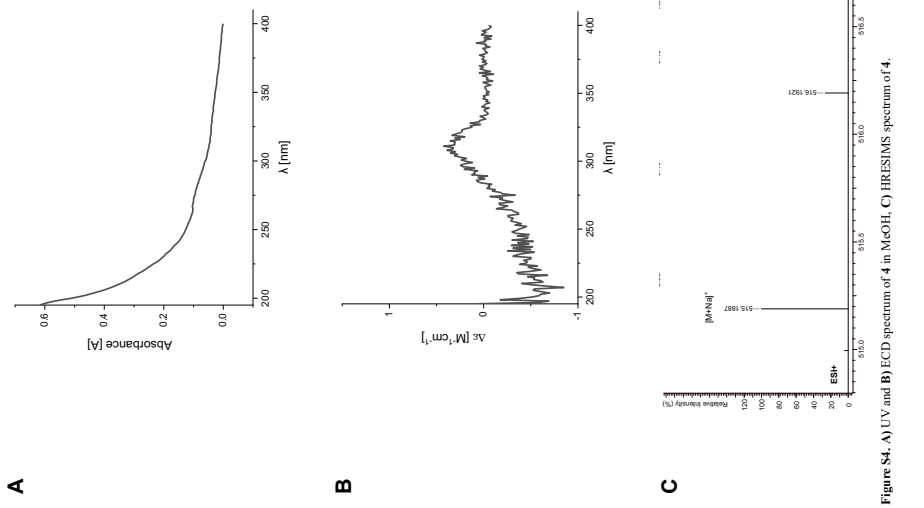

Figure S4. **A)** UV and **B)** ECD spectrum of **4** in MeOH, **C)** HRESIMS spectrum of **4**.

4

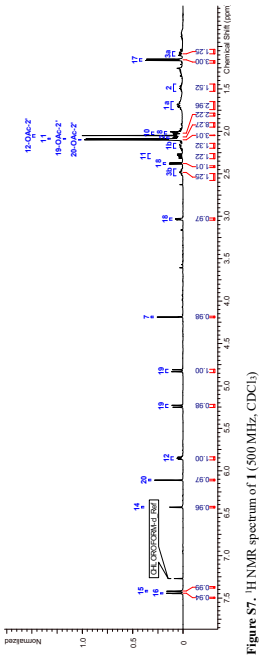

Figure S7. ^{1}H NMR spectrum of **1** (500 MHz, CDCl$_3$).

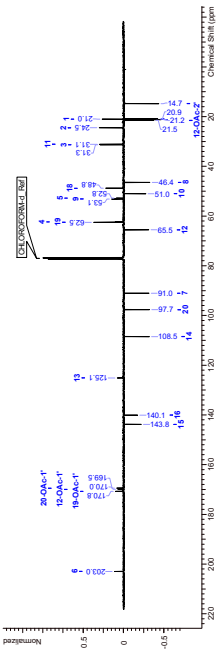

Figure S8. ^{13}C DEPTq spectrum of **1** (126 MHz, CDCl$_3$).

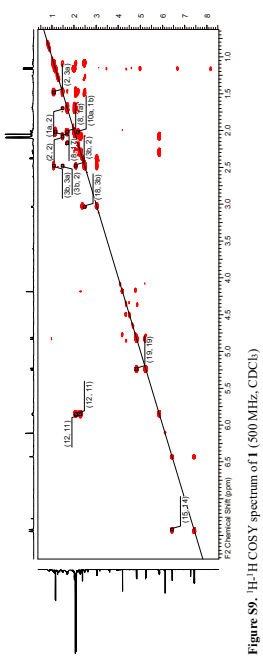

Figure S9. ^{1}H,^{1}H COSY spectrum of **1** (500 MHz, CDCl$_3$).

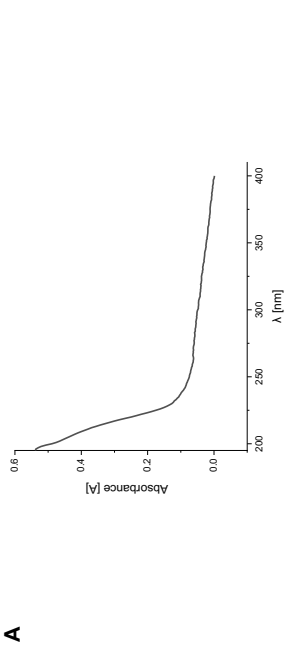

Figure S6. A) UV and **B)** ECD spectrum of **6** in MeOH, **C)** HRESIMS spectra of **6**.

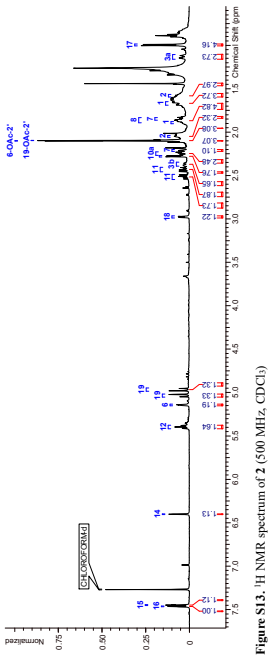

Figure S13. ^{1}H NMR spectrum of **2** (500 MHz, $CDCl_3$)

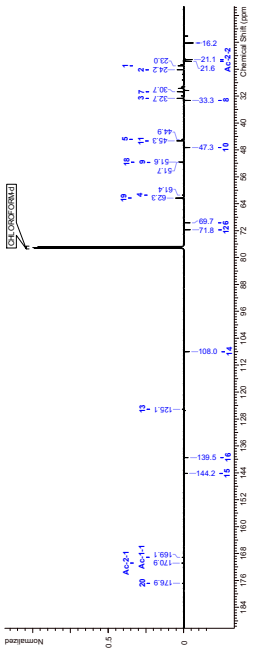

Figure S14. ^{13}C DEPTq spectrum of **2** (126 MHz, $CDCl_3$)

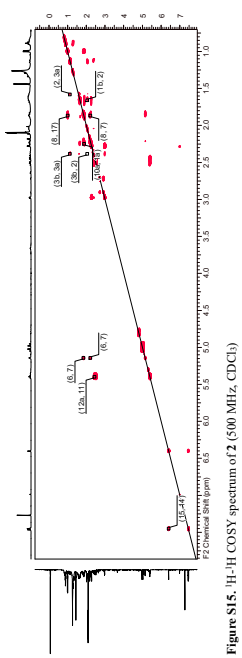

Figure S15. ^{1}H-^{1}H COSY spectrum of **2** (500 MHz, $CDCl_3$)

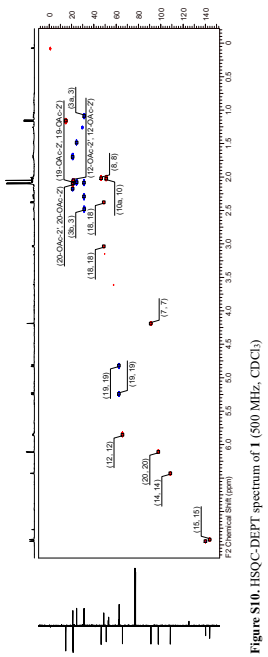

Figure S10. HSQC-DEPT spectrum of **1** (500 MHz, $CDCl_3$)

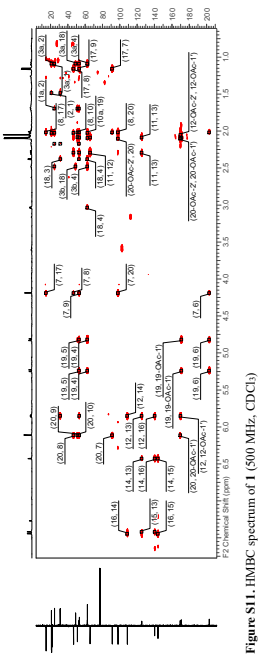

Figure S11. HMBC spectrum of **1** (500 MHz, $CDCl_3$)

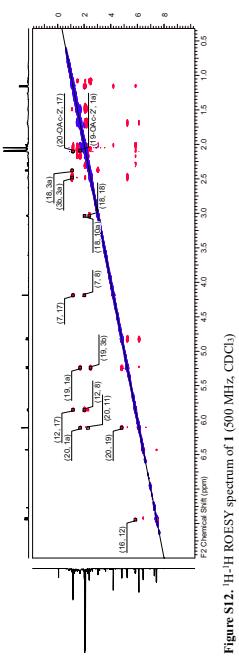

Figure S12. ^{1}H-^{1}H ROESY spectrum of **1** (500 MHz, $CDCl_3$)

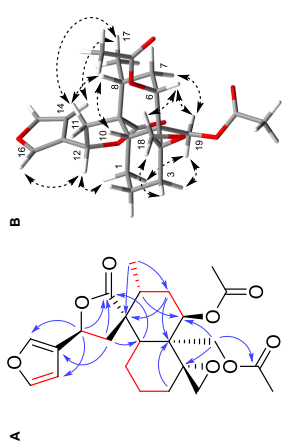

Figure S19. (A) COSY (red) and key HMBC correlations (blue arrows), (B) key ROESY correlations of **2**.

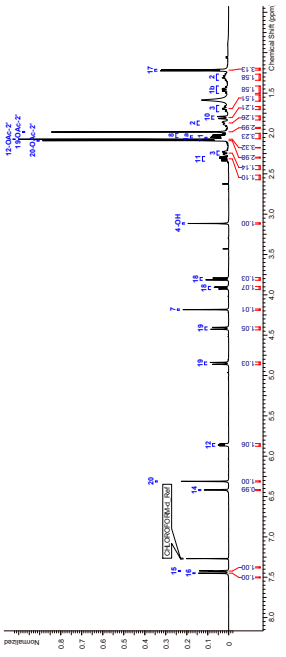

Figure S20. ^{1}H NMR spectrum of **3** (500 MHz, $CDCl_3$)

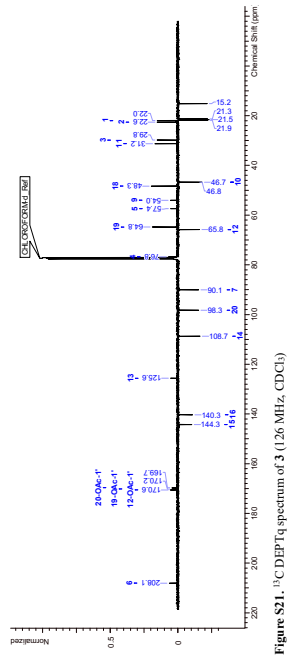

Figure S21. ^{13}C DEPTq spectrum of **3** (126 MHz, $CDCl_3$)

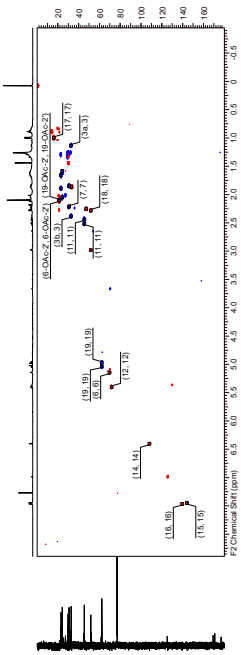

Figure S16. HSQC-DEPT spectrum of **2** (500 MHz, $CDCl_3$)

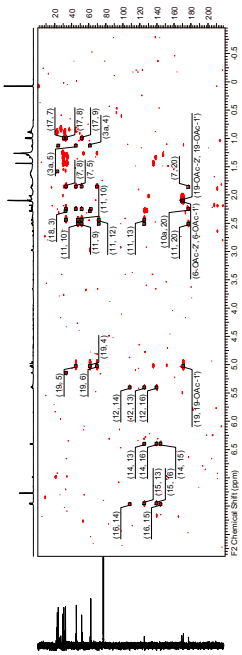

Figure S17. HMBC spectrum of **2** (500 MHz, $CDCl_3$)

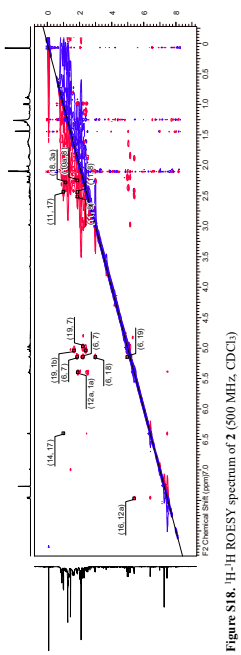

Figure S18. ^{1}H-^{1}H ROESY spectrum of **2** (500 MHz, $CDCl_3$)

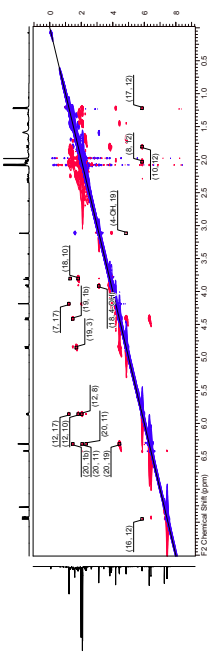

Figure S25. ^{1}H-^{1}H ROESY spectrum of **3** (500 MHz, $CDCl_3$)

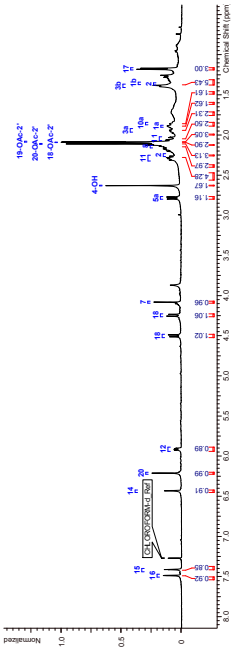

Figure S26. ^{1}H NMR spectrum of **4** (500 MHz, $CDCl_3$)

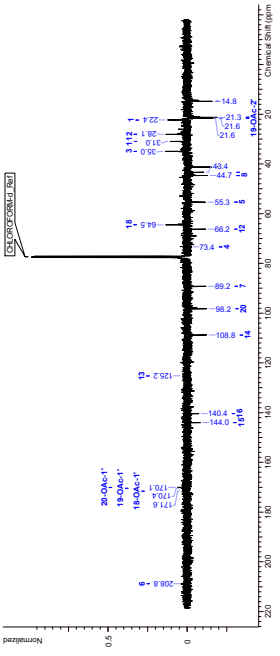

Figure S27. ^{13}C DEPTq spectrum of **4** (126 MHz, $CDCl_3$)

13

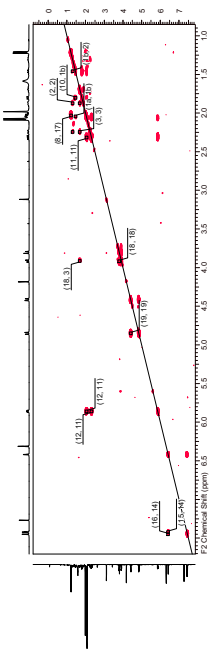

Figure S22. ^{1}H-^{1}H COSY spectrum of **3** (500 MHz, $CDCl_3$)

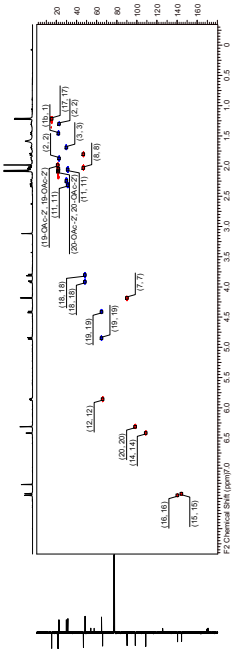

Figure S23. HSQC-DEPT spectrum of **3** (500 MHz, $CDCl_3$)

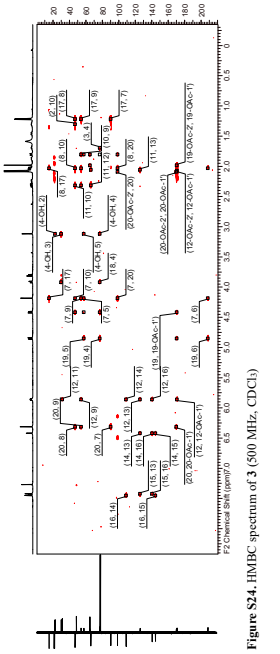

Figure S24. HMBC spectrum of **3** (500 MHz, $CDCl_3$)

12

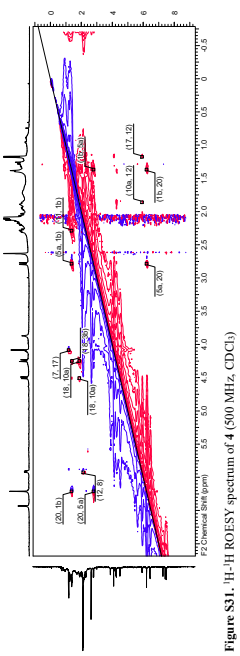

Figure S31. ^{1}H-^{1}H ROESY spectrum of **4** (500 MHz, $CDCl_3$).

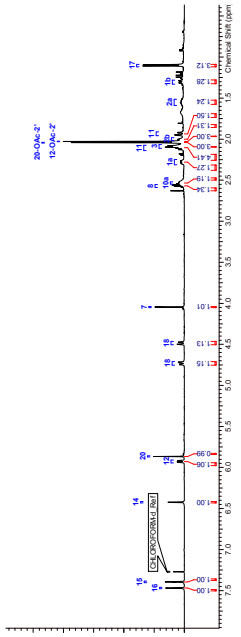

Figure S32. ^{1}H NMR spectrum of **5** (500 MHz, $CDCl_3$).

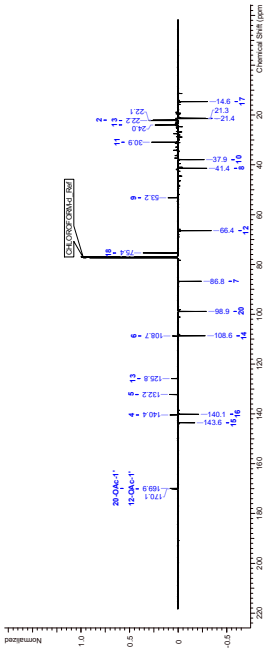

Figure S33. ^{13}C DEPTq spectrum of **5** (126 MHz, $CDCl_3$).

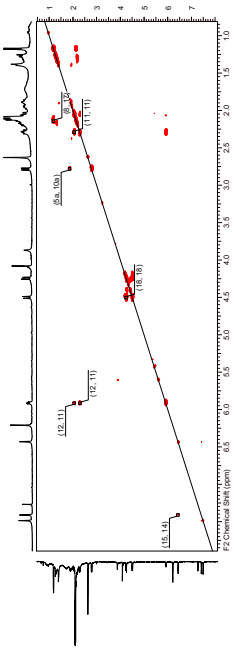

Figure S28. ^{1}H-^{1}H COSY spectrum of **4** (500 MHz, $CDCl_3$).

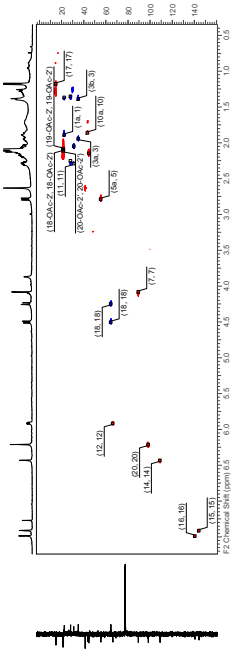

Figure S29. HSQC-DEPT spectrum of **4** (500 MHz, $CDCl_3$).

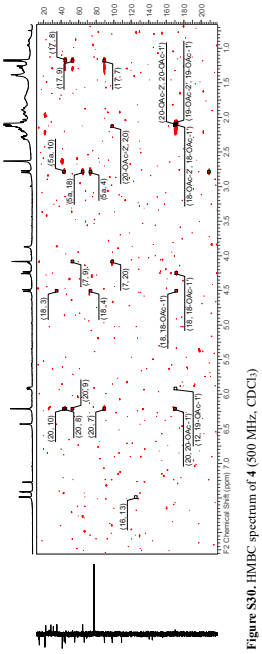

Figure S30. HMBC spectrum of **4** (500 MHz, $CDCl_3$).

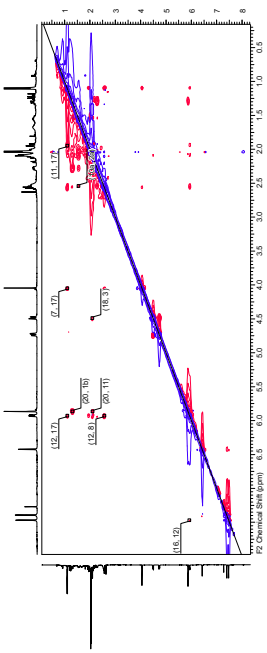

Figure S37. ^{1}H-^{1}H ROESY spectrum of **5** (500 MHz, CDCl$_3$)

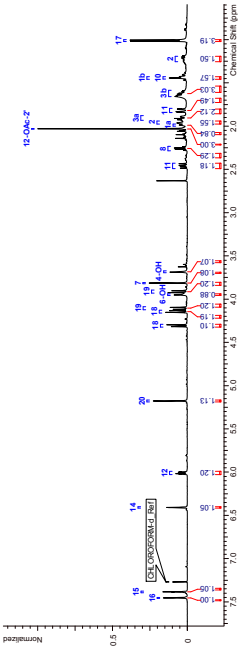

Figure S38. ^{1}H NMR spectrum of **6** (500 MHz, CDCl$_3$)

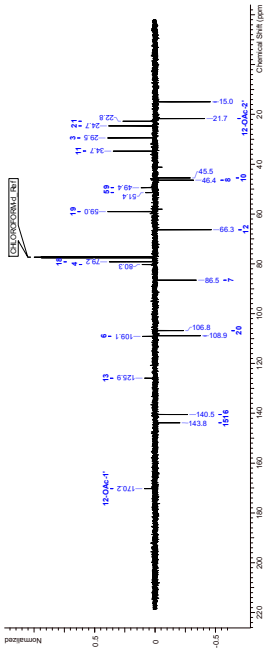

Figure S39. ^{13}C DEPTq spectrum of **6** (126 MHz, CDCl$_3$)

17

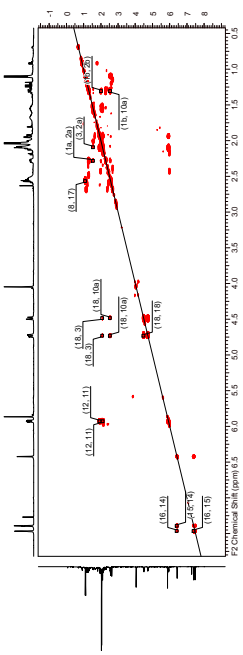

Figure S34. ^{1}H-^{1}H COSY spectrum of **5** (500 MHz, CDCl$_3$)

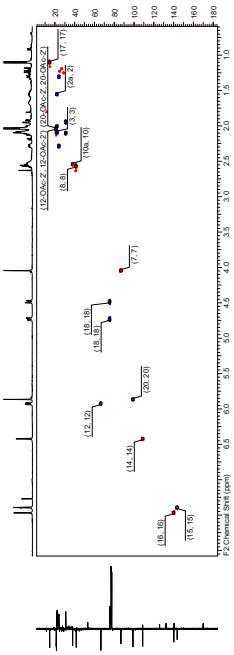

Figure S35. HSQC-DEPT spectrum of **5** (500 MHz, CDCl$_3$)

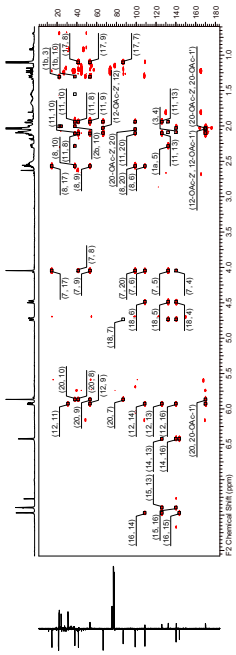

Figure S36. HMBC spectrum of **5** (500 MHz, CDCl$_3$)

16

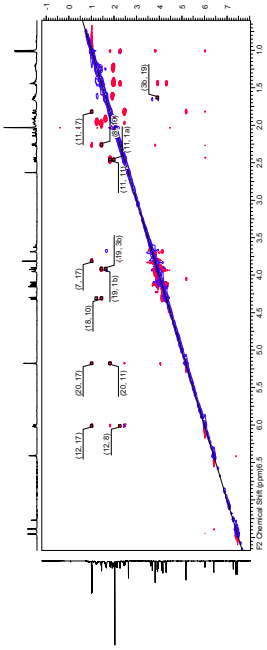

Figure S43. ^{1}H-^{1}H ROESY spectrum of **6** (500 MHz, CDCl$_3$)

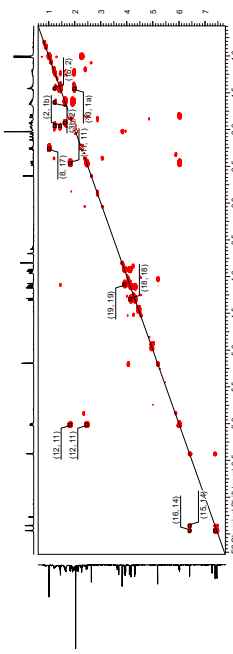

Figure S40. ^{1}H-^{1}H COSY spectrum of **6** (500 MHz, CDCl$_3$)

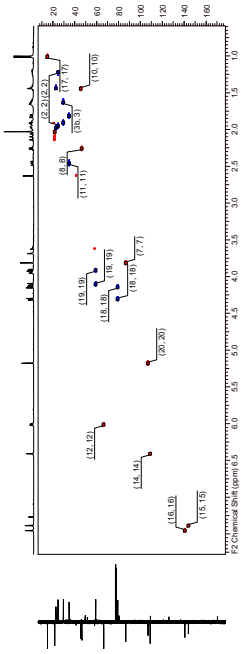

Figure S41. HSQC-DEPT spectrum of **6** (500 MHz, CDCl$_3$)

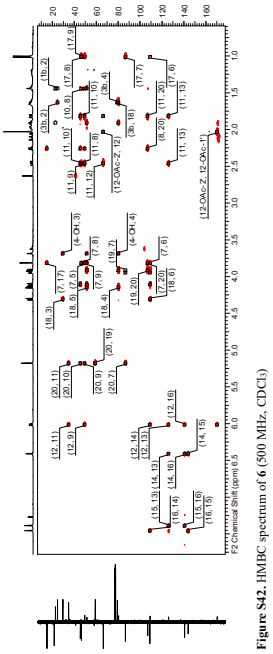

Figure S42. HMBC spectrum of **6** (500 MHz, CDCl$_3$)

Single Crystallographic Data and Experimental of 1

Diterpene 1 (20-Acetylauropolin)

OLEX²

Report created with **ReportPlus**

Submitted by: **Morris Keller**
University of Basel
Solved by: **Alessandro Prescimone**
Sample ID: **F15c2_D1_150K**

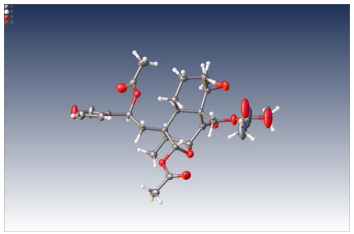

Experimental. Single colorless block-shaped crystals of **1** were recrystallized from a mixture of EtOAc and iso-ProOH by solvent layering. A suitable crystal 0.13×0.09×0.06 mm was selected and the crystal was mounted on a mylar loop in perfluoroether oil on a Stoe StadiVari diffractometer. The crystal was kept at a steady T = 150 K during data collection. The structure was solved with the **ShelXT** [1,2] structure solution program using the Intrinsic Phasing solution method and by using **Olex2** [3] as the graphical interface. The model was refined with version 2018/3 of **ShelXL** [1,2] using Least Squares minimization.

Crystal Data. $C_{26}H_{32}O_{10}$, M_r = 504.51, orthorhombic, $P2_12_12$ (No. 18), a = 17.3203(7) Å, b = 17.4805(9) Å, c = 8.3553(3) Å, $\alpha = \beta = \gamma = 90^\circ$, V = 2529.71(19) Å^3, T = 150 K, Z = 4, Z' = 1, $\mu(GaK_\alpha)$ = 0.547, 52085 reflections measured, 5209 unique (R_{int} = 0.1141) which were used in all calculations. The final wR_2 was 0.1418 (all data) and R_1 was 0.0557 ($I > 2(I)$).

Compound	1
Formula	$C_{26}H_{32}O_{10}$
$D_{calc.}$/ g cm^{-3}	1.325
m/mm^{-1}	0.547
Formula Weight	504.51
Color	colorless
Shape	block
Size/mm^3	0.13×0.09×0.06
T/K	150
Crystal System	orthorhombic
Flack Parameter	0.02(12)
Hooft Parameter	-0.03(11)
Space Group	$P2_12_12$
a/Å	17.3203(7)
b/Å	17.4805(9)
c/Å	8.3553(3)
α/°	90
β/°	90
γ/°	90
V/Å^3	2529.71(19)
Z	4
Z'	1
Wavelength/Å	1.34143
Radiation type	GaK_α
Q_{min}/°	3.125
Q_{max}/°	57.645
Measured Refl.	52085
Independent Refl.	5209
Reflections with I > 2(I)	4680
R_{int}	0.1141
Parameters	330
Restraints	16
Largest Peak	0.991
Deepest Hole	-0.369
GooF	1.140
wR_2 (all data)	0.1418
wR_2	0.1375
R_1 (all data)	0.0654
R_1	0.0557

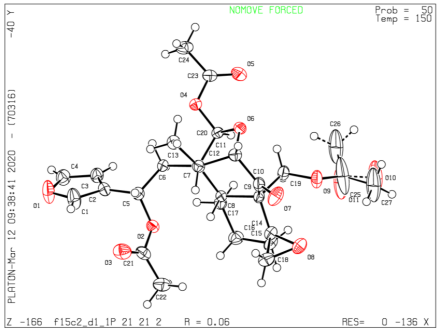

Figure S44. Ellipsoid plot of **1**.

Structure Quality Indicators of 1

Reflections: d min (1.34143) 0.79 | I/σ 24.1 | Rint 11.41% | complete 100%

Refinement: Shift 0.003 | Max Peak 1.0 | Min Peak -0.4 | GooF 1.140 | Flack .02(13)

A colorless block-shaped crystal with dimensions 0.13×0.09×0.06 mm was mounted on a mylar loop in perfluoroether oil. Data were collected using a Stoe StadiVari diffractometer equipped with an Oxford Cryosystems low-temperature device operating at T = 150 K.

Data were measured using rotation method, ω scans using GaK_α radiation. The total number of runs and images was based on the strategy calculation from the program STOE X-AREA (Stoe & Cie 2011) The maximum resolution that was achieved was Q = 57.645° (0.79 Å).

The diffraction pattern was indexed. The total number of runs and images was based on the strategy calculation from the program STOE X-AREA (Stoe & Cie 2011) and the unit cell was refined using STOE X-RED (Stoe & Cie 1996) on 44099 reflections, 85% of the observed reflections.

Data reduction, scaling and absorption corrections were performed using STOE X-RED (Stoe & Cie 1996). The final completeness is 99.90% out to 57.645° in Q. A multi-scan absorption correction was performed using STOE LANA, absorption correction by scaling of reflection intensities [4]. Afterwards a spherical absorption correction was performed within STOE LANA. The absorption coefficient m of this material is 0.547 mm^{-1} at this wavelength (l = 1.341Å) and the minimum and maximum transmissions are 0.500 and 3.400.

The structure was solved and the space group $P2_12_12$ (# 18) determined by the **ShelXT** [1,2]

structure solution program using Intrinsic Phasing and refined by Least Squares using version 2018/3 of **ShelXL** [1,2]. All non-hydrogen atoms were refined anisotropically. Hydrogen atom positions were calculated geometrically and refined using the riding model. Hydrogen atom positions were calculated geometrically and refined using the riding model.

_exptl_absorpt_process_details: STOE LANA, absorption correction by scaling of reflection intensities [4]. Afterwards a spherical absorption correction was performed within STOE LANA.

There is a single molecule in the asymmetric unit, which is represented by the reported sum formula. In other words: Z is 4 and Z' is 1.

The Flack parameter was refined to 0.02(12). Determination of absolute structure using Bayesian statistics on Bijvoet differences using the Olex2 results in -0.03(11). Note: The Flack parameter is used to determine chirality of the crystal studied, the value should be near 0, a value of 1 means that the stereochemistry is wrong and the model should be inverted. A value of 0.5 means that the crystal consists of a racemic mixture of the two enantiomers.

Data Plots: Diffraction Data of 1

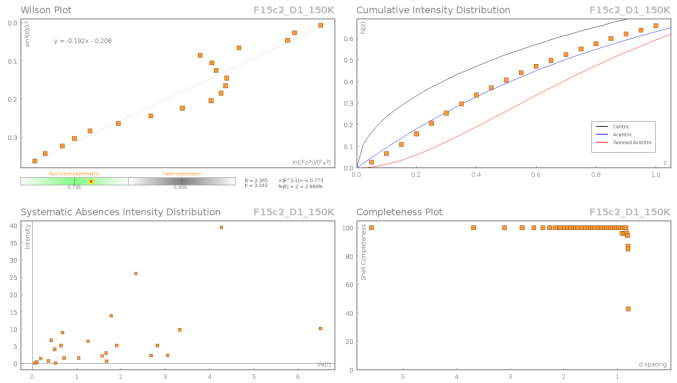

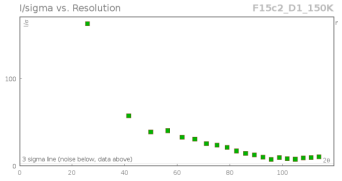

Data Plots: Refinement and Data of 1

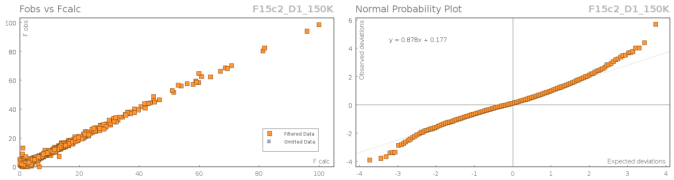

Reflection Statistics of 1

Total reflections (after filtering)	52110	Unique reflections	5209
Completeness	0.982	Mean I/s	19.76
hkl_{max} collected	(13, 21, 10)	hkl_{min} collected	(-21, -21, -10)
hkl_{max} used	(21, 21, 10)	hkl_{min} used	(-21, 0, 0)
Lim d_{max} collected	100.0	Lim d_{min} collected	0.67
d_{max} used	12.3	d_{min} used	0.79
Friedel pairs	3508	Friedel pairs merged	0
Inconsistent equivalents	2031	R_{int}	0.1141
R_{sigma}	0.0415	Intensity transformed	0
Omitted reflections	0	Omitted by user (OMIT hkl)	0
Multiplicity	(2697, 2457, 2168, 1622, 1418, 1108, 778, 585, 351, 216, 110, 57, 20, 10, 2)	Maximum multiplicity	26
Removed systematic absences	25	Filtered off (Shel/OMIT)	0

Table S1. Fractional Atomic Coordinates (×10⁴) and Equivalent Isotropic Displacement Parameters (Å²×10³) for **1**. U_{eq} is defined as 1/3 of the trace of the orthogonalised U_{ij}.

Atom	x	y	z	U_{eq}
O4	4198.7(15)	8129.7(14)	5575(3)	25.9(5)
O2	4501.7(15)	6106.4(14)	1219(3)	26.1(5)
O6	2909.1(15)	7794.3(14)	5454(3)	26.4(5)
O3	4315(2)	6324.8(17)	-1405(3)	43.2(8)
O9	1764.7(18)	6109.6(17)	6971(3)	39.6(7)
O5	3898(2)	8169.3(17)	8193(3)	41.6(7)
O8	1512.1(19)	5217.4(18)	4209(4)	44.5(8)
O7	1427.8(17)	6834.9(17)	3619(4)	42.7(7)
O1	6665.5(19)	7145(2)	-437(4)	53.6(9)
C2	5585(2)	6979(2)	996(4)	27.2(7)
C11	2521(2)	7635.5(19)	3955(4)	26.1(7)
C10	2092(2)	6876(2)	4045(4)	28.6(7)
C8	3430(2)	6274.9(18)	3948(4)	21.8(7)
C23	4259(2)	8417(2)	7079(4)	26.4(7)
C3	6250(2)	6881(2)	2005(5)	30.7(8)
C7	3757(2)	7112.3(18)	3769(4)	22.1(7)
C20	3675(2)	7509.4(19)	5400(4)	23.4(7)
C21	4277(2)	5905(2)	-263(4)	31.3(8)
C5	4746(2)	6904(2)	1421(4)	25.0(7)
C9	2585(2)	6207(2)	4674(4)	23.9(7)
C17	3972(2)	5697(2)	4737(4)	26.1(7)
C6	4597(2)	7135.8(19)	3163(4)	24.0(7)
C12	3179(2)	7576.2(19)	2741(4)	24.7(7)
C13	3440(2)	8373(2)	2199(4)	28.9(8)
C14	2322(2)	5398(2)	4198(5)	31.9(8)
C16	3675(3)	4879(2)	4454(5)	33.4(8)
C4	6876(2)	6990(2)	1087(5)	37.0(9)
C19	2553(2)	6256(2)	6527(4)	29.2(8)
C22	3977(3)	5101(2)	-311(5)	39.3(10)
C24	4808(2)	9070(2)	7104(6)	36.9(9)
C1	5877(3)	7138(3)	-461(5)	47.8(11)
C15	2823(3)	4770(2)	4879(5)	35.1(9)
C18	1912(3)	5253(3)	2702(5)	43.7(11)
C25	1609(4)	5789(6)	8292(8)	104(3)
O10	882(7)	5702(11)	8889(15)	94(2)
O11	2063(5)	5315(6)	8878(9)	94(2)
C26	2195(9)	6074(13)	9503(18)	94(2)
C27	702(7)	5725(11)	8336(15)	94(2)

Table S2. Anisotropic Displacement Parameters (×10⁴) **1**. The anisotropic displacement factor exponent takes the form: $-2p^2[h^2a^{*2} \times U_{11} + ... + 2hka^* \times b^* \times U_{12}]$

Atom	U_{11}	U_{22}	U_{33}	U_{23}	U_{13}	U_{12}
O4	25.8(13)	27.1(11)	24.7(11)	-3.0(10)	0.6(10)	-5.1(10)
O2	25.7(13)	29.3(12)	23.1(11)	-1.7(9)	0.1(10)	1.1(10)
O6	23.6(13)	29.5(12)	25.9(12)	-4.9(10)	1.3(10)	-1.0(10)
O3	55(2)	44.6(16)	29.7(14)	1.2(12)	-10.6(14)	-0.8(14)
O9	31.5(16)	54.6(18)	32.8(14)	7.2(12)	8.8(12)	-9.2(14)
O5	53(2)	45.0(16)	27.2(13)	-8.9(12)	4.3(13)	-8.2(14)
O8	29.9(16)	50.9(17)	52.6(18)	-7.3(14)	2.3(13)	-16.3(14)
O7	22.9(15)	47.6(17)	57.6(18)	12.8(14)	-9.9(13)	-6.5(13)
O1	27.9(17)	97(3)	36.3(16)	13.1(17)	7.7(13)	-4.5(17)
C2	28.1(19)	29.6(17)	23.9(16)	0.4(13)	3.5(14)	1.5(15)
C11	24.7(18)	25.7(16)	27.8(16)	-0.9(13)	-1.4(15)	1.8(14)
C10	22.8(18)	37.9(19)	25.0(16)	0.3(14)	2.2(14)	-2.9(15)
C8	22.3(17)	23.4(16)	19.7(15)	-1.9(12)	2.2(12)	-2.6(13)
C23	25(2)	24.9(16)	29.2(17)	-4.8(13)	-5.2(14)	3.5(14)
C3	23.6(19)	38.0(19)	30.5(17)	0.6(15)	0.1(15)	-1.0(16)
C7	23.5(17)	22.9(15)	19.8(14)	-1.6(12)	1.5(13)	-1.8(13)
C20	22.2(17)	22.1(15)	26.1(16)	-2.6(13)	0.5(13)	-2.4(13)
C21	28(2)	38(2)	28.1(18)	-7.9(15)	-1.9(15)	6.7(16)
C5	21.1(17)	27.8(16)	26.1(16)	-0.5(13)	-0.5(13)	1.8(14)
C9	19.6(17)	29.0(17)	23.1(15)	-0.3(13)	1.4(13)	-4.4(14)
C17	25.1(19)	26.6(17)	26.7(16)	0.5(13)	0.7(14)	0.5(14)
C6	21.1(18)	25.4(15)	25.3(16)	-1.9(13)	2.9(13)	-4.6(13)
C12	23.6(18)	25.8(16)	24.7(17)	-0.9(13)	-0.1(13)	0.3(14)
C13	31(2)	27.4(17)	28.2(17)	3.6(13)	0.4(14)	1.7(15)
C14	28(2)	32.9(18)	35.1(18)	-2.5(15)	3.0(15)	-7.7(16)
C16	38(2)	25.7(18)	36(2)	-0.1(15)	0.1(17)	0.6(16)
C4	26(2)	47(2)	38(2)	-1.9(17)	-0.5(16)	-1.6(18)
C19	24.3(19)	34.2(18)	29.0(17)	2.8(14)	2.9(14)	-4.2(15)
C22	42(3)	38(2)	38(2)	-8.9(17)	-7.2(19)	0.4(18)
C24	27(2)	32.6(19)	51(2)	-12.0(18)	-7.6(18)	2.1(16)
C1	27(2)	82(3)	35(2)	7(2)	3.1(18)	3(2)
C15	39(2)	25.3(19)	40(2)	1.8(15)	2.8(17)	-11.9(16)
C18	40(3)	44(2)	47(2)	-12.3(19)	-1.1(19)	-13.1(19)
C25	55(4)	191(8)	65(4)	70(5)	32(3)	30(5)
O10	60(3)	159(5)	62(4)	66(4)	17(3)	4(4)
O11	60(3)	159(5)	62(4)	66(4)	17(3)	4(4)
C26	60(3)	159(5)	62(4)	66(4)	17(3)	4(4)
C27	60(3)	159(5)	62(4)	66(4)	17(3)	4(4)

Table S3 Bond Lengths in Å for **1**.

Atom	Atom	Length/Å	Atom	Atom	Length/Å
O4	C23	1.357(4)	C8	C7	1.577(4)
O4	C20	1.422(4)	C8	C9	1.589(5)
O2	C21	1.344(4)	C8	C17	1.529(5)
O2	C5	1.467(4)	C23	C24	1.484(5)
O6	C11	1.448(4)	C3	C4	1.342(6)
O6	C20	1.417(4)	C7	C20	1.536(4)
O3	C21	1.205(5)	C7	C6	1.541(5)
O9	C19	1.438(5)	C7	C12	1.549(5)
O9	C25	1.266(6)	C21	C22	1.499(6)
O5	C23	1.203(5)	C5	C6	1.533(5)
O8	C14	1.438(5)	C9	C14	1.538(5)
O8	C18	1.439(6)	C9	C19	1.552(5)
O7	C10	1.207(5)	C17	C16	1.537(5)
O1	C4	1.352(5)	C12	C13	1.533(5)
O1	C1	1.366(6)	C14	C15	1.510(6)
C2	C3	1.437(5)	C14	C18	1.460(6)
C2	C5	1.501(5)	C16	C15	1.530(6)
C2	C1	1.348(6)	C25	O10	1.363(12)
C11	C10	1.524(5)	C25	O11	1.243(10)
C11	C12	1.529(5)	C25	C26	1.517(16)
C10	C9	1.539(5)	C25	C27	1.575(13)

Table S4 Bond Angles in ° for **1**.

Atom	Atom	Atom	Angle/°	Atom	Atom	Atom	Angle/°
C23	O4	C20	115.3(3)	O3	C21	C22	124.6(4)
C21	O2	C5	116.0(3)	O2	C5	C2	109.5(3)
C20	O6	C11	109.8(3)	O2	C5	C6	108.2(3)
C25	O9	C19	120.4(4)	C2	C5	C6	111.4(3)
C14	O8	C18	61.0(3)	C10	C9	C8	108.9(3)
C4	O1	C1	106.3(3)	C10	C9	C19	106.2(3)
C3	C2	C5	128.8(3)	C14	C9	C10	116.5(3)
C1	C2	C3	104.7(3)	C14	C9	C8	104.0(3)
C1	C2	C5	126.5(4)	C14	C9	C19	107.3(3)
O6	C11	C10	110.5(3)	C19	C9	C8	114.2(3)
O6	C11	C12	104.0(3)	C8	C17	C16	110.1(3)
C10	C11	C12	109.7(3)	C5	C6	C7	117.6(3)
O7	C10	C11	120.1(4)	C11	C12	C7	98.6(3)
O7	C10	C9	125.8(3)	C11	C12	C13	110.7(3)
C11	C10	C9	114.1(3)	C13	C12	C7	116.7(3)
C7	C8	C9	115.9(3)	O8	C14	C9	119.2(3)
C17	C8	C7	115.7(3)	O8	C14	C15	113.5(3)
C17	C8	C9	110.6(3)	O8	C14	C18	59.5(3)
O4	C23	C24	110.3(3)	C15	C14	C9	113.7(3)
O5	C23	O4	122.8(3)	C18	C14	C9	121.7(3)
O5	C23	C24	126.8(3)	C18	C14	C15	118.4(4)
C4	C3	C2	107.2(3)	C15	C16	C17	113.8(3)
C20	C7	C8	107.6(3)	C3	C4	O1	110.4(4)
C20	C7	C6	111.6(3)	O9	C19	C9	106.3(3)
C20	C7	C12	101.3(3)	C2	C1	O1	111.4(4)
C6	C7	C8	113.3(3)	C14	C15	C16	112.1(3)
C6	C7	C12	114.5(3)	O8	C18	C14	59.5(3)
C12	C7	C8	107.8(3)	O9	C25	O10	124.4(7)
O4	C20	C7	112.1(3)	O9	C25	C26	107.1(8)
O6	C20	O4	109.0(3)	O9	C25	C27	105.3(6)
O6	C20	C7	105.9(3)	O10	C25	C26	114.3(11)
O2	C21	C22	111.7(3)	O11	C25	O9	120.2(6)
O3	C21	O2	123.6(4)	O11	C25	C27	125.0(9)

Table S5 Hydrogen Fractional Atomic Coordinates (×10⁴) and Equivalent Isotropic Displacement Parameters (Å²×10³) for **1**. U_{eq} is defined as 1/3 of the trace of the orthogonalised U_{ij}.

Atom	x	y	z	U_{eq}
H11	2161.1	8060.75	3666.48	31
H8	3375.3	6088.15	2822.1	26
H3	6246.57	6762.43	3114.4	37
H20	3755.33	7130.37	6280.19	28
H5	4433.94	7238.22	696.98	30
H17A	4001.14	5798.72	5901.29	31
H17B	4496.86	5750.06	4283.7	31
H6A	4793.11	7663.12	3311.54	29
H6B	4909.64	6797.44	3858.55	29
H12	3010.81	7267.23	1795.77	30
H13A	3017.64	8625.37	1623.6	43
H13B	3887.93	8324.64	1489.3	43
H13C	3581.41	8679.18	3136.91	43
H16A	3750.84	4745.98	3313.44	40
H16B	3987.72	4520.01	5101.17	40
H4	7393.82	6962.09	1455.38	44
H19A	2900.2	5870.77	7012.13	35
H19B	2714.18	6770.51	6894.66	35
H22A	4232.3	4797.01	519.92	59
H22B	4083.15	4877.31	-1362.84	59
H22C	3418.57	5104.45	-119.95	59
H24A	5317.71	8895.65	6751.36	55
H24B	4844.38	9273.23	8194.2	55
H24C	4622.45	9472.2	6382.11	55
H1	5573.58	7232.15	-1387.34	57
H15A	2644.49	4270.74	4460.16	42
H15B	2765.92	4761.55	6057.93	42
H18A	1805.77	5694.46	1993.73	52
H18B	2017.33	4765.25	2139.64	52
H26A	2513.01	5644.3	9869.39	141
H26B	1924.96	6299.81	10418.78	141
H26C	2525.94	6460.79	9003.47	141
H27A	484.96	6189.59	8814.74	141
H27B	552.31	5279.82	8976.75	141
H27C	504.88	5666.48	7243.4	141

Table S6 Atomic Occupancies for all atoms that are not fully occupied in **1**.

Atom	Occupancy
O10	0.4
O11	0.6
C26	0.4
H26A	0.4
H26B	0.4
H26C	0.4
C27	0.6
H27A	0.6
H27B	0.6
H27C	0.6

References

[1] G.M. Sheldrick, SHELXT - integrated space-group and crystal-structure determination, Acta Crystallogr. Sect. A Found. Crystallogr. A71 (2015) 3–8. https://doi.org/10.1107/S2053273314026370.

[2] G.M. Sheldrick, Crystal structure refinement with SHELXL, Acta Crystallogr. Sect. C Struct. Chem. C71 (2015) 3–8. https://doi.org/10.1107/S2053229614024218.

[3] O.V. Dolomanov, L.J. Bourhis, R.J. Gildea, J.A.K. Howard, H. Puschmann, OLEX2: a complete structure solution, refinement and analysis program, J. Appl. Crystallogr. 42 (2009) 339–341. https://doi.org/10.1107/S0021889808042726.

[4] J. Koziskova, F. Hahn, J. Richter, J. Kožíšek, Comparison of different absorption corrections on the model structure of tetrakis(μ_2-acetato)-diaqua-di-copper(II), Acta Chim. Slovaca. 9 (2016) 136–140. https://doi.org/10.1515/acs-2016-0023.

checkCIF/PLATON report

Structure factors have been supplied for datablock(s) f15c2_d1_150k

THIS REPORT IS FOR GUIDANCE ONLY. IF USED AS PART OF A REVIEW PROCEDURE FOR PUBLICATION, IT SHOULD NOT REPLACE THE EXPERTISE OF AN EXPERIENCED CRYSTALLOGRAPHIC REFEREE.

No syntax errors found. CIF dictionary Interpreting this report

Datablock: f15c2_d1_150k

Bond precision: C-C = 0.0052 A Wavelength=1.34143

Cell: a=17.3203(7) b=17.4805(9) c=8.3553(3)
alpha=90 beta=90 gamma=90
Temperature: 150 K

	Calculated	Reported
Volume	2529.71(19)	2529.71(19)
Space group	P 21 21 2	P 21 21 2
Hall group	P 2 2ab	P 2 2ab
Moiety formula	C26 H32 O10	C26 H32 O10
Sum formula	C26 H32 O10	C26 H32 O10
Mr	504.52	504.51
Dx,g cm-3	1.325	1.325
Z	4	4
Mu (mm-1)	0.544	0.547
F000	1072.0	1072.0
F000'	1074.87	
h,k,lmax	21,22,10	21,21,10
Nref	5305[3010]	5209
Tmin,Tmax	0.941,0.968	0.500,3.400
Tmin'	0.931	

Correction method= # Reported T Limits: Tmin=0.500 Tmax=3.400
AbsCorr = MULTI-SCAN

Data completeness= 1.73/0.98 Theta(max)= 57.645

R(reflections)= 0.0557(4680) wR2(reflections)= 0.1418(5209)

S = 1.140 Npar= 330

The following ALERTS were generated. Each ALERT has the format
test-name_ALERT_alert-type_alert-level.
Click on the hyperlinks for more details of the test.

Alert level B

PLAT097_ALERT_2_B Large Reported Max. (Positive) Residual Density 0.99 eA-3

Alert level C

DIFMX02_ALERT_1_C The maximum difference density is > 0.1*ZMAX*0.75
The relevant atom site should be identified.
PLAT094_ALERT_2_C Ratio of Maximum / Minimum Residual Density .... 2.69 Report
PLAT213_ALERT_2_C Atom C25 has ADP max/min Ratio ..... 3.2 prolat
PLAT220_ALERT_2_C NonSolvent Resd 1 C Ueq(max) / Ueq(min) Range 4.8 Ratio
PLAT220_ALERT_2_C NonSolvent Resd 1 O Ueq(max) / Ueq(min) Range 3.6 Ratio
PLAT222_ALERT_3_C NonSolvent Resd 1 H Uiso(max)/Uiso(min) Range 5.4 Ratio
PLAT234_ALERT_4_C Large Hirshfeld Difference C25 --C26 . 0.17 Ang.
PLAT241_ALERT_2_C High MainMol Ueq as Compared to Neighbors of C25 Check
PLAT242_ALERT_2_C Low MainMol Ueq as Compared to Neighbors of O9 Check
PLAT309_ALERT_2_C Single Bonded Oxygen (C-O > 1.3 Ang) ..... O10 Check
PLAT340_ALERT_3_C Low Bond Precision on C-C Bonds ..... 0.00522 Ang.
PLAT410_ALERT_2_C Short Intra H...H Contact H19B ..H20 . 1.98 Ang.
x,y,z = 1_555 Check
PLAT906_ALERT_3_C Large K Value in the Analysis of Variance ..... 3.643 Check
PLAT911_ALERT_3_C Missing FCF Refl Between Thmin & STh/L= 0.600 2 Report

Alert level G

ABSMU01_ALERT_1_G Calculation of _exptl_absorpt_correction_mu
not performed for this radiation type.
PLAT002_ALERT_2_G Number of Distance or Angle Restraints on AtSite 12 Note
PLAT171_ALERT_4_G The CIF-Embedded .res File Contains EADP Records 1 Report
PLAT176_ALERT_4_G The CIF-Embedded .res File Contains SADI Records 5 Report
PLAT300_ALERT_4_G Atom Site Occupancy of O11 Constrained at 0.6 Check
PLAT300_ALERT_4_G Atom Site Occupancy of O10 Constrained at 0.4 Check
PLAT300_ALERT_4_G Atom Site Occupancy of C27 Constrained at 0.6 Check
PLAT300_ALERT_4_G Atom Site Occupancy of C26 Constrained at 0.4 Check
PLAT300_ALERT_4_G Atom Site Occupancy of H27A Constrained at 0.6 Check
PLAT300_ALERT_4_G Atom Site Occupancy of H27B Constrained at 0.6 Check
PLAT300_ALERT_4_G Atom Site Occupancy of H27C Constrained at 0.6 Check
PLAT300_ALERT_4_G Atom Site Occupancy of H26A Constrained at 0.4 Check
PLAT300_ALERT_4_G Atom Site Occupancy of H26B Constrained at 0.4 Check
PLAT300_ALERT_4_G Atom Site Occupancy of H26C Constrained at 0.4 Check
PLAT301_ALERT_3_G Main Residue Disorder .....(Resd 1) 6% Note
PLAT380_ALERT_4_G Incorrectly? Oriented X(sp2)-Methyl Moiety ..... C24 Check
PLAT398_ALERT_2_G Deviating C-O-C Angle From 120 for O1 106.4 Degree
PLAT398_ALERT_2_G Deviating C-O-C Angle From 120 for O6 109.8 Degree
PLAT398_ALERT_2_G Deviating C-O-C Angle From 120 for O8 61.0 Degree
PLAT412_ALERT_2_G Short Intra XH3 .. XHn H19A ..H26C . 2.06 Ang.
x,y,z = 1_555 Check
PLAT412_ALERT_2_G Short Intra XH3 .. XHn H19B ..H26C . 1.87 Ang.
x,y,z = 1_555 Check
PLAT413_ALERT_2_G Short Inter XH3 .. XHn H18A ..H26B . 1.70 Ang.
x,y,-1+z = 1_554 Check
PLAT413_ALERT_2_G Short Inter XH3 .. XHn H22C ..H26A . 1.83 Ang.
x,y,-1+z = 1_554 Check
PLAT432_ALERT_2_G Short Inter X...Y Contact C18 ..C26 3.07 Ang.
x,y,-1+z = 1_554 Check
PLAT791_ALERT_4_G Model has Chirality at C5 (Chiral SPGR) S Verify
PLAT791_ALERT_4_G Model has Chirality at C7 (Chiral SPGR) S Verify
PLAT791_ALERT_4_G Model has Chirality at C8 (Chiral SPGR) S Verify
PLAT791_ALERT_4_G Model has Chirality at C9 (Chiral SPGR) S Verify
PLAT791_ALERT_4_G Model has Chirality at C11 (Chiral SPGR) S Verify
PLAT791_ALERT_4_G Model has Chirality at C12 (Chiral SPGR) S Verify
PLAT791_ALERT_4_G Model has Chirality at C14 (Chiral SPGR) R Verify

```
PLAT791_ALERT_4_G Model has Chirality at C20         (Chiral SPGR)          R Verify
PLAT860_ALERT_3_G Number of Least-Squares Restraints .............         16 Note
PLAT912_ALERT_4_G Missing # of FCF Reflections Above STh/L=  0.600         27 Note
PLAT978_ALERT_2_G Number C-C Bonds with Positive Residual Density.          9 Info
PLAT984_ALERT_1_G The  C-f'=     0.0148 Deviates from the B&C-Value     0.0137 Check
PLAT984_ALERT_1_G The  O-f'=     0.0412 Deviates from the B&C-Value     0.0389 Check
```

```
  0 ALERT level A = Most likely a serious problem - resolve or explain
  1 ALERT level B = A potentially serious problem, consider carefully
 14 ALERT level C = Check. Ensure it is not caused by an omission or oversight
 37 ALERT level G = General information/check it is not something unexpected

  4 ALERT type 1 CIF construction/syntax error, inconsistent or missing data
 19 ALERT type 2 Indicator that the structure model may be wrong or deficient
  6 ALERT type 3 Indicator that the structure quality may be low
 23 ALERT type 4 Improvement, methodology, query or suggestion
  0 ALERT type 5 Informative message, check
```

It is advisable to attempt to resolve as many as possible of the alerts in all categories. Often the minor alerts point to easily fixed oversights, errors and omissions in your CIF or refinement strategy, so attention to these fine details can be worthwhile. In order to resolve some of the more serious problems it may be necessary to carry out additional measurements or structure refinements. However, the purpose of your study may justify the reported deviations and the more serious of these should normally be commented upon in the discussion or experimental section of a paper or in the "special_details" fields of the CIF. checkCIF was carefully designed to identify outliers and unusual parameters, but every test has its limitations and alerts that are not important in a particular case may appear. Conversely, the absence of alerts does not guarantee there are no aspects of the results needing attention. It is up to the individual to critically assess their own results and, if necessary, seek expert advice.

Publication of your CIF in IUCr journals

A basic structural check has been run on your CIF. These basic checks will be run on all CIFs submitted for publication in IUCr journals (*Acta Crystallographica*, *Journal of Applied Crystallography*, *Journal of Synchrotron Radiation*); however, if you intend to submit to *Acta Crystallographica Section C* or *E* or *IUCrData*, you should make sure that full publication checks are run on the final version of your CIF prior to submission.

Publication of your CIF in other journals

Please refer to the *Notes for Authors* of the relevant journal for any special instructions relating to CIF submission.

PLATON version of 22/12/2019; check.def file version of 13/12/2019

Datablock f15c2_d1_150k - ellipsoid plot

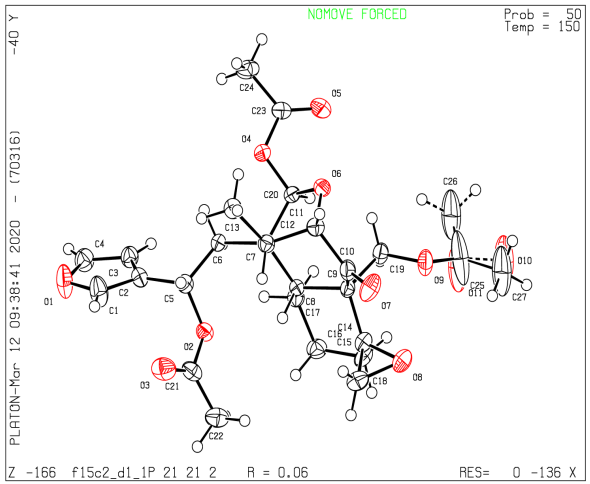

Curriculum Vitae

Morris Keller
Swiss, born 7th February 1992
Cuno-Amiet Strasse 30
3360 Herzogenbuchsee
Phone: +41 79 227 45 64
E-mail: keller-morris@gmx.ch

EDUCATION

01.2019 – 06.2023 **Doctor of Philosophy (PhD) in Pharmaceutical Sciences, University of Basel**
Title: Isolation and Characterization of Anti-Inflammatory and Immunomodulatory Compounds from Higher Plants
Supervisor: Prof. Dr. Olivier Potterat

09.2016 – 07.2018 **Master's Degree (MSc) in Drug Sciences, University of Basel**
Thesis: Phytochemical Profiling and Anti-Inflammatory Constituents from *Crocus sativus* corms
Supervisor: Prof. Dr. Matthias Hamburger & Prof. Dr Olivier Potterat

09.2013 – 07.2016 **Bachelor's Degree (BSc) in Pharmaceutical Sciences, University of Basel**

08.2006 – 06.2010 **Matura, Kantonsschule Solothurn**
Federal maturity in Mathematics and Sciences, focus on biology and chemistry

EMPLOYMENT HISTORY

08.2023 – present **Project Manager Analytical Chemistry (Method Validation)**
Dottikon Exclusive Synthesis AG, Dottikon
- Development and validation of analytical methods (GMP), Chromatography (HPLC, GC, IC), Evaluation of experimental data

01.2019 – 05.2023 **Research Scientist & Teaching Assistant**
University of Basel, Department of Pharmaceutical Sciences, Division of Pharmaceutical Biology, Basel
- Basic research in the field of natural product chemistry (Chromatography, HPLC, NMR, HRMS, Activity profiling, Teaching, Writing & Publishing)

08.2018 – 12.2018 **Research Scientist & Teaching Assistant**
Institute of Forensic Medicine, Division of Forensic Chemistry & Toxicology, Basel
- Development and validation of HPLC-based methods (GTFCh), Authoring of SOPs, Giving lectures

08.2015 – 10.2018 **Safety guard**
Securitas AG, Swiss Guarding Company, Olten & Thun
- Student part time job, Security staff

05.2010 – 08.2015 **Crew Trainer**
Mc Donald's Switzerland, Zuchwil
- Student part time job**,** Working in service, kitchen, and drive through

PUBLICATIONS

Keller, M., Chabane, S., Boudjelal, A., Danton, O., Prescimone, A., Hamburger, M. & Potterat, O. New neo-clerodane diterpenes from *Teucrium polium* subsp. *capitatum*. *J. Mol. Struct.* **1284**, 135447 (2023).
https://doi.org/10.1016/j.molstruc.2023.135447

Keller, M., Winker, M., Zimmermann-Klemd, A. M., Sperisen, N., Gupta, M. P., Solis, P. N., Hamburger, M., Potterat, O. & Gründemann, C. Aryltetralin lignans from *Hyptis brachiata* inhibiting T lymphocyte proliferation. *Biomed. Pharmacother.* **160**, 114328 (2023).
https://doi.org/10.1016/j.biopha.2023.114328

Hajib, A., Danton, O., **Keller, M.**, Potterat, O., Bougrin, K., Charrouf, Z. & Hamburger, M. Polyacetylenic caffeoyl amides from *Ammodaucus leucotrichus*. *Phytochemistry* **206**, 113555 (2023).
https://doi.org/10.1016/j.phytochem.2022.113555

Hell, T., Rutz, A., Dürr, L., Dobrzyński, M., Reinhardt, J. K., Lehner, T., **Keller, M.**, John, A., Gupta, M., Pertz, O., Hamburger, M., Wolfender, J.-L. & Garo, E. Combining activity profiling with advanced annotation to accelerate the discovery of natural products targeting oncogenic signaling in melanoma. *J. Nat. Prod.* **85**, 1540–1554 (2022).
https://doi.org/10.1021/acs.jnatprod.2c00146

Keller, M., Fankhauser, S., Giezendanner, N., König, M., Keresztes, F., Danton, O., Fertig, O., Marcourt, L., Hamburger, M., Butterweck, V. & Potterat, O. Saponins from saffron corms inhibit the gene expression and secretion of pro-inflammatory cytokines. *J. Nat. Prod.* **84**, 630–645 (2021).
https://doi.org/10.1021/acs.jnatprod.0c01220

Chabane, S., Boudjelal, A., **Keller, M.**, Doubakh, S. & Potterat, O. *Teucrium polium* - wound healing potential, toxicity and polyphenolic profile. *South African J. Bot.* **137**, 228–235 (2021).
https://doi.org/10.1016/j.sajb.2020.10.017

Drescher, C., **Keller, M.**, Potterat, O., Hamburger, M. & Brückner, R. Structure-elucidating total synthesis of the (polyenoyl)tetramic acid militarinone C. *Org. Lett.* **22**, 2559–2563 (2020).
https://doi.org/10.1021/acs.orglett.0c00431

CONTRIBUTIONS TO CONFERENCES

08.2023	Poster presentation at the Swiss Chemical Society (SCS) fall meeting 2023, Bern, Switzerland
03.2023	Poster presentation at the 14th Symposium of the Swiss Ethnobiology Network, Luzern, Switzerland
09.2022	Poster presentation at the Swiss Chemical Society (SCS) fall meeting 2022, Zürich, Switzerland
08.2022	Oral presentation at the Young Researchers' Workshop (YRW) at the 70th International Congress and Annual Meeting of the Society for Medicinal Plant and Natural Product Research (GA), Thessaloniki, Greece
08.2022	Poster presentation at the 15th Swiss Pharma Science Day 2022, Bern, Switzerland Awarded with the "Max Zeller Söhne AG Poster Award" – Prize for best poster in the category Pharmaceutical Biology

02.2022	Poster presentation at the Annual Research Meeting (ARM) of the Pharmacenter Basel, Switzerland
09.2021	Poster Presentation at the 6th Toyama-Basel Meeting 2021, virtual conference, Toyama, Japan
08.2021	"My Thesis in 180 seconds" presentation at the 34th Seminar in Pharmaceutical Sciences "New paradigms in natural product drug discovery: Bench to Bench Bench to Bedside", Leysin, Switzerland
08.2021	3 minutes flash talk and poster presentation at the PhD Retreat of the Bio- and Pharmacenter Basel 2021, virtual conference, Basel, Switzerland
08.2020	3 minutes video presentation at the Swiss Chemical Society (SCS) fall meeting 2020, virtual conference, Zürich, Switzerland
08.2019	Poster presentation at the 12th Swiss Pharma Science Day 2019, Bern, Switzerland

LANGUAGES

German	Native proficiency
English	Full professional proficiency
French	Professional working proficiency
Chinese	Elementary proficiency

ADDITIONAL TRAINING WITH CERTIFICATES

05.2023	LaTex Crash Course (2-day course)
11.2022	Information design – designing presentation slides, posters, reports, and handouts (2-day course)
01.2022	Communicate Effectively - Collaborate Constructively (3-day course)
10.2021	Learning How to Lead and to Build a Successful Work Environment (3-day course)
06.2021	Good Scientific Practice (3-day course)
05.2021	Project Management for Researchers (8 course module for 2 months)
04.2021	Storytelling, Message Distilling and Presentation Design for Natural and Life Scientists (2-day course)
06.2021	Preparing and Holding Presentations Effectively in the Natural and Life Sciences (2-day course)
01.2017	Good Clinical Practice (GCP) for Investigators and Study Teams (2-day course)